A Study of Small and Intermediate Conductance Calcium-Activated Potassium Channels in Sensory Neurones

Parmvir Kaur Bahia

Thesis submitted for the degree of Doctor of Philosophy

Department of Pharmacology

University College London

ProQuest LLC
789 East Eisenhower Parkway
P.O. Box 1346
Ann Arbor, MI 48106-1346

Abstract

The role of small and intermediate conductance calcium-activated potassium channels (SK and IK channels) in dorsal root ganglion (DRG) neurones was examined. Sixteen antibodies raised against human or rat SK/IK channel peptide epitopes were tested for their ability to stain cells expressing channel protein. Of sixteen antibodies, 12 (6 to SK1, 1 to SK2, 2 to SK3 and 3 to IK) were deemed suitable for immunohistochemistry in human or rat tissue.

Real-time quantitative PCR (qPCR) of rat DRG cDNA was performed to examine SK/IK expression levels. DRG neurones produce mRNA for all SK/IK channels and these mRNA levels were found to increase during development. Antibody staining experiments using DRG neurones cultured from different aged animals produced a positive stain with the anti-SK3 antibody only. The number of cells that stained positively and the intensity of staining for SK3 increased with age.

To investigate possible functional roles for SK/IK channels sensory neurones, action potential afterhyperpolarisations (AHPs) were recorded from cultured DRG and nodose cells. The majority of these AHPs proved to be insensitive to the SK channel blocker UCL 1848. Attempts to block medium duration AHPs in DRG cells using IK and calcium channel blockers, also failed in most cases, suggesting that some other potassium conductance(s) are responsible.

The possibility that SK3 is functional at the terminals of primary afferents was examined next. Spinal cord slices stained with SK/IK channel antibodies revealed positive SK3 staining in the outer laminae of the dorsal horn, where small and large diameter DRG fibres are expected to terminate. *In vivo* experiments (done by Dr Rie

Suzuki, Department of Pharmacology, UCL) using UCL 1848 and 1-ethyl-2-benzimidazolinone (1-EBIO; an SK channel opener) showed that SK channels are likely to be active at these terminals where they have a functional role in mediating innocuous mechanical and nociceptive responses.

Acknowledgements

I am incredibly grateful to my supervisor Guy Moss for his patience and good advice. Thanks also to Don Jenkinson for introducing me to sharp electrode recording, to Dennis Haylett, David Benton and Alan Monaghan for being my "Idiot's guide to electrophysiology" and for all their useful comments over the years. Thank you to Ramine Hosseini for demonstrating the antibody staining technique, to Gayle Passmore for helping me setup and troubleshoot the DRG preparation and to Wahida Rahman for preparing the rat spinal cord slices. I would also like to express my gratitude to Tony Dickenson and Rie Suzuki for agreeing to the collaboration that has contributed substantially to this thesis.

At GSK, I would like to thank Mark Chen and Derek Trezise for all their advice and particularly to JP Wahlin for patiently helping out with all aspects of the qPCR experiments. There are many other people (too numerous to mention) at both UCL and GSK who kindly took time out from their busy schedules to demonstrate a particular technique, provided me with reagents or allowed me to use their equipment. I hope they all know how much I appreciate it.

Last, but certainly not least, I would like to thank my very good friends Sarah Fisher, Nick Hayes, David Hillman, Tom Taylor-Clark, and the Mei Chuan crew for listening to my woes and keeping me sane.

This thesis is dedicated to my family.

Publications

Papers

Benton DC, Monaghan AS, Hosseini R, Bahia PK, Haylett DG, Moss GW (2003) Small conductance Ca2+-activated K+ channels formed by the expression of rat SK1 and SK2 genes in HEK 293 cells. J Physiol 553: 13-19.

Monaghan AS, Benton DC, Bahia PK, Hosseini R, Shah YA, Haylett DG, Moss GW (2004) The SK3 subunit of small conductance Ca2+-activated K+ channels interacts with both SK1 and SK2 subunits in a heterologous expression system. J Biol Chem 279: 1003-1009.

Bahia PK, Suzuki R, Benton DC, Jowett AJ, Chen MX, Trezise DJ, Dickenson AH, Moss GW (2005) A functional role for small-conductance calcium-activated potassium channels in sensory pathways including nociceptive processes. J Neurosci 25: 3489-3498.

Abstracts

Benton, D. C., Monaghan, A. S., Hosseini, R., Bahia, P. K., Haylett, D. G., and Moss, G. W. Interactions between rat SK channel subunits expressed in HEK 293 cells. J.Physiol 551P, C43. 2003.

Contents

Page no.

Title page..... 1

Abstract..... 2

Acknowledgements..... 4

Publications..... 5

Contents..... 6

List of figures..... 15

List of tables..... 23

Abbreviations and acronyms..... 24

Chapter 1: Introduction..... 26

1.1 Potassium channels – a general introduction..... 26

1.1.1 Classification of potassium channels..... 28

1.1.2 Assembly and selectivity of potassium channels..... 29

1.2 Calcium-activated potassium channels (K_{Ca})..... 30

1.2.1 BK channels..... 30

1.2.2 IK channels..... 33

1.2.3 SK channels..... 34

1.2.3.1 Biophysical properties..... 34

1.2.3.2 Molecular structure of SK channels..... 34

1.2.3.3 SK channel pharmacology..... 35

1.2.3.4 Overview of the distribution and functions of SK channels..... 36

1.3 Neuronal afterhyperpolarisations (AHPs) and their relation to cloned SK channels..... 37

1.3.1 The fAHP..... 38

1.3.2 The mAHP..... 39

1.3.3 The sAHP..... 40

1.3.3.1 Pharmacology of sAHPs..... 40

1.3.3.2 Are SK channels involved in the sAHP or the underlying current (I_{sAHP})?..... 42

1.4 AHPs generated by means other than K_{Ca} channels..... 44

1.4.1 Other channels that contribute to mAHPs: KCNQs..... 44

1.4.2 K_{Na} channels..... 45

1.5 Sensory neurones..... 46

1.5.1 Properties of nodose ganglion neurones..... 46

1.5.2 Properties of DRG neurones..... 47

1.5.2.1 The separation of DRG neurones based on conduction velocities..... 48

1.5.2.2 Cell bodies of DRG neurones..... 49

1.5.2.3 Electrophysiological differences between A- and C-type cells..... 49

1.5.2.4 Possible roles for SK channels in DRG AHPs..... 50

1.5.3 Termination of DRG fibres in the spinal cord..... 51

1.5.4 Pain..... 53

1.6 Aims of experiments..... 54

Chapter 2: Methods..... 56

2.1 Cell culture methods..... 56

2.1.1 Cell lines..... 56

2.1.2 Primary culture of peripheral ganglion neurones..... 56

2.2 Immunofluorescent antibody staining..... 58

2.2.1 Immunocytochemistry..... 58

2.2.2 Immunohistochemistry..... 61

2.3 Methods for molecular biology and gene expression..... 62

2.3.1 SK channel constructs..... 62

2.3.2 Cloning of the rat IK channel.....63
2.3.2.1 PCR of the rat IK channel.....63
2.3.2.2 Sub-cloning the rat IK into a mammalian expression vector.....64
2.3.2.3 Minipreps of plasmid DNA.....65
2.3.2.4 Large scale production of plasmid DNA.....65
2.3.2.5 DNA sequencing.....66
2.3.3 Transfection of cell lines.....67
2.4 Methods for electrophysiology.....68
2.4.1 Cell preparations.....68
2.4.2 Solutions.....68
2.4.3 Pipettes.....68
2.4.3.1 Intracellular electrodes.....68
2.4.3.2 Patch pipettes.....69
2.4.4 Equipment used for electrophysiological studies.....69
2.4.5 Methods for recording AHPs.....71
2.4.6 Pulse protocols.....71
2.4.7 Data analysis.....71
2.4.7.1 AHP duration in DRG neurones.....71
2.4.7.2 Nodose cells, dose-response curve to UCL 2027.....75
2.4.8 Drugs and reagents.....76
2.5 Quantitative PCR (qPCR).....77
2.5.1 Primer and probe design for qPCR.....77
2.5.2 Controls for primers and probes.....80
2.5.2.1 Plasmid controls for SK1, SK2 and SK3.....80
2.5.2.2 Cloning of rat IK fragment.....80
2.5.2.3 Transiently transfected HEK 293 cells.....82
2.5.3 Tissue extraction.....82

2.5.4 RNA isolation..... 83

2.5.5 Checking RNA integrity..... 84

2.5.6 RNA quantitation..... 84

2.5.7 Reverse Transcription (RT) to produce cDNA..... 86

2.5.8 qPCR (TaqMan®)..... 88

Chapter 3: Characterisation of primary antibodies targeted to SK channels and the IK channel..... 92

3.1 Introduction..... 92

3.2 Results..... 94

3.2.1 Negative controls..... 94

3.2.2 rSK1 antibodies..... 97

3.2.3 rSK2 staining..... 102

3.2.4 rSK3 staining..... 102

3.2.5 Distribution of SK channel proteins in transfected HEK 293 cells..... 102

3.2.6 rIK staining..... 107

3.2.6.1 Cloning the rIK channel..... 107

3.2.6.2 Formation of functional rIK channels..... 110

3.2.6.3 Staining in rIK transfected cells..... 111

3.2.6 Antibodies to human SK/IK channel proteins..... 113

3.2.7 Co-expression of SK channels in HEK 293 cells..... 115

3.2.7.1 hSK1 and rSK3 co-expression..... 117

3.2.7.2 rSK1 and rSK3 co-expression..... 119

3.2.7.3 rSK1 and rSK2 co-expression..... 121

3.2.7.4 rSK2 and rSK3 co-expression..... 123

3.2.8 Positive controls; staining of neurones..... 124

3.3 Discussion..... 126

3.3.1 Antibody screening and cloning of the rat IK channel..... 126

3.3.2 hSK1 and rSK3 co-expression..... 128

3.3.3 rSK1 and rSK3 co-expression..... 130

3.3.4 rSK1 and rSK2 interactions..... 132

3.3.5 rSK2 and rSK3 interactions..... 135

Chapter 4: Characterisation of AHPs seen in DRG and nodose ganglion cells.... 139

4.1 Introduction..... 139

4.1.1 Choice of cell preparation..... 139

4.1.2 Age of cultures..... 141

4.1.3 Characterising cells in culture..... 142

4.1.3.1 Cell size..... 142

4.1.3.2 Action potential inflection..... 143

4.1.3.3 The hyperpolarisation-activated current (I_H)..... 143

4.2 Results from studies in DRG neurones..... 144

4.2.1 Identification of DRG cell types..... 144

4.2.1.1 DRG cell sizes..... 144

4.2.1.2 Presence of an action potential inflection..... 146

4.2.1.3 Presence of the hyperpolarisation-activated current (I_H)..... 146

4.2.1.4 Criteria used to identify A- and C-type neurones..... 149

4.2.2 Variety of AHPs in cultured DRG cells..... 149

4.2.2.1 AHP_{80}..... 151

4.2.2.2 AHP decay time constants..... 152

4.2.3 Pharmacology of DRG AHPs..... 157

4.2.3.1 mAHPs in neurones from p17 rats..... 158

Effects of UCL 1848..... 159

Effects of 200 μM Cd^{2+}..... 159

Effects of other K^+ channel blockers..... 160

4.2.3.2 mAHPs in cells from p40-45 rats.....163

Effects of blockers on the mAHP..... 164

Effects of the SK/IK channel enhancer, 1-EBIO.....164

4.2.3.3 sAHPs in DRG cells from p17 rats.....167

4.3 Results from nodose ganglion neurones..... 173

4.3.1 Characteristics of the sAHP..... 173

4.3.2 Effects of histamine on the sAHP.....175

4.3.3 Effects of bradykinin on the sAHP..... 177

4.3.4 Effects of UCL 1848 on nodose AHPs.....178

4.3.5 Effects of UCL 2027 on the sAHP..... 179

4.3.6 Antibody staining of nodose ganglion cells..... 181

4.4 Discussion.....183

4.4.1 Analysis of AHP kinetics..... 183

4.4.1.1 AHP_{80} values..... 183

4.4.1.2 AHPs fitted to a modified GHK equation..... 184

4.4.2 Pharmacology of AHPs.....185

4.4.2.1 Pharmacology of mAHPs in DRG cells from p17 rats..... 186

4.4.2.2 Pharmacology of mAHPs in DRG cells from adult rats.....187

4.4.2.3 Possible candidates for the channel underlying the mAHP in DRG cells..... 188

4.4.2.4 Pharmacology of the sAHP in DRG cells..... 189

4.4.3 Pharmacology of AHPs in nodose ganglion cells.....192

4.4.4 Staining for SK/IK channel proteins in nodose neurones.....193

Chapter 5: Developmental regulation of SK/IK channel gene expression in DRGs..... 196

5.1 Introduction..... 196

5.2 Results..... 197

5.2.1 SK/IK channel mRNA expression in DRG cells..... 197

5.2.1.1 Positive controls using plasmid DNA..... 197

5.2.1.2 SK/IK channel transcripts found in DRG and other tissues..... 199

Choice of tissues..... 199

Controls..... 199

Tissue results..... 200

5.2.2 Increases in mRNA levels of SK/IK channels in DRG and adrenal gland tissue..... 202

5.2.3 Reproducibility of qPCR results..... 204

5.2.4 SK/IK channel proteins detected in DRG cells..... 206

5.2.5 Quantification of the SK3 changes in DRG cells with age..... 210

5.3 Discussion..... 212

5.3.1 qPCR controls using different rat tissues..... 212

5.3.1.1 SK/IK mRNA levels in brain tissues..... 212

5.3.1.2 SK/IK mRNA levels in colon..... 213

5.3.1.3 SK/IK mRNA levels in adrenal gland..... 214

5.3.1.4 SK/IK mRNA levels in DRG tissue..... 214

5.3.1.5 Levels of SK channel splice variants..... 215

5.3.2 Age-dependent changes in mRNA levels..... 216

5.3.3 SK/IK channel proteins expressed in cultured DRG neurones..... 216

5.3.5 Possible mechanisms by which SK/IK channels are up-regulated..... 217

5.3.6 Possible functional significance of SK3 up-regulation..... 217

Chapter 6: SK/IK channel gene expression in rat spinal cord and putative role in sensory nerve terminals..... 219

6.1 Introduction..... 219

6.2 Results..... 221

6.2.1 Controls..... 221

6.2.2 SK/IK channel staining in the spinal cord..... 221

6.2.3 SK3 staining in the spinal cord..... 221

6.2.4 Staining for other calcium-activated potassium channels..... 227

6.2.5 Staining for SK1 and SK2 with higher antibody concentrations..... 229

6.2.5.1 rSK1 staining at high antibody concentrations..... 229

6.2.5.2 rSK2 staining at high antibody concentrations..... 229

6.2.6 *In vivo* recordings from adult rat spinal cord..... 232

6.2.6.1 Method for *in vivo* recordings..... 233

6.2.6.2 Data analysis..... 235

6.2.6.3 Effects of drugs that alter SK channel activity..... 238

UCL 1848..... 238

1- EBIO combined with UCL 1848..... 242

6.3 Discussion..... 245

6.3.1 Antibody staining for K_{Ca} channels in the rat spinal cord..... 245

6.3.1.1 rSK1 staining..... 245

6.3.1.2 rSK2 staining..... 246

6.3.1.3 IK and BK staining..... 246

6.3.1.4 SK3 staining..... 247

6.3.2 *In vivo* recording from the rat spinal cord..... 248

6.3.2.1 Increasing concentrations of UCL 1848 increase firing in spinal neurones... 249

6.3.2.2 Activation of SK channels by 1-EBIO is reversed by UCL 1848..... 250

Chapter 7: Discussion..... 252

7.1 SK channel subunits and their interactions..... 252

7.2 SK/IK channel expression in DRGs..... 254

7.2.1 Expression of SK/IK mRNA splice variants in DRGs..... 254

7.2.2 Developmental regulation of SK/IK channels..... 255

7.3 The diversity of AHPs in DRG and nodose ganglion neurones..... 256

7.3.1 Which channel(s) underlie the mAHPs in DRG neurones?.....256

7.3.2 Which channel(s) underlie the sAHPs in DRG and nodose neurones?..... 257

7.3.2 SK channels in DRG neuronal cell bodies..... 259

7.4 SK/IK expression in rat spinal cord and putative role in sensory nerve terminals.....260

7.5 Do SK channels make suitable targets for analgesic drug development?..... 261

Appendix 1. A summary of some of the basic properties of all p17 DRG cells recorded from using the perforated patch technique.....262

Appendix 2. A summary of the effects of different drugs used to try and identify the K^+ channels underlying the AHPs in DRG cells..... 265

Appendix 3. A summary of the different components underlying the AHPs in DRG cells.....265

References.....266

List of figures

Page no.

Figure 1.1 A schematic representation of the three main groups of potassium channel α subunits..... 27

Figure 1.2 BK channels are different from other K_{Ca} channels in that the α subunits have seven TMDs..... 32

Figure 1.3 A current clamp recording from a neurone illustrating the hyperpolarisation components seen following a single action potential..... 38

Figure 1.4 A schematic representation of a transverse section of the lumbar spinal cord with its laminellar organisation..... 52

Figure 2.1 Antibody epitopes shown within an alignment of the predicted amino acid sequences for rat and human SK and IK channels..... 60

Figure 2.2 A Clampfit trace of an AHP from a DRG cell..... 72

Figure 2.3 Example of an AHP trace fitted using a modified Goldman-Hodgkin-Katz equation..... 75

Figure 2.4 A schematic representation of TaqMan® primer annealing..... 77

Figure 2.5 Alignment of the C terminal region of eight mouse and two rat SK1 splice variants..... 79

Figure 2.6 An example of a typical electropherogram obtained from samples run on an RNA 6000 nanochip..... 85

Figure 2.7 A typical example of a standard curve generated using the RiboGreen assay..... 87

Figure 2.8 A typical TaqMan® trace..... 89

Figure 2.9 A graph comparing the SK2 cDNA copy numbers calculated using two different methods..... 91

Figure 3.1 Negative control experiments using anti-SK/IK antibodies and the CY3 secondary antibody..... 95

Figure 3.2 The four different anti-rSK1 antibodies do not produce specific staining in a HEK 293 cell line stably expressing hSK1..... 96

Figure 3.3 The YFP-tagged construct expresses when transiently transfected in HEK 293 cells and is recognised by anti-rSK1 antibodies 98

Figure 3.4 C-terminal anti-rSK1 antibodies produce positive staining in HEK 293 cells transiently transfected with the native rSK1 construct 100

Figure 3.5 Staining with N-terminal anti-rSK1 antibodies of HEK 293 cells transiently transfected with the native rSK1 construct..... 101

Figure 3.6 The anti-SK2 antibody (M1) produces positive staining in HEK 293 cells transfected with rSK2..... 103

Figure 3.7 Anti-SK3 antibodies recognise the channel protein in HEK 293 cells transiently transfected with the rSK3 construct..... 104

Figure 3.8 Intensity profiles show the differences in distribution of fluorescence seen for rSK1, rSK2 and rSK3 antibody staining..... 106

Figure 3.9 Nucleotide and predicted amino acid sequence of the rIK channel cloned from rat DRG cDNA as described in the Methods..... 108

Figure 3.10 A comparison of the predicted amino acid sequences of the rIK channel..... 109

Figure 3.11 The DRG rIK clone forms functional channels when expressed in HEK 293 cells..... 110

Figure 3.12 Staining seen with rat specific anti-IK channel antibodies, of HEK 293 cells transiently transfected with the rIK construct..... 112

Figure 3.13 Positive staining produced by the L155 anti-hSK1 antibody using a CHO cell line stably expressing hSK1..... 114

Figure 3.14 Staining of hIK CHO cells with antibodies targeted to the hIK channel protein..... 114

Figure 3.15 Different patterns of distribution seen for rat SK channels expressed alone in HEK 293 cells..... 116

Figure 3.16 The rSK3 protein assumes a more intracellular distribution when co-expressed with hSK1..... 118

Figure 3.17 A largely intracellular rSK3 staining pattern is seen when co-transfected with rSK1..... 120

Figure 3.18 rSK1 staining remains largely unchanged when co-transfected with rSK3..... 120

Figure 3.19 Distributions of YFP-tagged rSK1 and rSK2 in HEK 293 cells co-transfected with cDNAs for both proteins..... 122

Figure 3.20 rSK3 staining appears more intracellular in HEK 293 cells when co-transfected with rSK2, compared with rSK3 alone..... 123

Figure 3.21 SK3 positive staining seen with the M75 antibody in peripheral neurones in culture..... 125

Figure 3.22 SK3 and MAP2 staining co-localises in the same subcellular regions of SCG neurones..... 125

Figure 3.23 Co-expression of hSK1 with the TEA-sensitive rSK3 mutant rSK3VF does not alter TEA sensitivity of channels..... 129

Figure 3.24 Co-expression of rSK1 with rSK3VF does not alter the TEA sensitivity..... 131

Figure 3.25 Co-expression of rSK1 with rSK2 alters sensitivity to block by apamin..... 133

Figure 3.26 Co-expression of rSK1 with rSK2 alters sensitivity to block by UCL 1848..... 133

Figure 3.27 Co-expression of rSK2 and rSK3 alters sensitivity to block by UCL 1848..... 136

Figure 4.1 Isolated DRG cells after 1 day in culture showing the variety of cell sizes..... 144

Figure 4.2 Action potential shapes in two different types of DRG cell recorded from cultured neurones..... 147

Figure 4.3 The presence of an action potential inflection in different sized DRG neurones in culture..... 147

Figure 4.4 Response of two different cultured DRG cells to a hyperpolarising current pulse..... 148

Figure 4.5 The presence of a voltage sag in different sized DRG neurones in culture..... 148

Figure 4.6 Different kinetics of the AHPs recorded from DRG cells grown in culture..... 150

Figure 4.7 Range of AHP_{80} values for AHPs recorded from DRG cells..... 151

Figure 4.8 Typical examples of AHP fits using the modified Goldman-Hodgkin-Katz equation..... 154

Figure 4.9 A histogram of the range of decay time constants for AHPs in DRG cell bodies..... 155

Figure 4.10 Scatterplots of the range of decay time constants seen for AHPs recorded from DRG cell bodies..... 156

Figure 4.11 Variable sensitivity of the DRG mAHPs to UCL 1848..... 161

Figure 4.12 Variable Cd^{2+} sensitivity of mAHPs in DRG neurones..... 161

Figure 4.13 Examples illustrating the effect of different K^+ channel blockers on the mAHPs in DRG cells..... 162

Figure 4.14 Examples of mAHPs in DRG cells from p40-45 rats, illustrating the effects of different drugs..... 166

Figure 4.15 A recording from a C-type p17 DRG cell which had a sAHP..... 168

Figure 4.16 Pharmacology of a sAHP recorded from an A-type cell..... 170

Figure 4.17 An example of a small Cd^{2+}-sensitive sAHP in a C-type DRG cell seen in response to a single action potential..... 171

Figure 4.18 The pharmacology of a sAHP from a C-fibre type cell..... 172

Figure 4.19 Typical examples of voltage recordings from two different nodose ganglion cells cultured for 1-3 days..... 174

Figure 4.20 The size and the duration of the sAHPs seen in nodose ganglion neurones is dependent upon the number of action potentials fired..... 174

Figure 4.21 Block of the sAHP in a nodose ganglion neurone in response to 3 μM histamine..... 176

Figure 4.22 Effect of bradykinin (10 μM) on the sAHP seen in a nodose ganglion cell..... 177

Figure 4.23 The absence of effects of UCL 1848 on the nodose ganglion cell sAHP..... 178

Figure 4.24 The response of a nodose sAHP to a 20 μM concentration of UCL 2027..... 179

Figure 4.25 Inhibition of the nodose ganglion neurone sAHPs by UCL 2027..... 180

Figure 4.26 Staining of guinea pig nodose ganglion cells with anti-SK/IK channel antibodies..... 182

Figure 4.27 Sequence alignments of SK peptide sequences from different species in the epitope regions..... 195

Figure 5.1 Positive controls for qPCR results show that the probes selectively amplify the appropriate gene..... 198

Figure 5.2 Levels of SK/IK channel mRNA expressed in different tissues detected by qPCR..... 201

Figure 5.3 SK/IK channel mRNA expressed in adrenal gland and DRG tissues for three different age groups..... 203

Figure 5.4 The variability of the results for different animals should not affect the overall trend of an age-dependent increase in DRG mRNA levels..... 205

Figure 5.5 SK channel antibody staining in p7 DRG cells..... 207

Figure 5.6 SK channel antibody staining in p17 DRG cells..... 208

Figure 5.7 SK/IK antibody staining in p40-45 DRG cells..... 209

Figure 5.8 Age-dependent increase in SK3 staining in DRG cells..... 211

Figure 6.1 Secondary antibodies produce very low levels of background staining in rat spinal cord slices..... 222

Figure 6.2 Anti-SK1 and SK2 antibodies do not produce positive staining in rat spinal cord slices..... 223

Figure 6.3 SK3 antibody staining is seen in several regions of the spinal cord.....225

Figure 6.4 SK3 antibody staining in spinal cord and cultured DRG neurones is consistent with expression in both A- and C-type cells.....226

Figure 6.5 The IK channel antibody produces selective staining in the spinal cord...228

Figure 6.6 The BK channel antibody produces positive staining throughout the grey matter of the spinal cord..... 228

Figure 6.7 Staining of spinal sections with higher concentrations of the anti-SK1 antibodies..... 230

Figure 6.8 Positive staining of spinal neurones with higher concentrations of the anti-rSK2 antibody (M1).....231

Figure 6.9 A schematic representation of the principal connections between primary afferents and spinal neurones..... 232

Figure 6.10 A diagram illustrating the set-up for *in vivo* recording from anaesthetised adult rats..... 233

Figure 6.11 Data separation from a single lamina V neurone..... 234

Figure 6.12 Raw data from two different A_β neurones along with histograms generated using the Rantest program to calculate the significance of the differences in means of data generated pre- and post-drug application (in this case following the application of 10 nM UCL 1848).....236

Figure 6.13 UCL 1848 increases spinal cord input from electrically evoked stimuli recorded as the firing of a lamina V neurone.....239

Figure 6.14 UCL 1848 increases spinal input from most naturally evoked responses..... 241

Figure 6.15 1-EBIO and UCL 1848 have very little effect on responses evoked using heat and innocuous brush..... 243

Figure 6.16 1-EBIO dramatically reduces nociceptive mechanically induced responses and this effect is inhibited by the SK channel blocker UCL 1848..... 244

List of tables

Page no.

Table 2.1 Primary antibody concentrations used..... 59

Table 2.2 Fluorescent secondary antibodies used to detect primary antibody binding..... 59

Table 2.3 Sequences of TaqMan primers and probes used for qPCR..... 81

Table 3.1 A table of the antibodies designed to recognise either human or rat SK/IK channel proteins.....93

Table 4.1 Ranges of DRG cell sizes adopted to try and identify them as C- or A-type cells..... 145

Table 4.2 A summary of various blockers used to characterise the mAHP in both A- and C-fibre cells isolated from p17 rats.....163

Table 4.3 Characterisation of the mAHP in DRG cells isolated from p40-45 rats.....167

Table 4.4 A summary table of the responses to drugs used to characterise the sAHP in DRG cells isolated from p17 rats..... 169

Table 5.1 A table showing increases in levels of SK/IK channel mRNA in rat DRGs with age.....204

Table 5.2 The number of SK3 positive cells increase with age..... 212

Abbreviations and acronyms

1-EBIO	1-ethyl-2-benzimidazolinone
4-AP	4-aminopyridine
ABS	antibody blocking solution
ADP	afterdepolarisation
AHP	afterhyperpolarisation
AHP_{80}	time taken for 80 % recovery of the AHP from the peak relative to the resting membrane potential
BK channel	large conductance calcium-activated K^+ channel
BSA	bovine serum albumin
$[Ca^{2+}]_i$	intracellular calcium concentration
CaM	calmodulin
CaMBD	calmodulin binding domain
cDNA	complementary DNA
CHO	chinese hamster ovary cell line
ChTx	charybdotoxin
CICR	calcium-induced calcium release
C_t	cross threshold for quantitative PCR reaction
d-TC	d-tubocurarine
DHS-1	dehdrosoyasponin-1
DMEM	Dulbecco's modified Eagle's medium
DMSO	dimethyl sulphoxide
DRG	dorsal root ganglion
E_K	K^+ reversal potential
fAHP	fast afterhyperpolarisation
FAM	6-carboxyfluorescein
FCS	foetal calf serum
GFP	green fluorescent protein
GHK equation	Goldman-Hodgkin-Katz equation
HEK 293	human embryonic kidney cell line
HEPES	N-(2-hydroxyethyl) piperazine-N'-(2-ethanesulfonic acid)
HBSS	Hanks' balanced salt solution
IbTx	iberiotoxin

I_H	hyperpolarisation-activated current
I_M	M current
I_{mAHP}	current underlying the mAHP
I_{sAHP}	current underlying the sAHP
IK channel	intermediate conductance calcium-activated K^+ channel
K_{Ca}	calcium-activated K^+ channel
K_{ir}	inwardly rectifying K^+ channel
K_{Na}	sodium-activated K^+ channel
K_V	voltage-gated K^+ channel
LTP	long-term potentiation
mAHP	medium afterhyperpolarisation
MAP2	microtubule-associated protein 2
MEM	minimal essential medium
NGF	nerve growth factor
NMJ	neuromuscular junction
PB	phosphate buffer
PBS	phosphate buffered saline
PD	postdischarge
qPCR	quantitative PCR
RCK domain	regulator of K^+ conductance domain
sAHP	slow afterhyperpolarisation
SCG	superior cervical ganglion
SK channel	small conductance calcium-activated K^+ channel
TAMRA	6-carboxytetramethylrhodamine
TE	tris-EDTA
TEA	tetraethylammonium
T_m	primer melting temperature
TMD	transmembrane domains
TTX	tetrodotoxin
TRPV1	transient receptor potential channel of the vanilloid subfamily type 1
VDCC	voltage-dependent calcium channel
VR1	vanilloid receptor type 1
WDR neurones	wide dynamic range neurones
YFP	yellow fluorescent protein

Chapter 1

Introduction

Ion channels are protein pores found in the lipid membranes of all cells. Though sometimes active in resting cells, they usually open in response to a specific stimulus, for example, ligand binding, a change in membrane potential, or a rise in intracellular calcium, to allow the passive movement of charged particles (ions, such as Na^+, K^+, Ca^{2+} or Cl^-) into or out of a cell.

1.1 Potassium channels – a general introduction

Though this is not intended to be a thorough review of potassium (K^+) channels, I hope to introduce a number of their important properties, to provide an outline of the different types, their structures and to briefly describe some of the functions. K^+ conductances were first described and characterised by Hodgkin and Huxley in the giant squid axon (Hodgkin and Huxley, 1952). The underlying potassium channels are now known to be members of the largest and most diverse group of all ion channels. This diversity is primarily due to the large number of genes for the pore-forming (alpha) subunits, but also because many of these genes have alternative splice variants. Furthermore, the individual subunit proteins can come together as heteromers, associate with auxiliary proteins, or undergo post-translational modifications to produce an amazing variety of channels. Their functions range from the repolarisation of nerves following action potentials to the control of insulin release from pancreatic β cells. However, despite progress with patch-clamp technology and various cloning techniques, we do not fully understand all of their physiological roles.

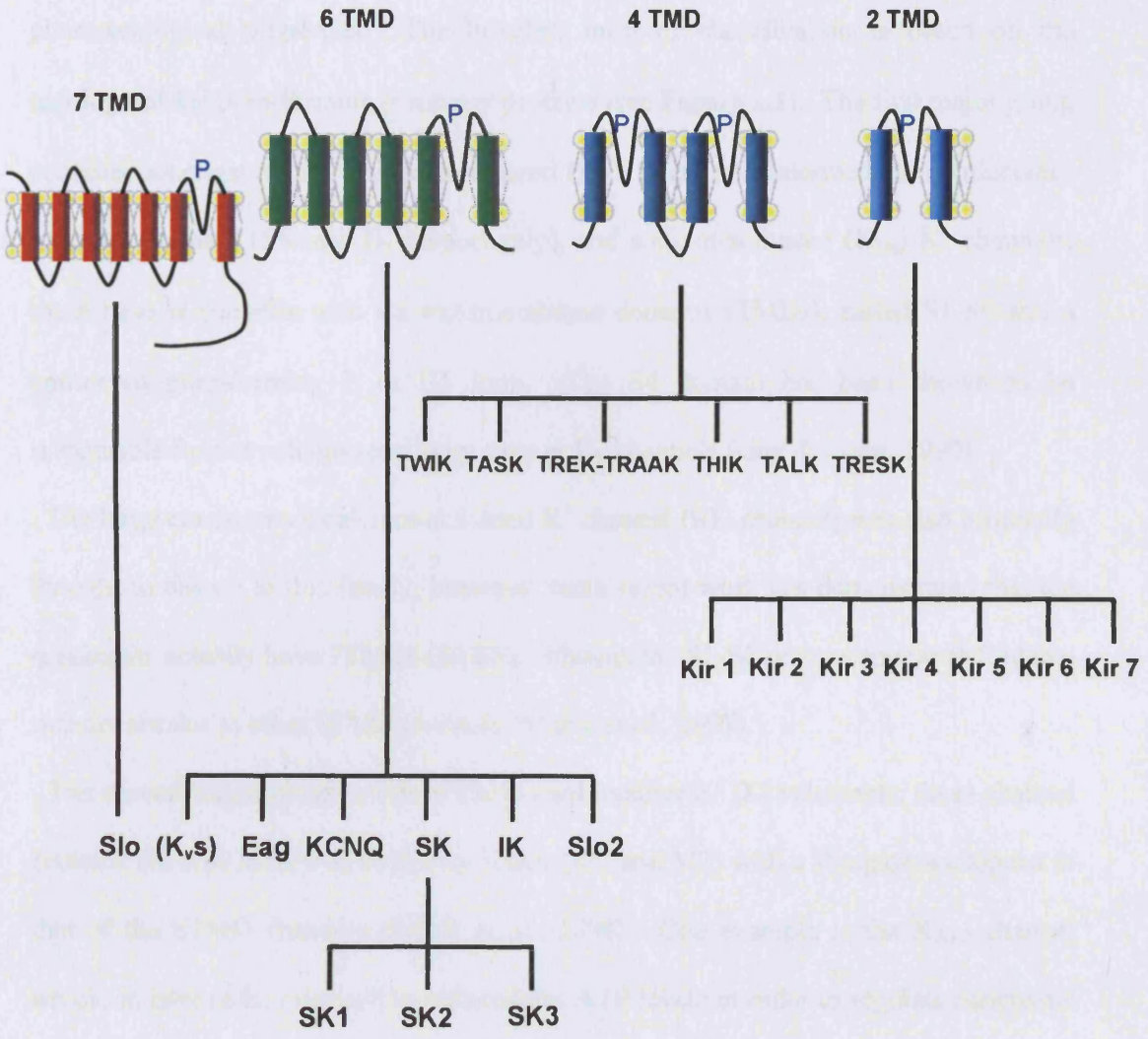

Figure 1.1. A schematic representation of the three main groups of potassium channel α subunits. They are separated on the basis of the number of membrane spanning domains. Each group of principal subunits is divided into families, most of which can, in turn, be further subdivided into a number of closely related members. In each illustration, "**P**" indicates the pore region.

1.1.1 Classification of potassium channels

Potassium channels are classified according to their structural, biophysical and pharmacological properties. The broadest form of classification is based on the topology of the pore-forming α subunit proteins (see **Figure 1.1**). The first major group contains, amongst others, the voltage-gated (K_V), small and intermediate conductance calcium-activated (SK and IK respectively), and sodium-activated (K_{Na}) K^+ channels; these have α subunits with six transmembrane domains (TMDs), called S1-S6 and a conserved pore-forming P or H5 loop. The S4 domain has been shown to be responsible for the voltage-sensitivity seen in K_V channels (Guy & Conti, 1990).

The large conductance calcium-activated K^+ channel (BK channel) was also originally thought to belong to this family, however, more recent work has demonstrated that the α-subunits actually have 7TMDs (S0-S6), although the S1-S6 regions appear to fold in a manner similar to other 6TMD channels (Meera *et al.*, 1997).

The second major group is that of the inward rectifier K^+ (K_{ir}) channels; these channel proteins are now known to have two TMDs (M1 and M2) with a P region analogous to that of the 6TMD channels (Doyle *et al.*, 1998). One example is the K_{ATP} channel which, in islet cells, responds to intracellular ATP levels in order to regulate pancreatic insulin release.

The final group of K^+ channel pore-forming subunit proteins are those that make up the "leak" or "two-pore" channels; these have 4 TMDs (M1-M4) and two pore (P) loops distinguishing them from the other groups. "Leak" channels are non-inactivating and are open at all membrane potentials (Lesage and Lazdunski, 2000).

1.1.2 Assembly and selectivity of potassium channels

Potassium channels (unlike their close relatives the voltage-gated Na^+ and Ca^{2+} channels) consist of several separate channel α subunits that come together to form a central pore region allowing the selective passage of K^+ ions. Several groups provided the initial evidence that K^+ channels are heteromers made up of several α subunits (MacKinnon *et al.*, 1988; Isacoff *et al.*, 1990; Ruppersberg *et al.*, 1990). However, definitive evidence for a tetrameric structure of K^+ channels has recently come from impressive work on the crystallisation and x-ray analysis of bacterial K^+ channels (Doyle *et al.*, 1998; Jiang *et al.*, 2002, Jiang *et al.*, 2003). In this respect the two-pore channel family differs from the others in that the 4TMD proteins come together to form dimers (Lesage & Lazdunski, 2000). However, by doing this they retain the four-fold symmetry of the channel. One common feature of the great majority of K^+ channels is that the pore sequence contains a GYG (gly-tyr-gly) motif, which conveys selectivity of the pore to K^+ ions (Heginbotham *et al.*, 1994), although there are also K^+ channels e.g. certain inward rectifiers with a GFG (gly-phe-gly) motif (Reimann & Ashcroft, 1999).

The fact that K^+ channels comprise several individual channel proteins allows for the possibility of heteromerisation and indeed this has been shown to occur with several members of the K^+ channel family; for example, different K_V channel α subunits can come together to form heteromultimers that are functionally different from the homomultimers formed from either set of subunits (Isacoff *et al.*, 1990; Ruppersberg *et al.*, 1990; Christie *et al.*, 1990). In some instances, different protein subunits may need to associate in order to reach the cell surface (Zhu *et al.*, 2003).

This thesis is concerned specifically with calcium-activated K^+ (K_{Ca}) channels, so in the following sections these are described in more detail.

1.2 Calcium-activated potassium channels (K_{Ca})

The first indications of the existence of K_{Ca} channels came from studies in red blood cells, which showed that increases in intracellular calcium ($[Ca^{2+}]_i$) led to an increase in potassium permeability (Gardos, 1958). The first recordings of a K^+-selective ionic current activated by a rise in $[Ca^{2+}]_i$ were made by Meech & Strümwasser (1970) from *Aplysia* neurones. Since this early work, much has been done to characterise K_{Ca} channels which fall into three subfamilies based on their biophysical and pharmacological properties: large conductance (BK), intermediate conductance (IK) and small conductance (SK) K_{Ca} channels. Functional studies, along with the completion of the human genome project, have identified five genes in the human body which code for the alpha pore-forming subunits of calcium-activated potassium channels. These are; KCNMA1, which codes for the α subunit of the BK channel; KCNN1, KCNN2, KCNN3 and KCNN4, which code for the α subunits of SK1, SK2, SK3 and IK channels respectively.

1.2.1 BK channels

BK or maxiK channels were first described in chromaffin cell membranes (Marty, 1981) and cultured rat skeletal muscle (Pallotta *et al.*, 1981). They are highly potassium selective with single channel conductances > 100 pS in symmetrical K^+ (Sah, 1996). These channels rapidly respond by opening upon application of Ca^{2+} to the cytosolic face and promptly close upon its removal. As well as requiring calcium for activation, BK channels are also strongly voltage sensitive. At depolarised membrane potentials (from + 20 mV to + 40 mV) the concentration of Ca^{2+} required to activate 50% of BK channels lies in the high nanomolar range (several hundred), while at resting membrane potentials this value is several micromolar (Barrett *et al.*, 1982). BK channel activation

is also altered by association with some of the β subunits that have been described (McManus *et al.*, 1995; Dworetzky *et al.*, 1996). The dependence of BK channels on Ca^{2+} and membrane potential is an important determinant of their role as a feedback mechanism to regulate voltage-dependent Ca^{2+} channels (VDCCs; Vergara *et al.*, 1998).

A number of compounds are known to block BK channels including tetraethylammonium (TEA), which acts at submillimolar concentrations (Blatz & Magleby, 1987), also charybdotoxin (ChTx) and iberiotoxin (IbTx), which are two scorpion toxins (Galvez *et al.*, 1990). Other blockers include paxilline and penitrem A (Sah & Faber, 2002). Of these compounds, IbTx and paxilline are the most selective for BK channels. In addition, dehydrosoyasponin-1 (DHS-1) has been shown to act as a selective BK channel opener (Sah & Faber, 2002).

The α pore-forming subunit of all BK channels is the product of a single gene, first cloned from *Drosophila*, which was named "Slowpoke" (Slo; Atkinson *et al.*, 1991; Adelman *et al.*, 1992). The resulting protein has a high degree of homology with K_V channels, particularly in the S4 TMD, which forms part of the voltage sensor (Larrson *et al.*, 1996). The BK channel is, however, quite different structurally in that it has seven TMDs (Meera *et al.*, 1997; see also **Figure 1.2**) and a large intracellular C-terminal tail that probably confers its Ca^{2+}-sensitivity (Schreiber & Salkoff, 1997). The C-terminal region has two RCK (or regulator of K^+ conductance) domains, and a region with a large number of negatively charged aspartic acid residues which has been termed the "calcium bowl" (Schreiber & Salkoff, 1997; Jiang *et al.*, 2001; 2002). Despite there being just one gene for the principal BK channel subunit, there is a great deal of functional diversity generated via alternative splicing, phosphorylation of the α subunit and assembly with β subunits (Sah & Faber, 2002). Thus native channels comprise either four α subunits that come together to form a tetramer, (Adelman *et al.*, 1992;

Shen *et al.*, 1994) or they may co-assemble with β subunits (Garcia-Calvo *et al.*, 1994; McManus *et al.*, 1995).

These β subunits have two putative TMDs and a large extracellular loop. Three different subunits, β1, β2/3 and β4, have been cloned (Dworetzky *et al.*, 1996; Knaus *et al.*, 1994; Tseng-Crank *et al.*, 1996; Brenner *et al.*, 2000; Meera *et al.*, 2000). When expressed with α subunits, β subunits have been shown to shift the voltage sensitivity of BK channels to potentials that are more negative, thereby increasing Ca^{2+} sensitivity, and to confer properties such as rapid inactivation (β2/3) and the insensitivity of BK channels to ChTx and IbTx (β4; Sah & Faber, 2002).

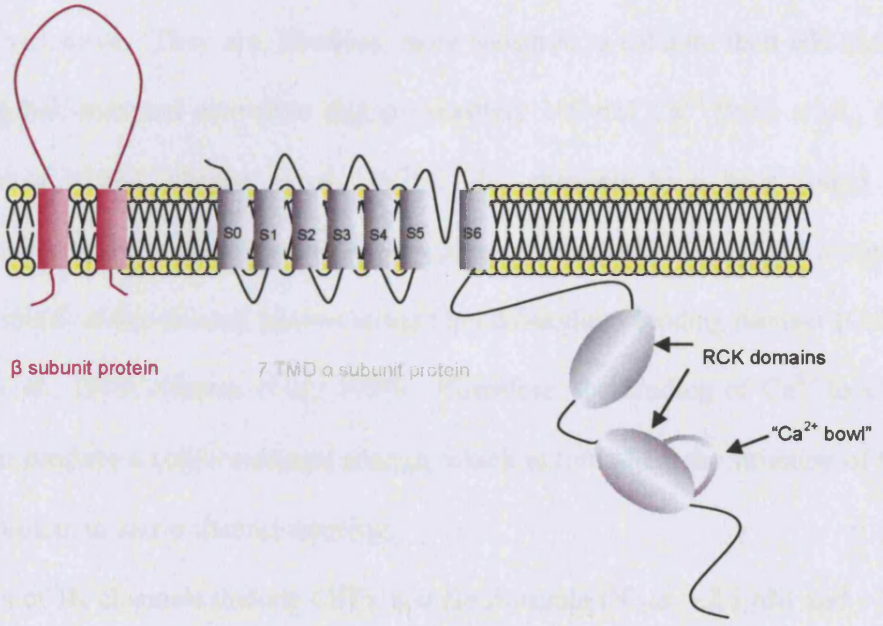

Figure 1.2 BK channels are different from other K_{Ca} channels in that the α subunits have seven TMDs. The large C terminus with two RCK domains and a "calcium bowl" region has been implicated in channel gating. BKs are also known to associate with β subunit proteins that alter their pharmacological and electrophysiological properties. On the basis of hydropathy analysis, the β subunits are believed to have two membrane-spanning domains (Knaus *et al.*, 1994; Brenner *et al.*, 2000).

1.2.2 IK channels

The first IK channel to be described was the Gardos channel seen in erythrocytes. The cloned KCNN4 gene gave rise to proteins that formed a channel which fell into the IK category, hence these channels were called IK1 (Ishii *et al.*, 1997a), though their close similarity to SK channels has also led to them being termed SK4 (Joiner *et al.*, 1997). IK channels have been cloned from a variety of tissues including the pancreas (Ishii *et al.*, 1997a), T lymphocytes (Lodgson *et al.*, 1997), placenta (Joiner *et al.*, 1997; Jensen *et al.*, 1998) and vascular smooth muscle (Neylon *et al.*, 1999).

Cloned IK channels, expressed in *Xenopus* oocytes have single channel conductances in the range of 20-80 pS (Ishii *et al.*, 1997a). IK channels are inward rectifiers and are voltage insensitive. They are, however, more sensitive to calcium than BK channels, achieving half-maximal activation at approximately 100 nM Ca^{2+} (Ishii *et al.*, 1997a; Joiner *et al.*, 1997; Neylon *et al.*, 1999). IK channels have been found to be constitutively bound to the calcium-binding protein calmodulin (CaM) via a region of the C-terminal of the channel protein termed the calmodulin binding domain (CaMBD; Fanger *et al.*, 1999; Khanna *et al.*, 1999). Therefore, the binding of Ca^{2+} to CaM is thought to produce a conformational change, which in turn alters the structure of the IK channel protein to cause channel opening.

Blockers of IK channels include ChTx and clotrimazole (IC_{50}s: ~2.5 nM and ~25 nM respectively; Ishii *et al.*, 1997a). Their activity can also be enhanced by the compound 1-ethyl-2-benzimidazolinone (1-EBIO) with an EC_{50} of ~74 μM (Devor *et al.*, 1996; Jensen *et al.*, 1998).

IK expression and function has been extensively studied in many non-excitable tissues. Although work by Greffrath *et al.* (1998) suggests that IK channels are involved in AHP

generation in the magnocellular neurones of the rat supraoptic nucleus, there is very little evidence to support a role for IKs in the majority of neuronal tissues.

1.2.3 SK channels

1.2.3.1 Biophysical properties

SK channels are so-called because of their small single channel conductances (2-20 pS) particularly when compared to BK channels (Romey & Lazdunski, 1984; Blatz & Magleby, 1986). As with all K_{Ca} channels, they are activated by a rise in $[Ca^{2+}]_i$ and, for the SK channels, maximal activation is seen at 400-800 nM (Blatz & Magleby, 1986; Park *et al.*, 1994). Like IK channels, SK channels show some inward rectification, are voltage insensitive and Ca^{2+} activation occurs via the constitutively bound CaM protein (Sah & Davies, 2000; Faber & Sah, 2003). Of the two Ca^{2+} binding sites available on the CaM protein, only one need be occupied for channel gating (Xia *et al.*, 1998; Keen *et al.*, 1999). So presumably, given the proposed tetrameric structure of the channels, four or more Ca^{2+} ions are needed for channel opening.

These channels were first characterised in skeletal muscle (Romey & Lazdunski, 1984) but have since been shown to be widely expressed in excitable and inexcitable tissues (Köhler *et al.*, 1996; Stocker & Pederzani, 2000; Barfod *et al.*, 2001; Ro *et al.*, 2001; Rhodes *et al.*, 2003).

1.2.3.2 Molecular structure of SK channels

The cloning of the SK channels revealed three distinct genes: SK1, SK2 and SK3 (Köhler et al., 1996) also known as KCNN1, KCNN2 and KCNN33. They belong to the six TMD family of potassium channels and have highly similar sequences, particularly in the regions of the transmembrane domains. However, whilst SK

channels show 80-90% sequence identity, the only significant similarity with other members of the 6TMD K_V channel family is seen in the pore region (Köhler et al., 1996). The closest relative of the SK channels, IK/SK4 channels, show ~40% sequence identity (Joiner *et al.*, 1997). Interestingly, whilst rat clones of SK2 (rSK2) and SK3 (rSK3) produce functional channels in mammalian cell lines, rSK1 fails to produce detectable current; therefore, the majority of SK1 studies to date have been performed on the human isoform hSK1, that can form functional channels.

As with other 6TMD K^+ channels, the SK pore-forming subunits are believed to come together to form a tetrameric structure. There is also recent evidence, some of which is presented in this thesis, to suggest that SK subunits may form homo- and heterotetramers (Ishii *et al.*, 1997b; Benton *et al.*, 2003; Monaghan *et al.*, 2004). In addition to the cloned pore-forming subunits, certain studies also suggest the existence of accessory subunits. Wadsworth and colleagues found that radiolabelled apamin (^{125}I-apamin), and photolabelled derivatives, bind to a ~30 kDa protein in a number of tissues (Wadsworth *et al.*, 1994; 1996; 1997), which raises the possibility of a putative regulatory β subunit for SK channels. However, the exact identity and role of this protein remains to be determined.

1.2.3.3 SK channel pharmacology

SK channels are unaffected by low concentrations of TEA, ChTx or IbTx. They are, however, potently blocked by the bee venom toxin apamin (Banks *et al.*, 1979; Romey & Lazdunski, 1984; Blatz & Magleby, 1986) with the IC_{50}s of expressed channels ranging from ~100 pM for rSK2 to low nanomolar concentrations for hSK1 (Shah & Haylett, 2000a; Strobæk *et al.*, 2000; however see also section 1.3.2). More recently, it has been shown that scyllatoxin and tamapin, two scorpion toxins, are also capable of

blocking SK channels (Strobæk *et al.*, 2000; Pederzani *et al.*, 2002) and these, like apamin, display selectivity for SK2 over SK3, which in turn is more sensitive than SK1. Other blockers include d-tubocurarine (d-TC; Jenkinson *et al.*, 1983), bicuculline (Johnson & Seutin, 1997; Seutin & Johnson, 1999) and a number of synthetic dequalinium analogues including the potent and selective blocker UCL 1848 (Campos Rosa *et al.*, 2000; Chen *et al.*, 2000). Experiments with UCL 1848 and apamin show that the concentrations required to block cloned channels are comparable to those needed to block native channels (Hosseini *et al.*, 2001).

As with IK channels, SK channels can be activated by 1-EBIO, which alters Ca^{2+} sensitivity, and thus the open probability of SK channels in the presence of Ca^{2+} (Oleson *et al.*, 1994; Syme *et al.*, 2000; Pedarzani *et al.*, 2001). It is thought that 1-EBIO increases Ca^{2+} sensitivity by stabilising the association of Ca^{2+}-CaM with the CaMBD (Pederzani *et al.*, 2001).

1.2.3.4 Overview of the distribution and functions of SK channels

SK channels are distributed in a number of different tissues including T-lymphocytes (Grissmer *et al.*, 1992), hepatocytes (Ogden *et al.*, 1990) epithelial cells (Wiener *et al.*, 1990; Pácha *et al.*, 1992) and throughout the central nervous system (CNS; Köhler *et al.*, 1996; Stocker & Pederzani, 2000). Accordingly they have a variety of functions. In gastrointestinal smooth muscle, for example, they are involved in muscle relaxation (Banks *et al.*, 1979; Ro *et al.*, 2001). Adrenal chromaffin cells have also been shown to express functional SK channels, which most likely provide part of a negative feedback mechanism for catecholamine release (Neely and Lingle, 1992; Park, 1994). These are just some of the known functions for SK channels.

As has already been stated, K^+ channels play a vital role in neurones. One well-documented way in which K^+ channels regulate neural activity is via the neuronal afterhyperpolarisation (AHP), which occurs following either a single action potential or a train in many types of nerve cell. The most widely studied mechanism is dependent on raised levels of intracellular Ca^{2+}. Since the only other calcium-activated potassium channel genes to be identified, are the BK and IK channel genes, SK channel would appear to provide the obvious candidates for the molecular counterparts of AHP channels. As this thesis centres on possible roles for SK/IK channels in sensory neurones, they are discussed in the following section within the context of the neuronal AHP. (Note, however, that there are a number of different potassium channels that can share this function as discussed in section 1.4).

1.3 Neuronal afterhyperpolarisations (AHPs) and their relation to cloned SK channels

Neuronal firing rates are regulated in various ways in order to modulate the transmission of information along nervous pathways. In general, AHPs are generated by an efflux of potassium through channels that open following action potential discharge. By making the cell membrane more negative than it would be at rest, AHPs reduce cell excitability.

At least three temporally distinct components of AHPs have been identified (see **Figure 1.3**), each of which acts to regulate action potential firing. These are the fast AHP (fAHP), the medium AHP (mAHP) and slow AHP (sAHP) components. Each of these components is discussed below.

1.3.1 The fAHP

The fast afterhyperpolarisation (fAHP) can be seen immediately following an action potential and lasts for 1-10 ms. The channels underlying the fAHP are those involved in action potential repolarisation, i.e. voltage-gated K^+ channels and BK channels (reviewed by Sah, 1996). The fAHP can be followed by a more prolonged AHP which peaks relatively rapidly (< 10 ms) and lasts between fifty and several hundred milliseconds.

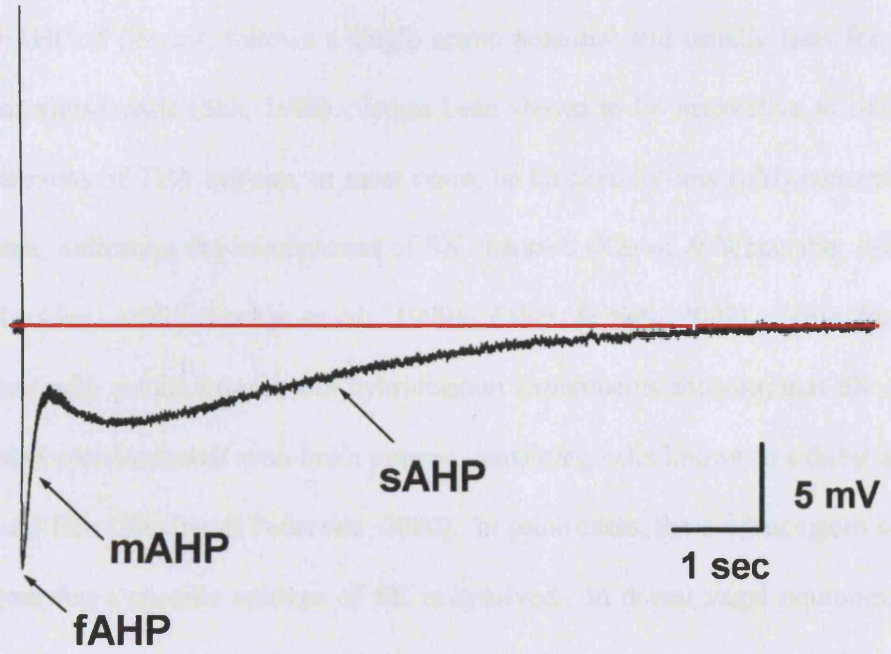

Figure 1.3 A current clamp recording from a neurone illustrating the afterhyperpolarisation (AHP) components seen following a single action potential. The fAHP has a duration of a few milliseconds (however, it is difficult to see a separate component on this timescale). The mAHP is more prolonged and lasts for several hundreds of milliseconds. The sAHP is usually only seen after a train of action potentials and has been shown in some cases to last for more than 10 s. The current example shows an exceptional cell where the sAHP was evident following just a single action potential. The red line represents the level of the resting membrane potential (-69 mV). This recording was made from a 17-day old rat DRG cell.

While in superior cervical ganglion (SCG) cells this is often termed the "slow" component, here it will be referred to as the medium AHP (mAHP). This is because certain cell types, for example hippocampal neurones, also exhibit a third type of AHP which is usually only seen after a train of action potentials. This third component has a slow rise time to peak and lasts several seconds and will be referred to in this thesis as the slow AHP (sAHP).

1.3.2 The mAHP

The mAHP, if present, follows a single action potential and usually lasts for several hundred milliseconds (Sah, 1996). It has been shown to be insensitive to millimolar concentrations of TEA but can, in most cases, be blocked by low (nM) concentrations of apamin, indicating the involvement of SK channels (Kawai & Watanabe, 1986; Sah & McLachlan, 1991; Stocker *et al.*, 1999a; Faber & Sah, 2002). This finding is consistent with results from *in situ* hybridisation experiments showing that SK channel expression correlates well with brain regions containing cells known to exhibit apamin-sensitive AHPs (Stocker & Pederzani, 2000). In some cases, the evidence goes so far as to suggest that a specific subtype of SK is involved. In dorsal vagal neurones, SCGs and dopaminergic neurones, SK3 is believed to be the major contributor to the apamin-sensitive AHP (Pederzani *et al.*, 2000; Hosseini *et al.*, 2001; Wolfart *et al.*, 2001), while in Purkinje fibre cells and interneurones in the hippocampal CA3 region, SK2 channel opening is thought to dominate (Savic *et al.*, 2001; Cingolani *et al.*, 2002). In many of these neurones the mAHP is believed to regulate the firing frequency (Pederzani *et al.*, 2001; Savic *et al.*, 2001; Wolfart *et al.*, 2001).

1.3.3 The sAHP

The sAHP is also thought to arise from a calcium-activated potassium current, but one that is quite distinct from that underlying the mAHP. In most cases the sAHP is only seen after a train of action potentials, has a slower rising phase and can last several seconds. Furthermore, in the majority of neurones it is insensitive to apamin at concentrations of up to 100 nM (Lancaster and Nicoll, 1987). Although it is known that the current underlying the sAHP (I_{sAHP}) is a potassium current, activated either directly or indirectly by the rise in intracellular calcium associated with the opening of calcium channels during action potential firing, the identity of the channel in question remains controversial. The single channel conductance has been estimated by noise analysis as 6.8 pS for channels in vagal motorneurones (Sah, 1995). Attempts to make more direct (single channel) measurements in myenteric neurones have put the value for the conductance at 9–15 pS (Vogalis *et al.*, 2001), but similar experiments in hippocampal neurones failed (Bekkers, 2000).

The sAHP builds up as action potentials are fired causing spike frequency adaptation i.e. the sAHP adapts neuronal firing rates in response to a constant stimulus.

1.3.3.1 Pharmacology of sAHPs

Despite the absence of selective blockers of the sAHP, a number of different drugs have been used in attempts to characterise the sAHP. Many cell types such as hippocampal pyramidal neurones (Lancaster & Nicoll, 1987), vagal motorneurones (Sah & McLachlan, 1991) and nodose ganglion neurones (Cordoba-Rodriguez *et al.*, 1999) have a sAHP that cannot be blocked even by high concentrations of apamin, but can be regulated by neurotransmitters such as noradrenaline, histamine and acetylcholine. The sAHPs seen in different cell types are diverse with respect to their sensitivities to

different drugs. For example, the sAHP in hippocampal cells seems to have a single component. However, the sAHP seen in neurones from the coeliac ganglion has a more complex pharmacology as it can be partially blocked by 20 nM IbTx and 100 nM apamin, but it also has a component insensitive to either of these toxins (Martinez-Pinna *et al.*, 2000). The differing sensitivities of sAHPs to the actions of different channel blockers suggests that several K_{Ca} channels may mediate the sAHP in some neurones.

sAHPs are characteristically inhibited by blockers of high threshold voltage-dependent Ca^{2+} channels (VDCCs), for example Co^{2+} and Cd^{2+} (Kubota *et al.*, 1984; Griffith, 1988). Interestingly, the use of more specific blockers, for example ω-conotoxin which targets N-type Ca^{2+} channels (Varadi *et al.*, 1995) and dihydropyridines, such as nifedipine, which is specific for L-type Ca^{2+} channels (Varadi *et al.*, 1995; Catterall & Striessnig, 1992), demonstrate that different subtypes of VDCC are involved in the sAHPs seen in different cell types (Shah & Haylett, 2000b). In some cases, there are suggestions that more than one type of channel may be important (Shah & Haylett, 2000b). Furthermore, drugs like ryanodine that deplete intracellular stores of Ca^{2+} can also inhibit sAHPs in certain neurones, supporting a role for CICR (Moore *et al.*, 1998; Cordoba-Rodriguez et al., 1999; Shah & Haylett, 2000b).

One recently described compound, UCL 2027 developed by C.R.Ganellin and his colleagues of the Department of Chemistry at UCL, has been shown to block the sAHP in cultured hippocampal cells without affecting the mAHP (Shah *et al.*, 2001). UCL 2027 was believed to act on the channels underlying the sAHP and it was thus suggested that it may present a means to identify this channel.

1.3.3.2 Are SK channels involved in the sAHP or the underlying current (I_{sAHP})?

When this thesis work was started it had long been suggested that an apamin-insensitive SK channel underlies the neuronal sAHP. Work by Köhler and colleagues (1996) seemed to provide an ideal candidate in the SK1 channel, which when expressed in *Xenopus laevis* oocytes, was insensitive to relatively high concentrations of apamin (100 nM). This fact, along with the detected single channel conductance of hSK1 (9.2 pS; Köhler *et al.*, 1996) and immunofluorescent staining experiments that appeared to show the presence of SK1 channels in rat hippocampal pyramidal neurones (Bowden *et al.*, 2001), led to the suggestion that SK1 channels may be responsible for the I_{sAHP}.

Subsequent experiments cast doubt on this theory as work in oocytes produced conflicting results. Grunnet and colleagues (2001) showed that all SK subtypes displayed some sensitivity to apamin. However, a much higher concentration of apamin was required to block SK1 and the dose-response curve was biphasic. In addition, when hSK1 was transiently transfected into HEK 293 cells and COS-7 cells (two mammalian cell lines), the SK current in most of these cells could be blocked by apamin concentrations in the low nanomolar range (Shah and Haylett, 2000a; Strobæk *et al.*, 2000). This finding is, however, further complicated by the fact that a small proportion of HEK 293 cells expressing hSK1 had currents that were only partially sensitive to apamin (Shah and Haylett, 2001a). In the hands of Dale and colleagues (2001), hSK1 and hSK2 when expressed in CHO cells, appear to exhibit only partial sensitivity to apamin. Therefore, in both oocytes and mammalian cells, it appears that SK channel subunits can form both apamin-sensitive and apamin-insensitive potassium channels.

As a recent review highlights (Vogalis *et al.*, 2003), there are several other problems with attempting to implicate a particular SK channel in sAHP generation. These include uncertainty about the timecourse of $[Ca^{2+}]_i$ changes and the time for the sAHP

to peak and decay; these may be explained by a need for highly localised increases in $[Ca^{2+}]$ that may not be reflected in bulk changes throughout the cell. (Hanani & Lasser-Ross, 1997, Lasser-Ross *et al.*, 1997, Hillsley *et al.*, 2000). Another problem is the ability of neurotransmitters such as noradrenaline to cause a profound reduction in the amplitude of the sAHP, putatively via phosphorylation of the underlying channel. Yet despite the presence of phosphorylation consensus sequences (Köhler *et al.*, 1996), there is no evidence to suggest that expressed SK channels are regulated by any such means. One explanation for the very different pharmacologies of SK channels and the sAHP channel is the possibility that the latter associates with a putative β subunit, making it insensitive to blockers such as apamin. An analogous case is the BK channel where certain β subunits confer insensitivity to charybdotoxin (Meera *et al.*, 2000). However, again there are no obvious candidates for such auxiliary proteins associating with SK channels.

More recent work on the rSK1 channel, some of which is presented in this thesis, indicates that rSK1 acts as a "silent subunit" and is therefore unlikely to be involved in generating the sAHP (Benton *et al.*, 2003; D'hoedt *et al.*, 2004). Furthermore, work by Bond *et al.* (2004), using SK knock-out mice, and Villalobos *et al* (2004), using a dominant negative strategy, shows that SK channels are not necessary for the I_{sAHP}, which is thought to be responsible for spike-frequency adaptation. So despite extensive work in the area, we are still no closer to finding out the identity of the channel involved in the sAHP.

1.4 AHPs generated by means other than K_{Ca} channels

As already discussed, there is substantial evidence to support the idea that K_{Ca} channels underlie the AHPs many in excitable cells. In one of the examples already discussed the pharmacology of the "medium" AHP in SCG neurones for example, provides a strong case for it being an exclusively SK-generated AHP (Kawai & Watanabe, 1986; Dunn, 1994; Hosseini *et al.*, 2001). However, in other cell types, there is work to suggest that SK channels only form one component of the AHP and that other K^+ channels also contribute.

1.4.1 Other channels that contribute to mAHPs: KCNQs

Initial experiments looking at the medium duration AHP in hippocampal pyramidal cells had suggested that the underlying current (I_{mAHP}) was due largely to a Ca^{2+}-independent K^+ channel. It was later realised that bicuculline, used as the quaternary salt to prevent spontaneous inhibitory activity in these cells, had the additional effect of blocking any SK channels present. While it is now known that SKs do contribute to the I_{mAHP} in these cells, the fact remains that there is a component resistant to Ca^{2+} channel block mediating this current.

The channel in question is thought to belong to the family of KCNQ K^+ channels, which fall into the voltage-gated 6TMD group. They are characteristically slowly activating and slowly deactivating channels that do not inactivate. Furthermore, the current generated, first described by Halliwell & Adams (1982), is sensitive to block by muscarinic agonists, which has led to it being termed the M-current (I_M).

A role for the I_M has been described in hippocampal pyramidal cells (Storm, 1989; Dutar & Nicoll, 1989) and in pyramidal neurones of the basolateral amygdala (Womble & Moises, 1993). This is based on the sensitivity of the current and the corresponding

AHP to carbachol and prevention of block by the muscarinic antagonist atropine (Storm, 1989; Womble & Moises, 1993). More direct evidence for KCNQ involvement in neuronal firing has now been provided using the specific blockers linopirdine and XE991 (Aiken *et al.*, 1995; Wang *et al.*, 1998).

1.4.2 K_{Na} channels

K_{Na} channels form yet another family belonging to the group of voltage-gated K^+ channels. Two genes have recently been cloned that correspond to the molecular counterparts of K_{Na} channels, Slo2.1 (Slick; Bhattacharjee *et al.*, 2003) and Slo2.2 (Slack; Joiner et al., 1998; Yuan *et al.*, 2003). These genes encode channels that have large single channel conductances (comparable to BK and K_{ATP} channels) whose opening is dependent upon rises in intracellular Na^+ and Cl^- (Bhattacharjee *et al.*, 2003; Yuan *et al.*, 2003). The K_{Na} channels first described in inside-out patches from guinea pig ventricular myocytes (Kameyama *et al.*, 1983) seem to have a defined protective role in cases of ischaemia or other metabolic stress (Dryer, 1994) and while this may also hold true in neurones, several other functions have also been suggested. One of these is that they may generate a prolonged AHP in response to repetitive firing (Schwindt *et al.*, 1989; Dryer, 1994, Safronov & Vogel, 1996, Franceschetti, *et al.*, 2003). Whether K_{Na} channels play a major role in regulating neuronal excitability is uncertain because the Na^+ influx through voltage-gated channels during action potential firing might not be sufficient to activate them (Dryer, 1994; 2003). However, certain circumstances may allow this; firstly, dendritic processes and axonal nodes may provide a sufficiently confined space for Na^+ to accumulate to levels high enough to activate local K_{Na} channels, particularly during a train of action potentials (Koh *et al.*, 1994; Safronov & Vogel, 1996). Another possibility is that K_{Na} channels are tightly clustered

around Na^+ channels and so are activated before there is significant diffusion of Na^+ within the cell (Koh *et al.*, 1994). Although the exact mechanisms have yet to be determined, several studies have provided evidence of a role for K_{Na} channels in AHP generation. It was shown that AHPs generated following trains of action potentials, in cat neocortical and rat motorneurones, reversed when close to E_K, were not dependent on increases in intracellular Ca^{2+} and were abolished in Na^+-free solutions (Schwindt *et al.*, 1989; Safronov & Vogel, 1996). Although the lack of selective inhibitors hampers the search for an exact role for K_{Na} there is support, in the literature cited above, for the idea that K_{Na} may underlie sAHPs that are responsible for spike-frequency adaptation in specific neuronal cell types.

1.5 Sensory neurones

The primary sensory unit, consisting of a single afferent neurone with its receptor endings in the periphery, forms the first link in a sensory pathway. The central processes of these cells terminate in the spinal cord where they synapse onto interneurones termed second-order neurones. These in turn may synapse onto third order neurones, and so on until the information eventually reaches the brain.

Mechanisms affecting the firing of a primary afferent neurone in turn affect, and thus regulate, the way sensory information is transmitted from the periphery to the central nervous system. The two types of sensory neurone studied in this thesis are those of the nodose and dorsal root ganglia.

1.5.1 Properties of nodose ganglion neurones

The nodose (or inferior vagal) ganglion is located at the rostral end of the vagus nerve and contains somata of afferents that innervate the abdominal and thoracic viscera. In

the guinea pig, the majority of nodose neurones (90%) have axonal conduction velocities consistent with those of unmyelinated C-fibres and it is among this population of cells that sAHPs can be found (Undem & Weinreich, 1993). Approximately 20% of guinea pig C-fibre neurones exhibit a sAHP (Cordoba-Rodriguez *et al.*, 1999).

Nodose neurones exhibit a particularly robust sAHP that can often be seen following just a single action potential. It is insensitive to a number of potassium channel blockers including apamin (100 nM), d–TC (10 μM), Cs^+ (5 mM), TEA (30 mM), 4–aminopyridine (4 mM) and ChTx (10 nM; Cordoba-Rodriguez *et al.*, 1999). It can however, be abolished through regulatory pathways by inflammatory mediators such as histamine (Jafri *et al.*, 1997), bradykinin or serotonin (Leal-Cardoso *et al.*, 1993; Weinreich *et al.*, 1995).

1.5.2 Properties of DRG neurones

The dorsal root ganglia (DRGs) lie within the vertebral column and can be divided up into five main groups. The uppermost ganglia comprise those of the cervical region (C1-8) followed by the thoracic (T1-13), lumbar (in rats L1-6), sacral (S1-4) and the coccygeal (3) ganglia (Waibl, 1973). DRGs contain the cell bodies of sensory afferent neurones originating from various structures including the skin, muscle and visceral organs, and terminate in the dorsal horn of the spinal cord, so that information from both the internal and external environments is conveyed to the central nervous system. Functionally cells can be classified as being one of three different types according to the kind of stimulus that is detected:

1. Low threshold mechanoreceptors, which normally detect innocuous touch/pressure in the skin, proprioception and kinæsthesis in joints and capsules and stretch in muscles.

2. Thermoreceptors which detect cooling and heating.

3. Nociceptors which detect noxious stimuli but can be sensitive to one or many different kinds of stimulus. For example, some cells are excited only by mechanical stimuli, others respond equally well to noxious mechanical and thermal stimuli and some are very high threshold, stimulated by chemical events associated with chronic tissue damage and inflammation.

DRG cells can also be separated into groups based on their conduction velocities and various anatomical and immunohistochemical properties as described in the following sections.

1.5.2.1 The separation of DRG neurones based on conduction velocities

The first group, called A-fibre neurones, consists of cells with very large cell bodies and myelinated axons. They can be further divided into $A_{\alpha/\beta}$ and A_{δ} subtypes. As the $A_{\alpha/\beta}$ fibres are more heavily myelinated, they have considerably faster conduction velocities (> 14 ms^{-1} compared with 2.2-8 ms^{-1} in A_{δ}). In contrast, C-fibres have small cell bodies and non-myelinated axons, which means that they have much slower conduction velocities (< 1.4 ms^{-1}; Harper & Lawson, 1985a). It is generally agreed that the majority of $A_{\alpha/\beta}$ fibres carry information resulting from innocuous stimuli, that C-fibres carry predominantly nociceptive signals and that A_{δ} fibres are sensitive to both noxious and non-noxious stimuli. However, there is good evidence to suggest that nociceptive signals are also carried by some large diameter $A_{\alpha/\beta}$ fibres and that certain C-type neurones may respond to low-threshold mechanical stimuli (Lawson, 2002; Light & Perl, 2003).

1.5.2.2 Cell bodies of DRG neurones

Distinctions between A- and C-type cells can be made based on cytological properties. When stained with, for example, the dye cresyl violet, the larger cell bodies display uneven staining due to large amounts of Nissl substance (aggregations of ribosomes with rough endoplasmic reticulum) and are hence referred to as "large light" neurones. The smaller somata, however, have a denser distribution of organelles resulting in more darkly stained cytoplasm, and the term "small dark" neurones. These two cell types can also be differentiated by staining for the intermediate filament proteins neurofilament that is predominantly found in large diameter A-type cells ("large light" neurones) and for peripherin, which is limited to C-type cells ("small dark" neurones; Lawson *et al.*, 1984; Ferri *et al.*, 1990; Troy *et al.*, 1990).

1.5.2.3 Electrophysiological differences between A- and C-type cells

Electrophysiological recordings show that there are two different types of action potential that can be recorded from DRG cells. The first is a long duration action potential showing an inflection on the falling phase, which is thought to arise due to an inward Na^{2+}/Ca^{2+} current (Görke & Pierau, 1980; Harper & Lawson, 1985b; Traub & Mendell, 1988; Blair & Bean, 2002). The second type has a much shorter duration and no inflection. It is thought, at least in the rat, that all C-fibre cells display action potentials with inflections whilst only 60% of A_δ and 20% of $A_{\alpha/\beta}$ fibres display such action potentials (Waddell & Lawson, 1990). It is likely that the presence of such action potentials corresponds more to the function of the cell, rather than the type of fibre, so inflections are more likely to be seen in high-threshold nociceptors than low threshold mechanoceptors, and their presence is thus not limited to C- or A-fibres (Waddell & Lawson, 1990, Ritter & Mendell, 1992).

Further differences are reported in response to long hyperpolarising current steps. The majority of C-fibres (87%) show a hyperpolarisation that decays with a single exponential timecourse. A-fibres are different in that they initially show a "voltage sag" which has been attributed to the anomalous inward-rectifying current or I_H (Villière & McLachlan, 1996; see also **Chapter 4**).

1.5.2.4 Possible roles for SK channels in DRG AHPs

Following one or more action potentials, DRG cells tend to display a robust AHP. As with other neurone types, the AHP appears to have several components which have durations ranging from a few milliseconds to several seconds, being longer in nociceptors and shorter in low threshold mechanoceptors (Villière & Mclachlan, 1996). In guinea pig DRGs cells, the use of the non-selective Ca^{2+} channel blocker Co^{2+} blocks a prominent outward current (Kameyama, 1983). There is also some evidence that DRGs exhibit AHPs sensitive to apamin. For example, Tokimasa *et al.*, (1990) made voltage-clamp recordings from bullfrog DRGs and showed that an outward current lasting several hundred milliseconds was reduced to approximately 25% in the presence of 3 nM apamin.

In rat DRGs, Boettger *et al.* (2002), provided some evidence to suggest that SK channel proteins are expressed, however, the evidence supporting a role for SK channels in generating AHPs is inconsistent. Amir & Devor (1997) and Gold *et al.* (1996a) report the presence of apamin-sensitive AHPs in rat DRG cells, albeit at relatively high concentrations of the blocker (1 μM) in the case of the latter work. In contrast to these studies, Abdulla & Smith (2001) found that apamin had little or no effect on the number of action potentials seen in response to a depolarising pulse, suggesting that SK channels do not regulate the firing frequency in these cells. Even more striking is the

work done by Villière & McLachlan (1996) who found that few AHPs in different sized cells were sensitive to block by Co^{2+} and those cells that were sensitive only showed partial block. This would suggest that the conductances underlying AHPs in DRG cells are unlikely to be due to the opening of K_{Ca} channels. So questions remain: to what extent are SK channels involved in AHP generation in rat DRG cells? Indeed, are they involved at all?

1.5.3 Termination of DRG fibres in the spinal cord

DRG afferents enter the spinal cord via the dorsal horn where they are distributed differentially depending upon the type of cell (i.e. A- or C-fibre). The spinal cord itself is divided into several regions, known as laminae, based on the differences in cell morphology throughout the butterfly-shaped grey matter. First described by Rexed (1952) using transverse sections of cat spinal cord, this laminellar arrangement is roughly the same in many different species. **Figure 1.4** illustrates the divisions into laminae I-IX and the area surrounding the central canal (area X) in a transverse section of the lumbar region of rat spinal cord.

It is known that lamina I and lamina II (also known as the substantia gelatinosa) receive input from both myelinated and unmyelinated fibres. C-fibres are known to terminate in both of these regions (Sugiura *et al.*, 1986; 1989). A_δ fibres appear to terminate preferentially in the superficial region of lamina II (called lamina II_o where the "o" stands for "outer") but also in lamina V (Nagy & Hunt, 1983). Larger afferent fibres terminate more ventrally in laminae III to IV. This provides a distribution pattern whereby nociceptive nerve terminals are found in the outer layers of the dorsal horn, while the non-nociceptive fibres penetrate deeper into the spinal cord.

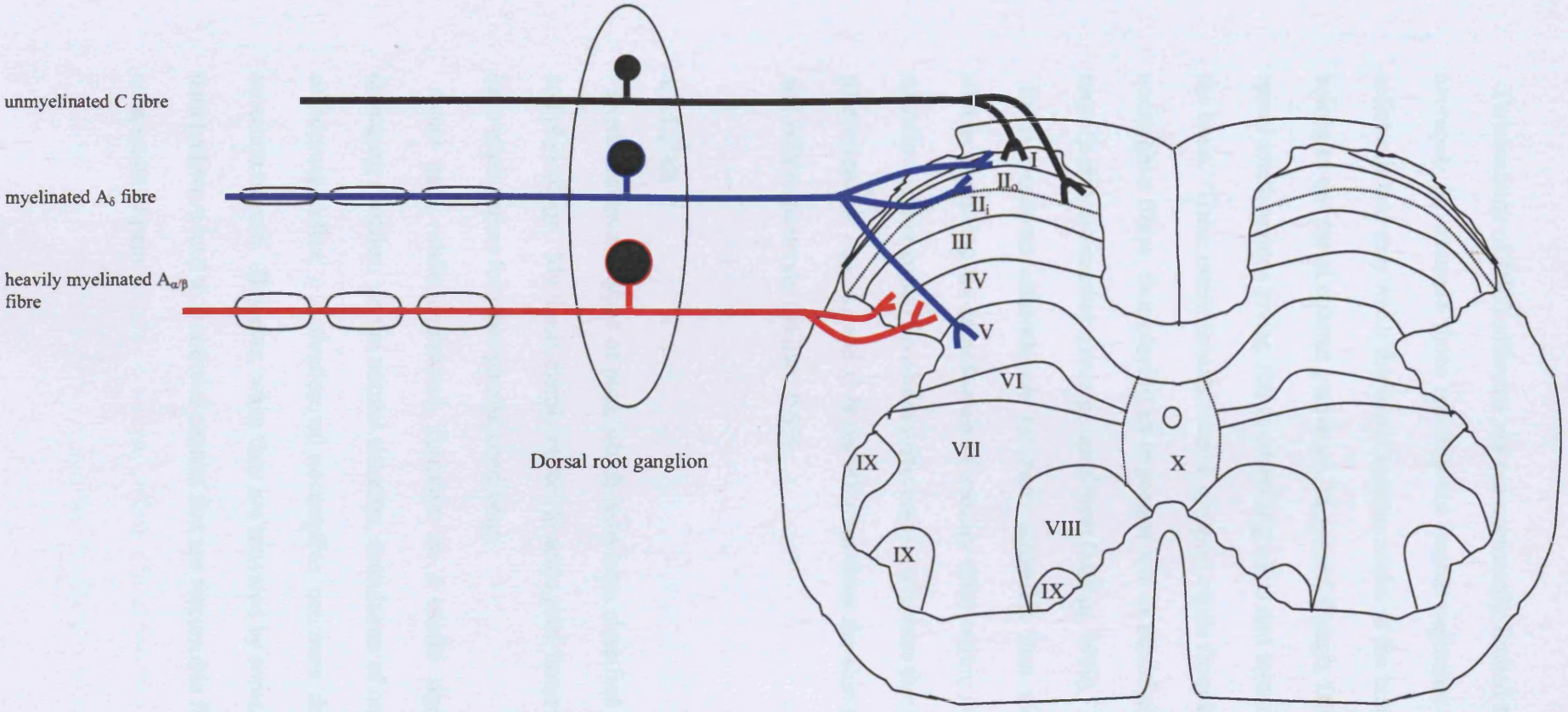

Figure 1.4 A schematic representation of a transverse section of the lumbar spinal cord with its laminellar organisation. Spinal cord laminae are indicated with roman numerals (I-X). Lamina II is further divided into inner (II_i) and outer (II_o) sections. Sensory nerves originating in the periphery with cell bodies in the DRGs terminate in different regions of the spinal cord. C fibres terminate in the most superficial laminae, I and II. The intermediate conducting A_δ fibres terminate in laminae I, II_o and V while fast-conducting $A_{\alpha/\beta}$ fibre terminals are predominantly seen in the deeper laminae (III/IV).

Terminations of DRG afferents are not necessarily limited to the spinal cord. Some neurones, for example those entering via lumbar segments of the spinal cord, have collaterals that may reach the dorsal column nuclei in the brain. Neurones of this type belong to the dorsal column pathways. In general though, DRG afferents synapse onto spinal interneurones giving rise to ascending tracts that terminate in various regions of the brain. These interneurones receive synaptic inputs from both nociceptive and non-nociceptive fibres, thus playing an important role in modulating the different forms of sensory information that converge upon them (Millan, 1999).

Since cutaneous afferents are far more accessible than visceral ones, most of the studies examining the transduction of sensory information; including the *in vivo* work described in this thesis, have been performed on neurones that originate in the skin. The proportions of $A_{\alpha/\beta}$, A_{δ} and C-fibres afferents from the skin are approximately 20, 10 and 70% respectively (Millan, 1999).

1.5.4 Pain

There are several types of pain, which have been classified according to their causes and physiology. My thesis mainly relates to acute pain, however, the findings may also have implications for other painful conditions.

Acute pain, while unpleasant, functions as a useful signal to withdraw from a damaging stimulus. In the normal situation, stimulation of nociceptors often leads to a withdrawal reflex. Activation of nociceptive neurones does not itself create the sensation of pain. However, when they are activated by some noxious stimulus, certain pain pathways lead to emotional centres that are responsible for the additional affective component of pain.

In cases involving inflammation or nerve damage, the manner in which painful stimuli are processed alters (Dickenson, 1995; Millan, 1999; Holden, 2003). These alterations can decrease the threshold of nociceptors to facilitate neuronal firing. This increase in sensitivity, termed hyperalgesia, may last for many hours after the original stimulus is over. Neuropathic pain is the term used to describe the pain that can be the result of disease, nerve trauma or compression, or centrally due to damage in specific brain or spinal cord regions (Suzuki & Dickenson, 2000). Symptoms include spontaneous pain and allodynia, i.e. pain in response to an innocuous stimulus. The chronic pain resulting from nerve damage serves no purpose and often leads to great distress (Scholz & Woolf, 2002).

Current treatments for chronic pain are often ineffectual, or cause unpleasant side effects; clearly the discovery of new analgesics that could overcome these problems would fill a significant gap in the treatment of chronic pain. Recent work on the KCNQ channels in DRGs has suggested novel pain therapy in the form of a K^+ channel opener (Passmore *et al.*, 2003). This seems highly logical as K^+ channels not only set the resting membrane potential, but also hyperpolarise cells to reduce neuronal excitability. As DRGs are also thought to express SK channels, these may form an equally important target for the development of novel analgesics.

1.6 Aims of experiments

The aim of my thesis was to try to determine whether SK and/or IK channels might have a functional role in the transmission of sensory information. Therefore, the ability to detect the expression of SK/IK channel proteins forms a pivotal part of this thesis. The method chosen to detect expression was that of immunofluorescent staining. The first step was to characterise antibodies kindly provided by Dr Mark Chen at

GlaxoSmithkline, Stevenage. Once the most suitable antibodies had been identified, the expression of SK and IK channels was examined in two different tissue types, the nodose ganglion of the guinea pig and the rat DRG.

As mentioned earlier, there are conflicting reports about the role of SK channels in AHP generation in DRG neurones. For this reason, and to complement the immunohistochemistry, these AHPs and their pharmacology were examined further. Using various electrophysiological markers to identify the type of cell being recorded from, intracellular and perforated-patch recordings were made to examine AHP characteristics and pharmacology. These studies were done using enzymatically-isolated cells in culture. In order to extend this work, spinal cord slices were stained with the SK/IK channel antibodies to establish whether SK channels synthesised in the cell body could be transported to DRG processes terminating in the spinal cord and thus play a wider role.

Finally, while *in vitro* studies provide a good basis for determining how SK channels work, their part in the transmission of sensory information can only be fully understood by observing effects in the whole animal. With the help of Prof Anthony Dickenson and Dr Rie Suzuki, extracellular recordings were made from deep spinal neurones of adult rats. The firing of these cells in response to innocuous and noxious stimuli was recorded and compared with recordings taken in the presence of the K_{Ca} channel opener 1-EBIO and specific SK blocker UCL 1848.

Taken together the work in this thesis looks at SK/IK channel expression in sensory neurones and possible functions at both the cellular and the whole-animal level.

Chapter 2

Methods

2.1 Cell culture methods

2.1.1 Cell lines

All human embryonic kidney 293 (HEK 293) cell lines (including one stably expressing the human SK1 gene) were maintained in Dulbecco's modified Eagle's medium (DMEM), while all chinese hamster ovary (CHO) cell lines (including one stably expressing the human SK4/IK gene) were maintained in alpha minimal essential medium (alpha MEM). Both media were supplemented with 10% foetal calf serum (FCS), 2 mM L-glutamine, penicillin (100 units/ml) and streptomycin (100 μg/ml). Cells were plated onto laminin-coated square glass coverslips a day before staining. All tissue culture materials for cell lines were obtained from Gibco BRL (Invitrogen).

2.1.2 Primary culture of peripheral ganglion neurones

Sprague Dawley rats of either sex were used to obtain dorsal root ganglion (DRG) and superior cervical ganglion (SCG) tissues. Nodose ganglia were obtained from Duncan Hartley guinea-pigs (~300 g) of either sex. All animals were killed in accordance with Home Office guidelines for Schedule 1 killing using a rising concentration of CO_2 followed by decapitation for rats or exsanguination for guinea-pigs. DRGs were dissected out and placed in L-15 medium. The nerve roots were trimmed off so that only the ganglia remained. SCGs and nodose ganglia were also dissected out and left in L-15 medium where they were de-sheathed and cut into small pieces. In all cases the

ganglia were then washed twice in Ca^{2+}- and Mg^{2+}- free Hanks' balanced salt solution (HBSS; mM composition) $CaCl_2$ 1.26, KCl 5.37, KH_2PO_4 0.44, $MgCl_2$ 0.49, $MgSO_4$ 0.41, NaCl 136.89, $NaHCO_3$ 4.17, Na_2HPO_4 0.34 and D-glucose 5.56) containing 10 mM N-(2-hydroxyethyl) piperazine-N'-(2-ethanesulphonic acid) (HEPES free acid). The ganglia were initially incubated in HBSS buffered with 10 mM HEPES, containing 400 u/ml type 1A collagenase and 6 mg/ml bovine serum albumin (BSA) for 20 min at 37 °C applied using a syringe with a 0.2 μm sterile filter (Nalgene). After this incubation period, they were washed twice in 10 mM HEPES buffered HBSS. Tissues then underwent a second incubation in HEPES buffered HBSS, this time containing 1 mg/ml trypsin and 6 mg/ml BSA for 30 min at 37 °C. This solution was also filtered. The dissociated cells were then transferred to a growth medium consisting of L-15 medium supplemented with 10% FCS, 0.6% w/v D-glucose, 0.19% w/v $NaHCO_3$, 100 u/ml penicillin, 100 μg/ml streptomycin and 50 ng/ml nerve growth factor (NGF). The cell suspension was then plated onto either 35 mm plastic culture dishes, plain glass coverslips (13 mm diameter or 15 mm x 15 mm) or CELLocate® coverslips pretreated with laminin as follows: laminin was made up in HBSS to a concentration of 10 μg/ml and 200 μl of this solution was applied to each coverslip. The coverslips were then incubated at 37 °C for 1 hr after which they were rinsed once with L15 medium.

All tissue culture reagents for these preparations were obtained from Sigma except for HBSS and $NaHCO_3$ (Gibco) and D-glucose (VWR). Plasticware was obtained from Nunc, plain glass coverslips from VWR and CELLocate® coverslips from Eppendorf.

2.2 Immunofluorescent antibody staining

2.2.1 Immunocytochemistry

All staining operations were carried out at room temperature (22 °C) unless otherwise indicated. First, cells were washed three times in phosphate buffered saline (PBS; composition (mM): NaCl 136.9, KCl 2.7, Na_2HPO_4 9.2, KH_2PO_4 1.8, pH to 7.2 with HCl). Cell lines were then fixed in PBS containing 4% paraformaldehyde (Sigma) for 10 min or, in the case of neurones, 1% paraformaldehyde for 20 min. Coverslips were then transferred to PBS for 5 min to allow the cells to rehydrate. At this stage, neurones underwent two additional steps to reduce excess levels of background staining from the secondary antibody. This involved the cells being incubated in a quenching solution consisting of 0.37% glycine/0.27% NH_4Cl (made up in PBS) for 10 min, a process which was repeated and followed by another 5 min wash in PBS. In order to permeabilise cells, the coverslips were placed in methanol (VWR) for 10 min. After another 5 min wash step in PBS, cells were incubated in an antibody blocking solution (ABS) consisting of 2% horse serum (Sigma) and 2% BSA (Sigma) in PBS for 1 hr. After the blocking step, used to prevent non-specific antibody binding, cells were incubated in the appropriate primary antibody for 4 hr. The relevant concentrations of primary antibody (see **Table 2.1**) were made up in ABS.

Primary antibodies to the SK/IK channels were the kind gift of Dr Mark Chen (GlaxoSmithKline, Stevenage). These were polyclonal rabbit antibodies raised to specific peptides (see **Figure 2.1** for epitopes). Three additional antibodies used to stain for rSK1 and SK3 were also polyclonal rabbit antibodies. These were UCL55 and UCL56 which were raised to two rSK1 peptides and an anti-SK3 antibody which was

Name of antibody	Target protein	Final antibody concentration
L155[1]	hSK1	1.0 μg/ml
Rb185[1]	rSK1	1.0 μg/ml
Rb196[1]	rSK1	1.0 μg/ml
Rb186[1]	rSK1	1.0 μg/ml
Rb200[1]	rSK1	1.0 μg/ml
M1[1]	hSK2 and rSK2	0.75 μg/ml
M75[1]	hSK3 and rSK3	0.5 μg/ml
M20[1]	hIK	1.0 μg/ml
M4[1]	hIK	1.0 μg/ml
R212[1]	rIK	1.0 μg/ml
R224[1]	rIK	1.0 μg/ml
UCL56[2]	Rat SK1	20 μg/ml
Anti-SK3[3]	SK3	0.3 μg/ml
Anti-BK channel[4]	BK	Dilution[6] 1:200
Anti-peripherin[3]	Reacts with rat peripherin	Dilution[6] 1:200
Anti-capsaicin receptor[3]	Reacts with rat VR1 receptor	Dilution[6] 1:200
Anti-MAP2[5]	Reacts with microtubule-associated protein 2	Dilution[6] 1:200

Table 2.1. Primary antibody concentrations used. [1]Antibodies obtained from Dr Mark Chen at GlaxoSmithKline. [2]Antibody raised by Dr Ramine Hosseini, UCL. [3]Purchased from Chemicon. [4]Kind gift from Prof Edward Moczydlowski (Yale University). [5]Purchased from Sigma. [6]Concentration not available.

Type of antibody	Species	Final antibody concentration
TRITC[1] conjugated (Alexa 568; Molecular Probes)	Goat anti-rabbit	20 μg/ml
CY2 conjugated (Amersham)	Goat anti-rabbit	5 μg/ml
CY3 conjugated (Amersham)	Goat anti-rabbit	5 μg/ml
CY5 conjugated (Amersham)	Goat anti-rabbit	5 μg/ml
FITC[2] conjugated (Chemicon)	Goat anti-guinea pig	5 μg/ml
Fluorescein conjugated (Chemicon)	Sheep anti-mouse	Dilution[3] 1:40

Table 2.2. Fluorescent secondary antibodies used to detect primary antibody binding. [1]Tetramethyl rhodamine isothiocyanate. [2]Fluorescein isothicyanate. [3]Concentration not available.

Figure 2.1 Antibody epitopes shown within an alignment of the predicted amino acid sequences for rat and human SK and IK channels

This alignment was made with the ClustalW software (http://www.ebi.ac.uk/clustalw/) using the Gonnet protein weight matrix with a gap open penalty of 10.0 and a gap extension penalty of 0.2. The sequences recognised by the different antibodies are as follows:

Antibody Epitopes
Anti-hSK1 (L155)
Anti-rSK1 (Rb185 & Rb196)
Anti-rSK1 (Rb186 & Rb200)
Anti-h/rSK2 (M1)
Anti-h/rSK3 (M75)
Anti-hIK (M16 & M20)
Anti-hIK (M4 & M5)
Anti-rIK (R212 & R224)
CQPPEPIQEAT
UCL55
UCL56
KLPPPWPGPSHLTAA
Sequence recognised by Chemicon anti-rSK3 antibody

The epitopes do not always match the target protein sequence perfectly because they are frequently altered in order to facilitate antibody purification. Deviations from the peptide sequences are underlined.

Genbank accession numbers for the sequences used in this alignment are as follows:

hSK1 AAB0956.2
rSK1 AF000973
hSK2 NP_067627.2
rSK2 U69882
hSK3 CAB61331
rSK3 AF292389
hIK NP_002241.1
rIK Sequence reported in this thesis, see Chapter 3 section 3.2.6.1.

obtained from Chemicon. The anti-peripherin and anti-VR1 antibodies were also purchased from Chemicon.

Following the 4 hr incubation, the primary antibody was washed off with three washes in PBS containing 1% Tween-20 (Promega). The cells were then incubated in a solution containing a fluorescently-labelled secondary antibody for 1 hr. Again, these antibodies were diluted to the relevant concentration (see **Table 2.2**) in ABS. The cells then underwent three final washes in PBS with 1% Tween-20 and the coverslips were mounted onto clean glass slides using an antifade mount (Vectashield, Vector Laboratories Incorporated).

Stained cells were viewed with a Leica TCS confocal microscope or a Zeiss LSM 510 microscope. Where practical, all images within a single experimental set were recorded with the same gain, offset and pinhole settings. However, occasionally, the intensity was increased in negative controls so that cell outlines were visible.

2.2.2 Immunohistochemistry

45 day old (150-200 g) Sprague-Dawley rats of either sex were first deeply anaesthetised using 0.5 mg/kg Hypnorm (fentanyl citrate and fluanisone) and 2.5 mg/kg diazepam. They then underwent transcardial perfusion with saline prior to a 15 min perfusion with 4% paraformaldehyde in phosphate buffer (PB; Na_2HPO_4 (124 g/L) and NaH_2PO_4 (15.6 g/L) with 0.1% sodium azide, final pH of 7.4). Following the perfusion, the lumbar section of the spinal cord was dissected out and fixed for a further 4 hr in 4% paraformaldehyde solution. The cords were then transferred to a 30% sucrose solution (made up in PB) and stored overnight at 4 °C. Serial transverse slices of 40 μm were cut using a freezing microtome (perfusion carried out and sections kindly produced by Dr Wahida Rahman, Department of Pharmacology, UCL).

Slices were transferred to separate wells of a four-well culture dish (NUNC). They were first incubated in blocking solution consisting of 3% goat serum and 0.3% Triton X-100 in PB and left on a horizontal shaker for 1 hr. Primary antibodies were made up to the required concentration in the blocking solution and added to the slices which were then left shaking overnight. Tissues next underwent three separate washes in PBS. Secondary antibodies were then made up to the required dilution in blocking solution (see **Table 2.2**) and left on the slices for 2 hr with shaking. After a final three washes in PBS, slices were mounted onto 0.5% gelatin-coated glass slides using Vectashield anti-fade mount.

Slices were viewed with a Leica TCS confocal microscope or a Zeiss LSM 510 microscope. As with individual cells, all images within a single experimental set were recorded with the same gain, offset and pinhole settings. When high antibody concentrations were used, the gain was reduced due to the increased background staining..

2.3 Methods for molecular biology and gene expression

2.3.1 SK channel constructs

The rSK1, rSK2 and hIK genes subcloned into pTracer or pcDNA3 plasmids were the generous gift of Prof Len Kaczmarek and Dr William Joiner, Yale university, USA. The rSK3 gene in pcDNA3.1 zeo was cloned from a rat SCG library as described in Hosseini *et al.*, (2001). The hSK1 clone used to generate transient transfections cells was the generous gift of Prof John Adelman (Vollum Institute, USA). The hSK1 stable cell line in HEK 293 cells was kindly provided by Dr Mark Chen (GlaxoSmithKline, Stevenage).

2.3.2 Cloning of the rat IK channel

2.3.2.1 PCR of the rat IK channel

The rat IK channel was cloned using cDNA that had been reverse-transcribed from rat DRG total RNA obtained from a 43 day old (p43) animal (see sections **2.5.3** to **2.5.7** for method). The initial PCR reaction was made up as follows: 1 unit Pfu turbo, 2 µl 10x Pfu enzyme buffer, 1 µl dNTPs (final concentration of 0.4 mM for each dNTP), 4 µl forward primer 1 (5'caccaagagctcggggccat 3'), 4 µl reverse primer 1 (5'caggcagctatgtggcctcct 3'; final concentration of 1.2 µM for each primer), 1 µl (1 µg) template cDNA and 1 µl DMSO made up to 20 µl in nuclease-free H_2O. The reaction was run using the following conditions: 94 °C for 2 min, then 35 cycles of 65 °C for 1 min, 72 °C for 2 min and 94 °C for 1 min with a final annealing step at 68 °C for 5 min and elongation step of 72 °C for 20 min. The resulting PCR product was run on a 0.9% agarose gel. However, at this stage it was not yet possible to visualise the expected 1.5 kb band so a section of the gel was cut out, where the band was anticipated, using the 1 kb and 2 kb bands of a marker as a guide. All DNA contained in this section of the gel was then purified using the QIAquick gel extraction kit (QIAGEN) following the manufacturers instructions. Briefly, the excised gel was incubated at 50 °C in Buffer QG. Once dissolved the gel mix was transferred to a QIAquick spin column and centrifuged at 13,000 rpm for 1 min. The column was then washed with Buffer PE and the cloned IK gene eluted in nuclease-free H_2O.

Of the gel purified DNA, 1 µl was used as the template to undergo a second round of PCR using the above conditions. A "second round" sample of this was run on a 0.9% agarose gel and on this occasion it was possible to see a band of ~1.5 kb. In order to increase the yield of DNA for subcloning, the gel purified product underwent a third round of PCR with an alternative set of primers, forward primer 2

(5'ggggtaccggggccatgggcggggagc 3') and reverse primer 2 (5'gctctagacaggcagctatgtggcctcctggatggg 3'). The conditions for PCR were as for the first round, however the reaction was scaled up so that the final volume was 50 µl. The PCR product from this reaction was also run on a 0.9% gel and purified using the gel extraction method.

Polymerases and dNTPs were obtained from Stratagene. Primers were purchased from either Invitrogen or Stratagene, nuclease-free water from Ambion and all other reagents from Sigma.

2.3.2.2 Sub-cloning the rat IK into a mammalian expression vector

As Pfu does not have terminal transferase activity, it was necessary to add the 3' overhangs needed for sub-cloning (Hu, 1993). This was done by incubation of 10 µl of gel purified DNA with 0.5 units of Taq polymerase, 1 µl Taq polymerase buffer and 1 µl dATP (final concentration of 0.8 mM) at 72 °C for 10 min. The resulting DNA was sub-cloned into the pcDNA3.1D/V5-His-TOPO® expression vector using the pcDNA3.1© Directional TOPO Expression Kit (Invitrogen). The TOPO cloning reaction was performed by incubating 4 µl A-tailed DNA, 1 µl of kit salt solution and 1 µl of the expression vector at room temperature for 30 min then placing on ice.

2 µl of the cloning reaction was added to a vial of One Shot® Chemically Competent *E.Coli* cells, which were incubated on ice for 5 min. The cells were heat-shocked at 42 °C for 30 sec and transferred to ice. After adding 250 µl of room temperature SOC medium (composition: 2% tryptone, 0.5% yeast extract, 10 mM NaCl, 2.5 mM KCl, 10 mM $MgCl_2$, 10 mM $MgSO_4$, 20 mM glucose) the tube was left shaking at 37 °C for 1 hr. Then either 50 µl or 200 µl of the transformation was spread onto an LB plate with 100 µg/ml ampicillin. The plates were then incubated at 30 °C overnight. The

following day 10 colonies were picked from the plates. Each colony was grown in 5 ml of LB medium containing 50 μg/ml ampicillin at 37 °C overnight (with shaking at ~ 225 rpm).

2.3.2.3 Minipreps of plasmid DNA

Plasmid DNA was isolated from the transformed *E.Coli* cells using the QIAquick kit for minipreps (QIAGEN). 3 ml of each overnight LB culture was spun down at 3500 rpm for 5 min at 4 °C in a Heraus centrifuge. The medium was then taken off and the pellet resuspended in buffer P1. Then 250 μl of P2 (lysis) buffer was added. When the cells had lysed, 350 μl of neutralisation buffer (N3) was added and the tubes were then spun down at maximum speed in a microcentrifuge for 10 min. The supernatant was transferred to a kit spin column and spun down at maximum speed for 1 min. The column was then washed in buffer PB followed by a wash in buffer PE. The DNA was finally eluted in 50 μl of nuclease-free H_2O.

To check which of the minipreps contained a plasmid with the correct sized insert in the correct orientation, 1μl of each prep was digested with *Stu*I which should have given two bands of approximately 2 kb and 4.7 kb in size. Digested DNA was run on a 2% agarose gel and clones that seemed to give the correct sized bands were identified.

2.3.2.4 Large scale production of plasmid DNA

The miniprep DNA identified as carrying an appropriate insert was then used to transform XL-10 Gold Ultra competent cells (Stratagene). 1 μl of plasmid, 1 μl of beta-mercaptoethanol and 30 μl XL-10 Gold were added to a pre-chilled falcon 2027 tube and then left on ice for 30 min. The mix was heat shocked at 42 °C for 30 secs and left on ice for a further 2 mins. Approximately 1 ml of NZY broth, preheated to 42 °C, was

added to the transformed cells. These were then left shaking at ~250 rpm (shaker model G25, New Brunswick Scientific Co. Inc.) at a temperature of 37 °C for 1 hr. 50 µl of the mix was plated on LB Agar with 50 µg/ml ampicillin and grown at 37 °C overnight.

Colonies were picked from the plates and transferred to LB medium containing 50 µg/ml ampicillin. This was incubated at 37 °C in a shaker (250 rpm) and left overnight. 10 µl of the culture was then transferred to 35 ml of LB medium with 50 µg/ ml ampicillin and again left shaking overnight at 37 °C.

Plasmid DNA was then midi-prepped using the Novagen Mobius 200 kit. The method was as follows: cultures were centrifuged in a Beckman JZ-M1 centrifuge at 6,000 rpm for 10 min with the temperature maintained at 4 °C. The pellet was resuspended with 2.1 ml of Bacterial Resuspension Buffer. 2.1 ml of Bacterial Lysis Solution was then added and the mix incubated at room temperature for 5 min. 2.1 ml of the pre-chilled Mobius Neutralization Buffer was then added and the mix was left on ice for 5 min. The lysate was then centrifuged at 9,000 rpm and 4 °C for 5 minutes. The Mobius 200 column storage buffer was decanted from a filter unit and 5 ml of the Mobius Equilibration Buffer was then poured into the column reservoir and allowed to drain through. The lysate was then transferred into the column reservoir and allowed to drain through. The column was then washed and the DNA was finally eluted using 2 ml of Mobius Elution Buffer.

2.3.2.5 DNA sequencing

Once the plasmids had been midi-prepped they were then sequenced using the Big Dye II sequencing kit (ABI) to confirm that the construct contained the rIK insert. Briefly, sequencing reactions were carried out using: 3.2-5 pmol of primer (either the T7 forward primer or the pcDNA3.1 reverse primer), 4 µl of sequencing buffer (900 mM

Tris, 5 mM $MgCl_2$, pH to 9.0), 10 µl of sterile H_2O, 1 µl of plasmid DNA, 4 µl of Big Dye II Terminator Mix and the following conditions: 96 °C for 2 min, 25 cycles of 96 °C for 30 sec, 50 °C for 15 sec and 60 °C for 4 min. The DNA was then separated from unincorporated dyes using 2 µl of 3 M NaOAc (pH 4.6) and 50 µl of 95% EtOH (made up fresh), vortexed and left at room temperature for 15 minutes. The DNA precipitate was then centrifuged at maximum speed for 20 minutes, the pellet rinsed with 250 µL of 70% ethanol and spun again for 5 min. The ethanol was then removed and the pellet was left to dry for 15 minutes at room temperature. The sequencing reactions were then resuspended in loading buffer and run on a ABI377 sequencer.

2.3.3 Transfection of cell lines

Conditions for transfection varied according to the experiment and the exact amounts of plasmid are indicated in the appropriate results chapter. However, the general method was as follows: HEK 293 cells were grown in 35 mm diameter culture dishes to ~70% confluency. 1-3 µg of SK/IK channel plasmid DNA and often 1 µg QBI plasmid DNA were used. The QBI plasmid expresses green fluorescent protein (GFP) and allows identification of transfected cells using fluorescence microscopy. The plasmid DNA, along with 2-3 µl (per µg of DNA) of the transfection reagent Lipofectamine™ 2000 (Invitrogen) were mixed in Optimem (Gibco BRL) and the mixture was then added to the cells. Cells were then grown overnight and plated onto 18 mm x 18 mm square glass coverslips in preparation of immunocytochemisty experiments.

2.4 Methods for electrophysiology

2.4.1 Cell preparations

All recordings were taken using isolated neurones in primary culture (as described in section 2.1.2). DRG and nodose neurones were left in culture for 1-3 days prior to recording. Nodose neurones were isolated and plated onto 35 mm plastic culture dishes. DRG cells were either plated onto the 35mm plastic culture dishes, 13 mm plain glass coverslips or CELLocate® coverslips.

2.4.2 Solutions

During experiments the cells were constantly perfused at a rate of 4-5 ml/min with an external solution of the following composition: NaCl 130 mM, KCl 3 mM, $CaCl_2$ 2.5 mM, $MgCl_2$ 1.2 mM, HEPES free acid 5 mM, glucose 10 mM, $NaHCO_3$ 26 mM and the pH was maintained at 7.5 by continuously bubbling the solution with 95% O_2/ 5% CO_2. A stainless steel inlet tube was positioned so that the external solution flowed directly over the cell being recorded from. The bathing solution was removed via a second stainless steel tube connected to a suction pump. Drugs stocks were made up in either DMSO or water as appropriate. These were diluted to the required concentration in the external solution and were applied by switching between reservoirs using a multiway tap. All experiments were carried out at 29-31 °C by passing the external solution through a heated coil.

2.4.3 Pipettes

2.4.3.1 Intracellular electrodes

Microelectrodes for intracellular recording were fabricated from 1.0 mm O.D. x 0.58 mm I.D. borosilicate glass (code: GC100F-15; Harvard instruments) using either a

Narishige PN-3 puller or a Brown and Flaming puller (Sutter instruments). When backfilled with a solution of 1 M KCl these microelectrodes had resistances of 90-150 MΩ.

2.4.3.2 Patch pipettes

Patch pipettes for perforated patch recordings were pulled from 1.5 mm O.D. x 1.17 mm I.D borosilicate glass (code: GC150TF-15; Harvard instruments) using an L-MP-30 vertical puller (List Medical). The tips of the pipettes were coated with Sylgard® (Dow Corning, USA) and fire polished using a microforge (Narashige, MF-9). These pipettes were dipped into a filling solution consisting of: $KMeSO_4$ 126 mM, KCl 14 mM, HEPES free acid 10 mM, $MgCl_2$ 3 mM, with the pH adjusted to 7.25 using 1 M KOH. They were then backfilled with the same solution containing 0.12 mg/ml amphotericin B (Sigma) to give resistances of 3-5 MΩ. The amphotericin "solution" was sonicated before use and was prepared on the day of the experiment.

2.4.4 Equipment used for electrophysiological studies

For experiments performed with cells plated onto plastic culture dishes, the dish was mounted onto the stage of a Nikon TMS inverted microscope using a perspex block with a circular slot to hold the dish. For later experiments where cells were plated onto glass coverslips, these were mounted in a perspex chamber. In these cases the coverslip rested on a base and was supported from above by an "o" ring and block of perspex with a diamond-shaped well which, when screwed into the base, formed the perfusion chamber. This perfusion chamber was mounted on the stage of a Leica DMIL microscope. Cells were photographed using a Nikon Coolpix 5000 digital camera attached to the microscope and live images could be captured from the camera on a

computer via a WinTV card (Hauppauge). The microscope was placed on steel and concrete slabs supported on a Micro-g vibration isolation table (Technical Manufacturing Corporation) to minimise external vibrations. The microscope was also shielded by a Faraday cage used to reduce electrical interference.

Recordings were made using an Axoclamp 2A amplifier (Axon Instruments) where stimulus pulse protocols were generated by a Master-8 stimulator (Intracel). Signals were amplified 5-fold and filtered at 5 kHz using an amplifier/filter built in-house. These signals were then digitized at 48 kHz using a VR-10 digital data recorder (Instrutech Corporation). Voltage signals were observed using an oscilloscope (Gould 20 MHz digital storage type 1424) and a computer monitor via pClamp6 software. Data were acquired at a sampling frequency of 20 kHz for fast events (action potentials and mAHPs) or 1 kHz for sAHPs. Signals were also recorded on a chart recorder (Gould Easy Graf TA240) and stored on a computer via the Axon TL1 Labmaster digitizer and pClamp6 software.

Patch pipettes and microelectrodes were held in perspex holders (Clark Electromedical Instruments). The holders were directly attached to the headstage of the Axoclamp amplifier. The headstage itself was mounted on a fine micromanipulator which in turn was mounted on a coarse manipulator attached to the microscope via a steel bar. Narashige hydraulic micromanipulators (model: MO 203) were used to make fine movements of the pipettes.

2.4.5 Methods for recording AHPs

All recordings were made using the patch amplifier in bridge mode. After dipping the electrode into the extracellular bathing solution, the resistance of the electrode was corrected for by balancing the bridge. Capacitance compensation was also applied.

Following cell penetration with an intracellular electrode or permeabilisation using a patch electrode the membrane potential was allowed to stabilise for at least 5 mins before any experimental procedures.

Cells were only deemed suitable for study if the membrane potential was more negative than or equal to -50 mV. All examples of recordings presented in this thesis are the average of three successive traces.

2.4.6 Pulse protocols

As mentioned already all pulse protocols were generated using the Master-8 stimulator. For single action potentials a pulse of 5 ms was used. For trains of action potentials the number of pulses was increased to 3, 7, 10 or 15 as necessary and pulses were generated so they were 50 ms apart. The amplitude of the current pulse (typically in the region of 200-300 pA) was adjusted to the lowest level that would initiate action potential firing and this was done using the Axoclamp amplifier.

To examine the effect of a hyperpolarising pulse on DRG cells a 200 pA negative current pulse was injected for 100 ms. For studies in rat DRG cells from p40-45 animals a depolarising pulse was employed to generate the AHP. This involved injecting 100 pA of current for 100 ms.

2.4.7 Data analysis

2.4.7.1 AHP duration in DRG neurones

AHPs seen after a single action potential were examined in two ways. The first was to measure the time taken for 80% recovery of the AHP relative to the resting membrane potential (AHP_{80}; see **Figure 2.2**).

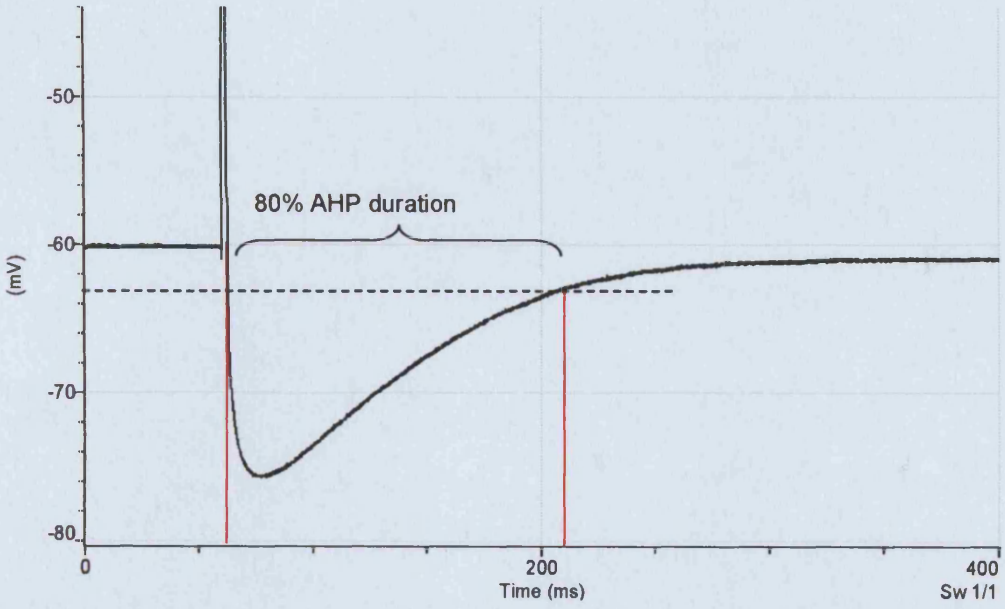

Figure 2.2 A Clampfit trace of an AHP from a DRG cell. The dotted line indicates the membrane potential at which the AHP has recovered by 80% (that is 80% of the peak amplitude of the AHP relative to the resting membrane potential). The vertical red lines then indicate the duration from the development of the AHP (the downstroke of the AP beyond the resting membrane potential) to the point of 80% recovery (AHP_{80}).

The second was to fit the AHPs with one or more exponential functions incorporated into a modified version of the Goldman-Hodgkin-Katz (GHK) voltage equation. This was done using Clampfit 8.2 (Axon Instruments). The unmodified equation is:

$$E_m = \frac{RT}{F} \ln \frac{P_K[K]_o + P_{Na}[Na]_o + P_{Cl}[Cl]_i}{P_K[K]_i + P_{Na}[Na]_i + P_{Cl}[Cl]_o}$$

where R is the gas constant 8.314 J K^{-1} mol^{-1}, T is the temperature, in this case assumed to be 303 °K and F is the Faraday constant 9.6485 x 10^4 C mol^{-1}. The values for $[K]_o$, $[K]_i$, $[Na]_o$, $[Na]_i$, $[Cl]_o$ and $[Cl]_i$ were set (in mM) to 4, 150, 145, 13, 150 and 31 respectively.

Several simplifying assumptions were made when fitting the DRG AHPs, one being that the resting membrane potential was set largely by K^+ and Na^+ conductances and that any contribution of Cl^- was negligible. This simplified the above equation somewhat to:

$$E_m = \frac{RT}{F} \ln \frac{P_K[K]_o + P_{Na}[Na]_o}{P_K[K]_i + P_{Na}[Na]_i}$$

A second assumption was that the conductances underlying the AHP decay exponentially and the shape of the AHP was due mostly to changes in K^+ conductance so the P_K values were adapted to try and account for this. For a single component AHP, P_K was substituted with the following expression: $Ae^{\frac{t-t_0}{\tau}}$ where A is the amplitude of the component, t is time, t_0 is the time at the beginning of the decay phase of the AHP and τ is the decay time constant. So the resulting equation looked as follows:

$$E_m = \frac{RT}{F} \ln \frac{Ae^{\frac{t-t_0}{\tau}}[K]_o + P_{Na}[Na]_o}{Ae^{\frac{t-t_0}{\tau}}[K]_i + P_{Na}[Na]_i}$$

For AHPs which appeared to have two K^+ components, P_K was substituted with the expression: $Ae^{\frac{t-t_0}{\tau}} + A_1 e^{\frac{t-t_0}{\tau_1}}$

so the equation looked as follows:

$$E_m = \frac{RT}{F} \ln \frac{(Ae^{\frac{t-t_0}{\tau}} + A_1 e^{\frac{t-t_0}{\tau_1}})[K]_o + P_{Na}[Na]_o}{(Ae^{\frac{t-t_0}{\tau}} + A_1 e^{\frac{t-t_0}{\tau_1}})[K]_i + P_{Na}[Na]_i}$$

for a three K^+ components the following was used:

$$E_m = \frac{RT}{F} \ln \frac{(Ae^{\frac{t-t_0}{\tau}} + A_1 e^{\frac{t-t_0}{\tau_1}} + A_2 e^{\frac{t-t_0}{\tau_2}})[K]_o + P_{Na}[Na]_o}{(Ae^{\frac{t-t_0}{\tau}} + A_1 e^{\frac{t-t_0}{\tau_1}} + A_2 e^{\frac{t-t_0}{\tau_2}})[K]_i + P_{Na}[Na]_i}$$

Finally, for a few AHPs, the best fit was achieved using an equation with two K^+ components and one depolarising Cl^- component. For these, the original GHK equation was used and P_K and P_{Cl} values substituted to give the following equation.

$$E_m = \frac{RT}{F} \ln \frac{Ae^{\frac{t-t_0}{\tau}} + A_1 e^{\frac{t-t_0}{\tau_1}}[K]_o + P_{Na}[Na]_o + A_2 e^{\frac{t-t_0}{\tau_2}}[Cl]_i}{Ae^{\frac{t-t_0}{\tau}} + A_1 e^{\frac{t-t_0}{\tau_1}}[K]_i + P_{Na}[Na]_i + A_2 e^{\frac{t-t_0}{\tau_2}}[Cl]_o}$$

An example of a fitted AHP can be seen in **Figure 2.3**.

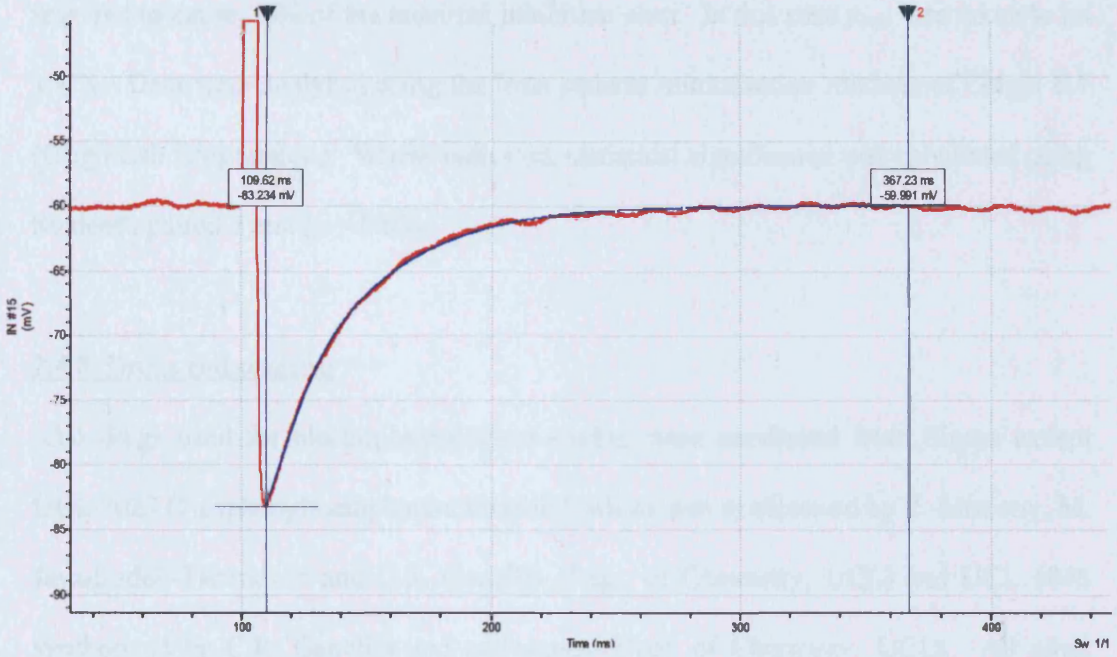

Figure 2.3 Example of an AHP trace fitted using the modified Goldman-Hodgkin-Katz equation. The red line shows the voltage trace from a DRG recording. The blue line shows the fit to two K^+ components which had decay time constants of 8.0 ms and 30.9 ms.

2.4.7.2 Nodose cells, dose-response curve to UCL 2027

The duration of a sAHP was taken as the length of time, from the last action potential, for the membrane potential return to the baseline (before the first action potential in a subsequent stimulatory set). The effects of the blockers used were expressed as the maximum amplitude of the sAHP in the presence of that drug as a percentage of that in its absence. (The sAHP amplitudes before drug addition and after washout were averaged in order to obtain the sAHP amplitude in the absence of drug). Data have been plotted as means ± the standard error of the mean (S.E.M).

The concentration-inhibition curve generated for UCL 2027 was fitted using the Hill equation in the modified form: $y / y_{max} = IC_{50}{}^{n} / (IC_{50}{}^{n} + [I]^{n})$

where y is the percentage inhibition, $[I]$ is the drug concentration, y_{max} is the maximum percentage inhibition and n is the Hill coefficient. The IC_{50} is the concentration of drug

required to cause 50% of the maximal inhibition seen. In this case y_{max} was taken to be 100%. Data were analysed using the least squares minimisation routines of Origin 6.1 (OriginLab Corporation). Where indicated, statistical significance was calculated using Student's paired T test ($p < 0.05$).

2.4.8 Drugs and reagents

All drugs used for electrophysiological studies were purchased from Sigma except UCL 2027 (2-triphenylmethylaminothiazole), which was synthesised by Z. Miscony, M. Javadzadeh-Tabatabaie and C.R. Ganellin (Dept. of Chemistry, UCL) and UCL 1848 synthesised by C.R. Ganellin and colleagues (Dept. of Chemistry, UCL). All other chemical reagents were obtained from Merck. Stock solutions of the drugs were made up in distilled water and stored at –20 °C or in dimethyl sulphoxide (DMSO) and stored at 4 °C as appropriate.

2.5 Quantitative PCR (qPCR)

2.5.1 Primer and probe design for qPCR

Quantitative PCR (qPCR) was carried out using the TaqMan® method (PE-Applied Biosystems) an approach that requires a set of conventional "outer" primers and a central fluorescently-labelled "probe" oligo which has both a "reporter" and a "quencher" dye bound (**Figure 2.4**). The TaqMan® reaction relies upon the exonuclease activity of the DNA polymerase. As with a normal PCR reaction, the primers anneal to the denatured template and the DNA polymerase begins to synthesize a new strand of DNA. However, when it reaches the probe oligo, the polymerase digests it so that the two dyes are no longer in close proximity. Once the reporter is released, a fluorescent signal can be detected and recorded. The probes, labelled at the 5' end with 6-carboxyfluorescein (FAM) and at the 3' end with 6-carboxytetramethylrhodamine (TAMRA), along with the primers, were obtained from Sigma.

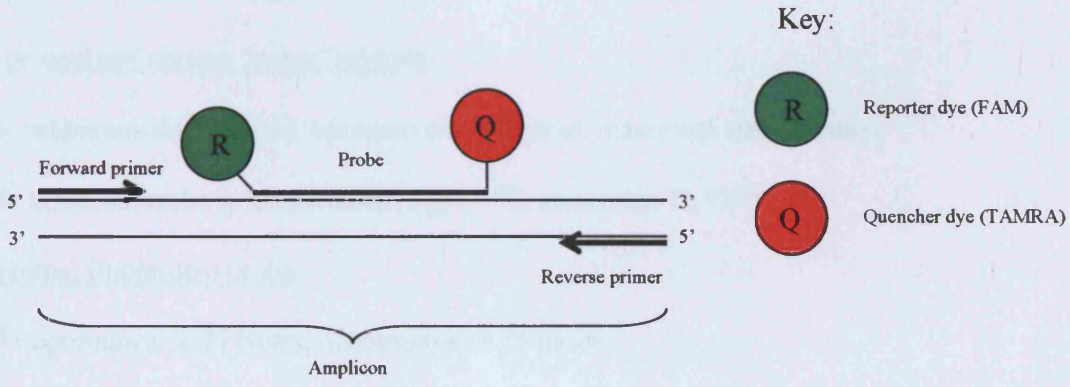

Figure 2.4 A schematic representation of TaqMan® primer annealing. TaqMan® reactions consist of the cDNA of interest, two external primers and a fluorescently labelled probe that hybridizes to the gene within the region that will be amplified (the amplicon). Exonuclease activity releases the labelled oligos and produces a fluorescent signal.

Primers and probes for the full length rSK3 channel had previously been designed at GlaxoSmithKline (Harlow) by Matthew Hall. Additional sets were designed for rSK1 to include all splice variants as well as those containing exon 7, and for rSK2 and rIK.

The rat SK1 (rSK1) sequence (Genbank accession NM_019313) was aligned with the mouse (mSK1; AF116525) sequence using the ClustalW program (available online at http://www.ebi.ac.uk/clustalw/) with the default settings. The aligned sequence was used to check where the sequences were conserved and where the splice sites in the rSK1 gene may lie. Once these had been determined primers were designed to specific targets so as to detect: all variants of rSK1 thus including truncated forms (there were two primer probe sets for this purpose) and variants containing exon 7 (see **Figure 2.5**). Primer design was limited to these two groups of splice variants as the other exons in the SK1 gene are too small to attempt to amplify using TaqMan® primers and probes.

Primer design was carried out using the Primer 3 program (available online at http://www-genome.wi.mit.edu/cgi-bin/primer/primer3_www.cgi; Rozen & Skaletsky, 2000) with the following parameters:

Forward and reverse "outer" primers

- minimum size 9 bases, optimum size 20 bases, maximum size 35 bases
- optimum melting temperature (T_m) 64 °C, maximum T_m 72 °C

Internal fluorescent probe

- optimum size 27 bases, maximum size 35 bases
- optimum T_m 72 °C, maximum T_m 75 °C

Target sequence

- product size range 80-150 bases

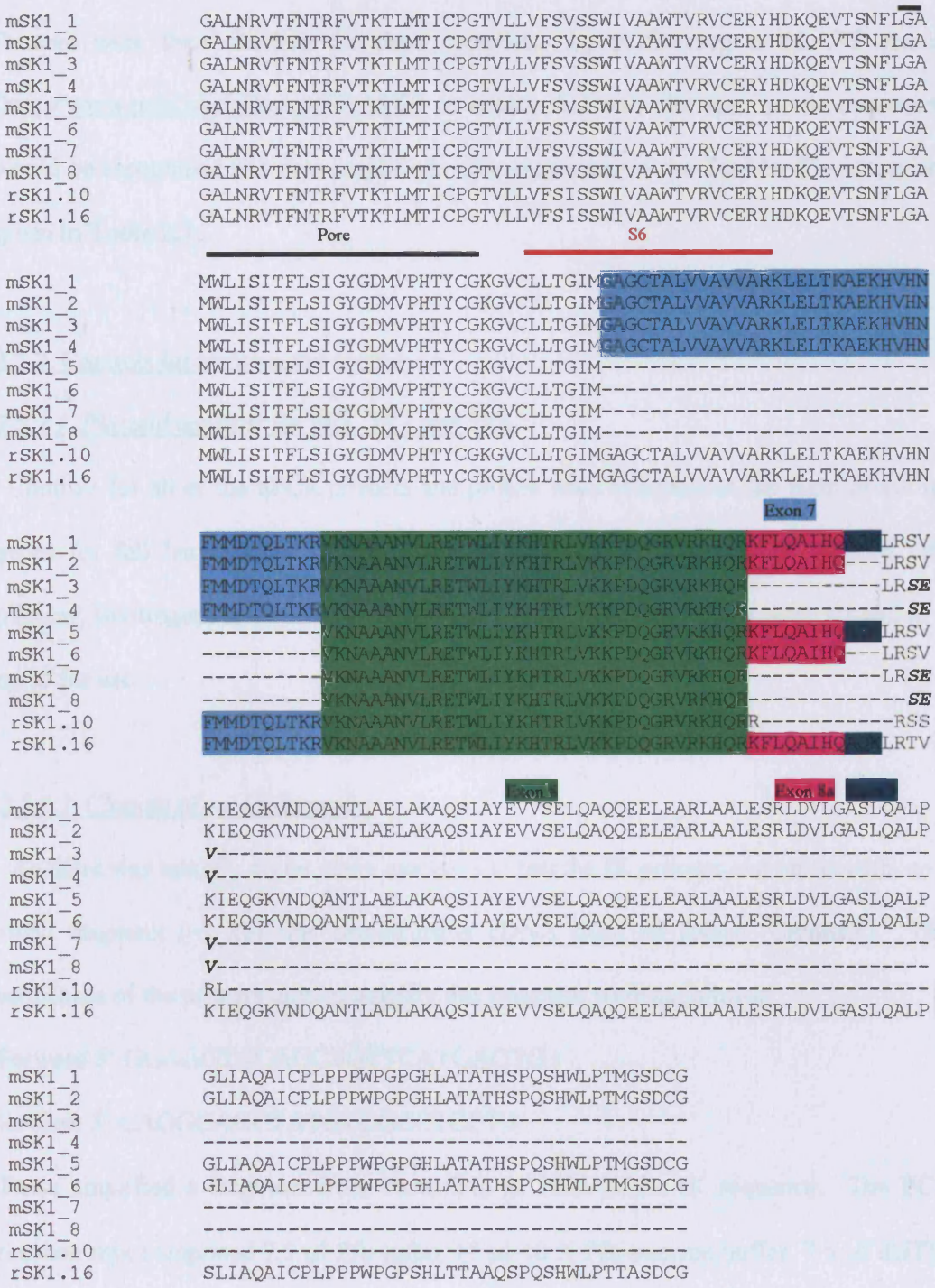

Figure 2.5 Alignment of the C terminal region of the eight mouse and two rat SK1 (mSK1 and rSK1 respectively) splice variants. Exons important in forming different splice variants are highlighted (see also Shmukler *et al.*, 2001). The pore region and the last transmembrane domain S6 are also shown. The splice variants that result in the truncated isoforms can be seen in bold and italic typeface.

Primers were then checked for their specificity by performing a BLAST search (http://www.ncbi.nlm.nih.gov/BLAST/) to ensure that only the appropriate sequences would be recognised and thus amplified. The sequences of the TaqMan® primers are given in **Table 2.3**.

2.5.2 Controls for primers and probes

2.5.2.1 Plasmid controls for SK1, SK2 and SK3

Controls for all of the qPCR primers and probes were available in the form of the rat genes for full length rSK1 (cloned into pcDNA3.1; Invitrogen), rSK2 (cloned into pTracer; Invitrogen) and rSK3 (cloned into pcDNA3.1 zeo+). These were diluted to 1 ng/µl for use.

2.5.2.2 Cloning of rat IK fragment

As there was initially no rat clone available to test the IK primers and probe with, so a small fragment (~1 kb) was cloned using cDNA from rat spleen (Clontech). The sequences of the primers used to amplify this fragment were as follows:

Forward 5' GGAGGTCCAGCTGTTCATGACTG 3'

Reverse 5' CAGGCAGCTATGTGGCCTCCT 3'

These amplified a fragment from bases 246 to 1425 in the IK sequence. The PCR reaction mix comprised 7.5 µl Pfu turbo, 15 µl 10 X Pfu enzyme buffer, 7.5 µl dNTPs (final concentration of each dNTP was 0.4 mM), 30 µl of each primer (final concentration of 1.2 µM), 7.5 µl of rat spleen cDNA as the template (0.9 ng/µl stock concentration), 7.5 µl

Gene	Primer	Sequence
Rat SK1 all variants	Forward primer	5' CATTCGCCCTGAAATGCCTA 3'
	Reverse primer	5' TCCACCAGGAACAGCTGGAT 3'
	Internal fluorescent probe	5' CACTGTCATCCTGCTTGGCCTTGTCAT 3'
Rat SK1	Forward primer	5' CCTGCAGGCCCTACCAAGTC 3'
alternative all variants	Reverse primer	5' CACAGTCTGATGCCGTGGTG 3'
	Internal fluorescent probe	5' AAGCCATATGCCCTCTACCACCACCCT 3'
Rat SK1	Forward primer	5' AAGGGCGTGTGTCTGCTCAC 3'
including exon 7	Reverse primer	5' CCGCTTGGTGAGCTGTGTGT 3'
	Internal fluorescent probe	5' GGAACTCACCAAGGCTGAGAAACACG 3'
Rat SK2	Forward primer	5' GGCTATAAGCTGGGCCATCG 3'
	Reverse primer	5' CCGAACATGCCGAAGATGAG 3'
	Internal fluorescent probe	5' AGAAGCGCAAGCGGCTCAGCGACTAT 3'
Rat SK3	Forward primer	5' TGGAATCCAAGCTGGAGCAC 3'
	Reverse primer	5' TGGCTAGTTCCCACAGCCAC 3'
	Internal fluorescent probe	5' AGCTTCAATTCCCTGCCCCTGCTCAT 3'
Rat IK	Forward primer	5' CAACAAGGCGGAGAAACACG 3'
	Reverse primer	5' TCGGGAGTCCTTCCTTCGAG 3'
	Internal fluorescent probe	5' TATGCCAAAGAGATGAAGGAGTCGGCC 3'
β-actin	Forward primer	5' GAGCTACGAGCTGCCTGACG 3'
	Reverse primer	5' GTAGTTTCGTGGATGCCACAGGA 3'
	Internal fluorescent probe	5'CATCACCATTGGCAATGAGCGGTTCC 3'

Table 2.3 Sequences of TaqMan primers and probes used for qPCR

DMSO made up to 150 µl in nuclease-free H_20. The PCR reaction was then performed using a PTC 200 Peltier thermalcycler (MJ research) and the following cycling conditions: 95 °C for 1 min, followed by 40 cycles of 95 °C for 1 min, 60 °C for 1 min, 72 °C for 1 min and finally one cycle of 60 °C for 5 min followed by 72 °C for 20 min. The product was run on a 1% agarose gel and the DNA extracted using the QIAquick gel extraction kit.

2.5.2.3 Transiently transfected HEK 293 cells

Additional controls used were in the form of HEK 293 cells transiently transfected with plasmids for rSK1, rSK2 and rSK3. The transfection was performed as described in section 2.3.3 using LipofectAMINE 2000™. RNA and cDNA were produced as described in sections 2.5.4 and 2.5.7.

2.5.3 Tissue extraction

To look at the developmental aspects of SK/IK channel expression, Sprague-Dawley rats of either sex and of three different ages were used. Animals at postnatal day 7, 17 and 40-45 (p7, p17 and p40-45 respectively) were terminally anaesthetised using a rising concentration of CO_2 followed by decapitation. The following tissues were dissected out into Ca^{2+}-free, Mg^{2+}-free HBSS: adrenal gland (medulla and cortex) and dorsal root ganglia (up to 20 individual ganglia). In addition, one p7 animal was used to obtain hippocampal and whole brain tissue, while a p17 animal was used to obtain a section of colon. All tissues were chopped into pieces of approximately 1 mm^3, rapidly transferred to cryovials (Nunc) and snap frozen in liquid nitrogen. Samples were stored at -80 °C until used (usually within 2 days).

2.5.4 RNA isolation

RNA was isolated from the above tissues using the Stratagene Absolutely RNA™ Isolation kit following the manufacturer's instructions. Initially tissues were weighed out and transferred to a microcentrifuge tube containing lysis buffer.

The samples were then homogenised using an Ultra-Turrax T8 tissue homogeniser (IKA Labortechnik) previously washed with lysis buffer. Samples were either stored on dry ice or at -80 °C until used (always within 24 hours). The lysed tissue samples were first transferred to a prefilter spin cup which was spun in a microcentrifuge (Biofuge pico, Heraeus instruments) at maximum speed (13,000 rpm) for 1 min. The filtrate was then transferred to a clean RNase-free microcentrifuge tube and an equal volume of 70% v/v ethanol added. The samples were mixed by vortexing and the solution was then transferred to an RNA-binding spin cup placed in a 2 ml collection tube. These were then spun at maximum speed for 1 min. Samples were washed and incubated in RNase-free DNase I for 15 mins at 37 °C. The matrix was then washed again, first in high salt and then in low salt wash buffers. Next the purified RNA was eluted into a microcentrifuge tube with Elution Buffer (10 mM Tris-HCl (pH 7.5) and 0.1 mM EDTA) and stored at -80 °C. All samples underwent an additional DNase step to ensure that there was no genomic DNA contamination as follows, 1 µl of RNase-free DNase I (Ambion) was added for each 10 µl of isolated RNA and the samples were incubated at 37 °C for 10 min followed by an additional 75 °C incubation for 5 min to inactivate the enzyme.

2.5.5 Checking RNA integrity

RNA samples were analysed using an RNA 6000 Nano LabChip kit run on a 2100 Bioanalyzer (Agilent Technologies). The chip was filled with a gel dye and 1 µl of each sample, along with an RNA standard, were run. The results are seen in the form of an electropherogram where peaks correspond with different sized fragments of RNA (a typical result is shown in **Figure 2.6**). Results were also "translated" so that they could be seen in gel format (**Figure 2.6** bottom left-hand corner).

The RNA integrity was determined by examining the peaks for 18S and 28S ribosomal RNA. The trace in **Figure 2.6** provides three examples of successfully purified total RNA and one example of degraded RNA in lane 4 (the electropherogram for "DRG cells" shows no peaks and the gel trace appears as a smear which is consistent with the RNA being degraded into fragments of various sizes). Samples showing evidence of degradation were not used for further study.

2.5.6 RNA quantitation

The amount of RNA for each sample was quantified using the RiboGreen® RNA quantitation kit (Molecular Probes). Initially each sample was diluted 1:100 in water. Each of the diluted samples was then transferred to separate wells of a 96-well plate. These then underwent serial dilutions in Tris-EDTA (TE) buffer as follows: 1:200; 1:400; 1:800; 1:1600 and 1:3200. A separate set of wells of the plate also contained known standards of RNA in the form of 16S and 23S rRNA from *E. coli* (provided with kit at a concentration of 100 µg/ml). The standard was diluted in TE buffer so as to produce final concentrations of: 1000 ng/ml, 500 ng/ml, 250 ng/ml, 125 ng/ml, 62.5 ng/ml, 31.25 ng/ml and 15.63 ng/ml

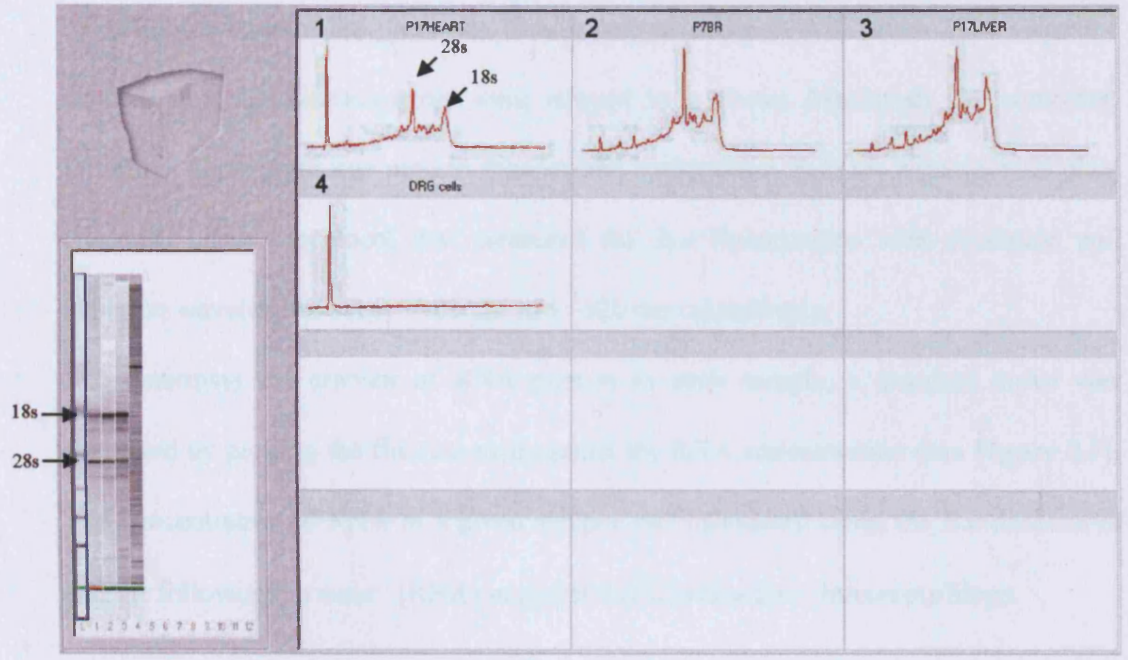

Figure 2.6 An example of a typical electropherogram obtained from samples run on an RNA 6000 nanochip: (1) p17 heart, (2) p7 brain, (3) p17 liver and (4) RNA from isolated DRG cells. Samples were deemed suitable for qPCR if they showed two peaks/bands corresponding to 28s and 18s ribosomal RNA (see arrows) indicating that samples had not undergone significant degradation. The image on the right hand side show the same samples in "gel format". The left hand lane shows marker bands while the four subsequent lanes show the RNA samples p17 heart, p7 brain, p17 liver and DRG cells respectively.

once the RiboGreen® dye was added. The dye itself was diluted 1:4000 in TE buffer and 100 µl of the resulting solution was dispensed into each well.

The fluorescence of the plate was then measured using an ABI prism 7700 sequence detector and the measurements were relayed to a Power Macintosh G3 computer. Initially a blank plate was used to measure the background, then the experimental plate was read using a protocol that measured the dye fluorescence with excitation and emission wavelengths set at ~480 nm and ~520 nm respectively.

To determine the amount of RNA present in each sample, a standard curve was generated by plotting the fluorescence against the RNA concentration (see **Figure 2.7**). The concentration of RNA in a given sample was calculated using the standard curve and the following formula: [RNA] in µg/ml = (Fluorescence – Intercept)/Slope

2.5.7 Reverse Transcription (RT) to produce cDNA

Isolated RNA was reverse transcribed using 1 µg of total RNA. For 10 reactions, a reagent mix was made up as follows: 23.3 µl 10X RT buffer, 9.3 µl 25X dNTP mix, 23.3 µl 10X random hexamers and 11.6 µl reverse transcriptase using the High Capacity cDNA Archive kit (Perkin-Elmer Applied Biosystems). The reactions were carried out using a GeneAmp® PCR system 9700 thermal cycler (PE-Applied Biosystems) and the following conditions: 10 min at 21 °C to allow annealing of primers, 60 min at 42 °C for the reverse transcriptase activity, 5 min at 70 °C to inactivate the enzyme and 10 min at 25 °C to store the cDNA once synthesized.

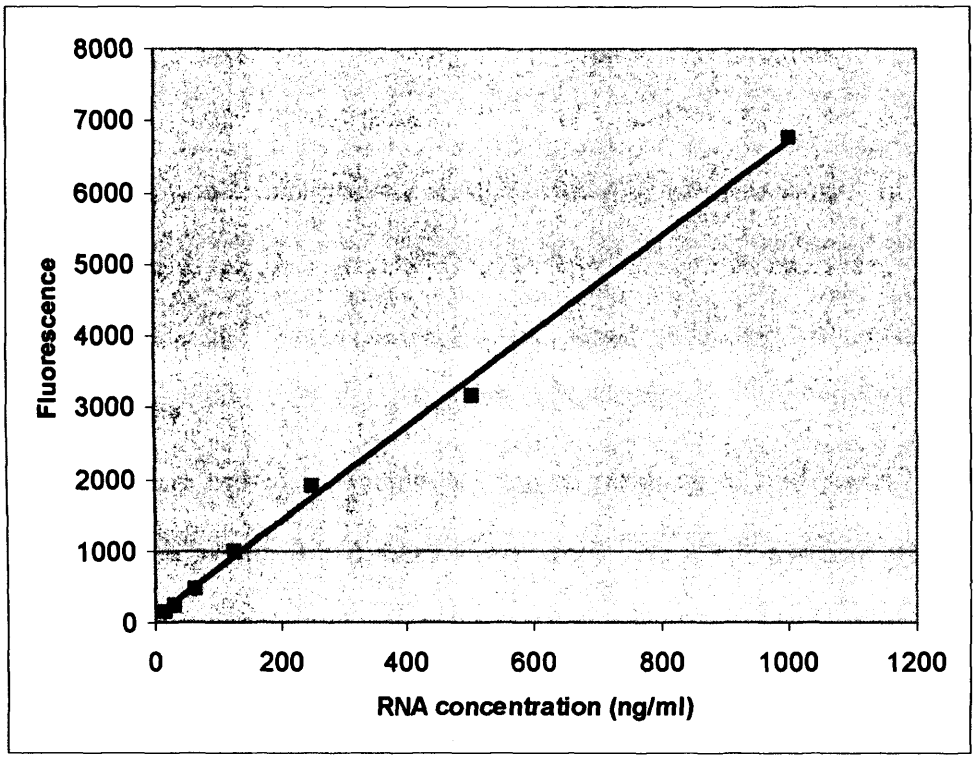

Figure 2.7 A typical example of a standard curve generated using the RiboGreen assay. The line of best-fit is determined by the ABI Prism 7700 software. RNA concentrations were determined as described in section 2.5.6.

2.5.8 qPCR (TaqMan®)

cDNA from the RT reactions was used at a final concentration of 4 ng/µl. The reaction mix for the qPCR consisted of (per sample): 4.6 µl TaqMan® universal PCR master mix (containing dNTPs, Taq polymerase from PE-Applied Biosystems), 2 µl of cDNA, 0.37 µl of 10 µM forward primer, 0.37 µl of 10 µM reverse primer, 0.19 µl of 5 µM probe made up to a final volume of 10 µl with nuclease-free water. In addition, four sets of standards using rat genomic DNA (Clontech) were set up so that a standard curve could be generated. These consisted of 10^5 copies, 10^4 copies, 10^3 copies and 10^2 copies of each gene.

The reactions were carried out in 384-well optical plates on an ABI prism 7900HT® sequence detection system (PE-Applied Biosystems). The PCR protocol was set up using the following conditions: 2 min at 50 °C, 10 min at 95 °C and 45 cycles of 5 min at 95 °C followed by 1 min at 60 °C. All data were recorded and analysed on a PC using SDS 2.0 software. For each PCR reaction, the cross threshold (C_t) was set to ~0.05 to ensure that it lay within the exponential phase of the reaction (see **Figure 2.8**). Copy numbers of the SK/IK channels expressed in each sample were calculated by comparing fluorescence values for samples with a standard curve generated from rat genomic DNA.

In the case of certain primer probe sets it was not possible to use the standards. This was because the amplicon region extended across two different exons. In these cases the copy number was generated using the following equation which assumes that the PCR reaction occurred under ideal conditions: mRNA copy number = $10^{(\frac{C-Ct}{3.5})}$

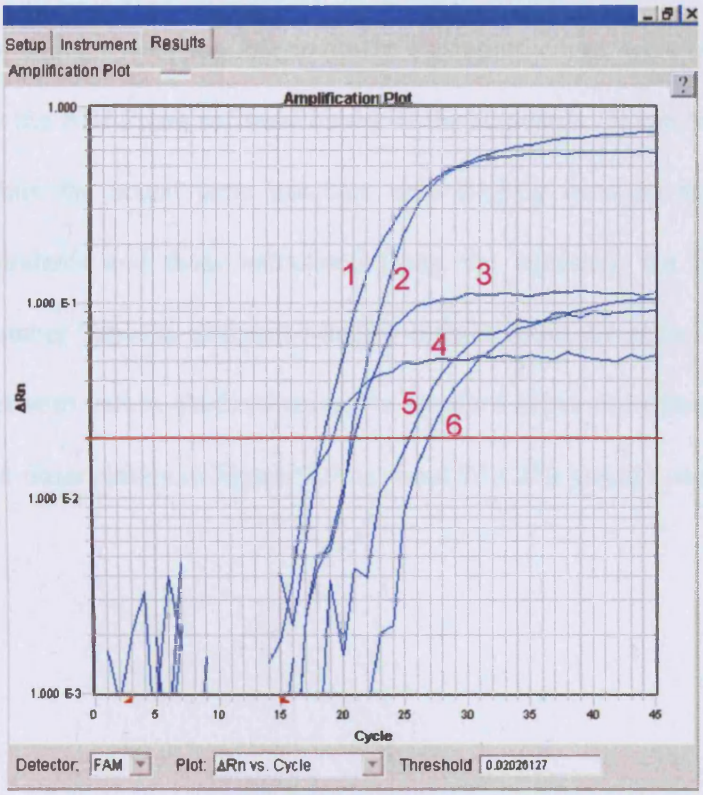

Key:
1 SK1 plasmid amplified with the SK1 all variants primer/probe set

2 IK fragment amplified with IK primer/probe set

3 SK1 plasmid amplified with SK1 exon 7 primer/probe set

4 SK2 plasmid amplified with the SK2 primer/probe set

5 SK1 plasmid amplified with the SK1 alternative all variants primer/probe set

6 SK3 plasmid amplified with the SK3 primer/probe set

Figure 2.8 A typical TaqMan® trace. The ΔR_n is plotted against the number of reaction cycles. $\Delta R_n = (R_n+)-(R_n-)$, where R_n+ denotes the ratio of: reporter emission intensity/quencher emission intensity during the reaction and R_n- is the emission intensity/quencher intensity before amplification begins. The bold horizontal line indicates the cross threshold (C_t). The target DNAs and the primer/probe sets are identified in the key.

where C represents a number of PCR cycles during the reaction (in this case 40) and C_t represents the cross threshold (see **Figure 2.8**). In order to ensure that this equation gave a reasonable estimate of the copy number, the results for the SK2 primer probe set, for which it was possible to obtain a standard curve, were compared to those generated by the ABI Prism software based on the standards. It can be seen from **Figure 2.9** that while the actual copy numbers vary slightly between the data generated from the standards and those calculated using the equation, the overall differences in copy number between different samples remain about the same. The percentage difference between values obtained using the standard curve and those using the equation, for the ten observations in **Figure 2.9**, is about 30 ± 2% (mean ± standard error of the mean).

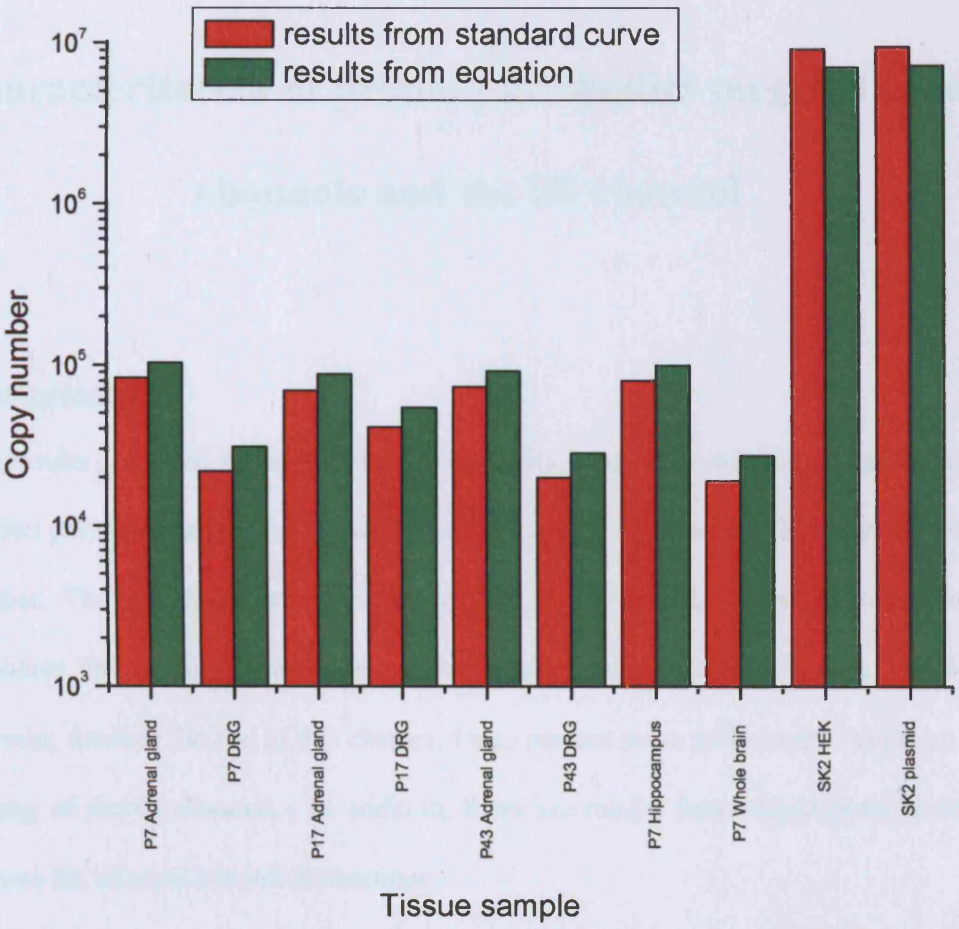

Figure 2.9 A graph comparing the SK2 cDNA copy numbers calculated using two different methods. The red bars show data derived from a standard curve generated by using rat genomic DNA with known copy numbers. The green bars show copy numbers generated using the equation described in the text. It can be seen that the relative copy numbers for all samples are essentially the same for both groups.

Chapter 3

Characterisation of primary antibodies targeted to SK channels and the IK channel

3.1 Introduction

The results presented in this chapter are primarily concerned with the characterisation of rabbit polyclonal antibodies raised against both rat and human SK/IK channel peptide epitopes. The main focus is on experiments designed to establish the suitability of these antibodies for immunohistochemistry, by testing them on recombinant channels. However, towards the end of this chapter, I also present some preliminary results on the staining of native channels. In addition, there are results from experiments done to examine SK channel subunit interactions.

Table 3.1 lists the antibodies by name and gives their intended target subunits as well as the peptide epitope used to raise the antibody. Most of the antibodies listed in **Table 3.1** (the exception being the anti-rIK antibodies) had been successfully tested in western blots but had previously not been used in staining experiments (see Chen *et al.*, 2004 for examples). To determine whether these antibodies detect proteins in their folded conformations, as opposed to in a denatured state, cell lines transfected with SK/IK channels were stained as described in the **Methods (Chapter 2)**. The antibodies which gave the best results were subsequently used to try to detect the presence of channels in native tissues and investigate the possibility of co-assembly of SK channels in cell lines.

Name of antibody	Target protein	Epitope
L155	hSK1	CSSPYRWTPVAPSDYG
rb185	rSK1	PEAGRPRQPTQGPGLQMC
rb196	rSK1	PEAGRPRQPTQGPGLQMC
rb186	rSK1	CSPQSHWLPTTASDYG
rb200	rSK1	CSPQSHWLPTTASDYG
UCL55	rSK1	MSSRSHNGSVGRPLGSGPGY
UCL56	rSK1	KLPPPWPGPSHLTAA
M1	hSK2 and rSK2	CRRSSSTAPPTSSESS
M75	hSK3 and rSK3	DTSGHFHDSGVGDLDC
Anti-SK3	hSK3 and rSK3	DTSGHFHDSGVGDLDEDPKC
M16	hIK	GGDLVLGLGALRRRKC
M20	hIK	GGDLVLGLGALRRRKC
M4	hIK	CALGPRQLPEPSQQSK
M5	hIK	CALGPRQLPEPSQQSK
R212	rIK	CQPPEPIQEAT
R224	rIK	CQPPEPIQEAT

Table 3.1 A table of the antibodies designed to recognise either human or rat SK/IK channel proteins. Each antibody epitope is shown. These epitopes do not always match the target protein sequence perfectly because a cysteine is frequently added to the sequence in order to facilitate antibody purification. Deviations of the epitopes from the exact peptide sequences are indicated in red.

3.2 Results

3.2.1 Negative controls

Several types of "negative" control experiments were carried out. First, experiments were performed to confirm that the anti-SK/IK antibodies would not cross react with native proteins in the HEK 293 cells. Each individual antibody was therefore initially tested on the untransfected HEK cell line. Secondly, as a control for the CY3-conjugated secondary antibody, it was applied alone to ensure that levels of background staining were suitably low. rSK2 and rSK3 are the most closely related of the rSK channels on the basis of sequence similarity. For this reason, a third type of control experiment was performed using the anti-rSK2 antibody (M1) to stain CHO cells stably expressing rSK3, to ensure that there was no cross-reactivity of the M1 antibody with the rSK3 channel protein. One final experiment was designed to look at whether antibodies raised against one species might recognise the channel protein of another. For this purpose, the anti-rSK1 antibodies were applied to HEK 293 cells stably expressing the hSK1 channel protein. Although there are similarities between the anti-rSK1 antibody epitopes and the corresponding regions of the hSK1 peptide sequence, there may be enough difference to ensure that there is no cross-reactivity between the rat-specific antibodies and the hSK1 channel protein.

Figure 3.1 (A-D) gives typical examples of the staining produced when the anti-SK/IK channel antibodies are used with untransfected HEK 293 cells. In each case it can be seen that there is no specific staining and only a fairly minimal level of non-specific background staining. This was true for all of the primary antibodies tested in this chapter. In addition,

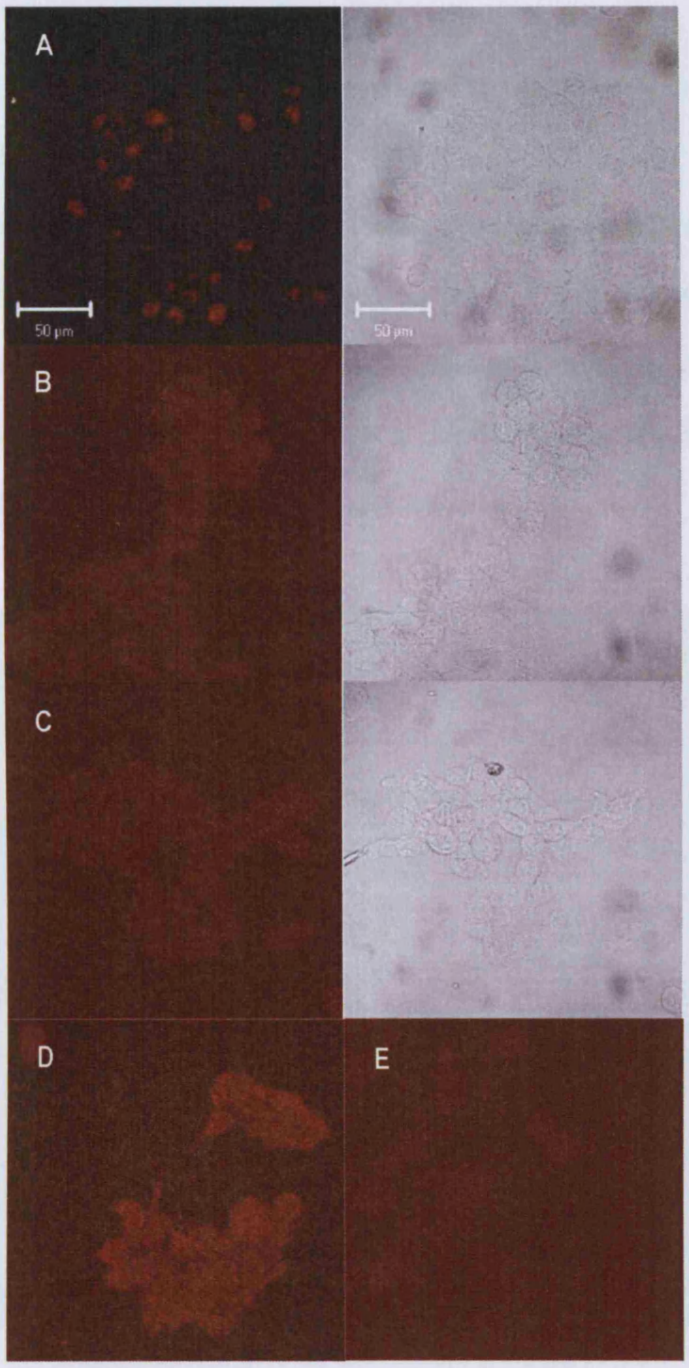

Figure 3.1 Negative control experiments using anti-SK/IK antibodies and the CY3 secondary antibody. Typical examples of staining of cells from two mammalian cell lines; HEK 293 cells (**A**-**D**) and CHO cells stably transfected with rSK3 (panel **E**), were stained with primary antibodies for SK1, SK2 and SK3 and the CY3 labelled goat anti-rabbit secondary antibody. **A**, Cells stained with the anti-SK1 antibody rb200. **B**, cells stained with the anti-SK2 antibody M1. **C**, cells stained with the anti-SK3 antibody M75. **D**, cells stained with the CY3-labelled secondary antibody. **E**, CHO cells stably expressing rSK3 stained with the anti-rSK2 antibody (M1) to ensure there is no cross reactivity of the antibody the rSK3 channel protein. For **A**, **B** and **C**, the left-hand panel shows the stained cells while the right-hand panel shows the corresponding brightfield. The scalebar in **A** also applies to **B**, **C**, **D** and **E**.

the staining results for the anti-rSK2 antibody produced negative results in rSK3 CHO cells (**Figure 3.1 E**).

Finally, experiments using the anti-rSK1 antibodies show that they did not produce any positive staining in the HEK 293 cells expressing hSK1. **Figure 3.1** and **3.2** shows that the antibodies designed to target the rSK1 channel appear to be species specific. Also, the results depicted in **Figure 3.1** establish the suitability of HEK 293 cells and the Cy3-conjugated secondary antibody for the positive controls.

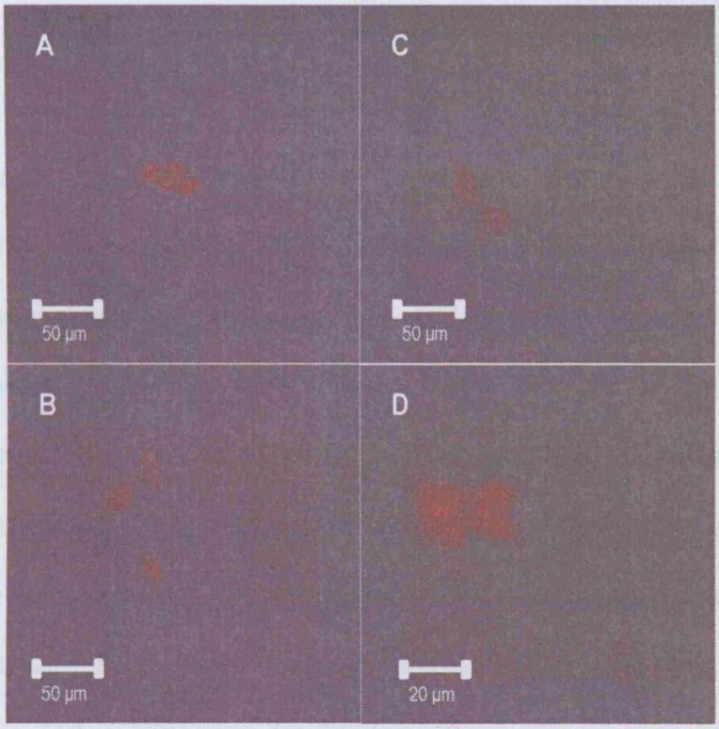

Figure 3.2 The four different anti-rSK1 antibodies do not produce specific staining in a HEK 293 cell line stably expressing hSK1. **A** and **B** show the results with the two N-terminal antibodies rb185 and rb196 respectively and **C** and **D** with the two C-terminal antibodies rb186 and rb200.

3.2.2 rSK1 antibodies

Of the six antibodies available to test on the rSK1 protein, three were raised against N-terminal epitopes (rb185, rb196 and UCL55) while the remaining three were designed to different regions of the C-terminal domain (rb186, rb200 and UCL56). Two different plasmids were employed to transfect HEK 293 cells in order to determine whether these antibodies would be useful in identifying the rSK1 channel protein. One plasmid was designed to express the native rSK1 protein while the other was modified to express a fusion protein of rSK1 and the yellow fluorescent protein (YFP). To identify transfected cells when using the native rSK1, the rSK1 plasmid was co-transfected with the QBI plasmid which expresses the green fluorescent protein (GFP).

The rSK1 channel has been reported not to produce detectable SK current in transfected cell lines (Bowden *et al.*, 2001; Benton *et al.*, 2003; D'Hoedt *et al.*, 2004). This may have been due to several reasons, one of which is that the channel protein is simply not expressed. This makes it difficult to test the antibodies as a negative result could occur because the antibody does not work, or because there is no protein to detect. It was for this reason that the YFP-tagged rSK1-containing plasmid was used. **Figure 3.3** shows that YFP fluorescence can be detected in transfected cells indicating that the plasmid is expressed. Furthermore, the C-terminal anti-rSK1 antibodies (rb186 and UCL56) produce a pattern of positive staining that closely resembles the distribution of the YFP tag, indicating that the antibodies recognise the channel protein. Interestingly both the YFP and antibody staining signals indicate that it is mostly within intracellular compartments of transfected cells.

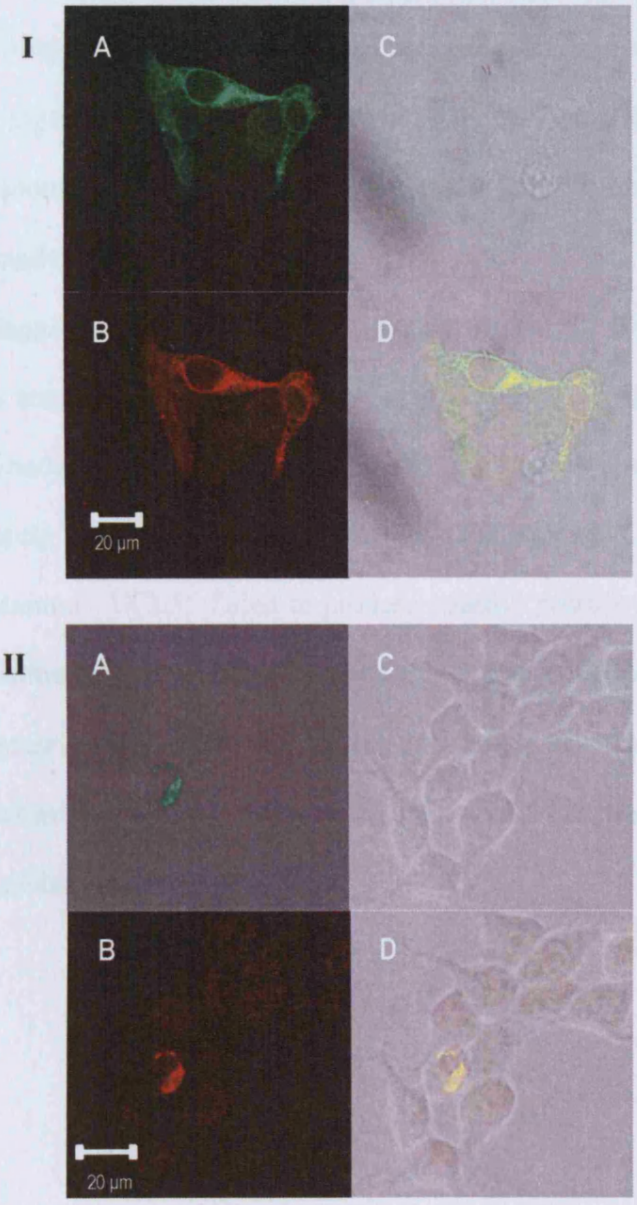

Figure 3.3 The YFP-tagged construct expresses when transiently transfected in HEK 293 cells and is recognised by anti-rSK1 antibodies. **IA** and **IIA** show YFP fluorescence. The rSK1 channel protein is also positively stained with the C-terminal antibodies rb186 (**IB**) and UCL56 (**IIB**). The bright-field images (**C**) and overlays of **A**, **B** and **C** (**D**) are also shown. In both cases the overlay shows that the YFP fluorescence and the antibody staining coincide well indicating that the antibodies do indeed recognise the channel protein. (YFP fluorescence appears green due to the use of a green filter).

Next, the C-terminal antibodies were tested on HEK 293 cells expressing the native rSK1 construct along with a plasmid containing GFP. The positive staining signal seen in **Figure 3.4** illustrates that the C-terminal anti-rSK1 antibodies also recognise the native channel protein. As with experiments using the YFP-tagged rSK1 construct, the rSK1 channel protein does not seem to localise at the cell membrane but is frequently distributed throughout the cell.

As the YFP-tagged rSK1 construct has the tag inserted at the N-terminal end, it was decided not to test rb185, rb196 or UCL55 using this plasmid as the YFP may have prevented antibody binding. However, **Figure 3.5** shows the results of staining experiments using the N-terminal antibodies on HEK 293 cells transfected with the native rSK1 plasmid. UCL55 failed to produce specific positive staining, so was not used in any further experiments. However, rb185 and rb196 produced comparable results to the other anti-SK1 antibodies in that they gave a bright positive signal with a distribution that gives the impression that the majority of the channel protein remains trapped intracellularly.

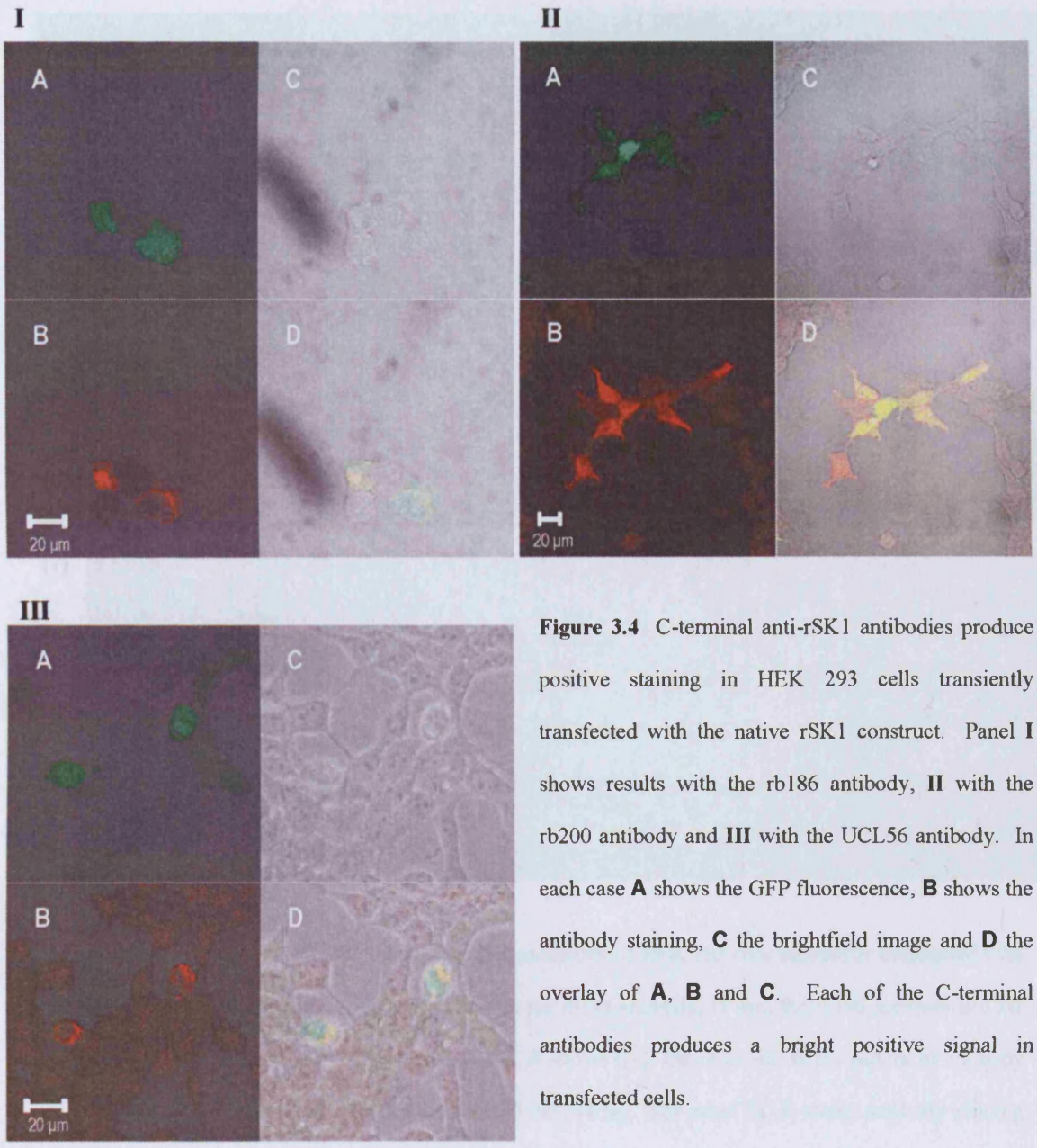

Figure 3.4 C-terminal anti-rSK1 antibodies produce positive staining in HEK 293 cells transiently transfected with the native rSK1 construct. Panel **I** shows results with the rb186 antibody, **II** with the rb200 antibody and **III** with the UCL56 antibody. In each case **A** shows the GFP fluorescence, **B** shows the antibody staining, **C** the brightfield image and **D** the overlay of **A**, **B** and **C**. Each of the C-terminal antibodies produces a bright positive signal in transfected cells.

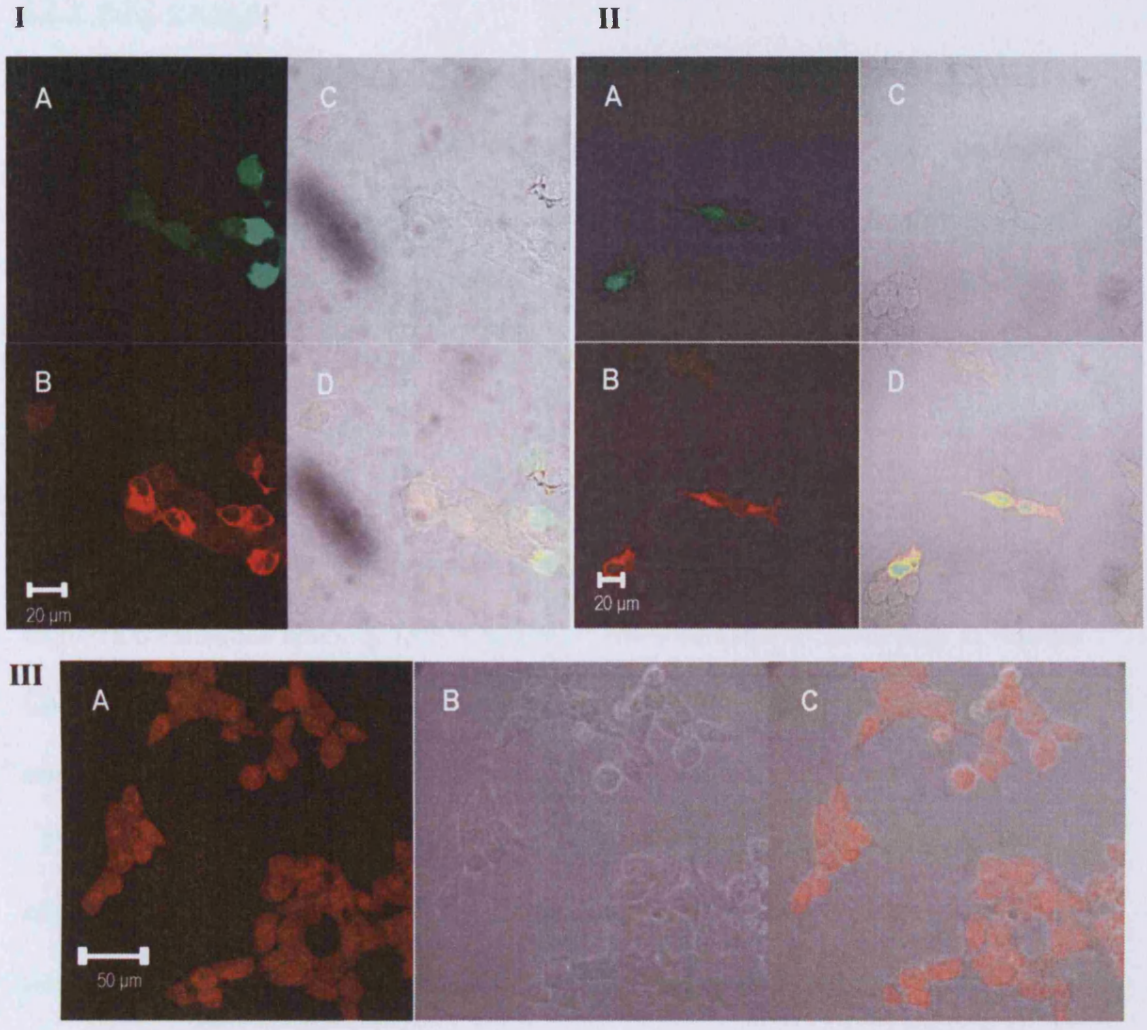

Figure 3.5 Staining with N-terminal anti-rSK1 antibodies of HEK 293 cells transiently transfected with the native rSK1 construct. **I**, staining seen with the rb185 antibody, **II** with the rb196 antibody and **III** with the UCL55 antibody. For panels I and II, **A** shows GFP fluorescence, **B** the pattern of antibody staining, **C** the brightfield image of cells and **D** the overlay. For panel III, **A** shows antibody staining results, **B** the brightfield and **C** the overlay. While there is a strong positive signal seen in transfected cells with the rb185 and rb196 antibodies, there does not appear to be any specific positive staining with the UCL55 antibody, just a high level of background.

3.2.3 rSK2 staining

The M1 antibody is specific to the last seventeen amino acids of the rSK2 sequence (see **Table 3.1** and **Figure 2.1** of **Methods**). When HEK 293 cells transiently transfected with the SK2 plasmid are stained with this antibody, a strong positive signal is seen (see **Figure 3.6**). Interestingly the fluorescence from the SK2 staining is dispersed quite densely throughout the cell.

3.2.4 rSK3 staining

There were two antibodies available to test for rSK3 the first being M75 and the second a commercial antibody from Chemicon. The two epitopes differ only in that the Chemicon antibody includes an additional four amino acids at the C-terminal end. Both are directed towards the N-terminal region of the SK3 protein.

Figure 3.7 demonstrates that both M75 and the commercial antibody produce a bright and specific positive signal. The vast majority of the protein seems to be present at or near the cell surface membrane with comparatively little seen in the intracellular region.

3.2.5 Distribution of SK channel proteins in transfected HEK 293 cells

The distributions of the rSK1, rSK2 and rSK3 channel proteins appear to differ quite substantially. This is perhaps best illustrated using intensity profiles of the antibody staining seen for the cells depicted in **Figures 3.3 IB, IIB, 3.6 B** and **3.7 IIB** as shown in **Figure 3.8**. The peaks seen correspond with the regions showing the brightest fluorescence.

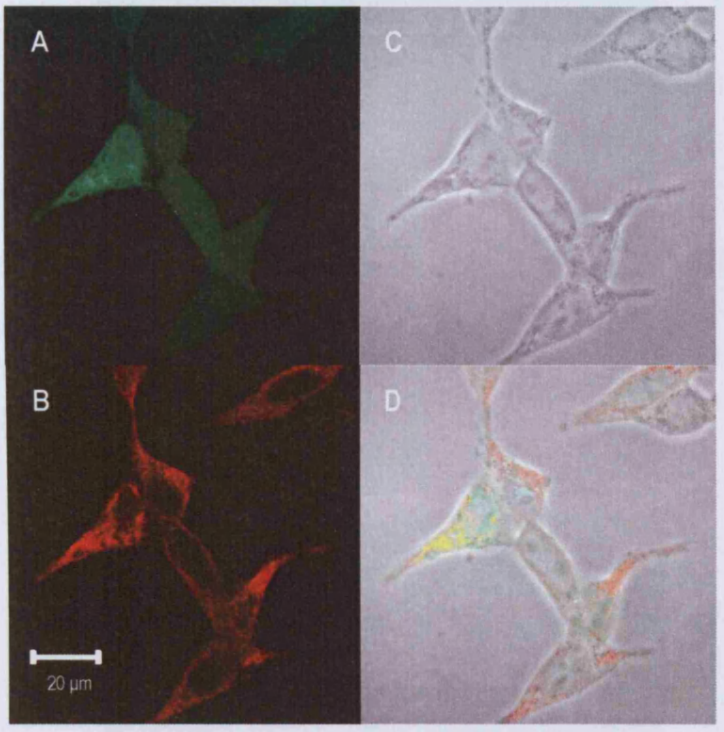

Figure 3.6 The anti-SK2 antibody (M1) produces positive staining in HEK 293 cells transfected with rSK2. **A**, GFP fluorescence from transfected cells. **B**, staining with the anti-SK2 antibody M1. **C**, brightfield image. **D**, overlay of images **A**, **B** and **C**. SK2 appears to be expressed throughout the cell with the exception that the signal is excluded from the nucleus.

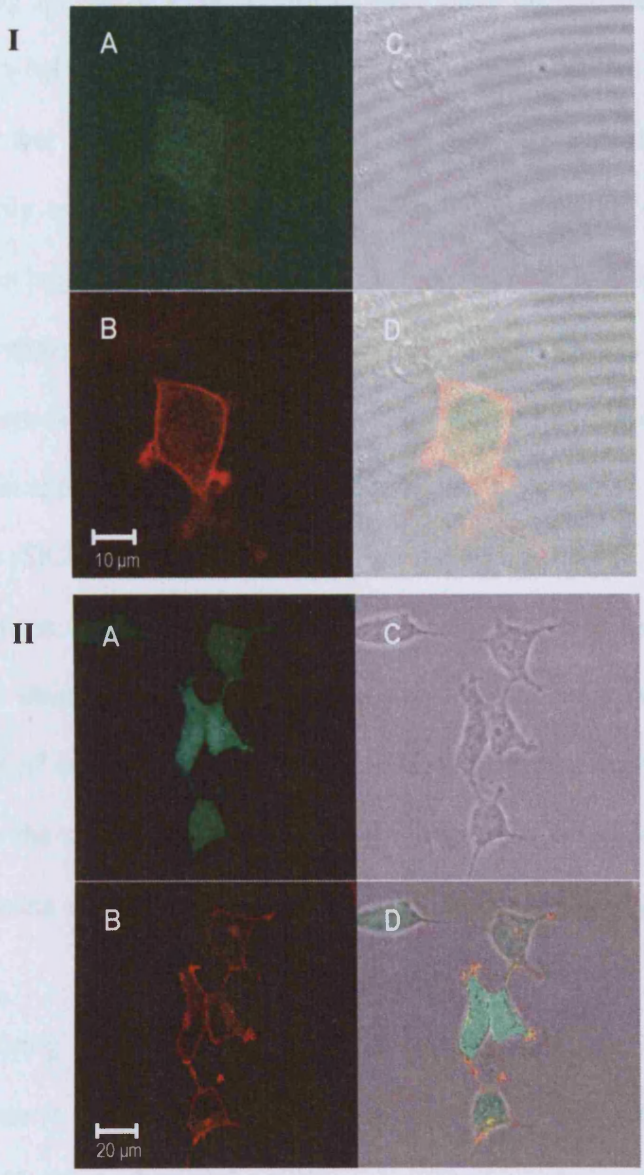

Figure 3.7 Anti-SK3 antibodies recognise the channel protein in HEK 293 cells transiently transfected with the rSK3 construct. **I,** staining results seen using the M75 antibody. **II,** staining seen using the Chemicon anti-SK3 antibody. In both **I** and **II, A** shows GFP fluorescence from transfected cells. **B**, staining with the anti-SK3 antibodies. **C**, brightfield image. **D**, overlay of images **A**, **B** and **C**. SK3 can clearly be seen at or near the plasma membrane of transfected cells using both anti-SK3 antibodies.

Of the three different channel proteins, rSK1 appears to show the greatest diversity in terms of distribution across the cell. **Figure 3.8 A** shows a cell transfected with rSK1 where the staining appears as a fine meshwork throughout the cell with the exception of a large area excluded by the nucleus. This is reflected in the profile of the intensity of staining. In another cell transfected with rSK1, the protein appears to be "clumped together" primarily on one side of the cell (**Figure 3.8 B**). In this case, the intensity profile shows one large set of peaks that are relatively uniform in height indicating that the fluorescence appears to be restricted to one region. Again there is a large area of the profile where there is no staining seen due to the exclusion by the cell's nucleus, but little or no protein appears on the opposite side of the nucleus.

In contrast, the rSK2 and rSK3 channel proteins showed very little variability in their cellular distributions. **Figure 3.8 C** shows a typical example of the rSK2 pattern of staining. rSK2 staining consistently had a "web-like" appearance which extended throughout most of the cell. This is illustrated well by the intensity profile of a cell transfected with the rSK2 plasmid. There are a large number of peaks showing that there are high levels of fluorescence across the cell, although the signal is excluded by the nucleus.

The rSK3 staining appears as a bright punctate signal at, or close to, the cell membrane. There is no bright intracellular staining seen, which makes the pattern of staining very different to that of the rSK1 and rSK2 channel proteins. The intensity profile shows two clear peaks in the region of the cell membrane.

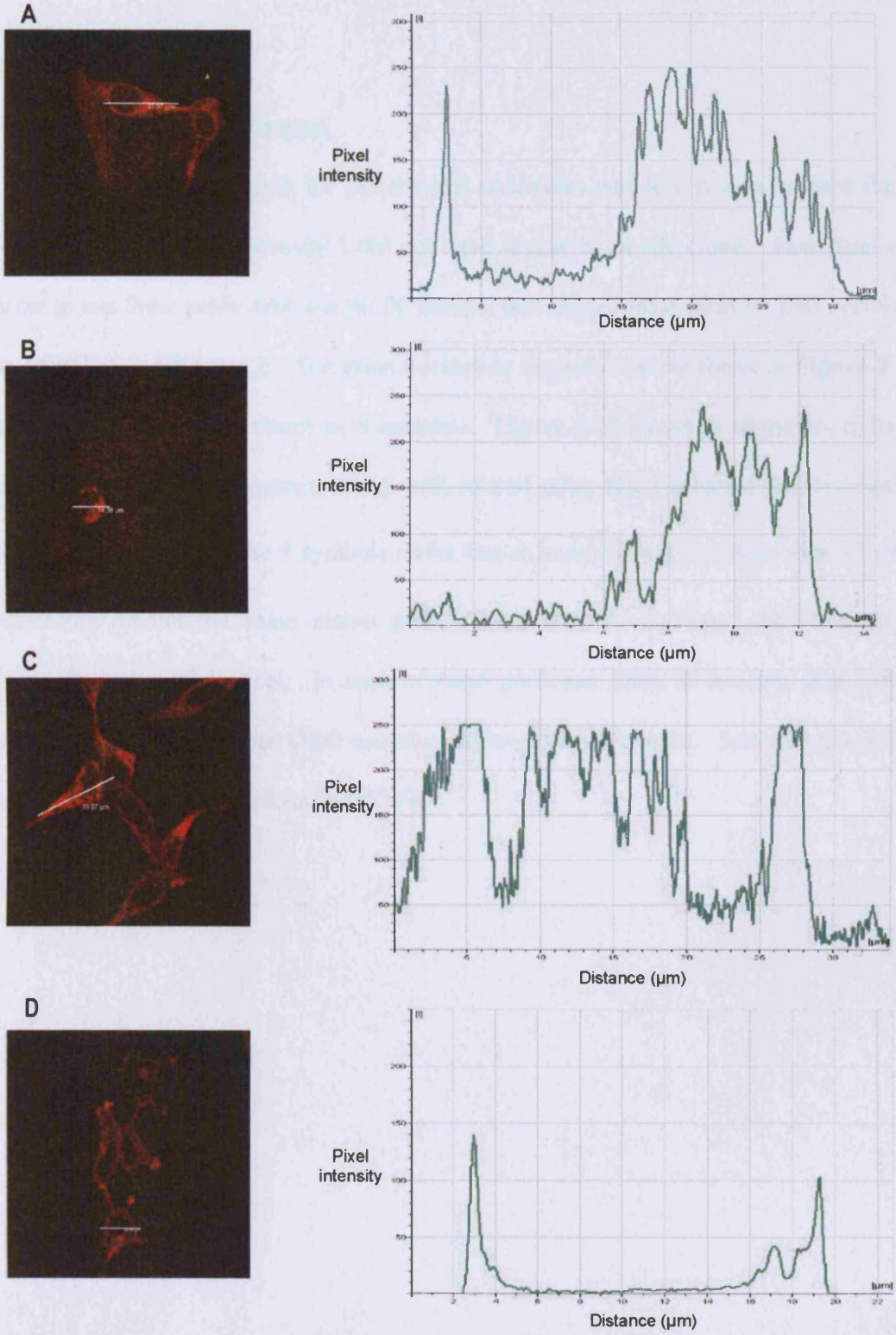

Figure 3.8 Intensity profiles show the differences in distribution of fluorescence seen for rSK1, rSK2 and rSK3 antibody staining. **A**, staining seen with the anti-rSK1 antibody rb186. **B**, staining seen with the anti-rSK1 antibody UCL56. **C**, staining seen with the anti-rSK2 antibody M1. **D**, staining seen with the Chemicon anti-SK3 antibody. In each case the staining is shown in the image on the left. The white bar indicates the section represented by the profile on the right. Peaks correspond to the regions of brightest fluorescence.

3.2.6 rIK staining

3.2.6.1 Cloning the rIK channel

Producing positive controls for the anti-rIK antibodies was less straightforward than for the SK channels as initially I did not have access to an rIK clone. Therefore, in order to test these antibodies, the rat IK channel was cloned from adult rat DRG cDNA as described in **Chapter 2**. The exact nucleotide sequence can be found in **Figure 3.9** along with the predicted amino acid sequence. **Figure 3.10** shows an alignment of this predicted rIK protein sequence along with several other rIK sequences as previously reported in Genbank. The * symbols under this alignment mark positions where in all sequences predict the same amino acid. There are six positions where the four sequences are not identical. In each of these positions, three of the four sequences agree. In all cases the rat DRG sequence follows the consensus. Interestingly, it is identical to the Genbank clone Q9QYW1.

```
M  G  G  E  L  V  T  G  L  G  A  L  R  R  R  K  R  L  L  E
atgggcggggagctggtgactggcctgggggccctgagacggagaaagcgcctgctggag
---------+---------+---------+---------+---------+---------+---------+60
tacccgcccctcgaccactgaccggacccccgggactctgcctctttcgcggacgacctc
Q  E  K  R  V  A  G  W  A  L  V  L  A  G  T  G  I  G  L  M
caggagaagagggtggccggctgggcactggtactggcgggaactggcatcggactcatg
---------+---------+---------+---------+---------+---------+---------+120
gtcctcttctcccaccggccgacccgtgaccatgaccgcccttgaccgtagcctgagtac
V  L  H  A  E  M  L  W  F  L  G  C  K  W  V  L  Y  L  L  L
gtgctgcacgctgagatgttgtggttcctgggttgcaagtgggtgctgtacctgctcttg
---------+---------+---------+---------+---------+---------+---------+180
cacgacgtgcgactctacaacaccaaggacccaacgttcacccacgacatggacgagaac
V  K  C  L  I  T  L  S  T  A  F  L  L  C  L  I  V  V  F  H
gttaagtgtttaatcacgctgtccactgccttcctcctttgtcttattgtggtcttccat
---------+---------+---------+---------+---------+---------+---------+240
caattcacaaattagtgcgacaggtgacggaaggaggaaacagaataacaccagaaggta
A  K  E  V  Q  L  F  M  T  D  N  G  L  R  D  W  R  V  A  L
gccaaggaggtccagctgttcatgactgacaacgggctccgggactggcgcgtggcgctg
---------+---------+---------+---------+---------+---------+---------+300
cggttcctccaggtcgacaagtactgactgttgcccgaggccctgaccgcgcaccgcgac
T  R  R  Q  V  A  Q  I  L  L  E  L  L  V  C  G  V  H  P  V
acccggcggcaggtggcgcagatcctgctggagctgctggtatgcggggtgcacccggtg
---------+---------+---------+---------+---------+---------+---------+360
tgggccgccgtccaccgcgtctaggacgacctcgacgaccatacgccccacgtgggccac
P  L  R  S  P  H  C  T  L  A  G  E  A  T  D  S  Q  A  W  P
cccctacggagcccgcactgcaccctggcgggggaggccacagactcacaggcctggccg
---------+---------+---------+---------+---------+---------+---------+420
ggggatgcctcgggcgtgacgtgggaccgccccctccggtgtctgagtgtccggaccggc
G  F  L  G  E  G  E  A  L  L  S  L  A  M  L  L  R  L  Y  L
ggcttcctgggcgaaggcgaggcgttgctgtccctggccatgctgctacgtctctacctg
---------+---------+---------+---------+---------+---------+---------+480
ccgaaggacccgcttccgctccgcaacgacagggaccggtacgacgatgcagagatggac
V  P  R  A  V  L  L  R  S  G  V  L  L  N  A  S  Y  R  S  I
gtgcctcgcgcggtacttctgcgtagcggggtcctgctcaacgcgtcttaccgcagcatc
---------+---------+---------+---------+---------+---------+---------+540
cacggagcgcgccatgaagacgcatcgccccaggacgagttgcgcagaatggcgtcgtag
G  A  L  N  Q  V  R  F  R  H  W  F  V  A  K  L  Y  M  N  T
ggggcgctcaaccaagtccgattccgccactggttcgtggccaaactatacatgaacacg
---------+---------+---------+---------+---------+---------+---------+600
ccccgcgagttggttcaggctaaggcggtgaccaagcaccggtttgatatgtacttgtgc
H  P  G  R  L  L  L  G  L  T  L  G  L  W  L  T  T  A  W  V
cacccgggtcgcctgcttctgggcctcacgctgggcctntggctcaccacagcttgggtg
---------+---------+---------+---------+---------+---------+---------+660
gtgggcccagcggacgaagacccggagtgcgacccgganaccgagtggtgtcgaacccac
L  S  V  A  E  R  Q  A  V  N  A  T  G  H  L  T  D  T  L  W
ctgtctgtggctgagaggcaggctgtcaatgccacgggacacctcacagacacactgtgg
---------+---------+---------+---------+---------+---------+---------+720
gacagacaccgactctccgtccgacagttacggtgccctgtggagtgtctgtgtgacacc
L  I  P  I  T  F  L  T  I  G  Y  G  D  V  V  P  G  T  L  W
ctgatacccatcacgttcctgaccattggctatggggacgtcgtacctggcaccctatgg
---------+---------+---------+---------+---------+---------+---------+780
gactatgggtagtgcaaggactggtaaccgataccctgcagcatggaccgtgggatacc
G  K  I  V  C  L  C  T  G  V  M  G  V  C  C  T  A  L  L  V
ggcaagattgtctgcttgtgcaccggagtcatggggtctgctgcacggctctactagtg
---------+---------+---------+---------+---------+---------+---------+840
ccgttctaacagacgaacacgtggcctcagtacccccagacgacgtgccgagatgatcac
A  V  V  A  R  K  L  E  F  N  K  A  E  K  H  V  H  N  F  M
gctgtggtggcccggaagctggagttcaacaaggcggagaaacacgtgcacaacttcatg
---------+---------+---------+---------+---------+---------+---------+900
cgacaccaccgggccttcgacctcaagttgttccgcctctttgtgcacgtgttgaagtac
M  D  I  H  Y  A  K  E  M  K  E  S  A  A  R  L  L  Q  E  A
atggacatccattatgccaaagagatgaaggagtcggccgctcggctgctgcaggaagcc
---------+---------+---------+---------+---------+---------+---------+960
tacctgtaggtaatacggtttctctacttcctcagccggcgagccgacgacgtccttcgg
W  M  Y  Y  K  H  T  R  R  K  D  S  R  A  A  R  R  H  Q  R
tggatgtactacaaacacactcgaaggaaggactcccgagcggctcgcaggcatcagcgc
---------+---------+---------+---------+---------+---------+---------+1020
acctacatgatgtttgtgtgagcttccttcctgagggctcgccgagcgtccgtagtcgcg
K  M  L  A  A  I  H  T  F  R  Q  V  R  L  K  H  R  K  L  R
aagatgctggctgccatccacacgttccgccaggtacggctgaaacatcggaagctccgg
---------+---------+---------+---------+---------+---------+---------+1080
ttctacgaccgacggtaggtgtgcaaggcggtccatgccgactttgtagccttcgaggcc
E  Q  V  N  S  M  V  D  I  S  K  M  H  M  I  L  C  D  L  Q
gaacaagtgaattccatggtggacatctccaagatgcacatgatcctgtgcgacctgcag
---------+---------+---------+---------+---------+---------+---------+1140
cttgttcacttaaggtaccacctgtagaggttctacgtgtactaggacacgctggacgtc
L  G  L  S  A  S  H  L  A  L  E  K  R  I  D  G  L  A  G  K
ctcgggctcagcgcctcgcaccttgccctggagaagagaatcgatgggctggcagggaag
---------+---------+---------+---------+---------+---------+---------+1200
gagcccgagtcgcggagcgtggaacgggacctcttctcttagctacccgaccgtccttc
L  D  A  L  T  E  L  L  S  T  A  L  Q  Q  Q  Q  P  P  E  P
ctggatgccctgactgaactgctcagtactgccctgcagcagcagcagccgccagaaccc
---------+---------+---------+---------+---------+---------+---------+1260
gacctacgggactgacttgacgagtcatgacgggacgtcgtcgtcgtcggcggtcttggg
I  Q  E  A  T
atccaggaggcca
---------+---1273
taggtcctccggt
```

Figure 3.9 Nucleotide and predicted amino acid sequence of the rIK channel cloned from rat DRG cDNA as described in **Chapter 2**. The amino acids are represented by single letter codes.

```
Cloned rIk      MGGELVTGLGALRRRKRLLEQEKRVAGWALVLAGTGIGLMVLHAEMLWFLGCKWVLYLLL 60
CAB40141.2      MGGELVTGLGALRRRKRLLEQEKRVAGWALVLAGTGIGLMVLHAEMLWFLGCKWVLYLLL 60
Q9QYW1          MGGELVTGLGALRRRKRLLEQEKRVAGWALVLAGTGIGLMVLHAEMLWFLGCKWVLYLLL 60
NP_075410.1     MGGELVTGLGALRRRKRLLEQEKRVAGWALVLAGTGIGLMVLHAEMLWFLGCKWVLYLLL 60
                ************************************************************

Cloned rIk      VKCLITLSTAFLLCLIVVFHAKEVQLFMTDNGLRDWRVALTRRQVAQILLELLVCGVHPV 120
CAB40141.2      VKCLITLSTAFLLCLIVVFHAKEVQLFMTDNGLRDWRVALTRRQVAQILLELLVCGVHPV 120
Q9QYW1          VKCLITLSTAFLLCLIVVFHAKEVQLFMTDNGLRDWRVALTRRQVAQILLELLVCGVHPV 120
NP_075410.1     VKCLITLSTAFLLCLIVVFHAKEVQLFMTDNGLRDWRVALTRRQVAQILLELLVCGVHPV 120
                ************************************************************

Cloned rIk      PLRSPHCTLAGEATDSQAWPGFLGEGEALLSLAMLLRLYLVPRAVLLRSGVLLNASYRSI 180
CAB40141.2      PLRSPHCTLAGEATDSQAWPGFLGEGEALLSLAMLLRLYLVPRAVLLRSGVLLNASYRSI 180
Q9QYW1          PLRSPHCTLAGEATDSQAWPGFLGEGEALLSLAMLLRLYLVPRAVLLRSGVLLNASYRSI 180
NP_075410.1     PLRSPHCTLAGEATDSQAWPGFLGEGEALLSLAMLLRLYLVPRAVLLRSGVLLNASYRSI 180
                ************************************************************

Cloned rIk      GALNQVRFRHWFVAKLYMNTHPGRLLLGLTLGLWLTTAWVLSVAERQAVNATGHLTDTLW 240
CAB40141.2      GALNQVRFRHWFVAKLYMNTHPGRLLLGLTLGFWLTTAWVLSVAERQAVNATGHLTDTLW 240
Q9QYW1          GALNQVRFRHWFVAKLYMNTHPGRLLLGLTLGLWLTTAWVLSVAERQAVNATGHLTDTLW 240
NP_075410.1     GALNQVRFRHWFVAKLYMNTHPGRLLLGLTLGLWLTTAWVLSVAERQAVNATGHLTDTLW 240
                ********************************:***************************

Cloned rIk      LIPITFLTIGYGDVVPGTLWGKIVCLCTGVMGVCCTALLVAVVARKLEFNKAEKHVHNFM 300
CAB40141.2      LIPITFLTIGYGDVVPGTLWGKIVCLCTGVMGVCCTALLVAVVARKLEFNKAEKHVHNFM 300
Q9QYW1          LIPITFLTIGYGDVVPGTLWGKIVCLCTGVMGVCCTALLVAVVARKLEFNKAEKHVHNFM 300
NP_075410.1     LIPITFLTIGYGDVVPGTLWGKIVCLCTGVMGVCCTALLLAVVARKLEFNKAEKHVHNFM 300
                ************************************:*******************

Cloned rIk      MDIHYAKEMKESAARLLQEAWMYYKHTRRKDSRAARRHQRKMLAAIHTFRQVRLKHRKLR 360
CAB40141.2      MDIHYAKEMKESAARLLQEAWMYYKHTRRKDSRAARRHQRKMLAAIHTFRQVRLKHRKLR 360
Q9QYW1          MDIHYAKEMKESAARLLQEAWMYYKHTRRKDSRAARRHQRKMLAAIHTFRQVRLKHRKLR 360
NP_075410.1     MDIHYAKEMKESAARLLQEAWMYYKHTRRKDSRAARRHQRKMLAAIHTFRQVRLKHRKLR 360
                ************************************************************

Cloned rIk      EQVNSMVDISKMHMILCDLQLGLSASHLALEKRIDGLAGKLDALTELLSTALQQQQPPEP 420
CAB40141.2      EQVNSMVDISKMHMILCDLQLGLSASHLALEKRIDGLAGKLDALTELLSTALQQQQPPEP 420
Q9QYW1          EQVNSMVDISKMHMILCDLQLGLSASHLALEKRIDGLAGKLDALTELLSTALQQQQPPEP 420
NP_075410.1     EQVNSMVDISKMHMILCDLQLGLSASHLALEKRIHGLARKLDALTELLSSALQQQ-PPEP 419
                **********************************.*** **********:***** ****

Cloned rIk      IQEAT 425
CAB40141.2      IQEAT 425
Q9QYW1          IQEAT 425
NP_075410.1     IQEAT 424
                *****
```

Figure 3.10 A comparison of the predicted amino acid sequences of the rIK channel. The alignment was performed with ClustalW software using sequences reported under the following Genbank accession numbers: CAB40141.2, Q9QYW1 and NP_075410.1 and the sequence of the rIK cloned from DRG cDNA reported in this thesis. The cloned rIK sequence is identical to the Q9QYW1 sequence. The "*" symbol marks positions where the amino acids are identical in all sequences while the ":" and "." symbols mark conservative or semi-conservative differences respectively.

3.2.6.2 Formation of functional rIK channels

Once the rIK clone had been sequenced to ensure its integrity and identity, whole-cell voltage clamp using transiently transfected HEK 293 cells was carried out (by Dr David Benton, Department of Pharmacology, UCL) to determine whether it expressed functional IK channels. Typical whole-cell currents seen in response to a series of voltage steps are shown in **Figure 3.11** Such currents are not seen in untransfected wild-type cells. The currents produced when HEK 293 are transfected with the rIK channel are substantially blocked in the presence of 10 μM clotrimazole (**Figure 3.11**), a known IK channel blocker

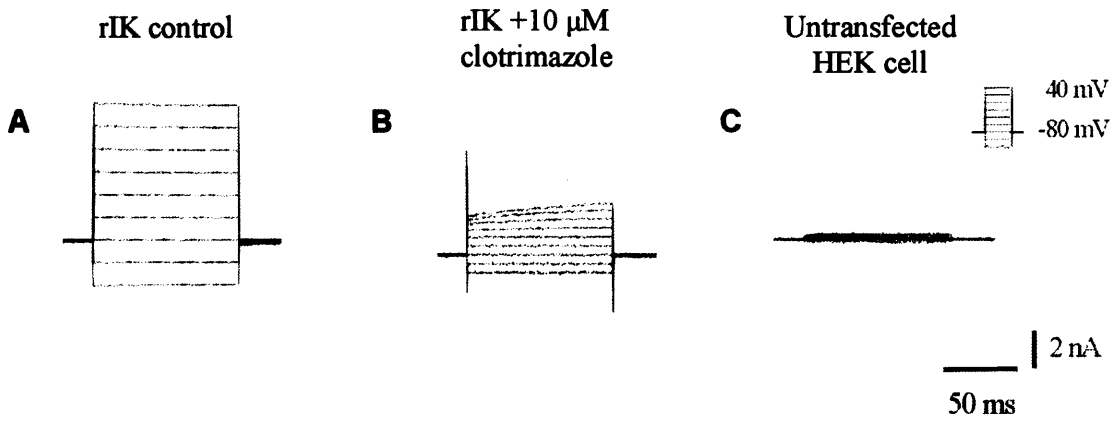

Figure 3.11 The DRG rIK clone forms functional channels when expressed in HEK 293 cells. **A**, typical whole-cell currents recorded from a cell transfected with the rIK clone, which are not seen in untransfected WT cells (**C**). The cells were held at -80 mV and subjected to 100 ms voltage steps in 20 mV increments from -120 mV to +40 mV (see inset). **B**, the currents are substantially reduced in the presence of 10 μM clotrimazole. Channels were activated by including 1 μM free Ca^{2+} in the pipette solution. The composition of the bathing solution was (in mM): NaCl 140, KCl 5, $MgCl_2$ 1, $CaCl_2$ 2, glucose 10, HEPES 10, adjusted to pH 7.4 with NaOH. The pipette solution contained (in mM): KCl 130, HEPES 10, K_2HEDTA 5 and 1.2 $CaCl_2$ adjusted to pH 7.2 with KOH. Data were digitised at 5kHz and filtered at 1 kHz.

(Alvarez *et al.*, 1992; Brugnara *et al.*, 1993; Jensen *et al.*, 1998). These results together suggest that the rIK pore-forming subunit protein is expressed in HEK 293 cells where the protein subunits assemble to form functional channels.

3.2.6.3 Staining in rIK transfected cells

Having cloned the rIK channel and established that it is functional when expressed in mammalian cells, further transfections were carried out to test the anti-rIK antibodies R212 and R224. The results are presented in **Figure 3.12**. Although both antibodies are designed to the same C-terminal epitope, the results are quite different. With R224, there is no clear sign of any specific staining in the cells that show GFP expression. Thus R224 would be unsuitable for the purpose of examining rIK expression in native tissues. In contrast, the R212 antibody produces a clear positive stain for the rIK channel protein, which correlates well with GFP expression. **Figure 3.12** illustrates that R212 gives a strong positive signal, most of which appears to be located close to the cell surface membrane.

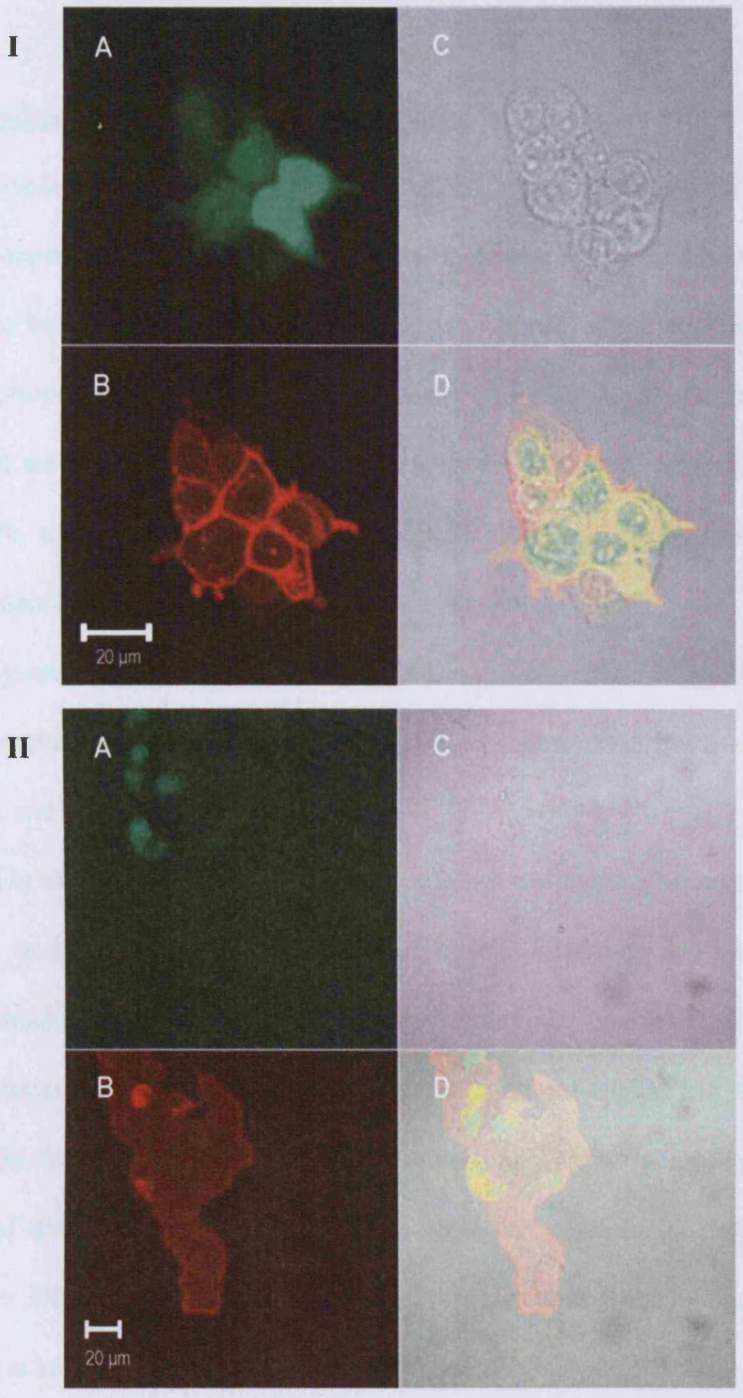

Figure 3.12 Staining seen with rat specific anti-IK channel antibodies, of HEK 293 cells transiently transfected with the rIK construct. **I,** staining results seen using the R212 antibody. **II,** staining seen using the R224 antibody. **A** shows GFP fluorescence from transfected cells. **B**, staining with the anti-IK antibodies. **C** shows the brightfield image and **D** an overlay of images **A**, **B** and **C**. Only the R212 antibody produces a positive signal (**IB**), which is located at or close to the cell membrane.

3.2.6 Antibodies to human SK/IK channel proteins

Of the antibodies described so far, M1 (anti-SK2) and M75 (anti-SK3) have been raised to epitopes in regions that are conserved between the rat and human sequences and so would be expected to work in both species. However the anti-rSK1 antibodies recognise epitopes in regions that are significantly different in the rat and human channels and the staining results in **Figure 3.2** showed that the rat specific antibodies (rb185, rb186, rb196 and rb200) were not able to recognise the human SK1 channel protein in a stable cell line established in HEK 293 cells.

An antibody specific to the human isoform was also available. When tested on CHO cells stably expressing hSK1 this antibody, L155, did produce a positive signal, albeit quite a weak one (see **Figure 3.13**)

In addition to the anti-SK1 channel antibodies, there were also a number of antibodies designed to recognise the human IK (hIK) channel. M16 and M20 are N-terminal specific antibodies while M4 and M5 are targeted to the C-terminal. **Figure 3.14 (A** and **B)** illustrates that, in CHO cells, M16 and M20 do not appear to produce staining that is specific for the channel protein. The staining appears to be more pronounced in the region of the cell nucleus. However, M4 and M5 seem to be more suitable for detecting the hIK channel. Panel (**C** and **D)** shows that these antibodies produce staining that is located at or near the cell membrane.

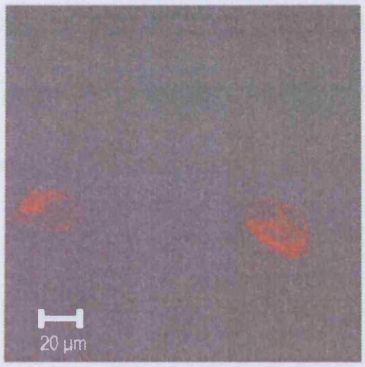

Figure 3.13 Positive staining produced by the L155 anti-hSK1 antibody using a CHO cell line stably expressing hSK1. The cells show a weak but clearly detectable signal.

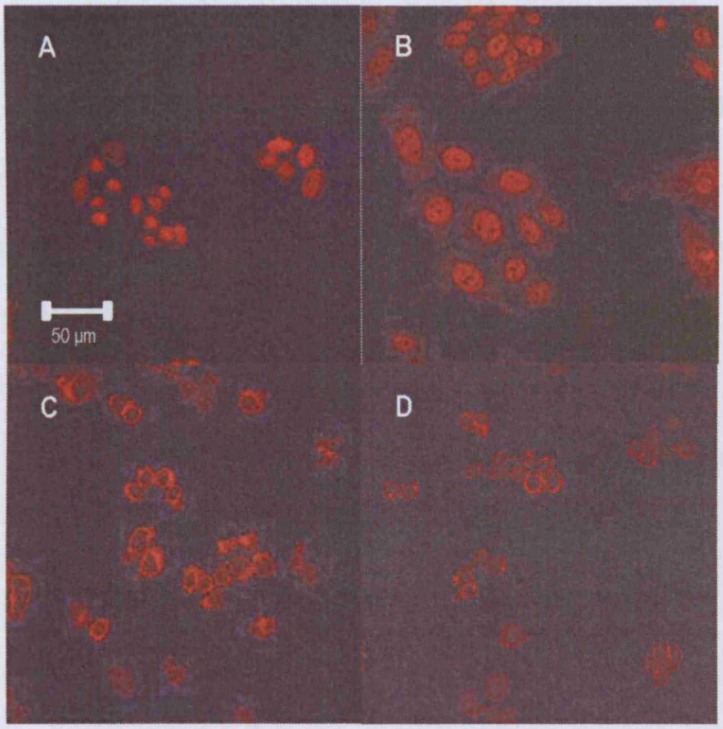

Figure 3.14 Staining of hIK CHO cells with antibodies targeted to the hIK channel protein. **A,** staining seen with the M16 antibody and **B**, with the M20 antibody. Both of these antibodies produce staining that seems to be limited to the nuclei of the cells. **C**, the M4 antibody and **D**, the M5 antibody, both of which are designed to a C terminal epitope, detect the channel protein in the area of the cell membrane. The scale bar in **A** also applies to **B**, **C** and **D**.

3.2.7 Co-expression of SK channels in HEK 293 cells

As noted earlier, and as shown in **Figure 3.15**, when expressed alone, the rat SK channels show distinctly different distributions within the cell. It is interesting, therefore to determine whether the distributions change when two subunits are expressed together. If they do, it would provide evidence of subunit interactions, possibly indicating co-assembly. This section, therefore, describes experiments using HEK 293 cells co-transfected with two different SK channel genes in order to determine whether evidence for subunit interactions can be found.

Figure 3.15 shows that rSK1 distribution is variable but the protein appears to remain trapped intracellularly. rSK2 produces a more constant staining pattern distributed across the cell probably reaching cell membrane. rSK3 differs again in that antibody staining consistently produces an "outline" of the cell, so appears at or in the region of the plasma membrane of transfected cells. This corresponds qualitatively quite well with what is known of the functional properties of these three different subtypes of channel when they are expressed in *Xenopus* oocytes or mammalian cell lines. Both rSK2 and rSK3 produce functional channels that exhibit typical SK channel properties (Köhler *et al.*, 1996; Shah & Haylett, 2000a; Strobæk *et al.*, 2000; Grunnet *et al.*, 2001; Hosseini *et al.*, 2001). rSK1, however, is not able to produce functional channels in heterologous expression systems (Bowden *et al.*, 2001, D'Hoedt *et al.*, 2004). The antibody staining results suggest that the channel protein remains trapped in the intracellular compartments of the cell. If rSK1 is somehow prevented from reaching the cell surface membrane, this would explain why there are no currents detected in cells transfected with the rSK1 construct (Bowden *et al.*, 2001; Benton *et al.*, 2003).

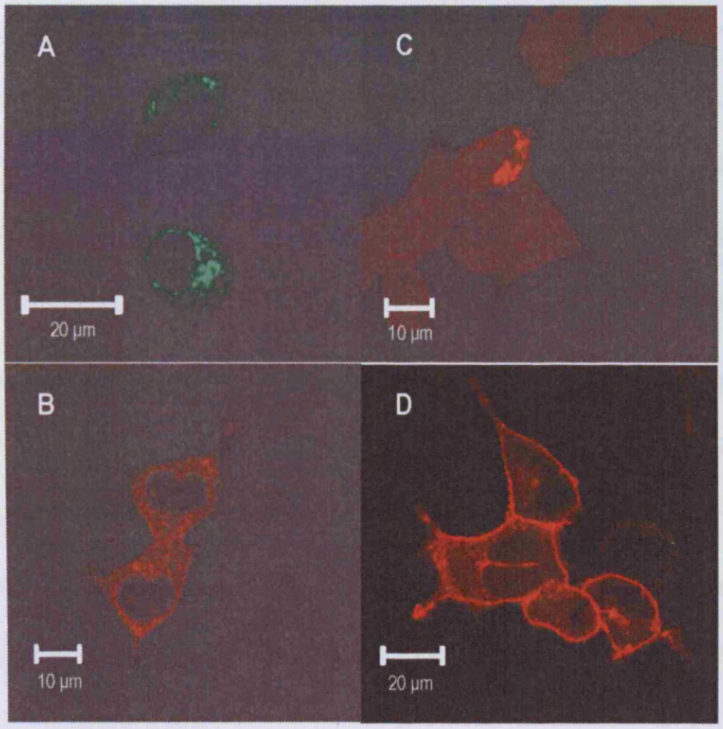

Figure 3.15 Different patterns of distribution seen for rat SK channels expressed alone in HEK 293 cells. **A**, fluorescence seen due to the YFP-tagged rSK1. **B**, staining of the untagged rSK1 channels with the UCL56 antibody. **C**, SK2 transfected cells stained with the M1 antibody. **D**, SK3 transfected cells stained with the M75 antibody. All transfections were performed using 1 µg of the relevant plasmid.

3.2.7.1 hSK1 and rSK3 co-expression

Since rSK1 does not form functional channels in heterologous expression systems but hSK1 does, much of the work exploring the properties of SK1 has, to date, been done using the human channel. For the same reason, the first staining experiments examining the co-expression of different SK channels were performed using hSK1 and rSK3.

Figure 3.16 shows that when cells are co-transfected with hSK1 and rSK3, the staining for SK3 is very different from that of cells transfected with rSK3 alone (see **Figure 3.15**). It is known that hSK1 expresses functional channels at the cell surface, however when co-expressed with rSK3, the bright signal for rSK3 appears to be clumped in the intracellular regions implying that in the presence of hSK1 less of the rSK3 protein reaches the cell surface than otherwise. These images strongly imply an interaction between the hSK1 and rSK3 subunits. However, this situation is somewhat artificial because the human SK1 clone does not normally encounter the rat SK3 clone.

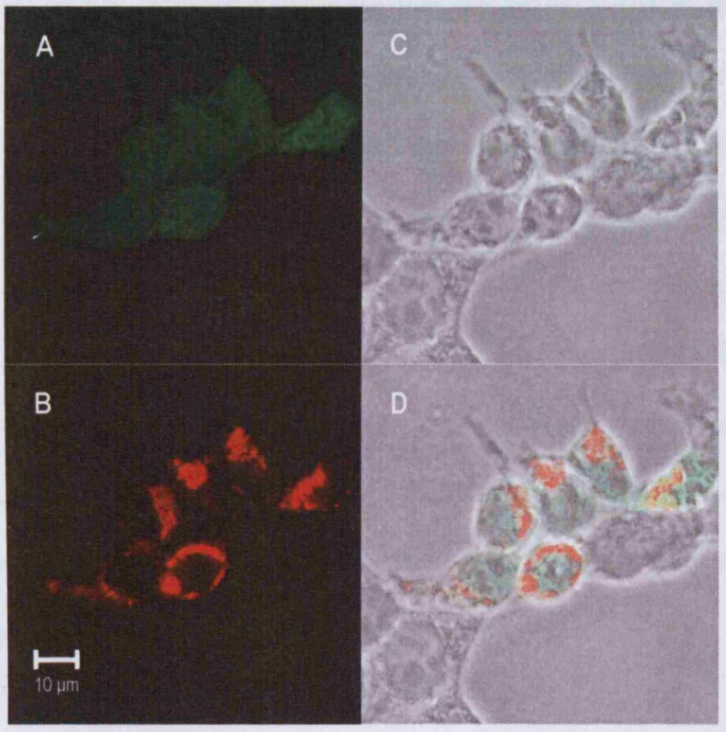

Figure 3.16 The rSK3 protein assumes a more intracellular distribution when co-expressed with hSK1. **A** shows the GFP fluorescence in transfected cells. **B**, staining of rSK3 with the Chemicon antibody. **C**, brightfield image of cells. **D**, overlay of images in **A**, **B** and **C**. HEK 293 cells were transfected with 2 µg of hSK1 and 0.5 µg of rSK3.

3.2.7.2 rSK1 and rSK3 co-expression

To determine whether the intracellular location of rSK3, when co-expressed with hSK1, was due to some effect of the human isoform of the channel, rSK3 was also co-transfected with rSK1. **Figure 3.17** shows that the staining pattern for rSK3 in the presence of the rat SK1 homologue is very similar to that seen when it is co-transfected with human SK1. It would thus appear that the presence of rSK1 also has the effect of changing the distribution of the rSK3 channel protein.

Figure 3.18 shows the pattern of staining for rSK1 in cells co-transfected with rSK1 and rSK3. The rSK1 channel protein can be seen to be "clumped" in the intracellular regions of the cell. This result is comparable to many of the other examples of rSK1 staining described in this chapter and shows that while the distribution of rSK3 is greatly altered in the presence of rSK1, the pattern of staining for rSK1 remains largely unchanged by rSK3.

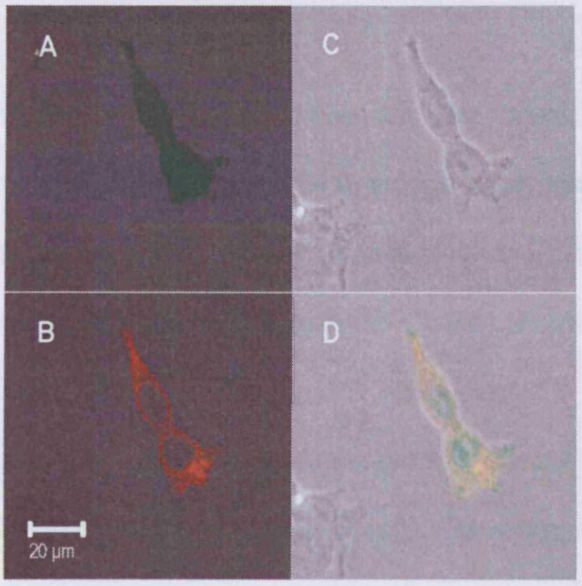

Figure 3.17 A largely intracellular rSK3 staining pattern is seen when co-transfected with rSK1. **A**, GFP fluorescence used as a marker of transfected cells. **B**, staining of rSK3 with the Chemicon antibody. **C**, brightfield image of cells. **D**, overlay of **A**, **B** and **C**. HEK 293 cells were transfected with 2 µg of rSK1 and 0.5 µg of rSK3.

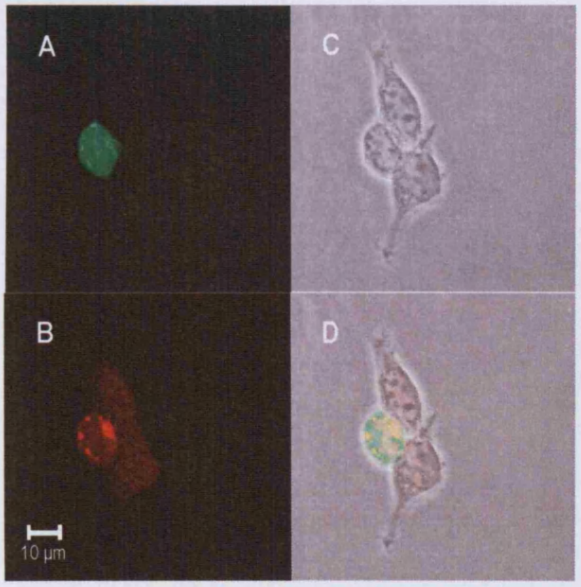

Figure 3.18 rSK1 staining remains largely unchanged when co-transfected with rSK3. **A**, GFP fluorescence. **B**, staining of rSK1 with the UCL56 antibody. **C**, brightfield image of cells. **D**, overlay of **A**, **B** and **C**. HEK 293 cells were transfected with 2 µg of rSK1 and with 0.5 µg of rSK3.

3.2.7.3 rSK1 and rSK2 co-expression

As both the anti-rSK1 and rSK2 antibodies had been raised in rabbits, it was not possible to use both antibodies to stain cells in a single experiment. For this reason, to explore whether there was any interaction between rSK1 and rSK2 subunits, HEK 293 cells were transfected with the YFP-tagged rSK1 construct and rSK2. **Figure 3.19** shows that both rSK1 (green) and rSK2 (red) can be detected in the cells and that vast majority of the fluorescent signal for the two respective channel proteins appears to be within intracellular compartments. Looking at panel **D** of **Figure 3.19** it can also be seen that the red and green signals show a good degree of overlap suggesting that the two subunit proteins may be closely associated in similar regions of the cell. The pattern of staining resembles that of rSK1 staining alone, however, rSK1 and rSK2 co-expression produces functional channels that are clearly different from those seen with rSK2 alone (see discussion).

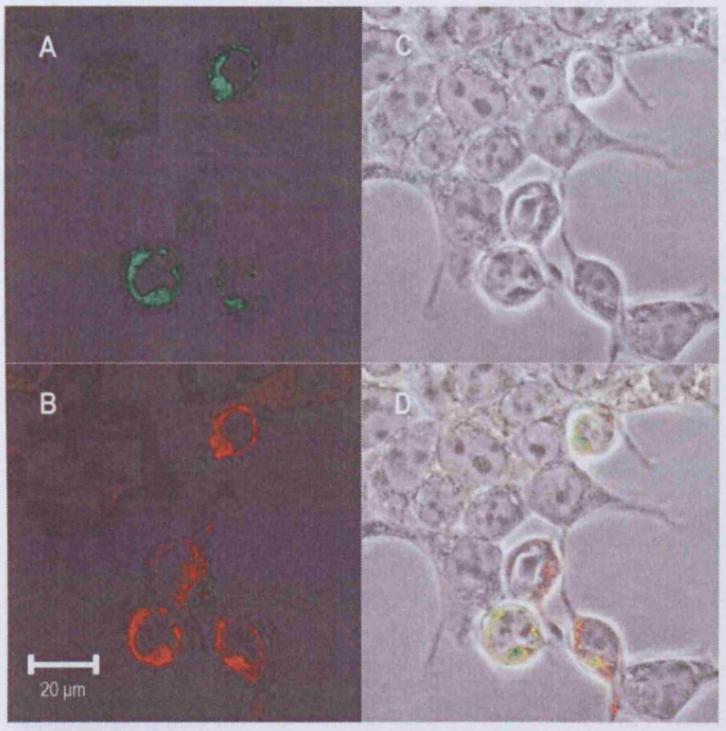

Figure 3.19 Distributions of YFP-tagged rSK1 and rSK2 in HEK 293 cells co-transfected with cDNAs for both proteins. **A**, fluorescence due to the YFP-tagged rSK1. **B**, staining of the rSK2 channel protein with the M1 antibody. **C**, brightfield image of cells. **D**, overlay of **A**, **B** and **C**. HEK cells were transfected with 0.5 µg of rSK1 and 5 µg of rSK2.

3.2.7.4 rSK2 and rSK3 co-expression

Figure 3.20 shows the pattern of staining seen for rSK3 when co-transfected with rSK2. Although the pattern of the fluorescent signal differs greatly from that seen with cells expressing SK3 alone, there is some similarity with the staining seen for the cells co-transfected with rSK3 and SK1. As with the rSK1/rSK3 transfected cells there is a bright intracellular signal for rSK3. These results suggests that there is an interaction between the rSK2 and rSK3 subunits.

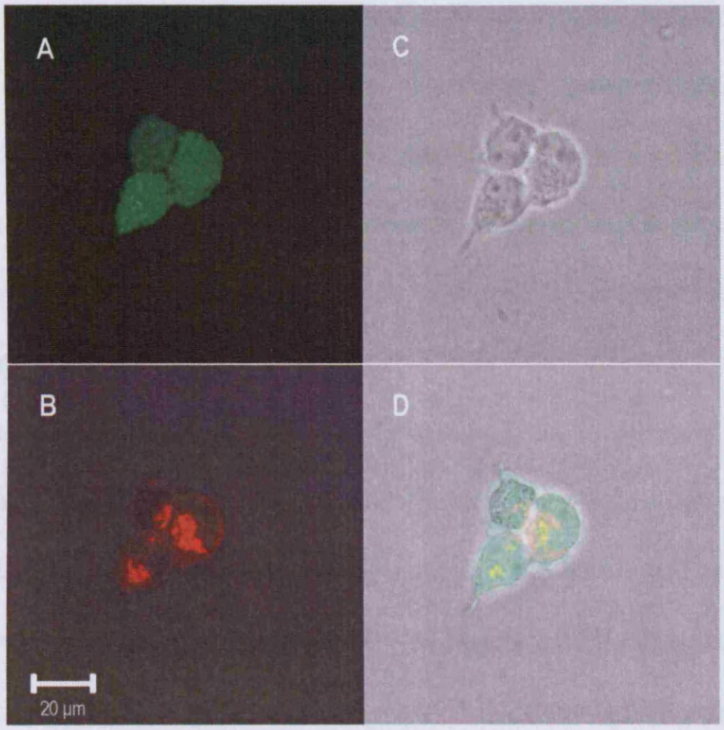

Figure 3.20 rSK3 staining appears more intracellular in HEK 293 cells when co-transfected with rSK2, compared with rSK3 alone. **A** shows GFP fluorescence, **B** shows staining of rSK3 with the Chemicon antibody, **C** shows the brightfield image and **D** shows the overlay of **A**, **B** and **C**. Cells were transfected with 2 µg of rSK2 and 0.5 µg of rSK3.

3.2.8 Positive controls; staining of neurones

Additional experiments were carried out in order to determine whether the antibodies would also stain native SK channels in neurones where the protein will be expressed at physiologically relevant levels. These experiments comprised a brief look at both superior cervical ganglion (SCG) and dorsal root ganglion (DRG) neurones. The reason for looking at SCG neurones is that Hosseini *et al.* (2001) previously described positive SK3 staining in cultured SCG cells. This work was done using a commercial antibody available from Chemicon. The M75 antibody has an almost identical epitope to the Chemicon antibody (see **Table 3.1**) and so was expected to work in a similar fashion. **Figure 3.21** shows that this is indeed the case. Clear membranous staining can be seen with the M75 antibody in SCGs. **Figure 3.21** also shows that some DRG neurones in culture display a similar staining pattern. However, while all SCGs appear to be SK3 positive, only a subset of DRG neurones appear to express the channel protein. This is discussed in more depth in **Chapter 5**.

What is particularly interesting about the SCG staining is the localisation of SK3. This was investigated by co-staining with an antibody to the microtubule-associated protein 2 (MAP2). MAP2 is important in neurite outgrowth and can be utilised as a marker for dendrite-like processes (Gordon-Weeks, 2004). In **Figure 3.22** it can be seen that while there is strong positive staining for SK3 in the cell body, there is also punctate staining in the processes that are MAP2-positive. This suggests that SK3 may play a functional role not only in the soma but also that the expressed protein is transported to the dendritic processes to play a further role there.

At the time these experiments were performed, there were no examples of appropriate neurones that would provide good positive controls for SK1, SK2 and IK1.

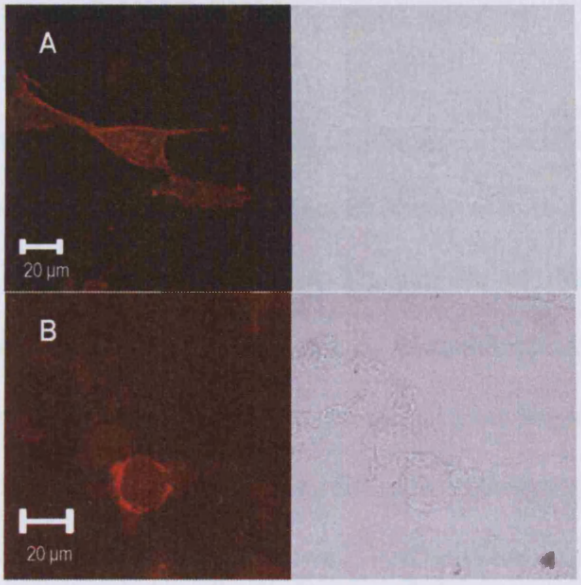

Figure 3.21 SK3 positive staining seen with the M75 antibody in peripheral neurones in culture. **A** an SCG cell and **B** a DRG neurone. In each case, the first panel shows rSK3 staining and the second the corresponding brightfield image of that cell. Both cell types show clear staining which appears to be at or close to the cell surface.

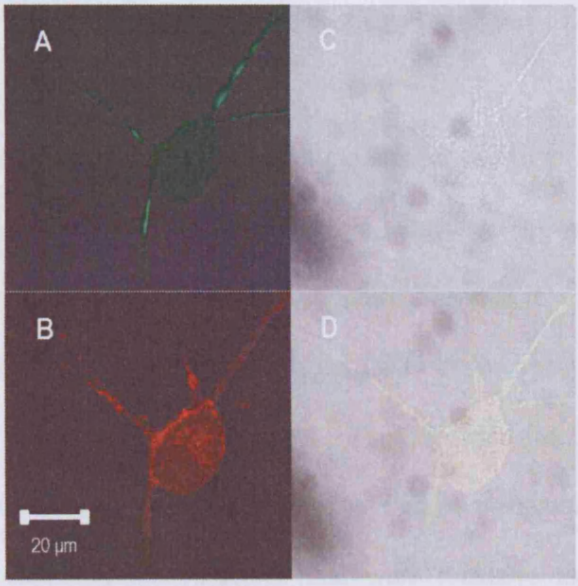

Figure 3.22 SK3 and MAP2 staining co-localises in the same subcellular regions of SCG neurones. **A**, MAP2 staining (green). **B**, SK3 staining with the M75 antibody (red). **C**, brightfield image of the SCG cell. **D**, overlay of **A, B** and **C**. The MAP2 staining is restricted to the dendrite-like processes of the cell. SK3 can be seen in the soma and there is also bright, punctate staining in the MAP2-positive processes.

3.3 Discussion

3.3.1 Antibody screening and cloning of the rat IK channel

The main aim of the work described in this chapter was to ascertain the suitability of a number of anti-SK/IK channel antibodies for the purpose of immunocytochemical staining. Before these antibodies could be tested on neuronal tissues, it was necessary to establish positive controls, which was done using cell lines transfected with SK/IK channel constructs. Of the antibodies tested on HEK 293 cells expressing a given SK or IK channel, several failed to provide a positive signal and were not used for further study. These were: UCL55 (anti-rSK1), R224 (anti-rIK), M16 and M20 (anti-hIK). However, most of the other antibodies gave a bright positive signal in transfected cells, indicating that these may be useful in examining which SK channels are expressed in native tissues. These antibodies were adopted for later studies in DRG neurones: rb196, rb200, UCL56 (anti-rSK1), M1 (anti-SK2), M75, Chemicon (anti-SK3) and R212 (anti-rIK).

The rIK channel had to be cloned in order to generate a positive control for the anti-rIK antibodies. Only in a very few instances have IK channels been shown to play a role in neurones (Greffrath *et al.*, 1998) so it is interesting that it was possible to PCR the rIK gene using cDNA isolated from adult rat DRG tissue because it demonstrates that message for the channel protein is present. The sequence for the cloned rIK was found to be identical to Genbank entry Q9QYW1 and when expressed in HEK 293 cells produced functional channels with currents that were sensitive to block by 10 μM clotrimazole, as expected (Alvarez *et al.*, 1992, Jensen *et al.*, 1998).

From the initial experiments carried out to characterise SK channel antibodies it was clear that the subcellular distributions of these proteins are quite different. It is known that rSK2 forms functional channels at the cell surface (Köhler *et al.*, 1996; Shah &

Haylett, 2000a; Strobæk *et al.*, 2000) but the staining is largely intracellular. This may be due to the very strong promoter systems that mammalian expression vectors contain that would result in the channel proteins being greatly over-expressed. It is likely that a small proportion of channels are needed at the cell surface and the remainder might remain trapped in intracellular compartments such as the endoplasmic reticulum. The outcome would be a bright intracellular signal that is likely to mask a signal at the cell membrane. However, there are similar distributions are seen for other K^+ channels (including hSK1, see **Figure 3.13**), which when expressed in cell lines, form functional channels that exhibit robust currents (Ishii *et al.*, 1997b; Kuryshev *et al.*, 2000).

rSK3 is predominantly seen at or close to the cell membrane with very little present intracellularly. This distribution pattern agrees with previous work (Hosseini *et al.*, 2001). The intracellular distributions of rSK2 and rSK1 are also in accordance with previously published data (Cingolani *et al.*, 2002; D'hoedt *et al.*, 2004). This gives rise to the possibility that the subunit distribution could change when two or more subunits are expressed because interactions might occur between the different SK channel proteins. To explore this possibility, the anti-SK channel antibodies were used in an additional set of experiments where plasmids encoding two different members of the SK channel subfamily were co-transfected into the same cell. These were done as part of a collaborative study with Drs David Benton and Alan Monaghan (Department of Pharmacology, UCL) who examined the electrophysiological properties of the channels formed by co-expression of the channel cDNAs. As their results are intimately related to the findings in this chapter, I have included some of these in the current discussion.

3.3.2 hSK1 and rSK3 co-expression

The rSK3 staining observed in cells co-transfected with hSK1, reveals that much of the SK3 channel protein trapped intracellularly, much more than when it is expressed alone. To investigate the interaction between hSK1 and rSK3, an rSK3 change-of-function mutant was employed, that dramatically alters the sensitivity to block by TEA (Monaghan *et al.*, 2004). The valine (V) residue at position 515 of the amino acid sequence was changed to a phenylalanine (F) to yield a channel (rSK3VF) that is highly sensitive to TEA. The currents produced by hSK1 are shown to be blocked by TEA with an IC_{50} of 14.1 ± 1.0 mM (**Figure 3.23**). For the native rSK3 channel this value was estimated to be 8.6 ± 1.6 mM but for the rSK3VF mutant the IC_{50} was found to be 0.31 ± 0.05 mM. This TEA sensitivity varies with the number of mutant subunits. Thus, if the rSK3VF subunits are co-expressed with wild-type rSK3 rather than getting an "all-or-nothing" TEA sensitivity, channels display an intermediate sensitivity to the blocker.

When the TEA-sensitive rSK3 mutant is co-expressed with hSK1, the concentration-inhibition curve for the resulting channels was almost identical to that of hSK1 alone (TEA IC_{50} when hSK1/rSK3 were co-expressed: 16.0 ± 1.5 mM).

The outcome of this experiment suggests that while functional hSK1 channels reach the cell surface in co-transfected cells, there appears to be little or no contribution of rSK3 subunits to the currents recorded. The staining results suggest a possible explanation for this, namely that hSK1 causes rSK3 to be retained intracellularly. However, the results presented here are not definitive in this regard.

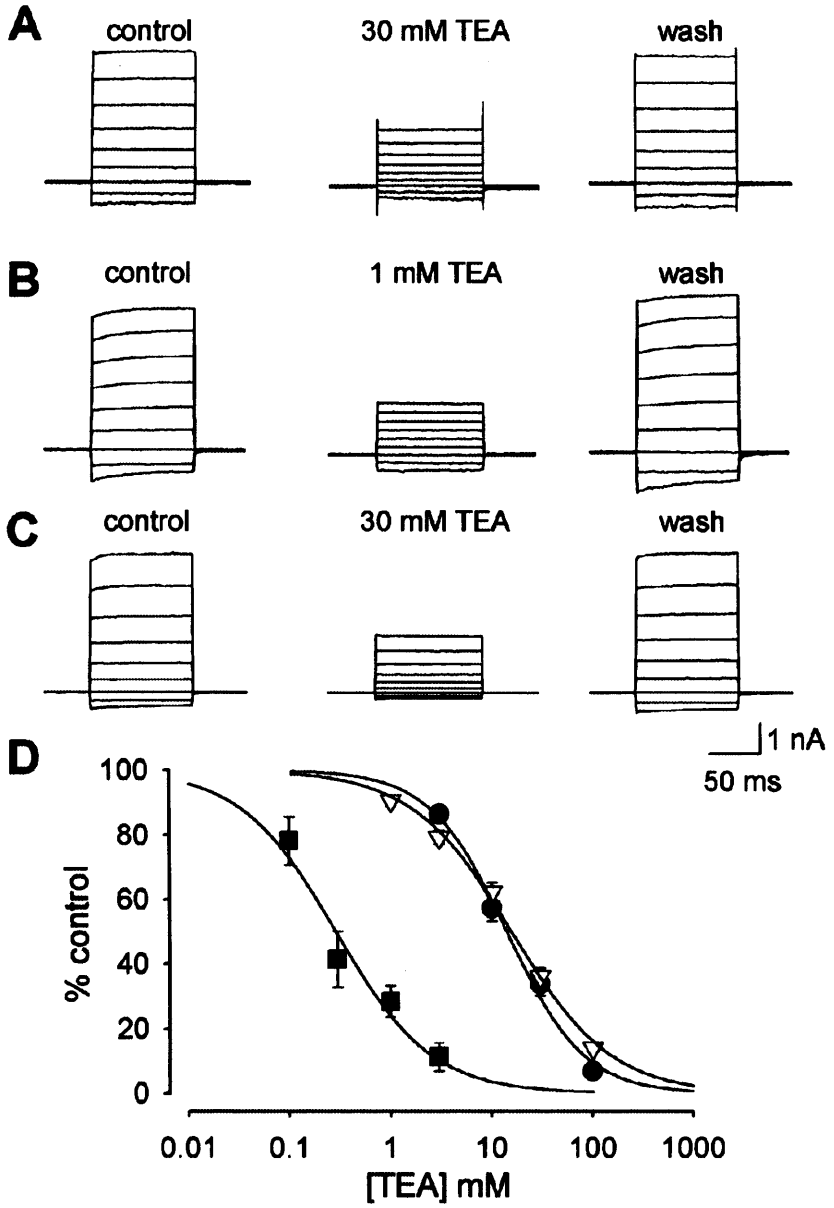

Figure 3.23 Co-expression of hSK1 with the TEA-sensitive rSK3 mutant rSK3VF does not alter TEA sensitivity of channels. **A**, example of a typical current trace showing the effect of 30 mM TEA on a cell transfected with hSK1 alone. **B**, typical current traces from an rSK3VF transfected cell showing the block seen with 1 mM TEA. **C**, current traces showing the effect of 30 mM TEA on a cell co-transfected with both hSK1 and rSK3VF. **D**, TEA concentration-inhibition curves for hSK1 (●), rSK3VF (■)and hSK1-rSK3 co-expression (▽). The lines are fits of the Hill equation with IC_{50} values of 14.1 ± 1.0 mM, 0.31 ± 0.07 mM and 16.0 ± 1.5 mM respectively. Hill coefficients were 1.2 ± 0.1, 0.9 ± 0.2 and 0.8 ± 0.1 respectively. (1 μg of each plasmid was used). Each point shows the mean of 3-5 observations. Results were obtained by D.C.H. Benton and A.S. Monaghan.

3.3.3 rSK1 and rSK3 co-expression

When expressed alone, rSK3 channels produce robust currents. However, these are substantially reduced when rSK3 is co-expressed with rSK1 (see **Figure 3.24**). The reason for this may be that rSK1 and rSK3 together form a heteromeric channel with a reduced conductance. Alternatively it may be that rSK1 affects rSK3 trafficking and prevents the formation of functional channels in the cell membrane, as appears to be the case with hSK1. This is indicated by the staining because when co-transfections were repeated using rSK1 instead of hSK1, the pattern of staining seen was very similar. To test which of these two possibilities was most likely, rSK1 was co-expressed with rSK3VF and the functional properties of the channels were assessed. When co-expressed with rSK1, the size of the current decreased as expected, however there was no obvious change in the TEA IC_{50} (0.24 ± 0.02 mM as compared to 0.31 ± 0.07 mM without rSK1). From this it would appear that the reduction in current size is due to a reduction in the number of functional rSK3 channels at the cell surface, but of the channels that are present there, it is unlikely that the resulting currents arise due to rSK1 and rSK3 heteromers.

From these results it appears that both the human and rat isoforms of SK1 have a "dominant negative"-like effect on rSK3. However, while hSK1 forms functional channels at the cell surface, rSK1 appears not to do so. In either case, when expressed with rSK3, SK1 is unlikely to form functional heteromeric channels at the cell surface.

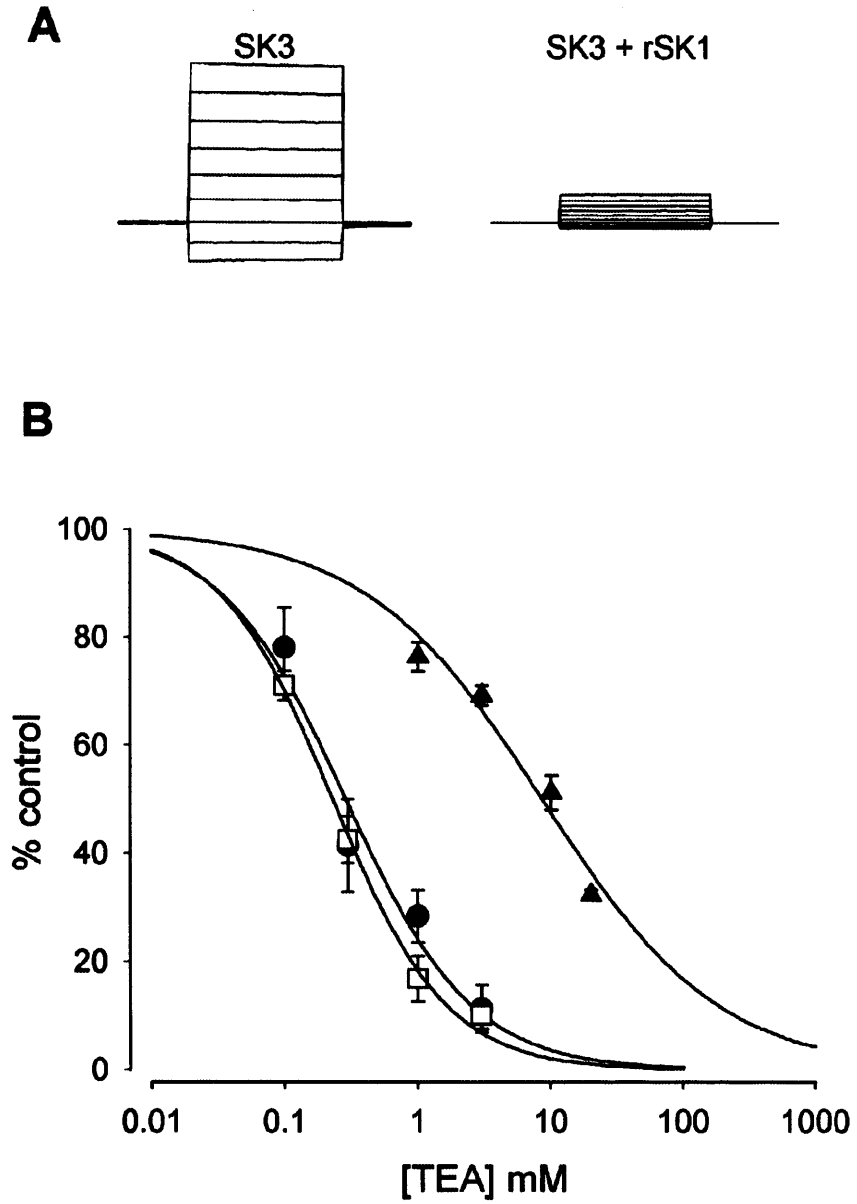

Figure 3.24 Co-expression of rSK1 with rSK3VF does not alter the TEA sensitivity. **A**, typical currents from a cell transfected with 1 μg of the native rSK3 alone (left) or co-transfected with rSK3 and rSK1 (1 μg and 2 μg respectively; right). It can be seen that when rSK1 is co-transfected with rSK3 the current amplitude is significantly reduced. **B**, TEA concentration-inhibition curves for wild-type rSK3 (▲), rSK3VF (●) or rSK3VF co-expressed with rSK1 (□). When fitted with the Hill equation the curves yielded IC_{50}values of 8.6 ± 1.6, 0.31 ± 0.07 and 0.24 ± 0.02 mM respectively. Hill coefficients were 0.65 ± 0.12, 0.9 ± 0.2 and 1.02 ± 0.08 respectively. Each point shows the mean of 3 or more observations.

3.3.4 rSK1 and rSK2 interactions

The staining results using HEK 293 cells transfected with the YFP-tagged rSK1 and rSK2 show that the fluorescence from the YFP and the anti-rSK2 antibody appear to co-localise well. While it is difficult to determine, from the current experiments, how well the results with the YFP-tagged rSK1 might compare with the native rSK1, they provide some indication that rSK1 and rSK2 interact.

Electrophysiological studies demonstrate that the interaction between SK1 and rSK2 is quite different from that between SK1 and SK3. It has already been shown that human SK1 subunits and rat SK2 subunits can co-assemble to produce channels with a pharmacology different to either of the homomers (Ishii *et al.*, 1997b; Benton *et al.*, 2003). This also appears to hold true for rSK1 and rSK2. When these two genes are co-expressed, the average current recorded in transfected cells increases two-fold. In addition to this consistent increase in the amplitude of the currents recorded, the channels expressed have a novel pharmacology clearly different to currents produced in cells expressing rSK2 alone. Apamin blocks rSK2 channels with an IC_{50} in the region of 100 pM (Köhler *et al.*, 1996; Grunnet *et al.*, 2001; Benton *et al.*, 2003) which is similar to the IC_{50} value for block by UCL 1848 (~120 pM in Hosseini *et al.*, 2001 and ~110 pM in Benton *et al.*, 2003). However, as shown in **Figures 3.25 and 3.26**, co-expression causes a right-ward shift in the concentration-inhibition curves for apamin and UCL 1848. When fitted with the Hill equation, the IC_{50}s for apamin and UCL 1848 come to 1.4 ± 0.3 nM and 2.9 ± 0.3 nM respectively. There is also a reduction in the Hill coefficients for apamin and UCL 1848 when rSK2 is co-expressed with rSK1 compared with rSK2 alone. Hill coefficients for

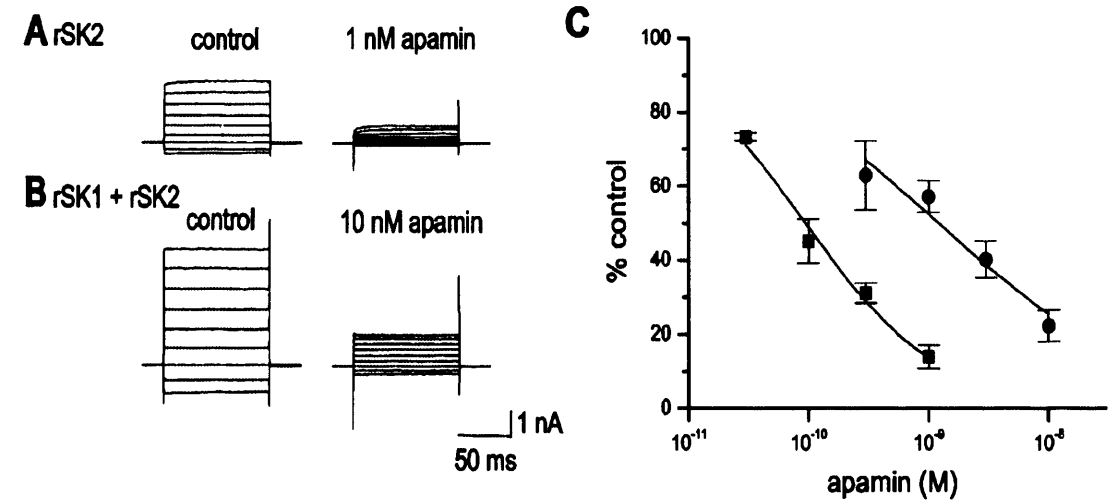

Figure 3.25 Co-expression of rSK1 with rSK2 alters sensitivity to block by apamin. **A**, The effect of 1 nM apamin on currents produced by transfecting rSK2 alone. **B**, current traces showing the effect of 10 nM apamin on a cell co-transfected with rSK1 and rSK2. The scale-bar is applicable to both **A** and **B**. **C**, apamin concentration-inhibition curves for rSK2 (■) or rSK1 and rSK2 (●). IC_{50} values obtained when these curves were fit with the Hill equation were: 95 ± 8 pM for rSK2 alone and 1.4 ± 0.3 nM for rSK2 co-expressed with rSK1. Hill coefficients were 0.8 ± 0.06 and 0.6 ± 0.1 respectively. Each point is the mean of 4 to 9 observations.

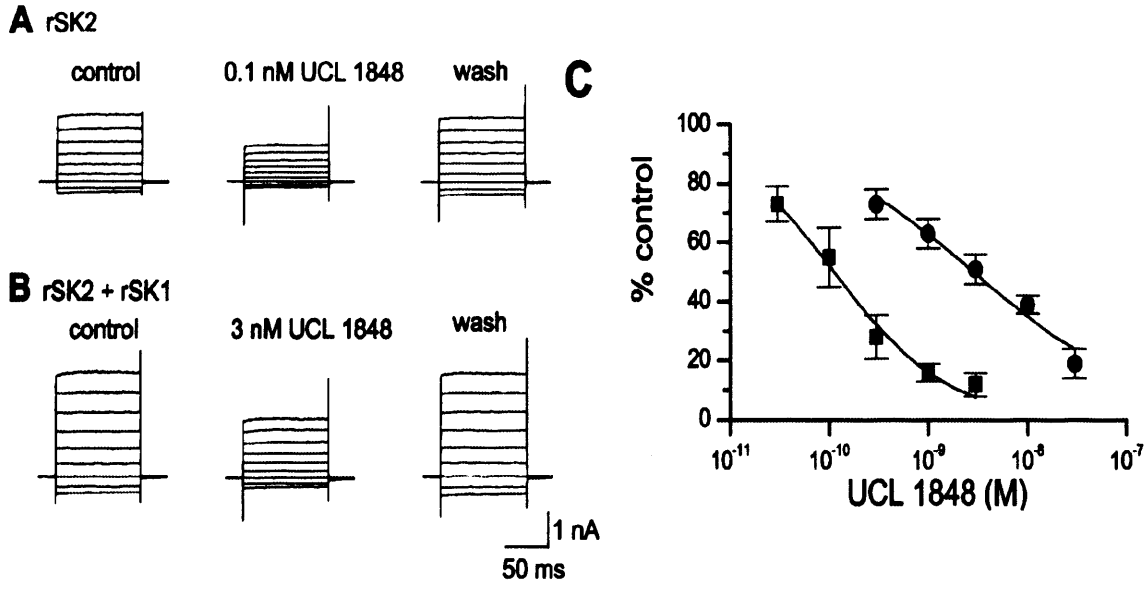

Figure 3.26 Co-expression of rSK1 with rSK2 alters sensitivity to block by UCL 1848. **A**, The effect of 0.1 nM UCL 1848 on currents produced by transfecting rSK2 alone. **B**, block seen with UCL 1848 of currents from cells co-expressing rSK1 and rSK2. The scale-bar applies to **A** and **B**. **C**, UCL 1848 concentration-inhibition curves for cells transfected with SK2 alone (■) or both rSK1 and rSK2 (●). Curves were fit with the Hill equation to give IC_{50} values of 110 ± 26 pM for rSK2 and 2.9 ± 0.3 nM for rSK1 with rSK2. Hill coefficients were 0.7 ± 0.1 and 0.49 ± 0.04 respectively. Each point shows the mean of 3 to 5 observations.

rSK2 alone with apamin and UCL 1848 were 0.8 ± 0.06 and 0.7 ± 0.1 respectively, compared with rSK1 and rSK2 where Hill coefficients were 0.6 ± 0.1 and 0.49 ± 0.04 respectively. These shifts in concentration-inhibition curves and reduction of the Hill coefficients are consistent with the idea that rSK1 and rSK2 form heteromeric channels. This implies that whatever the mechanism that allows hSK1, but not rSK1, to reach the cell surface alone it doesn't seem to affect ability of either of these two channel proteins to form functional channels with rSK2.

The behaviour of rSK1 is similar to that of certain K_V (Post *et al.*, 1996; Ottschytsch, *et al.*, 2002) and K_{ir} (Krapivinsky *et al.*, 1995) channels that have been referred to as being "electrically silent". That is, while they are not functional alone, they can assemble with related channel subunits to form active channels. With rSK3 the effect of rSK1 is comparable to that of $K_V9.1$ on $K_V3.4$ (Stocker *et al.*, 1999b). $K_V3.4$ expressed alone shows robust currents which are reduced or even abolished in the presence of $K_V9.1$. With rSK2 the effect of rSK1 is like the effect of $K_V6.1$ on $K_V2.1$ (Post *et al.*, 1996). $K_V2.1$ alone produces functional channels with characteristic delayed rectifying currents. When co-expressed with $K_V6.1$, a "silent" subunit, the resulting channels show altered kinetics and a decreased sensitivity to TEA. The similarities between rSK1 and rSK2/rSK3 interactions and those previously reported for other K^+ channels strongly suggests that rSK1 is able to form direct interactions with other rat SK channel subunits, although it only forms functional channels when co-expressed with rSK2.

3.3.5 rSK2 and rSK3 interactions

Miller *et al.* (2001) have shown that the N-terminal fragment of SK3 suppresses native SK2 currents in Jurkat cells, indicating there may be an interaction between the two subunits. This was explored in more depth using rSK2 and a UCL 1848-insensitive mutant of rSK3, rSK3VK. The mutant (rSK3VK) has a lysine (K) in place of the valine (V) at position 491 of the amino acid sequence. Currents in control cells expressing rSK3VK alone were largely unaffected (10 ± 5% inhibition) by 300 nM UCL 1848 (**Figure 3.27**). Cells transfected with rSK2 alone, on the other hand, showed currents that were blocked by UCL 1848 with an IC_{50} of 110 ± 26 pM. When these two channel proteins were expressed together the resulting concentration-inhibition curve was found to be shifted to the right (**Figure 3.27**). This strongly suggests that the co-expression of rSK2 and rSK3 leads to the formation of functional heteromeric channels.

The staining patterns for rSK1 with rSK2 and rSK2 with rSK3 may, at first sight, seem surprising given the electrophysiological data as the former would suggest that there is very little protein reaching the cell surface. However, this might be explained by the over-expression of plasmids which would make it appear as if all the protein is being trapped intracellularly and clearly indicates that the immunostaining experiments must be treated with caution.

There are several implications of heteromeric SK channels co-assembly with respect to their possible functions in native cells. One of these is that if rSK1 is indeed a "silent" subunit that needs rSK2 to form functional channels at the cell surface, it would seem unlikely that homomeric rSK1 underlies the sAHP seen in neurones. There is, as yet, no

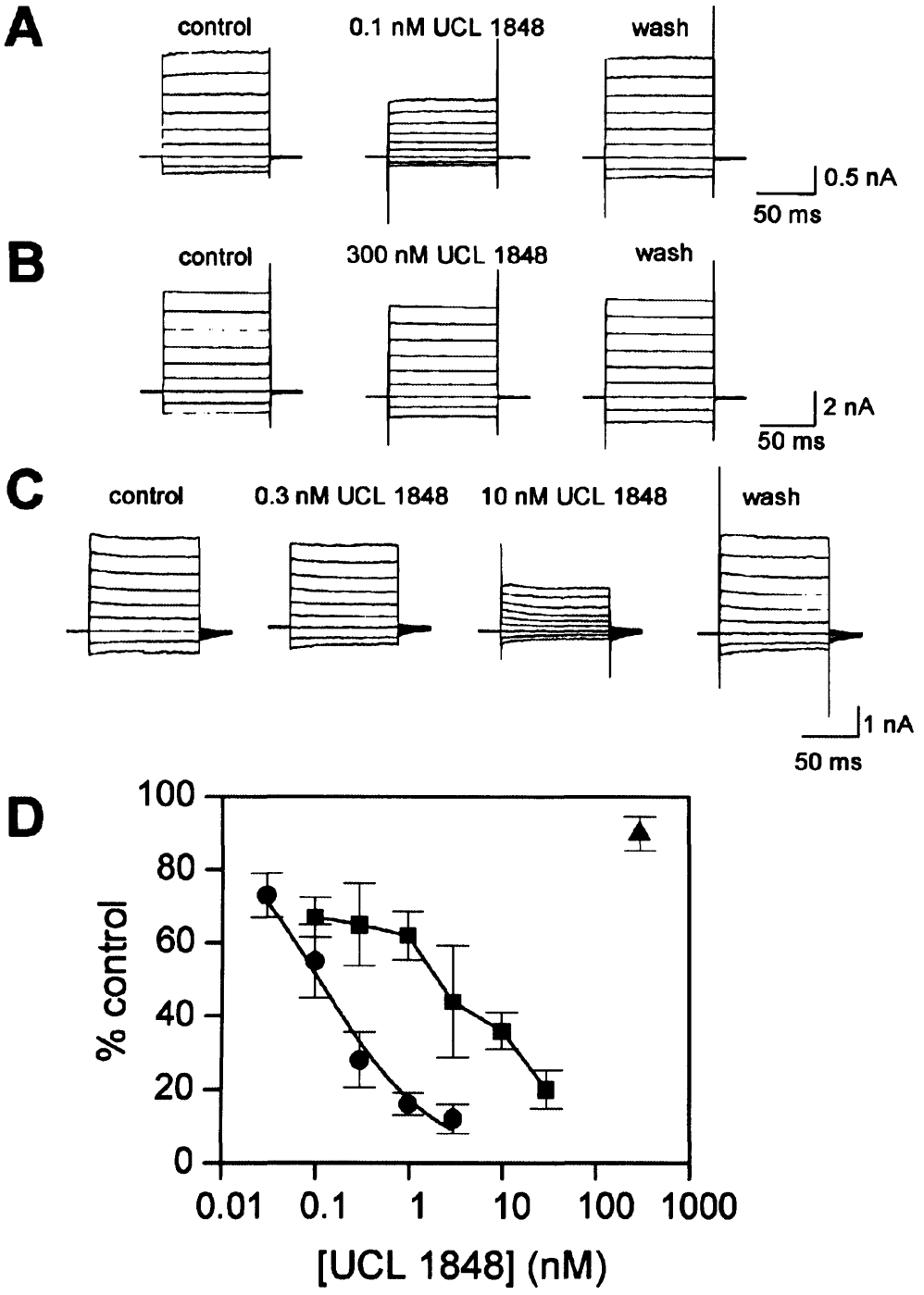

Figure 3.27 Co-expression of rSK2 and rSK3 alters sensitivity to block by UCL 1848. **A**, current traces showing the effect of 0.1 nM UCL 1848 on a cell transfected with rSK2. **B**, traces showing the effect of 300 nM UCL 1848 on rSK3VK. **C**, current recording showing the effect of 0.3 and 10 nM UCL 1848 on cells co-transfected with rSK2 and rSK3VK. **D**, UCL 1848 concentration-inhibition curves for cells transfected with rSK2 (●) or those transfected with rSK2 and rSK3VK (■). The effect of UCL 1848 was tested using a single concentration (300 nM) on homomeric rSK3VK transfected cells (▲). The rSK2 curve was fitted with the Hill equation to give an IC_{50} value of 110 ± 26 pM. The Hill coefficient was 1.05 ± 0.04. Each point shows the mean of 3 or more observations.

direct evidence to show that rSK1 and rSK2 form heteromeric channels *in vivo*, however there are suggestions from in-situ experiments which show that rSK1 is almost always seen with rSK2 (Stocker & Pederzani, 2000).

There is no putative role for SK2/SK3 heteromers. Co-immunoprecipitation experiments using antibodies against rSK2 and rSK3 have been done by Sailer *et al.* (2002) using SK channels solubilised from rat brain synaptosomes. However, attempts to isolate SK2 using the SK3 antibody failed. The same was true for the SK2 antibody which only seemed to detect homomeric SK2 channel and not SK3. While this suggests that the two channels probably do not co-assemble frequently in the CNS, it doesn't discount the possibility that SK2/SK3 heteromers may be functional in the periphery.

Although it is possible that the interactions of SK channels may be indirect this seems unlikely, particularly in the cases of SK1 with SK2 and SK2 with SK3. This is because channels formed when SK1/rSK2 and rSK2/rSK3 are co-transfected show an intermediate sensitivity to blockers when compared with that of the two channel proteins in their homomeric forms. So the work described here supports the hypothesis that different members of the SK channel subfamily form heteromers with varying properties. However, this type of heteromerisation only offers a limited amount of diversity for SK channels as only rSK1/rSK2 and rSK2/rSK3 co-expression appears to result in the production of functional heteromeric channels. Further SK channel diversity may arise as a result of associations with, as yet unidentified, β subunits (Wadsworth *et al.*, 1994; 1996; 1997).

As a first test to see whether the SK antibodies would recognise the channel protein in native tissues, isolated SCG and DRG cells in primary culture were stained with the anti-SK3 antibodies. Positive SK3 immunoreactivity was seen in both SCG and DRG neurones. Importantly, co-staining with MAP2 in SCG cells shows overlap between the

MAP2 and the SK3 signals. MAP2 is a dentritic marker and is indicative of developing neurites. The co-localisation of MAP2 and SK3 in these processes suggests that SK3 is transported from the cell bodies of neurones to peripheral dendritic processes. It is not clear whether SK3 would also be expected along axonal processes but the presence of SK channels in axonal termini has been described in other rat and mouse neurones (Sailer *et al.*, 2002; Obermair *et al.*, 2003; Roncarati *et al.*, 2001; Womack & Khodakhah, 2003). The expression of presynaptic SK3 channels in mouse hippocampal neurones (Obermair *et al.*, 2003) along with the presence of functional SK2 channels in the dendrites of cerebellar purkinje neurones (Womack & Khodakhah, 2003) and the work in SCG neurones is interesting as it could imply that the role for SK3 lies in regulating neurotransmision in neuronal processes rather than in generating AHPs in the cell body.

M75 also gave a positive signal in DRG cells. However, not all DRG cells expressed SK3. Given that DRG neurones comprise a hugely diverse group of cell types this is perhaps not surprising. The presence of SK3 immunoreactivity suggests it is appropriate to look for a functional role for SK channels in DRG cells and this is investigated further in **Chapters 4** and **6**.

Chapter 4

Characterisation of AHPs in DRG and nodose ganglion cells

4.1 Introduction

The aim of work reported in this chapter was to examine some of the properties of the AHPs seen in rat DRG and guinea-pig nodose afferent neurones and to characterise their pharmacology. Specifically, the emphasis was on examining the role of K_{Ca} channels.

4.1.1 Choice of cell preparation

All of the electrophysiological work described in this chapter was carried out on isolated cells grown in culture. There were several reasons for this. While *in vivo* experiments provide the most physiological situation, examining the effects of pharmacological compounds is complicated for several reasons. Firstly, it is not easy to determine the exact concentration of a given drug at the site of action and secondly, once applied, drugs are then difficult to wash out, so it is difficult to confirm that the effects are reversible. An isolated cell preparation provides a system whereby drug concentrations are known, and application and wash out can be performed with relative ease. This allows for several drugs to be applied in order to better characterise the properties of a given cell.

In addtion to the advantages of drug application offered by cultured cells, they have been shown to retain many of the properties of their counterparts *in vivo*. This holds

true in the case of DRG cells, particularly with respect to nociception. *In vitro* studies have demonstrated that certain populations of cells are activated by the algogenic agents capsaicin and bradykinin, express substance P and are sensitised by prostagladin E_2, all of which are associated with nociceptors *in vivo* (Baccaglini & Hogan, 1983; Cesare & McNaughton, 1996; Gold *et al.*, 1996b). In addition, characteristics such as small cell bodies (McCarthy & Lawson, 1989; 1990) and inflections on the falling phase of an action potential (Ritter & Mendell, 1992; Traub & Mendell, 1988), which can be seen in cultured cells, are all associated with nociceptors *in vivo*. This shows that at least some of the characteristics of isolated cells reflect what occurs in the whole animal. As a result they have been used to examine a number of membrane properties in sensory neurones including currents generated due to potassium channel opening (Kostyuk *et al.*, 1981a; McFarlane & Cooper, 1991; Gold *et al.*, 1996a), Na^+ currents (Kostyuk *et al.*, 1981b; Caffrey *et al.*, 1992; Roy & Narahashi, 1992), Ca^{2+} currents (Kostyuk *et al.*, 1981c; Scroggs & Fox, 1992) and non-selective cation currents generated by members of the TRPV family of channels (Cesare & McNaughton, 1996; Reichling & Levine, 1997).

Finally, since SK channels frequently provide a molecular basis for AHP generation it is important to note that isolated neurones in culture often provide good models for neuronal AHPs *in vivo*, particularly those AHPs mediated by Ca^{2+}-activated K^+ channels. Examples include those from the coeliac ganglion (Coggan et al., 1991), SCG neurones (Pennefather *et al.*, 1985; Kawai & Watanabe, 1986) and hippocampal neurones (Shah & Haylett, 2000b; Shah *et al.*, 2001). DRGs and nodose neurones in culture also have robust AHPs (Leal-Cardoso *et al.*, 1993; Gold *et al.*, 1996a; Lüscher *et al.*, 1994; Abdulla & Smith, 2001) which are also seen in cells using whole ganglion *in vitro* preparations (Fowler *et al.*, 1985; Weinreich & Wonderlin, 1987; McCarthy &

Lawson, 1990; Villière & McLachlan, 1996) and those from *in vivo* experiments (Görke & Pierau; 1980; Harper & Lawson, 1985b; Ritter & Mendell; 1992; Djouhri & Lawson, 1998).

In examining these DRG cultures I have recorded from their cell bodies. This is because the possibility of recording from the nerve terminals and the central projections of primary afferents, which are likely to be the most informative about sensory mechanisms, presents considerable problems. These processes, which can be less than 1 μm in size, are embedded in tissue thus making them inaccessible for cellular recording (Kress & Reeh, 1996). However, cell bodies show many of the properties associated with the whole neurone. For instance ion channels, such as members of the TRPV family, which are expressed in cell bodies can also be detected in nerve terminals (Zhang *et al.*, 1994; Brumovsky *et al.*, 2002). Furthermore, physiological characteristics such as the presence of an AHP, which have been reported in cell bodies of hippocampal neurones, have also been recorded in dendrites of these cells (Lancaster & Zucker, 1994; Andreasen & Lambert, 1995). Thus, though caution is needed, particularly since DRG properties can change with axotomy, recordings from the soma can give some indication of the properties of the neurone overall.

4.1.2 Age of cultures

One aim of the present investigation was to determine whether SK channels play a role in AHP generation in sensory neurones. As staining results showed that the SK3 channel protein is expressed in DRG cells within the first 3 days of culture (see **Chapter 3**) and voltage recordings showed that AHPs can also be detected in DRG cells this age (Gold *et al.*, 1996a), the electrophysiological data described in this chapter has been obtained from cells cultured for 1-3 days. An additional justification for this is

that there is evidence for up-regulation of SK channels in cultured cells over time (Obermair *et al.*, 2003) so, other things being equal, young cells may be closer to cells *in vivo*. One final reason for using 1-3 day old cultures was that cell survival rate of the very large (A-fibre) cells is much lower than that of the smaller diameter cells. Thus to have a more heterogeneous and representative population of cells to work with, a younger culture was more desirable.

4.1.3 Characterising cells in culture

All studies on guinea-pig nodose cells were done using intracellular recording techniques. In the case of rat DRGs, recordings were taken from either p17 or p45 animals using the perforated patch technique to characterise AHP duration and either perforated patch or intracellular recording to look at AHP pharmacology.

DRG neurones are highly heterogeneous, and as part of this study looks at the correlation between the type of cell and the AHP(s) present, it was necessary to be able to identify the type of cell being recorded from. Several properties of DRG cells in culture have been used to ascribe them to a certain subpopulation of cells *in vivo*; an obvious example is cell size. However, there are also currents that appear to be activated specifically in certain cell types and so may be exploited to try and establish which cell type is being recorded from. Three properties used to attempt to identify "A-type" and "C-type" cells in the current study are outlined below.

4.1.3.1 Cell size

In vivo, neurones with the smallest diameter axonal fibres, which comprise primarily nociceptors (Lawson, 2002), tend to have correspondingly small cell bodies (mean cell size of ~450 μm^2; Harper & Lawson, 1985a). At the other extreme, the largest neurones

(> 1000 μm^2 μm) represent $A_{\alpha/\beta}$ afferents. Thus cell size can be used as one indicator of whether a neurone is of the A- or C-type.

4.1.3.2 Action potential inflection

In some DRG neurones, an inflection on the falling phase of the action potential can be seen in the form of a "shoulder" (illustrated in **Figure 4.2**) that is thought to be due to a Ca^{2+} inward current (Görke & Pierau, 1980; Harper & Lawson, 1985b; Traub & Mendell, 1988) possibly in combination with a Na^{+} current (Blair & Bean, 2002). Harper & Lawson (1985b) have shown from recordings in DRG cells, made using whole ganglion preparations, that 76% of $A_{\alpha/\beta}$ and 18% of A_{δ} cells repolarise in a monophasic manner. However, 82% of A_{δ} and 100% of C cells show biphasic action potential repolarisation. Therefore, the presence of an inflection on the falling phase of the action potential indicates a decreased probability that it is an $A_{\alpha/\beta}$.type neurone.

4.1.3.3 The hyperpolarisation-activated current (I_H)

The I_H current can be detected as a voltage sag in response to the application of a hyperpolarising current pulse (see **Figure 4.4**). Its presence has been demonstrated in 90% of $A_{\alpha/\beta}$ and 70% of A_{δ} cells and is absent in 87% of C-fibre cells (Villière & McLachlan, 1996). In isolated DRG cells, Abdulla & Smith (2001) report that the I_H current is seen in 49/49 large cells, 33/37 medium cells and 14/24 small cells. Thus the absence of a voltage sag indicates an increased probability that a cell is of the C-type.

4.2 Results from studies in DRG neurones

4.2.1 Identification of DRG cell types in p17 rats

4.2.1.1 DRG cell sizes

DRG primary afferents comprise a very mixed group of cells as is apparent just by looking at the sizes of cell bodies in culture (see **Figure 4.1**). For p17 animals, cell diameters ranged from 20 to 50 μm. In adult rats this range increased to between 22.5 and 60 μm.

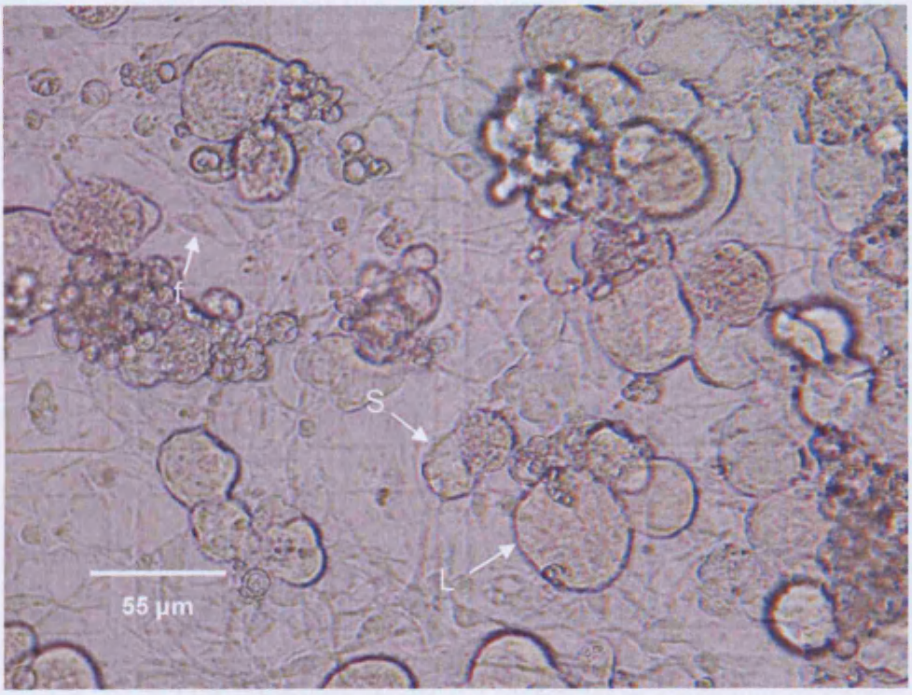

Figure 4.1 Isolated DRG cells after 1 day in culture showing the variety of cell sizes. The larger rounder cells make up the DRG population (**L** shows a large diameter neurone, **S** a small diameter neurone) while the smaller flatter cells constitute fibroblast-like supporting cells (see **f**). A large number of cells survive the isolation procedure and they have widely varying diameters. In this example the range is from 20 μm to about 50 μm. Sizes were estimated using a calibrated eye-piece graticule. The diameters expressed are the means of the height and width of the cells.

Villière & McLachlan (1996) found that the mean cell diameters of C-, A_δ- and $A_{\alpha/\beta}$-fibre neurones, identified on the basis of their conduction velocities, were 25 μm, 36 μm and 47 μm respectively. As it was not possible to use conduction velocities in the current work, a range of cell diameters were used to group neurones on the basis of size (see **Table 4.1**). Attempts were then made to choose cells with diameters that were least likely to overlap with other groups. The values for the division of cell groups were chosen to be able to compare certain properties (such as an inflection on the downstroke of the action potential) with the literature and are shown in **Table 4.1** (see also p144 and appendix).

Age of animal	small cells	medium cells	large cells
p17	20-25 μm	30-35 μm	> 40 μm
p40-45	22.5-27.5 μm	35-40 μm	> 45 μm

Table 4.1 Ranges of DRG cell sizes adopted to help identify them as C- or A-type cells. DRG cells from p17 and p40-45 rats were grouped into small (C-type) and medium or large (A-type) cells. Medium and large cells are likely to correspond to A_δ and $A_{\alpha/\beta}$ types respectively, however due to overlap in cell sizes (Harper & Lawson, 1985) these neurones were grouped together as "A-type" neurones.

4.2.1.2 Presence of an action potential inflection

Of the DRG cells obtained from p17 animals 82% of the small diameter neurones (20-25 μm) showed an inflection (n=45). Harper & Lawson (1985b) report that all C-type neurones show an inflection, so the 18% of small cells without an inflection in the current study may represent a small number of A_δ fibre cells, as some of these cells have diameters that overlap with C-fibre cells (Harper & Lawson, 1985b). Inflections were also present in 17% of medium diameter cells (30-35 μm; n=35) but absent in large cells with diameters > 40 μm (n=38).

4.2.1.3 Presence of the hyperpolarisation-activated current (I_H)

A second property that was employed for the purpose of identifying A-type and C-type neurones was the presence of the I_H current. Only 13/27 small diameter cells showed a voltage sag, however it was present in 20/23 medium diameter cells and 25/25 large diameter cells. Again, it is possible that a number of the small cells actually correspond to A_δ cells. Although these values (from p17 rat DRGs) are not very discriminatory cells with a voltage sag are unlikely to be C-type neurones.

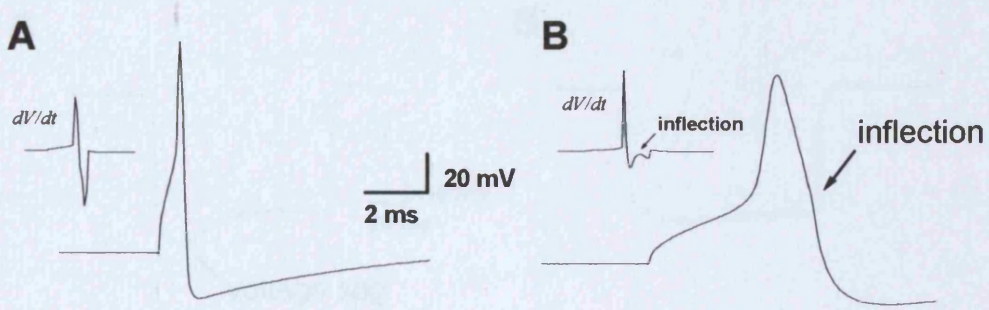

Figure 4.2 Action potential shapes in two different types of DRG cell recorded from cultured neurones. **A**, an action potential recorded from a large diameter cell (~40 μm) which does not show an inflection. **B**, an action potential recorded from a small diameter cell (~22 μm) which shows an inflection on the falling phase. The presence of an inflection was confirmed by differentiating the action potential using Clampfit 8.2 software. Results are shown in the insets (*dV/dt*). The presence of an inflection on the rising phase is likely to be an artefact of the recording technique. The scale-bar in **A** also applies to **B**. Recordings were made using the perforated patch technique.

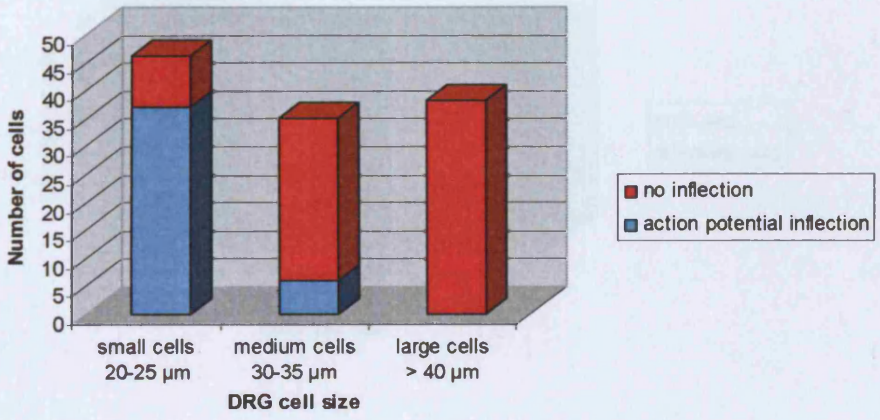

Figure 4.3 The presence of an action potential inflection in different sized DRG neurones in culture. 82% of small cells and 17% of medium sized cells show an inflection on the falling phase of the action potential. None of the large cells (> 40 μm) showed an inflection.

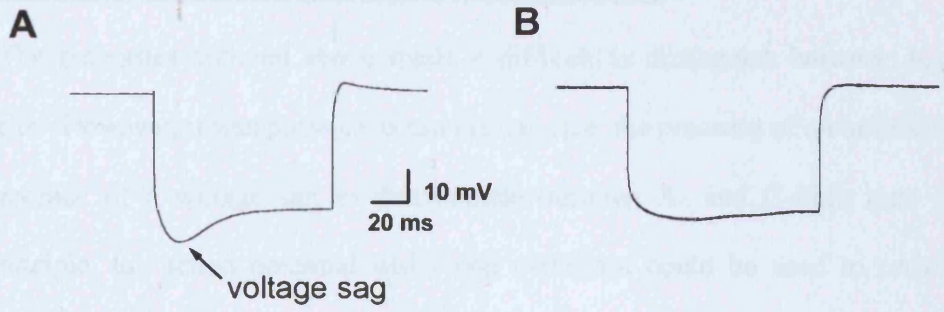

Figure 4.4 Response of two different cultured DRG cells to a hyperpolarising current pulse. **A**, a recording from a large diameter cell (>40 μm) showing a voltage sag in response to the hyperpolarising pulse. **B**, a recording from a small diameter cell (25 μm) that does not show a pronounced sag. The scale-bar in **A** also applies to **B**. Recordings were made using the perforated patch technique.

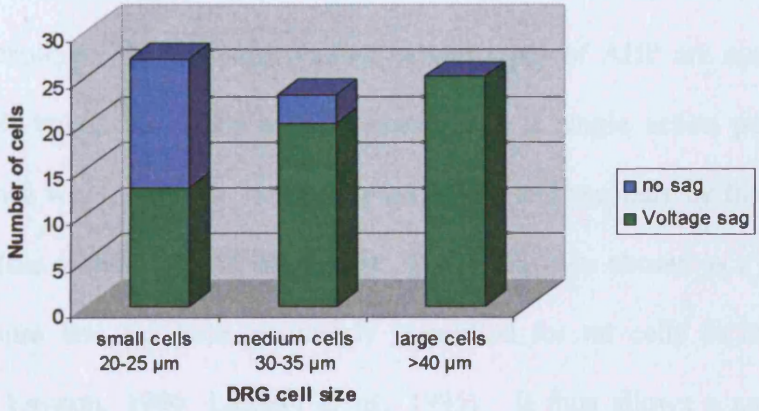

Figure 4.5 The presence of a voltage sag in different sized DRG neurones in culture. 42% of small cells do not show a voltage sag. 87% of medium sized and 100% of large cells showed a voltage sag in response to a hyperpolarising pulse.

4.2.1.4 Criteria used to identify A- and C-type neurones

The properties outlined above made it difficult to distinguish between $A_{\alpha/\beta}$ and A_{δ} cells. However, it was possible to use the cell size, the presence of an inflection and the presence of a voltage sag to discriminate between A- and C-fibre type cells. In principle, the action potential width and overshoot could be used to provide better separation, but these cannot be accurately measured with the current stimulation and recording methods. Nevertheless, the decision was made to use the absence of a voltage-sag and the presence of an action potential inflection to designate a cell as C-fibre type.

4.2.2 Variety of AHPs in cultured DRG cells from p17 rats

The AHPs recorded from DRG cells varied greatly in their timecourses. **Figure 4.6** illustrates some of the AHPs seen in C-type and A-type cells using the perforated patch recording technique. To examine whether certain types of AHP are associated with particular cell types, the AHPs seen in response to a single action potential were analysed in two ways. First, by measuring the AHP_{80} and secondly by fitting the AHP timecourses (see section 2.4.7 of **Methods**). The AHP_{80} was chosen as a parameter to analyse because this has been previously quantified for rat cells in intact ganglia (Waddell & Lawson, 1990; Lawson *et al.*, 1996). It thus allows a comparison of conditions in culture with those in a more physiological setting. It has also been shown to provide some correlation with the cell type (Waddell & Lawson, 1990). The second approach of fitting the timecourse of the AHP was chosen in an attempt to pursue these correlations in greater detail. Both sets of analyses are described below.

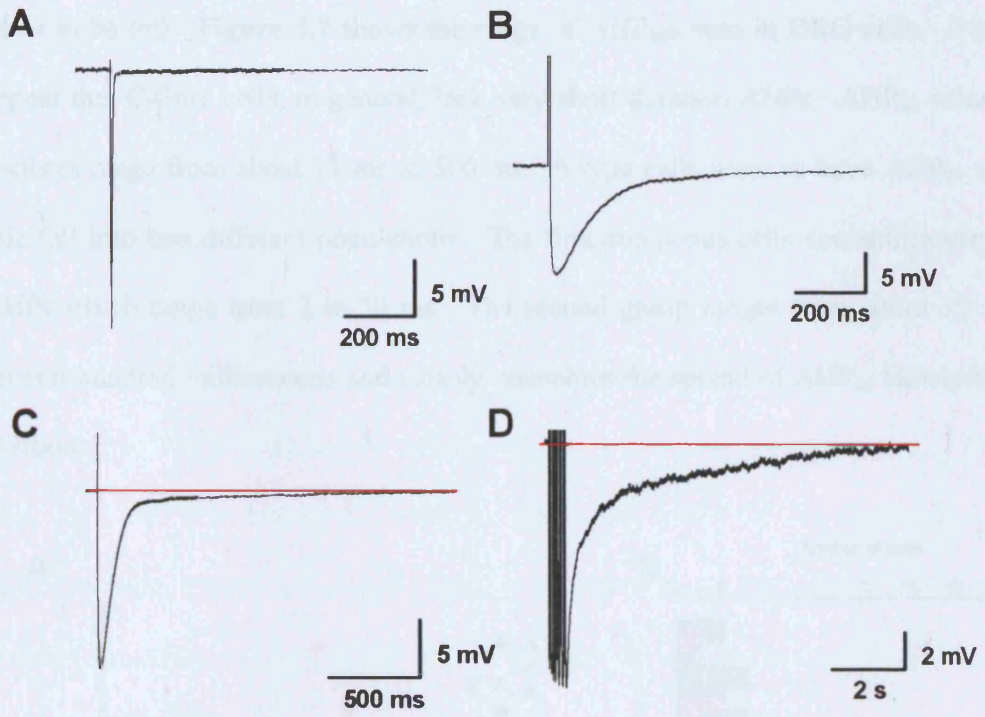

Figure 4.6 Different kinetics of the AHPs recorded from DRG cells grown in culture. **A**, a very fast duration AHP lasting only a few milliseconds. **B**, an AHP with a duration of a few hundred milliseconds. **C**, a cell with an AHP similar to that seen in **B**, but also showing a small, much slower component lasting several seconds. **D**, the AHP seen in the cell depicted in **C** when stimulated to fire a train of action potentials. A longer, more slowly decaying phase is seen. The extremes of the action potentials have been truncated in order to show the AHPs more clearly.

4.2.2.1 AHP_{80}

The AHP_{80} was measured as the time taken for 80% "recovery" from the AHP where the downstroke of the action potential, as it crosses the resting membrane potential, was taken to be t=0. **Figure 4.7** shows the range of AHP_{80}s seen in DRG cells. It would appear that C-fibre cells, in general, lack very short duration AHPs. AHP_{80} values for C-fibres range from about 11 ms to 500 ms. A-type cells seem to have AHP_{80} values that fall into two different populations. The first comprises cells containing very fast AHPs which range from 2 to 30 ms. The second group ranges from about 35 ms to several hundred milliseconds and closely resembles the spread of AHP_{80} values for the C-fibres.

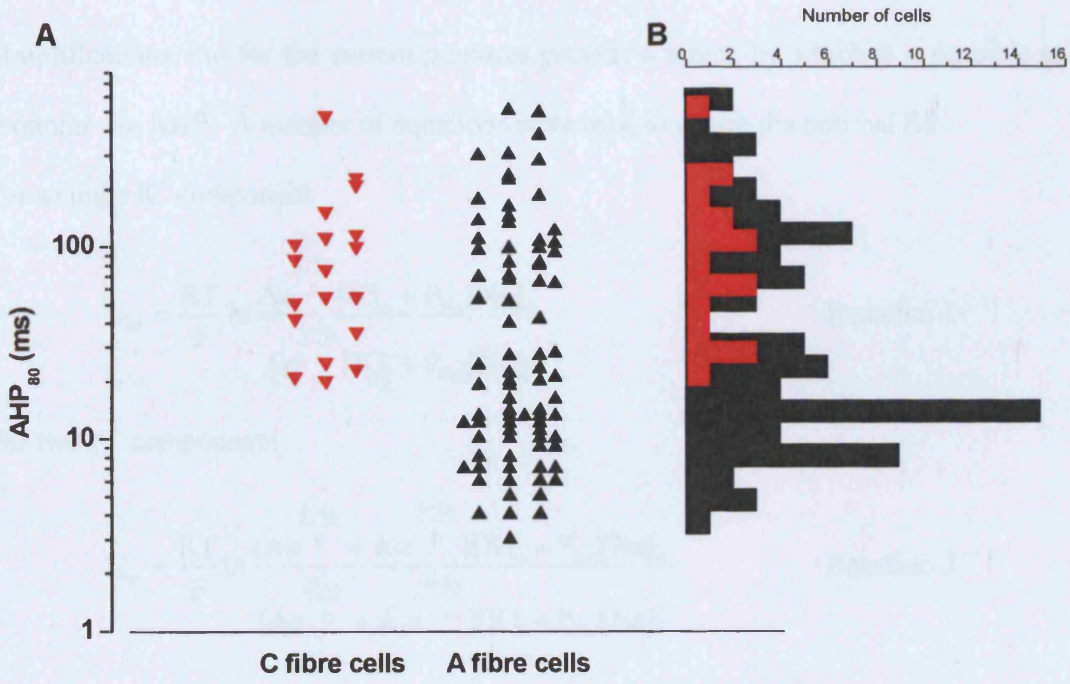

Figure 4.7 Range of AHP_{80} values for AHPs recorded from DRG cells. **A**, a scatter plot of the AHP_{80} values for C and A fibre cells. **B**, a histogram showing the range of AHP_{80} values for C- and A-fibre cells (the bars of the histogram correspond to a log bin size of 1.2). The pattern of spread from the scatter plot and the histogram indicate that the C-fibres (red) generally do not have fast duration AHPs. Also there seem to be two discrete populations of AHP_{80} values for the A-fibre cells (black) possibly reflecting two different cell types.

4.2.2.2 AHP decay time constants

One of the possible limitations of using the AHP_{80} value to compare AHP durations is that many of the AHPs in DRG cells appeared to have several components with different timecourses. The AHP_{80} might be dominated by the components with the largest amplitude. To explore the timecourses of different AHPs in greater detail, and to find out whether certain types were associated with either A- or C-type neurones, the AHPs were fitted using a modified version of the Goldmann-Hodgkin-Katz equation which assume that the conductances underlying the AHP undergo exponential decay (see section 2.4.7 of the **Methods**). It was also assumed that the resting potential was dominated by Na^+ and K^+ conductances, and that the internal Cl^- concentration in DRG cells was 31 mM (Kenyon, 2000). These are likely to be substantial over-simplifications, but for the current purposes provide a means by which it is possible to examine the AHP. A number of equations were used to obtain the optimal fit:

for a single K^+ component

$$E_m = \frac{RT}{F} \ln \frac{Ae^{\frac{t-t_0}{\tau}}[K]_o + P_{Na}[Na]_o}{Ae^{\frac{t-t_0}{\tau}}[K]_i + P_{Na}[Na]_i} \qquad \text{Equation 1}$$

for two K^+ components

$$E_m = \frac{RT}{F} \ln \frac{(Ae^{\frac{t-t_0}{\tau}} + A_1 e^{\frac{t-t_0}{\tau_1}})[K]_o + P_{Na}[Na]_o}{(Ae^{\frac{t-t_0}{\tau}} + A_1 e^{\frac{t-t_0}{\tau_1}})[K]_i + P_{Na}[Na]_i} \qquad \text{Equation 2}$$

for three K^+ components

$$E_m = \frac{RT}{F} \ln \frac{(Ae^{\frac{t-t_0}{\tau}} + A_1 e^{\frac{t-t_0}{\tau_1}} + A_2 e^{\frac{t-t_0}{\tau_2}})[K]_o + P_{Na}[Na]_o}{(Ae^{\frac{t-t_0}{\tau}} + A_1 e^{\frac{t-t_0}{\tau_1}} + A_2 e^{\frac{t-t_0}{\tau_2}})[K]_i + P_{Na}[Na]_i} \qquad \text{Equation 3}$$

for two K^+ and one Cl^- component

$$E_m = \frac{RT}{F} \ln \frac{(Ae^{\frac{t-t_0}{\tau}} + A_1 e^{\frac{t-t_0}{\tau_1}})[K]_o + P_{Na}[Na]_o + A_2 e^{\frac{t-t_0}{\tau_2}}[Cl]_i}{(Ae^{\frac{t-t_0}{\tau}} + A_1 e^{\frac{t-t_0}{\tau_1}})[K]_i + P_{Na}[Na]_i + A_2 e^{\frac{t-t_0}{\tau_2}}[Cl]_o} \qquad \text{Equation 4}$$

where R is the gas constant (8.314 J K^{-1} mol^{-1}), T is the temperature (303 °K) and F is the Faraday constant (9.6485 x 10^4 C mol^{-1}). The values for $[K]_o$, $[K]_i$, $[Na]_o$, $[Na]_i$, $[Cl]_o$ and $[Cl]_i$ were set (in mM) to 4, 150, 145, 13, 150 and 31 respectively. Also, A is the amplitude of the component, t is time, t_0 is the time at the beginning of the decay phase of the AHP (not equal to the t=0 for the AHP_{80} values and τ, τ_1 and τ_2 are the decay time constants.

In fitting the data there was no set minimum value for the standard deviation of the fit because of variable 50 Hz noise and minor fluctuations in the baseline. These fluctuations made it impossible to use a single criterion used to decide when a satisfactory fit was obtained. The fit was thus assessed by eye and by checking that adding an additional component produced either an "A" value not significantly different from zero, or both a positive and negative component with identical time constants.

Figure 4.8 shows typical examples of the kinds of fit seen for different AHPs. In total, AHPs from 34 (26 A-type and 8 C-type) cells were fitted. Most cells (26) were best fitted using two decaying exponential K^+-permeability components (Equation 2 above). Interestingly, among these were two "fAHPs" (with AHP_{80} values < 20 ms) which one might expect to arise from a single K^+ component, but were actually best fit with a two-component equation. The τ values for these two cells were: 2.14 and 9.26 ms and 3.24 and 10.36 ms respectively.

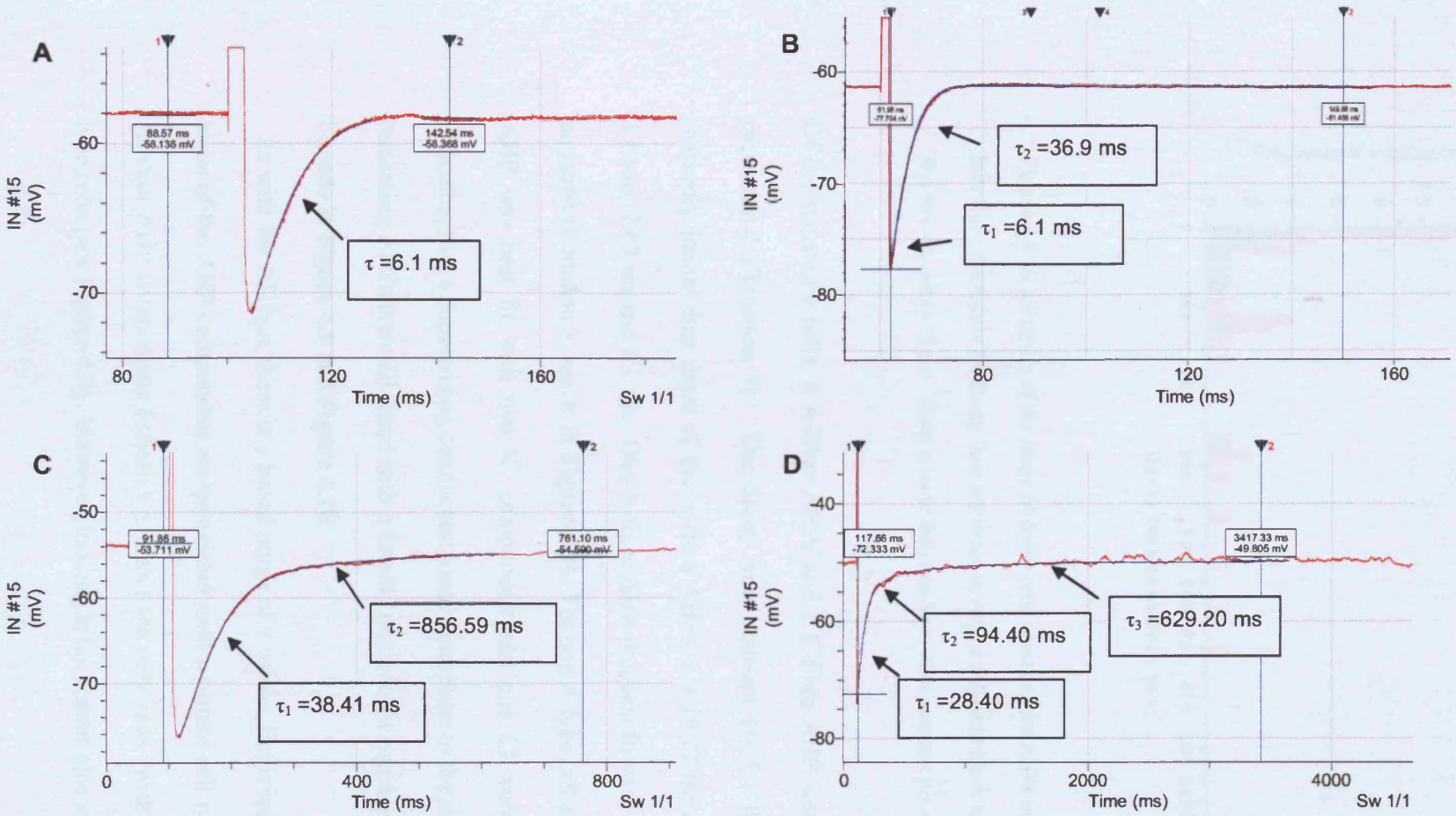

Figure 4.8 Typical examples of AHP fits using the modified Goldman-Hodgkin-Katz equation. The AHPs from most cells could be fit with a single (**A**) or a double exponential (**C**) K^+-permeability model. One cell was fit with a three K^+ component equation (**D**) and another with a hyperpolarising K^+ component and depolarising Cl^- component model (**B**). Decay time constants are indicated in the different panels. In each case the red trace shows the AHP and the blue shows the fit. The arrows indicate, approximately, regions where components with the indicated time constants are more dominant.

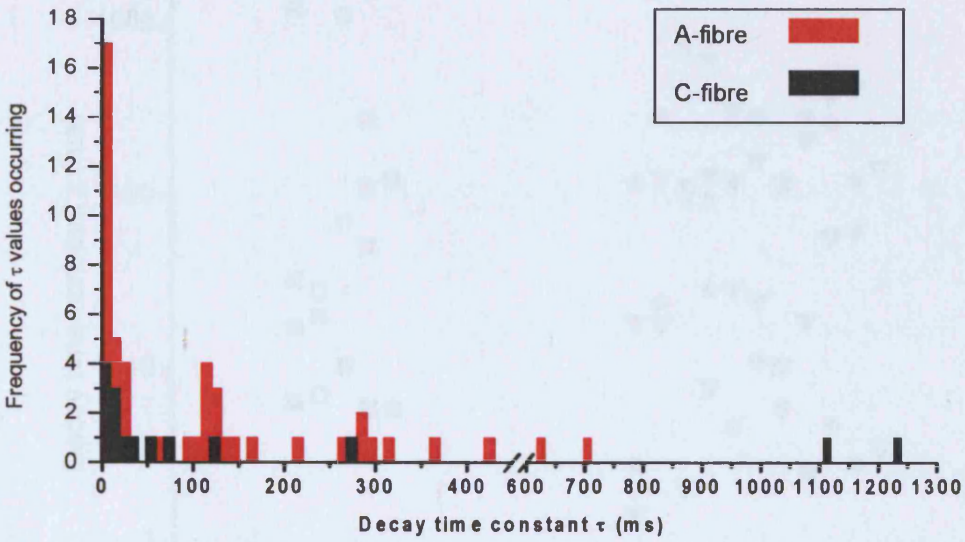

Figure 4.9 A histogram of the range of decay time constants for AHPs in DRG cell bodies. Red bars show the values for decay time constants in A-type cells and black bars for the C-type cells. Bin size was set to 10 ms. There is more than one decay time constant per neurone plotted.

Of the remaining cells, 4 A-fibre AHPs and 1 C-fibre AHP were fitted with a single exponential (Equation 1). The decay time constant (τ) for the C-fibre AHP was markedly longer than those of the A-fibre AHPs, τ = 19.77 ms compared to 0.93 ms, 1.86ms, 2.63 ms and 6.1 ms. One A-fibre AHP was best fit with a three K^+ component equation (Equation 3; see ★ in **Figure 4.9**). For one A-type cell and one C-type cell the AHP was best fit with two K^+ components and one Cl^- component (Equation 4) indicating that a depolarising conductance may contribute to the shape of the AHP. The remaining AHPs were all fitted with a two K^+ component equation and the τ values can be seen in **Figure 4.9** and **Figure 4.10**.

As with the AHP_{80}s, there is a broad range of τ values, but it would seem that at least some of the AHP components are associated with a certain cell type. For example, the shortest AHP components (where $\tau \leq 5$ ms) are only seen (with one exception) in A-type cells (see **Figure 4.9**). However, looking at the scatter-plot in **Figure 4.10** (top),

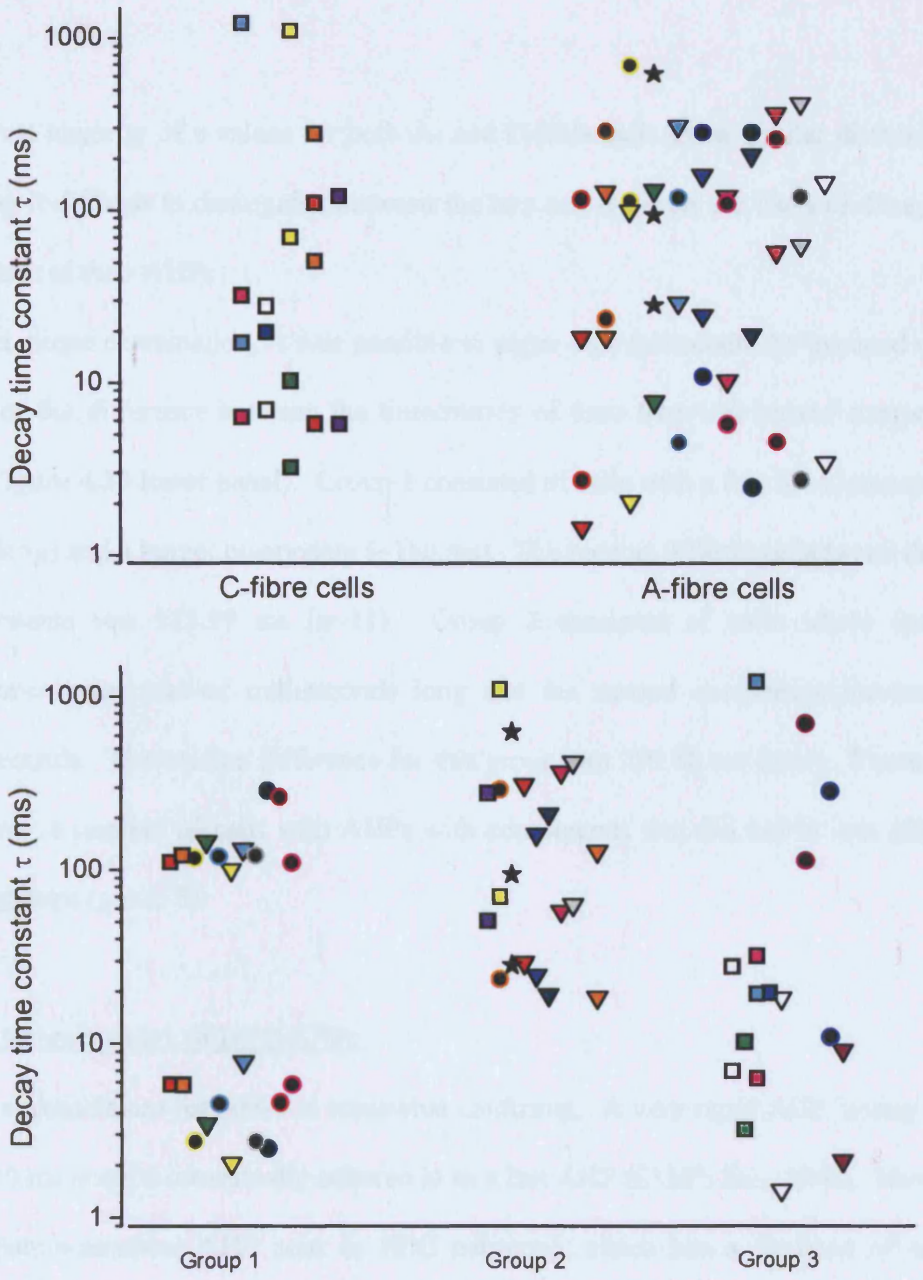

Figure 4.10 Scatterplots of the range of decay time constants seen for AHPs recorded from DRG cell bodies. Upper panel, a scatter-plot of the two-component AHPs seen in A- and C-type cells and one three component AHP (★) in an A-type cell. Lower panel, there are three main groups of cells based on the difference between the two different time constants. Group 1 includes cells with AHP time constants that are separated by one order of magnitude, with the first component < 10 ms and a second, slower component, of 100-300 ms. Group 2 neurones do not have a fast (< 10 ms) component and their two time constants are more closely matched. Group 3 shows the τ values for the AHPs that do not fall into either of these groups. The τ values for the AHP for any individual cell are plotted using the same colour and symbol. A-type cells are shown as circles (●) and triangles (▼) while C-type cells are cells are shown as squares (■).

the great majority of τ values for both A- and C-fibre cells show similar distributions, making it difficult to distinguish between the two cell types on the basis of decay time constants of their AHPs.

Upon closer examination, it was possible to argue that cells could be grouped on the basis of the difference between the timecourses of their first and second components (see **Figure 4.10** lower panel). Group 1 consisted of cells with a fast K^+ component (2-8 ms long) and a longer component (~110 ms). The median difference between the two components was 115.99 ms (n=11). Group 2 consisted of cells where the first component was tens of milliseconds long and the second component hundreds of milliseconds. The median difference for this group was 295.86 ms (n=8). There were, however, a number of cells with AHPs with components that did not fit into either of these groups (group 3).

4.2.3 Pharmacology of DRG AHPs

The nomenclature for AHPs is somewhat confusing. A very rapid AHP lasting fewer than 10 ms is quite consistently referred to as a fast AHP (fAHP; Sah, 1996). However, the apamin-sensitive AHP seen in SCG neurones, which has a duration of several hundred milliseconds, is often described as the slow AHP (Pennefather et al., 1985; Dunn, 1994). This would be fine but for the fact that in many other types of neurone, an apamin-sensitive AHP, with the same timecourse, is followed by an AHP lasting several seconds and in these cases the two components are termed the medium AHP (mAHP) and the slow AHP (sAHP) respectively (Storm, 1989). Further, there is little justification for such clear divisions when it comes to identifying mAHPs in DRG neurones, as can be seen by the range durations of the AHPs described by Waddell & Lawson (1990) and those reported in the preceding sections, as well as the timecourses

of the underlying currents studied by Villière & McLachlan (1996). Nevertheless, in this thesis, for the purpose of reporting the pharmacology of the AHPs recorded from DRG cells, they were separated into two groups. First, AHPs recorded after a single action potential, with durations of 50-500 ms, were classified as mAHPs and secondly, AHPs lasting several seconds usually evoked by a train of action potentials were classified as sAHPs. Whilst this division is somewhat artificial, because in some cases it was possible to observe a small sAHP following a single action potential, the amplitude was usually far more pronounced after repetitive firing. As a result, a train of 10 action potentials was used to generate what is referred to in the section as a sAHP to examine its pharmacology. Both mAHPs and sAHPs were recorded in small and large diameter cells and thus the presence of a sAHP did not appear to correlate with cell type.

Of 152 cells recorded from (using DRGs from p17 animals and perforated patch recording), 77 exhibited a mAHP, 50 displayed a sAHP (30 cells showed both a mAHP and a sAHP). An additional 11 cells showed a long lasting afterdepolarisation (ADP) which, like the sAHP, had a duration of several seconds. One such cell was tested with the Cl^- channel blocker niflumic acid (125 μM). The ADP was abolished, suggesting that there was an underlying Cl^- conductance, though this was not investigated further. The remaining cells showed only a very fast AHP (AHP_{80} < 20 ms).

4.2.3.1 mAHPs in neurones from p17 rats

As mentioned previously, many studies have described a mAHP with an underlying conductance that is due to SK channel activation. To determine whether this was also the case in DRG cells, mAHPs were tested using the SK channel blocker UCL 1848. This compound has been shown to potently block both recombinant (Benton *et al.*,

1999; Shah & Haylett, 2000a) and native neuronal SK channels (Hosseini *et al.*, 2001; Shah *et al.*, 2001; Faber & Sah, 2002) with IC_{50}s similar to those for apamin. However, UCL 1848 has two major advantages over apamin in that its onset of block is fast and its effects are rapidly reversible.

Effects of UCL 1848

Initially, in order to ascertain whether there was any SK involvement in mAHPs, UCL 1848 was applied at concentrations of either 10 nM or 50 nM. These values are quite high compared with the IC_{50} values of cloned channels: ~120 pM for SK2, ~2.1 nM for SK3 (Hosseini *et al.*, 2001) and ~2.9 nM for channels formed from rSK1 and rSK2 co-expression (Benton *et al.*, 2003), but were chosen so that any contribution of SK channels to the AHP could quickly be established.

At these concentrations, UCL 1848 had no effect on either the resting membrane potential or on action potentials. Surprisingly, it also failed to have any significant effect on the majority of mAHPs (results are summarised in **Table 4.2**). Only 1 of 11 cells tested, appeared to show any UCL 1848 sensitivity and this was seen as the reversible block of a component of the AHP (see **Figure 4.11**). Thus despite the evidence for SK channel expression in DRG cells from staining experiments (see **Chapters 3** and **5**), it would appear that they do not contribute substantially to generating mAHPs in the cell body.

Effects of 200 μM Cd^{2+}

AHPs were also tested with the non-selective voltage-dependent Ca^{2+} channel (VDCC) blocker Cd^{2+}. This was designed to indicate whether the mAHP was calcium-dependent. DRG cells exhibit a number of Ca^{2+} currents including some mediated by

L-type and N-type Ca^{2+} channels (Scroggs & Fox, 1992) and these Ca^{2+} channels are known to be sensitive to non-specific blockers such as Ni^{2+} and Cd^{2+} (Hagiwara & Byerly, 1981). Five of the cells which were insensitive to UCL 1848 were also unaffected by Cd^{2+} suggesting that neither SK nor IK channels are likely to be involved in generating the mAHP in these neurones. A further four cells were tested and of these, two showed partial sensitivity to Cd^{2+} (see **Figure 4.12**).

Effects of other K^+ channel blockers

Charybdotoxin (ChTx) is a known blocker of BK and IK channels (Sah & Faber, 2002). As a few cells apparently show some sensitivity to Cd^{2+} but not to UCL 1848 it is possible that this Ca^{2+}-dependent component may have been due to some other K_{Ca} channel i.e. either of the BK or IK type. For this reason, some of these cells were also tested with 10 nM ChTx. In the two cells where the toxin was applied, however, there was no sign of any block of the mAHP (**Figure 4.13**) indicating that K_{Ca} channels do not make any obvious contribution to the underlying conductance.

TEA when applied at 5 mM should block a number of voltage-activated K^+ channels including the BK channel (Blatz & Magleby, 1987; Coetzee et al., 1999). As with ChTx, there was no effect on the mAHP (n=5) although it was usually possible to observe broadening of the action potential (**Figure 4.13**). One final K^+ channel blocker tested was 4-amino pyridine (4-AP) which is known to act on a number of members of the K_V family of K^+ channels (Coetzee *et al.*, 1999). Again, there was no blocking effect of the mAHP observed in the presence of 4-AP (**Figure 4.13**) ruling out many of the K_V family.

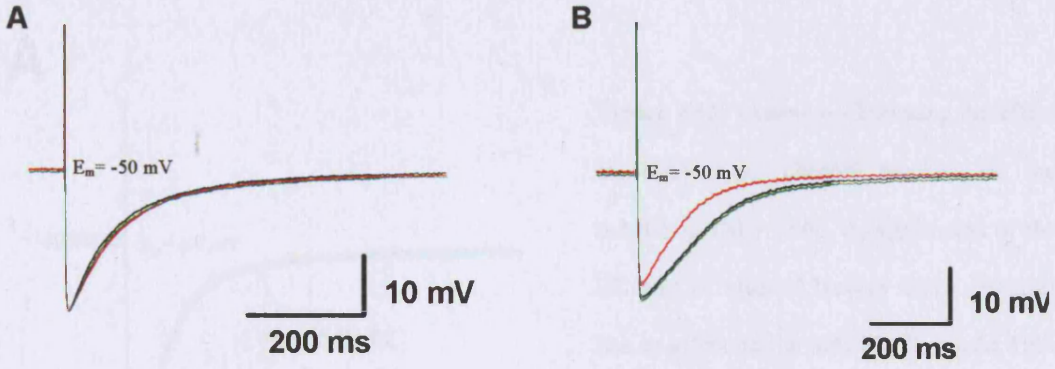

Figure 4.11 Variable sensitivity of the DRG mAHPs to UCL 1848. **A**, a typical example of a cell that did not show any block in response to the application of UCL 1848 at a 10 nM concentration. **B**, the mAHP in one cell, out of eleven tested, showed partial sensitivity, but not complete block, on application of 10 nM UCL 1848. In these and all subsequent electrophysiological figures in this chapter, the black trace shows the control recording, the red trace shows the AHP in the presence of the drug and the green trace shows the recovery.

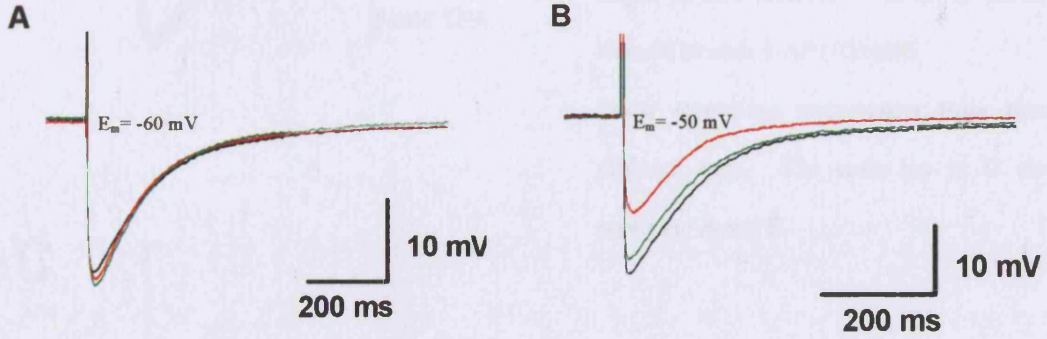

Figure 4.12 Variable Cd^{2+} sensitivity of mAHPs in DRG neurones. **A**, an example of a cell with a mAHP insensitive to block by Cd^{2+}. **B**, a mAHP showing a small component that is blocked by 200 μM Cd^{2+}. Block was only seen in two out of nine cells.

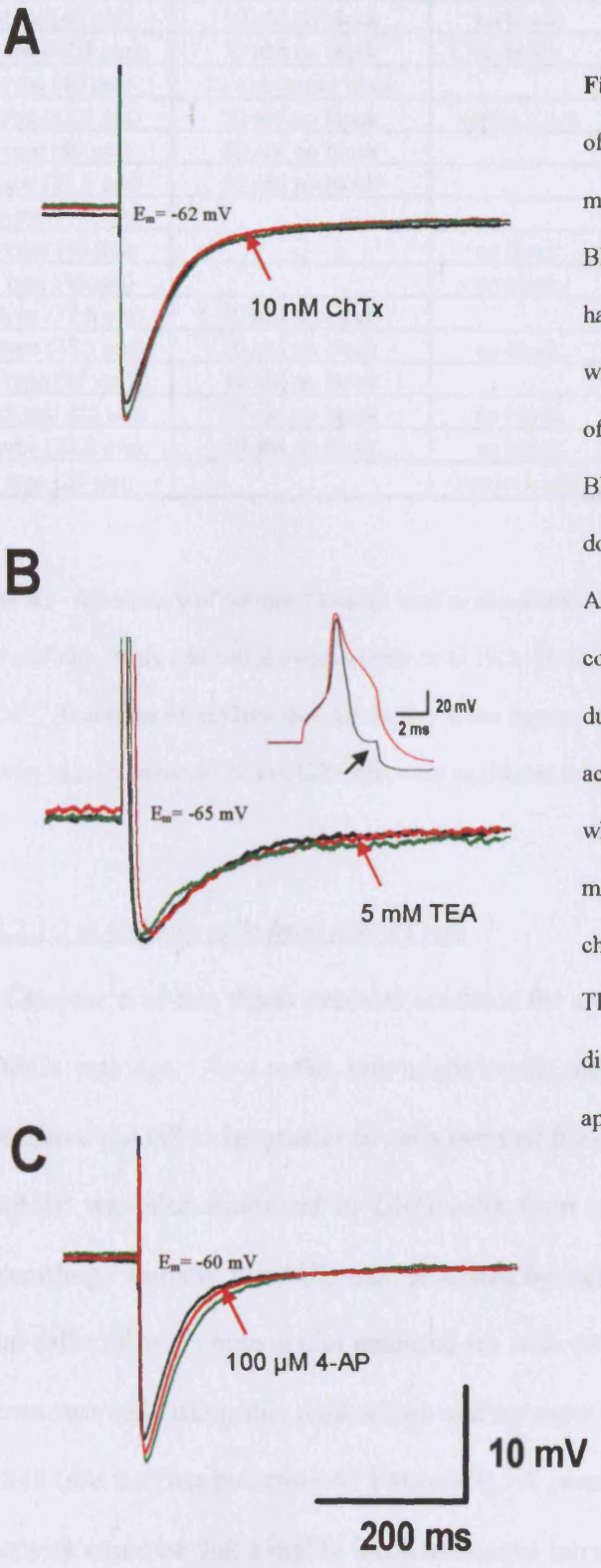

Figure 4.13 Examples illustrating the effect of different K^+ channel blockers on the mAHPs in DRG cells. **A**, application of the BK and IK channel blocker ChTx (10 nM) has no effect on the mAHP. **B**, 5 mM TEA which would be expected to block a number of voltage-gated K^+ channels including the BK channel has no effect on the mAHP. It does, however, increase the duration of the AP (shown in inset). The small step in the control recording (see arrow) is an artefact due to the depolarising pulse out-lasting the action potential. The step is seen at the point where the depolarising pulse ends. **C**, the mAHP is also resistant to block by the K_V channel blocker 4-AP (100 µM).

These recordings were taken from three different cells. The scale bar in **C** also applies to **A** and **B**.

Cell type (diameter)	UCL 1848 (10/50 nM)	200 μM Cd^{2+}	10 nM ChTx	5 mM TEA	100 μM 4-AP
A-type (40 μm)	10 nM no block				
A-type (40 μm)	10 nM no block	no block			
A-type (42.5 μm)	10 nM no block	no block			
A-type (40 μm)	10 nM partial block				
A-type (42.5 μm)	50 nM no block	partial block			
A-type (40 μm)	50 nM no block			no block	
A-type (37.5 μm)	50 nM no block			no block	
A- type (37.5 μm)				no block	
A- type (40 μm)		no block			
A- type (40 μm)		no block			
A- type (37.5 μm)	10 nM no block		no block		
A- type (37.5 μm)	10 nM no block	no block	no block		no block
C- type (25 μm)	10 nM no block				
Small cell (25 μm)	10 nM no block	no block			
C- type (22.5 μm)	10 nM no block	no block		no block	
C- type (25 μm)		partial block		no block	no block

Table 4.2 A summary of various blockers used to characterise the mAHP in both A- and C-fibre cells isolated from p17 rats. Only one cell showed sensitivity to UCL 1848, and two had mAHPs that were partially blocked by Cd^{2+}. Examples of mAHPs that did display some degree of block are illustrated in the figures. The great majority of cells, however, had mAHPs that were unaffected by any of the blockers used.

4.2.3.2 mAHPs in cells from p40-45 rats

Chapter 5 of this thesis presents evidence for an up-regulation of SK channels in rat DRGs with age. As a result, one might expect the likelihood of observing an apamin-sensitive mAHP to be greater in cells isolated from adult animals. For this reason, the mAHP was also examined in DRG cells from rats aged p40-45 using intracellular recording. Initially the AHP was generated by using a 5 ms current pulse to stimulate the cell to fire a single action potential (as with p17 cells). However, good recordings from two cells using this method showed no signs of block in response to 50 nM UCL 1848 (see the first two rows of **Table 4.3**). A possible reason for a lack of SK channel activity could be that a highly localised rise in intracellular Ca^{2+} is needed. If this were

so, a single action potential may not allow enough Ca^{2+} influx via VDCCs to cause SK channel opening. To overcome this possible problem, the pulse protocol for generating a mAHP was adjusted to a 100 pA depolarising current pulse lasting 100 ms.

Effects of blockers on the mAHP

The effects of different drugs on the mAHPs seen in DRG cells from p40-45 aged rats are summarised in **Table 4.3**. There was no effect of 50 nM UCL 1848 on any of the mAHPs recorded from isolated cells (n=8). Two of the cells tested with UCL 1848 also proved to be insensitive to 10 μM clotrimazole, a potent blocker of the IK channel (Alvarez *et al.*, 1992; Brugnara *et al.*, 1993; Jensen *et al.*, 1998). Furthermore, the mAHP in one of these cells also showed insensitivity to 5 mM TEA. However, one mAHP (of three tested) from the p40-45 cells had a component sensitive to block by 200 μM Cd^{2+}.

Effects of the SK/IK channel enhancer, 1-EBIO

1-EBIO has been shown to potentiate currents of cloned SK and IK channels (Pedersen *et al.*, 1999; Syme *et al.*, 2000; Pederzani *et al.*, 2001). In addition, Pederzani and colleagues (2001) have demonstrated that 1-EBIO increases the amplitudes of medium and slow AHP currents in hippocampal neurones. In contrast to these findings in the hippocampus, the great majority of DRG mAHPs appear to be unaffected by 1-EBIO application (**Table 4.3**). The frequency of a functional SK channel response appears unrelated to age when recording from the cell bodies. One cell, however, that has a mAHP enhanced by 300 μM 1-EBIO. This, along with the partial sensitivity of one mAHP (see **Figure 4.11**) to UCL 1848, provides some evidence for functional SK channels being formed in DRG cells. It also leaves open the possibility that while SK

channels may not normally play a substantial role in AHPs of DRG cell bodies, they may be brought into play by channel openers such as 1-EBIO. However, it is important to note that the effects of 1-EBIO seen in **Figure 4.14** could also be mediated by IK channels and this could only be ruled out by addition of either UCL 1848 or clotrimazole in the presence of 1-EBIO to see if either of these drugs could block the activated current.

Although only one cell appeared to be sensitive to 1-EBIO, this could perhaps be an underestimate. This is because several cells (3/10) had AHPs that approached the expected value for the potassium reversal potential (E_K; expected to be about -96 mV). It would then be difficult to observe any enhancement of the AHP due to SK/IK channel activation. Against this, 1-EBIO should also have prolonged the AHP so that any enhancement would have been evident.

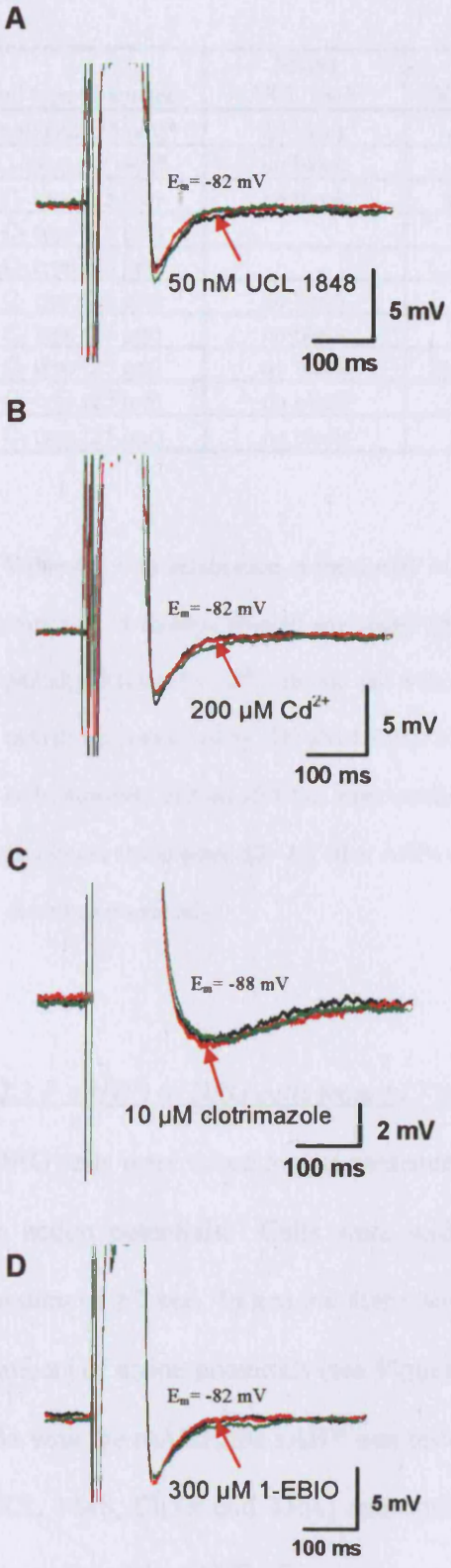

Figure 4.14 Examples of mAHPs in DRG cells from p40-45 rats, illustrating the effects of different drugs. **A**, no block is seen after applying UCL 1848 at a concentration of 50 nM. **B**, example of a mAHP insensitive to block by 200 µM Cd^{2+}. **C**, a mAHP insensitive to 10 µM clotrimazole. **D**, a mAHP that is unaffected by 300 µM 1-EBIO. **E** shows a set of recordings from a cell with an mAHP increased by 300 µm 1-EBIO.

All the AHPs depicted here were generated using a 100 pA current pulse that was 100 ms long. **A**, **B** and **D** are recordings taken from the same cell. **C** and **E** show recordings from a second cell.

Cell type (diameter)	50 nM UCL 1848	300 μM 1-EBIO	200 μM Cd^{2+}	10 mM clotrimazole	5 mM TEA
small cell (25 μm)*	no block	no change			
C- type (25 μm)*	no block		partial block	no block	no block
C- type (25 μm)	no block	no change			
C- type (25 μm)		no change			
C- type (25 μm)		no change			
C- type (25 μm)	no block				
C- type (25 μm)	no block	no change			
C- type (25 μm)	no block	Small increase		no block	
C- type (25 μm)	no block	no change	No block		
C- type (25 μm)	no block	no change	No block		

Table 4.3 Characterisation of the mAHP in DRG cells isolated from p40-45 rats. None of the cells from p40-45 animals showed any sensitivity to 50 nM UCL 1848, but one had a mAHP that was partially blocked by Cd^{2+}. In one cell with a mAHP insensitive to UCL 1848 and clotrimazole, the mAHP was enhanced by 300 μM 1-EBIO suggesting K_{Ca} channel activation. The great majority of cells, however, had mAHPs that were unaffected by any of the drugs used. *AHPs seen in response to a single action potential. All other AHPs were generated using a long depolarising current pulse as described previously.

4.2.3.3 sAHPs in DRG cells from p17 rats

DRG cells were tested for the presence of a sAHP by stimulating them to fire a train of ten action potentials. Cells were said to have a sAHP if the resulting AHP had a duration of ≥ 2 sec. In general there was an increase in sAHP amplitude with increasing numbers of action potentials (see **Figure 4.15**).

As with the mAHP, the sAHP was tested with a number of known K^+ channel blockers (UCL 1848, ChTx and TEA) and again, Cd^{2+} (200 μM) was used to check for Ca^{2+} sensitivity of the sAHP. Further, since many neuronal sAHPs are abolished by agonists for certain G-protein coupled receptors (Vogalis *et al.*, 2003), and since histamine is

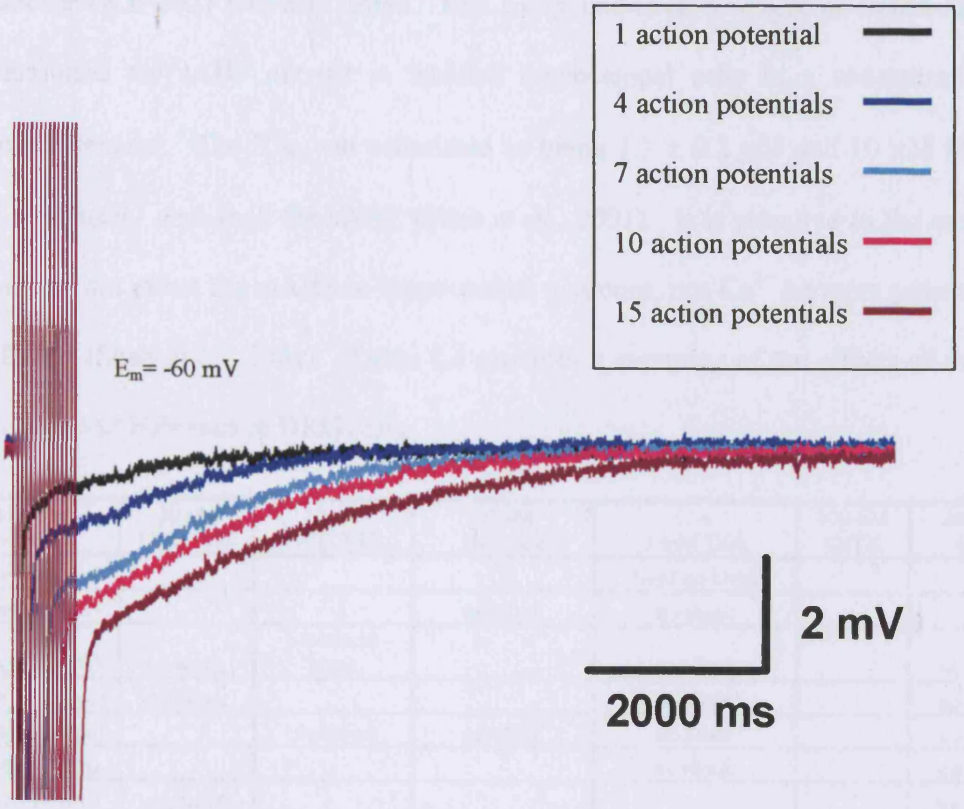

Figure 4.15 A recording from a C-type p17 DRG cell which had a sAHP. This sAHP increased in amplitude and duration with increasing numbers of action potentials (at a frequency of 20 Hz).

known to produce such an effect in sensory neurones of the nodose ganglion (Leal-Cardoso *et al.*, 1993; Undem & Weinreich, 1993) it was also tested here at a concentration of 10 μM to determine if it had a similar effect on DRG sAHPs. Finally the blocker UCL 2027 was also tested. This compound is an analogue of clotrimazole that inhibited the sAHP current in isolated hippocampal cells in a concentration-dependent manner. The IC_{50} was calculated as being 1.1 ± 0.2 μM and 10 μM UCL 2027 completely abolished the sAHP (Shah *et al.*, 2001). It is selective to the extent that it does not affect the mAHP in hippocampal neurones, nor Ca^{2+} currents generated by VDCCs (Shah *et al.*, 2001). **Table 4.4** provides a summary of the effects of these drugs on the sAHPs seen in DRG cells.

Cell type (diameter)	10 nM UCL 1848	10 μM UCL 2027	10 μM histamine	5 mM TEA	100 nM ChTX	200 μM Cd^{2+}
A-type (40 μm)				3mM no block		
A-type (40 μm)			no block	no block		
A-type (40 μm)	no block	prominent block		no block		no block
A-type (47.5 μm)	no block			no block		no block
A-type (42.5 μm)		abolished	no block	no block		no block
A-type (40 μm)				no block		no block
A-type (40 μm)	no block					no block
A-type(42.5 μm)	no block			no block		no block
C-type (25 μm)	no block	abolished	prominent block	prominent block		
C-type (25 μm)	no block	abolished	prominent block	prominent block	no block	
C-type(25 μm)	no block			no block		abolished

Table 4.4 A summary table of the responses to drugs used to characterise the sAHP in DRG cells isolated from p17 rats. A-fibre cells were generally insensitive to all of the blockers used except UCL 2027. In contrast three stable recordings from C-type cells, the sAHPs could be blocked by UCL 2027, histamine, TEA and in one case Cd^{2+}.

The sAHPs seen in the large diameter A-fibre cells were insensitive to all of the blockers used over the range of concentrations tested, with the exception of 10 μM UCL 2027 which blocked a small component of one AHP and abolished a second (see **Figure**

4.16). The lack of Ca^{2+} sensitivity suggests that these sAHPs are different to those described in a variety of other neuronal cell types (Sah & Faber, 2002; Vogalis *et al.*, 2003). The sAHPs in C-fibre cells were all insensitive to 10 nM UCL 1848. There appeared to be at least two kinds of sAHP in C-fibre cells, those that were TEA-insensitive and those that were TEA-sensitive. The cell that did not have a TEA-sensitive sAHP was completely blocked by 200 μM Cd^{2+} and the sAHP was evident after a single action potential (see **Figure 4.17**). Intriguingly, two cells with sAHPs that were sensitive to 10 μM histamine and UCL 2027, could also be almost completely blocked by 5 mM TEA (**Figure 4.18**). A sAHP sensitive to TEA block has not, to my knowledge, been previously reported.

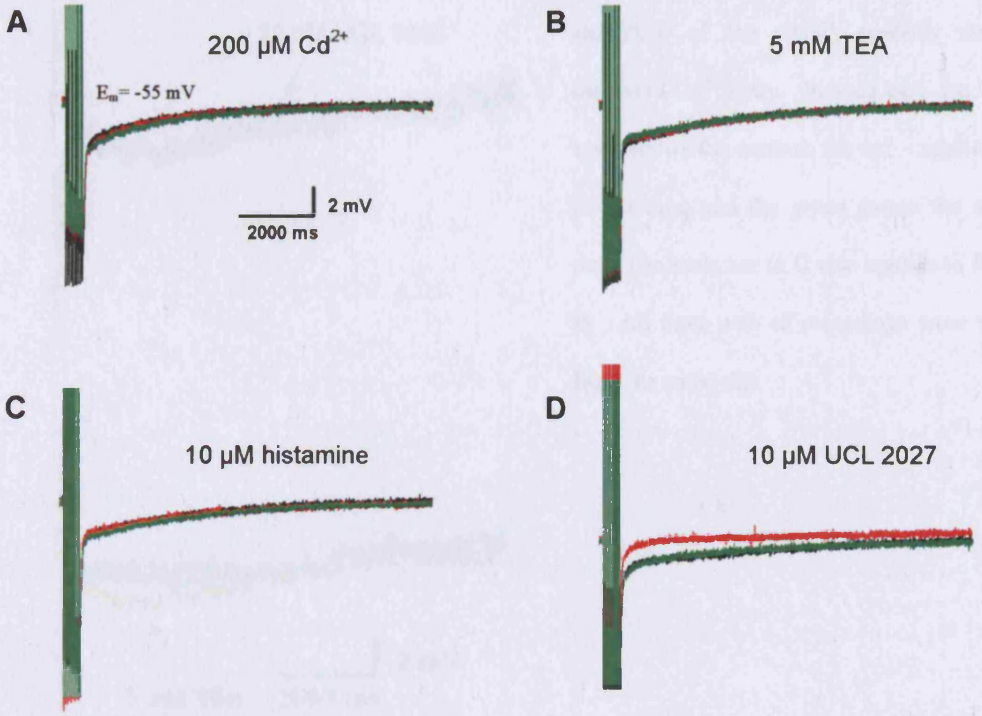

Figure 4.16 Pharmacology of a sAHP recorded from an A-type cell. The sAHP was tested with the following drugs: 200 μM Cd^{2+} (**A**), 5 mM TEA (**B**), 10 μM histamine (**C**) and 10 μM UCL 2027 (**D**). This sAHP is insensitive to Cd^{2+}, histamine and TEA. It is, however, blocked by UCL 2027. The scale-bar in **A** also applies to **B**, **C** and **D**.

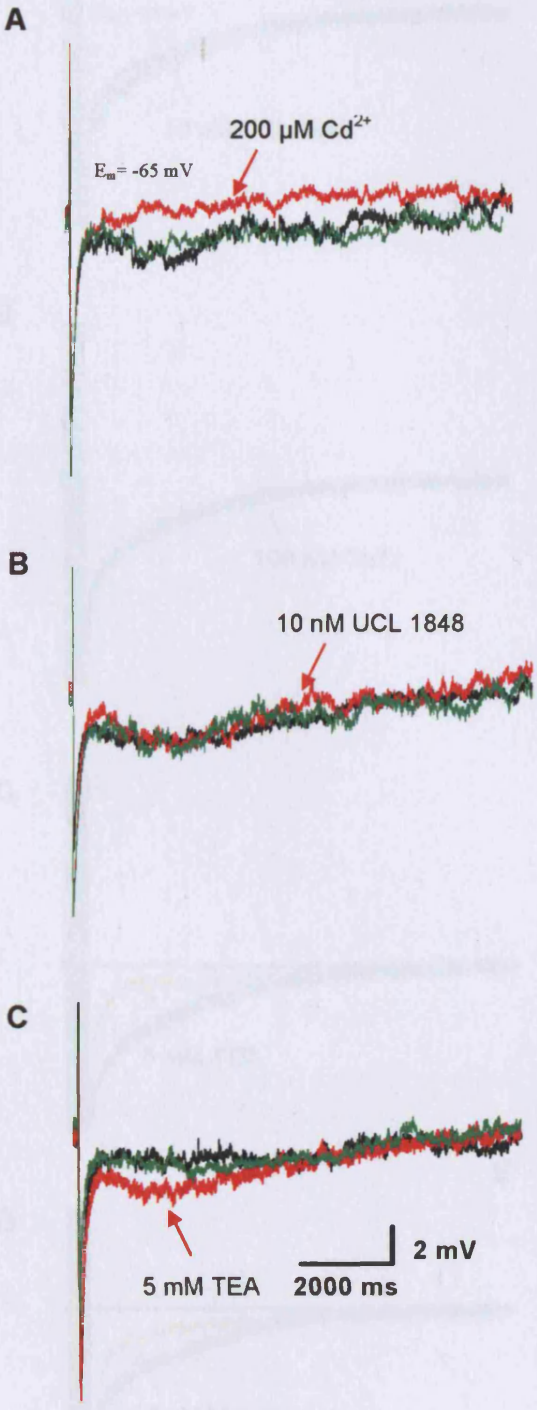

Figure 4.17 An example of a small Cd^{2+}-sensitive sAHP in a C-type DRG cell seen in response to a single action potential. **A**, effect seen with 200 μM Cd^{2+}. **B**, no block seen with 10 nM UCL 1848. **C**, no block seen with 5 mM TEA. In fact, if anything, there appears to be an increase in the peak amplitude of the sAHP, possibly due to increased Ca^{2+} entry. In each case the black trace shows the control, the red – application of the drug and the green shows the wash-out. The scale bar in **C** also applies to **A** and **B**. All three sets of recordings were taken from the same cell.

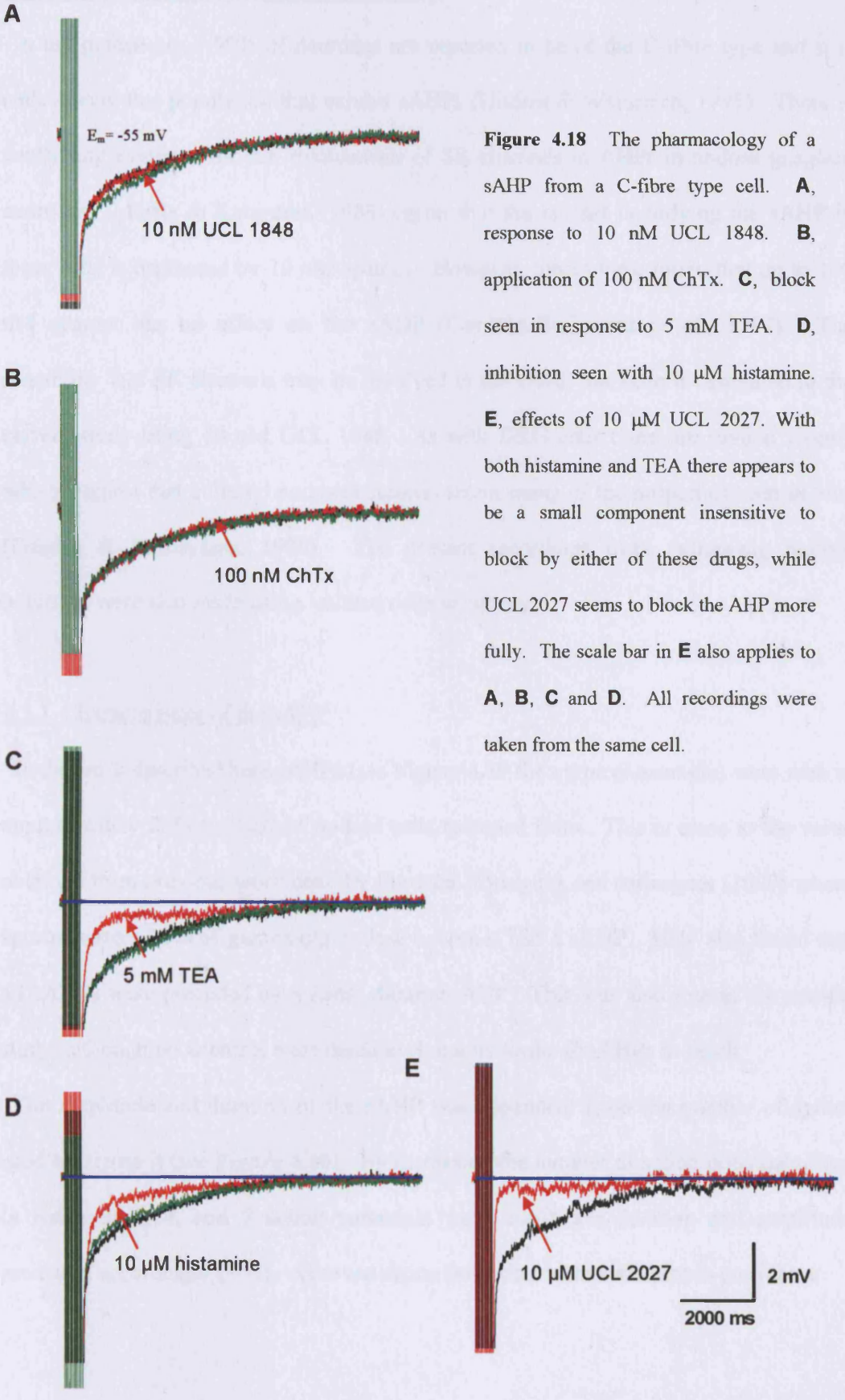

Figure 4.18 The pharmacology of a sAHP from a C-fibre type cell. **A**, response to 10 nM UCL 1848. **B**, application of 100 nM ChTx. **C**, block seen in response to 5 mM TEA. **D**, inhibition seen with 10 µM histamine. **E**, effects of 10 µM UCL 2027. With both histamine and TEA there appears to be a small component insensitive to block by either of these drugs, while UCL 2027 seems to block the AHP more fully. The scale bar in **E** also applies to **A**, **B**, **C** and **D**. All recordings were taken from the same cell.

4.3 Results from nodose ganglion neurones

In the guinea-pig, ~90% of neurones are reported to be of the C-fibre type and it is cells among this population that exhibit sAHPs (Undem & Weinreich, 1993). There is conflicting evidence for the involvement of SK channels in AHPs in nodose ganglion neurones. Morita & Katayama (1989) report that the current underlying the sAHP in these cells is depressed by 10 nM apamin. However, others have found that up to 100 nM apamin has no effect on the sAHP (Cordoba-Rodriguez *et al.*, 1999). The possibility that SK channels may be involved in the sAHP has been investigated in the current study using 10 nM UCL 1848. As with DRG cells there are several reports which suggest that cultured nodose neurones retain many of the properties seen *in vivo* (Fukuda & Kameyama, 1980). The present recordings from guinea-pig nodose neurones were also made using isolated cells in culture.

4.3.1 Characteristics of the sAHP

In the work described here sAHPs (see **Figure 4.19** for a typical example) were seen in approximately 25% (n=102) of nodose cells recorded from. This is close to the value obtained from previous work done by Cordoba-Rodriguez and colleagues (1999) where approximately 20% of guinea-pig nodose neurones had a sAHP. They also found that all sAHPs were preceded by a faster duration AHP. This was also true in the current study, although no attempts were made to characterise the f/mAHPs in depth.

The amplitude and duration of the sAHP was dependent upon the number of spikes used to initiate it (see **Figure 4.20**). By increasing the number of action potentials fired (a series of 1, 4, and 7 action potentials were used), the duration and amplitude increased accordingly (n=3). As seven action potentials were sufficient to produce a

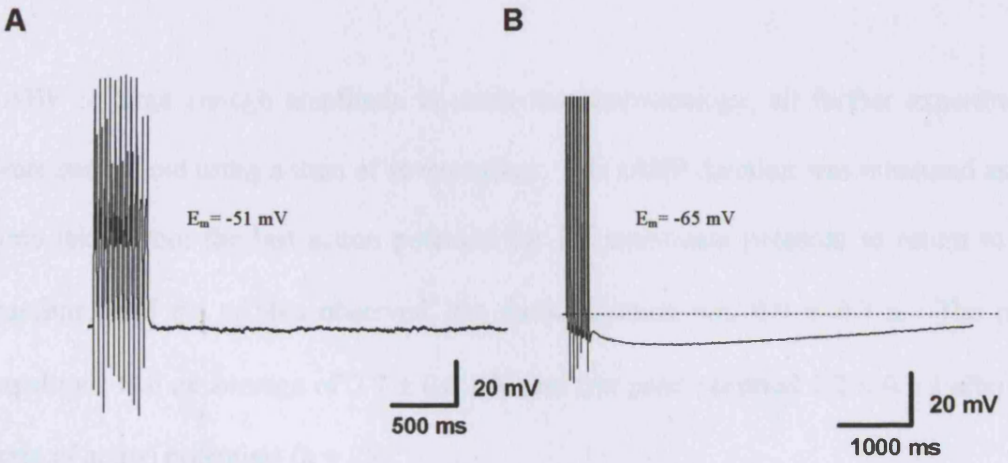

Figure 4.19 Typical examples of voltage recordings from two different nodose ganglion cells cultured for 1-3 days. **A**, a cell in which the sAHP is absent even in response to ten action potentials. **B**, a recording from a cell with a robust sAHP, seen in response to seven action potentials. The dotted line represents the resting membrane potential. The action potentials in **B** have been truncated to show the AHP more clearly.

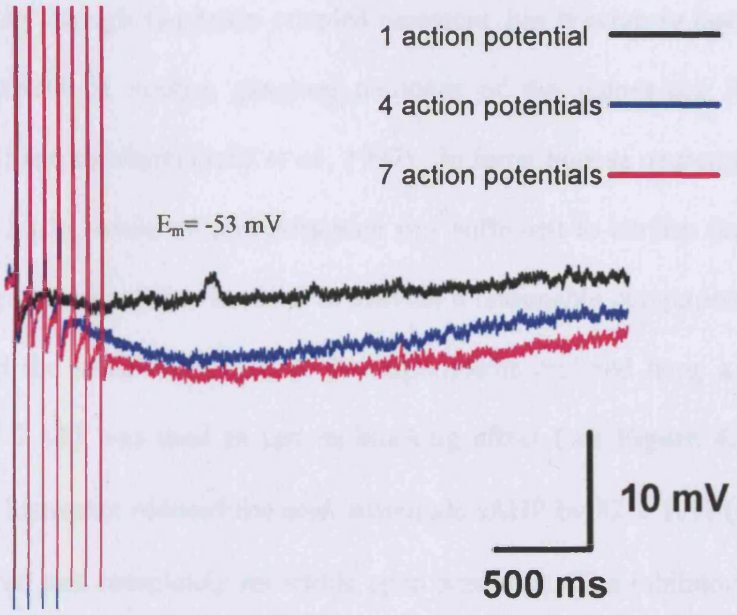

Figure 4.20 The size and the duration of the sAHPs seen in nodose ganglion neurones is dependent upon the number of action potentials fired. As the number of spikes initiated increases, so does the peak amplitude and the duration of sAHP. Extremes of the action potentials have been truncated for clarity.

sAHP of large enough amplitude to study the pharmacology, all further experiments were carried out using a train of seven spikes. The sAHP duration was measured as the time taken from the last action potential for the membrane potential to return to the baseline. Of the sAHPs observed, the mean duration was 6.9 ± 0.3 s. The peak amplitude had an average of 7.7 ± 0.6 mV and this peak occurred 1.2 ± 0.1 s after the train of action potentials (n = 26).

Before any novel pharmacology was carried out, the sAHP was tested with histamine and bradykinin. These two drugs are known to modulate the sAHP in nodose cells and so were used to ensure that responses seen with the neurones in culture were comparable to those previously reported in the literature.

4.3.2 Effects of histamine on the sAHP

Histamine, acting through G-protein coupled receptors, has previously been reported to abolish the sAHP in nodose ganglion neurones of the guinea-pig (Undem & Weinreich, 1993) and the ferret (Jafri *et al.*, 1997). In ferret nodose neurones the EC_{50} was reported as 2 μM, while 10 μM histamine was sufficient to abolish the sAHP in both ferret and guinea-pig cells. In order to provide a reasonable comparison between these results and the sAHPs recorded in the experiments outlined here, a histamine concentration of 3 μM was used to test its blocking effect (see **Figure 4.21**). This concentration of histamine reduced the peak amplitude sAHP by 82 ± 13% (n = 2) and the block observed was completely reversible upon wash-out. The inhibitory effect of histamine was also accompanied by a membrane depolarization of 8.5 ± 1 mV which suggests that it may act on more than one kind of channel (those underlying the sAHP and those responsible for setting the resting membrane potential). Another possibility is that some of the channels underlying the sAHP are open in the resting cell.

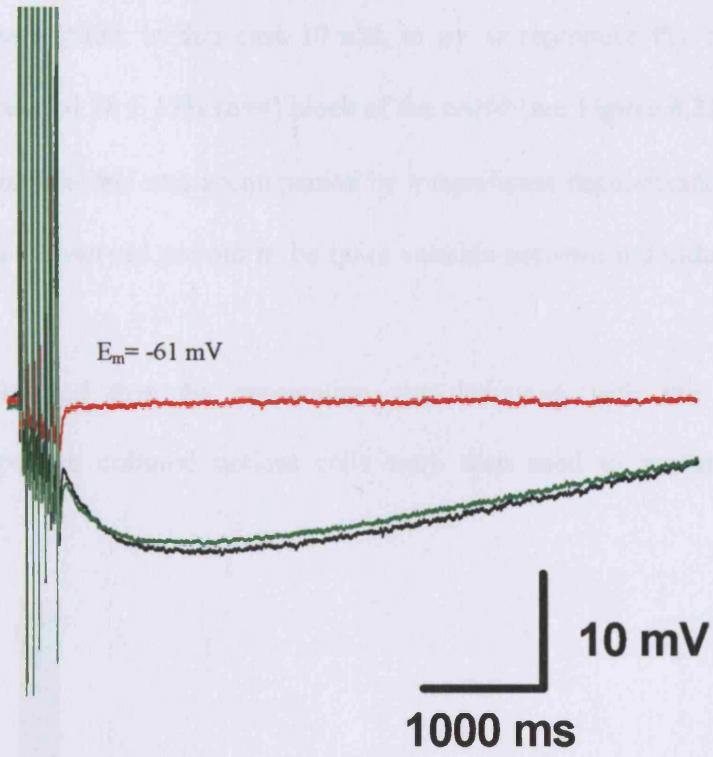

Figure 4.21 Block of the sAHP in a nodose ganglion neurone in response to 3 μM histamine. The block of the AHP was accompanied by a depolarisation of the resting membrane potential by 10 mV though this cannot be seen in the current figure, as the traces have been superimposed to illustrate the block of the sAHP.

4.3.3 Effects of bradykinin on the sAHP

As with histamine, the effects of bradykinin have been investigated previously and a concentration of 100 nM has been shown to produce complete inhibition of the sAHP in guinea-pig nodose neurones (Weinreich *et al.*, 1995). Again a single concentration of bradykinin was applied, in this case 10 nM, to try to reproduce this result. 10 nM bradykinin produced 58 ± 15% (n=4) block of the sAHP (see **Figure 4.22**). In a similar manner to histamine this was accompanied by a significant depolarisation of 7.4 ± 2.2 mV. The block observed proved to be quite variable between individual cells (range 25–100%).

Having established that the preparation was behaving with the characteristics previously reported, cultured nodose cells were then used to explore some novel pharmacology.

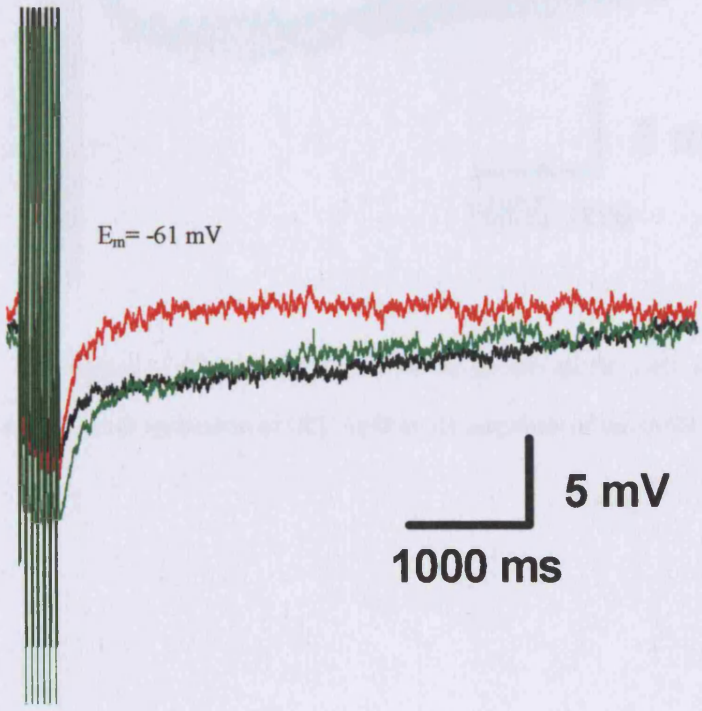

Figure 4.22 Effect of bradykinin (10 nM) on the sAHP seen in a nodose ganglion cell. Bradykinin completely abolishes the sAHP. This is accompanied by a depolarisation which cannot be seen here as the traces have been superimposed to show the effect on the sAHP.

4.3.4 Effects of UCL 1848 on nodose AHPs

In order to determine whether the sAHP in nodose cells exhibits SK-like pharmacology, the response to UCL 1848 was tested. At a concentration of 10 nM no block of the sAHP observed (n = 4; see **Figure 4.23**).

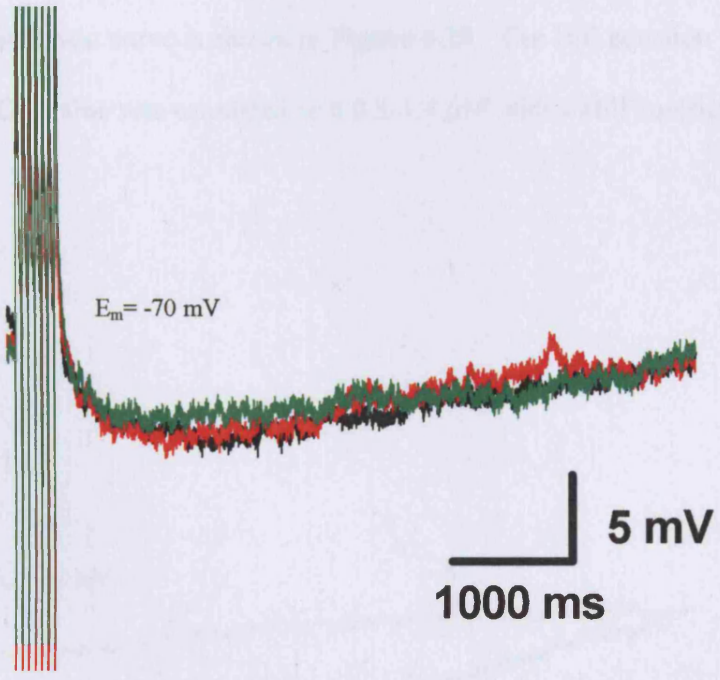

Figure 4.23 The absence of effects of UCL 1848 on the nodose ganglion cell sAHP. No block produced by a 10 nM bath application of UCL 1848 on the amplitude of the sAHP.

4.3.5 Effects of UCL 2027 on the sAHP

When tested with a high concentration of UCL 2027 (20 μM; **Figure 4.24**), the nodose sAHP showed obvious block. The majority, but not all, of this inhibition was reversed upon washout. In order to investigate this further, and to compare the inhibition with that reported for the sAHP in hippocampal neurones, UCL 2027 was applied to nodose neurones possessing a sAHP at concentrations of 1, 3, 6 and 10 μM and 20 μM. The reduction of the peak amplitude of the sAHP was determined and the resulting concentration-inhibition curve is shown in **Figure 4.25**. The Hill equation was fitted to the data. The IC_{50} value was estimated as 6.0 ± 1.4 μM with a Hill coefficient of 0.9 ± 0.2.

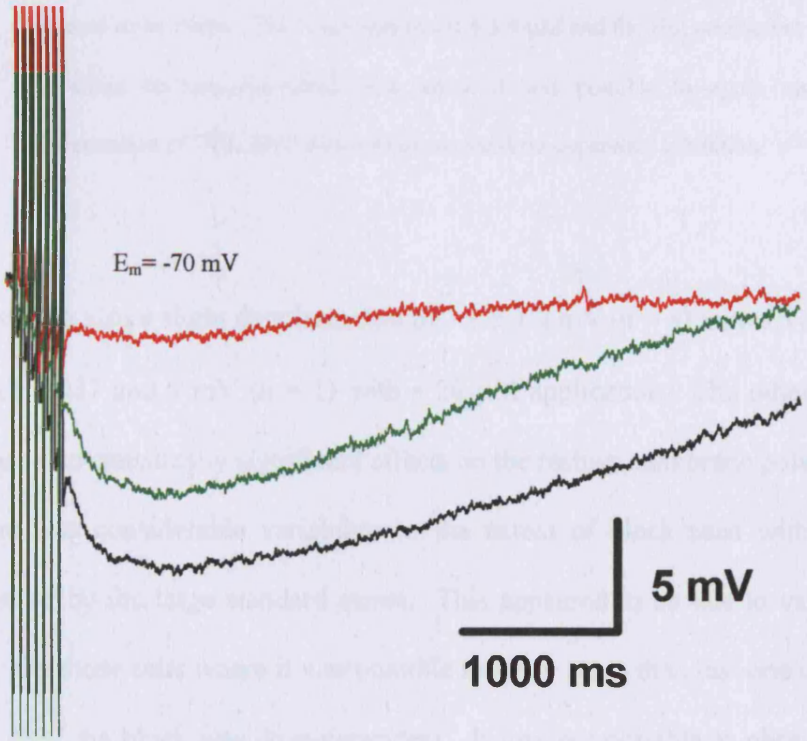

Figure 4.24 The response of a nodose sAHP to a 20 μM concentration of UCL 2027. This particular cell exhibits 78% inhibition of the peak amplitude of the sAHP (red trace). The effects are, however, not completely washed out up to 10 minutes after drug application (green trace).

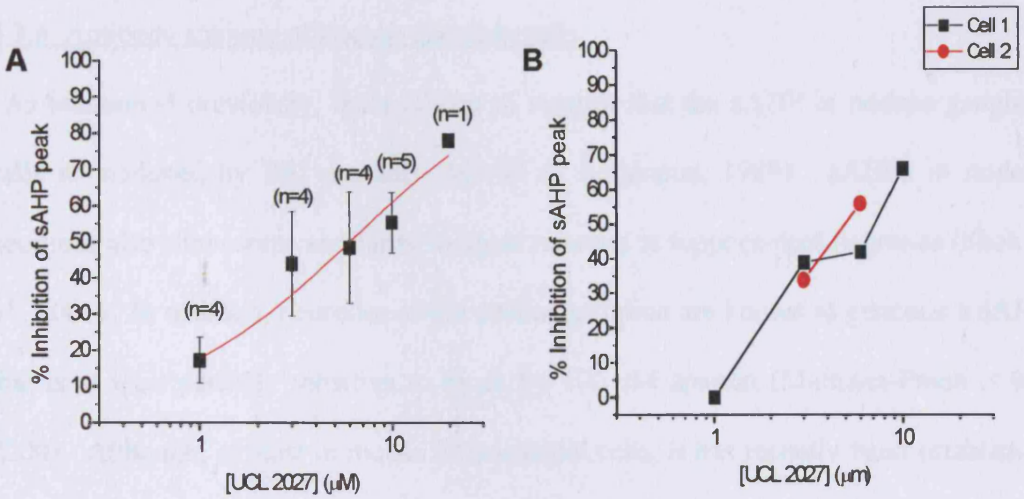

Figure 4.25 Inhibition of the nodose ganglion neurone sAHPs by UCL 2027. **A,** The concentration-inhibition curve for the effects of UCL 2027 on the sAHP amplitude. Each point shows the mean ± S.E.M of observations from 4–5 different cells (except for the 20μM point where n = 1). The curve has been fitted using the Hill equation where y_{max} is assumed to be 100%. The IC_{50} value is 6.0 ± 1.4 μM and the Hill coefficient 0.9 ± 0.2. **B,** the effect on two individual cells where it was possible to apply more than one concentration of UCL 2027 which illustrate the dose-dependent inhibition.

There was also a slight depolarisation of 3.9 ± 1.2 mV (n = 4) with 10 μM applications of UCL 2027 and 9 mV (n = 1) with a 20 μM application. The other concentrations produced no statistically significant effects on the resting membrane potential.

There was considerable variability in the extent of block seen with UCL 2027 as evidenced by the large standard errors. This appeared to be due to variation between cells. On those cells where it was possible to apply more than just one concentration of UCL 2027 the block was dose-dependent. It was not possible to observe 100% block with any of the concentrations of UCL 2027 used in the current study.

4.3.6 Antibody staining of nodose ganglion cells

As mentioned previously, there is data to suggest that the sAHP in nodose ganglion cells is mediated by SK channels (Morita & Katayama, 1989). sAHPs in nodose neurones also show some similarity to those reported in hippocampal neurones (Shah *et al.*, 2001). In addition, neurones of the coeliac ganglion are known to generate a sAHP that is at least partially sensitive to block by 100 nM apamin (Martinez-Pinna *et al.*, 2000). Although, at least in mouse hippocampal cells, it has recently been established that SK channels do not underlie the sAHP (see Bond *et al.*, 2004), at the time these experiments were pursued, it was believed that SK1 may be involved (see section 1.3.3.2. of **Introduction**; Vergara *et al.*, 1999; Bond *et al.*, 1999; Bowden *et al.*, 2001). Thus, isolated nodose ganglion cells in culture were stained with the anti-SK/IK channel antibodies to look for the presence of these channel proteins. All staining results are shown in **Figure 4.26**.

There was no obvious positive staining for SK1, SK2 or the IK channel proteins in nodose neurones. The results for the SK3 protein were variable. The M75 did not produce clear SK3 immunoreactivity, whilst the Chemicon antibody produced a fine punctate staining pattern in the region of the cell membrane.

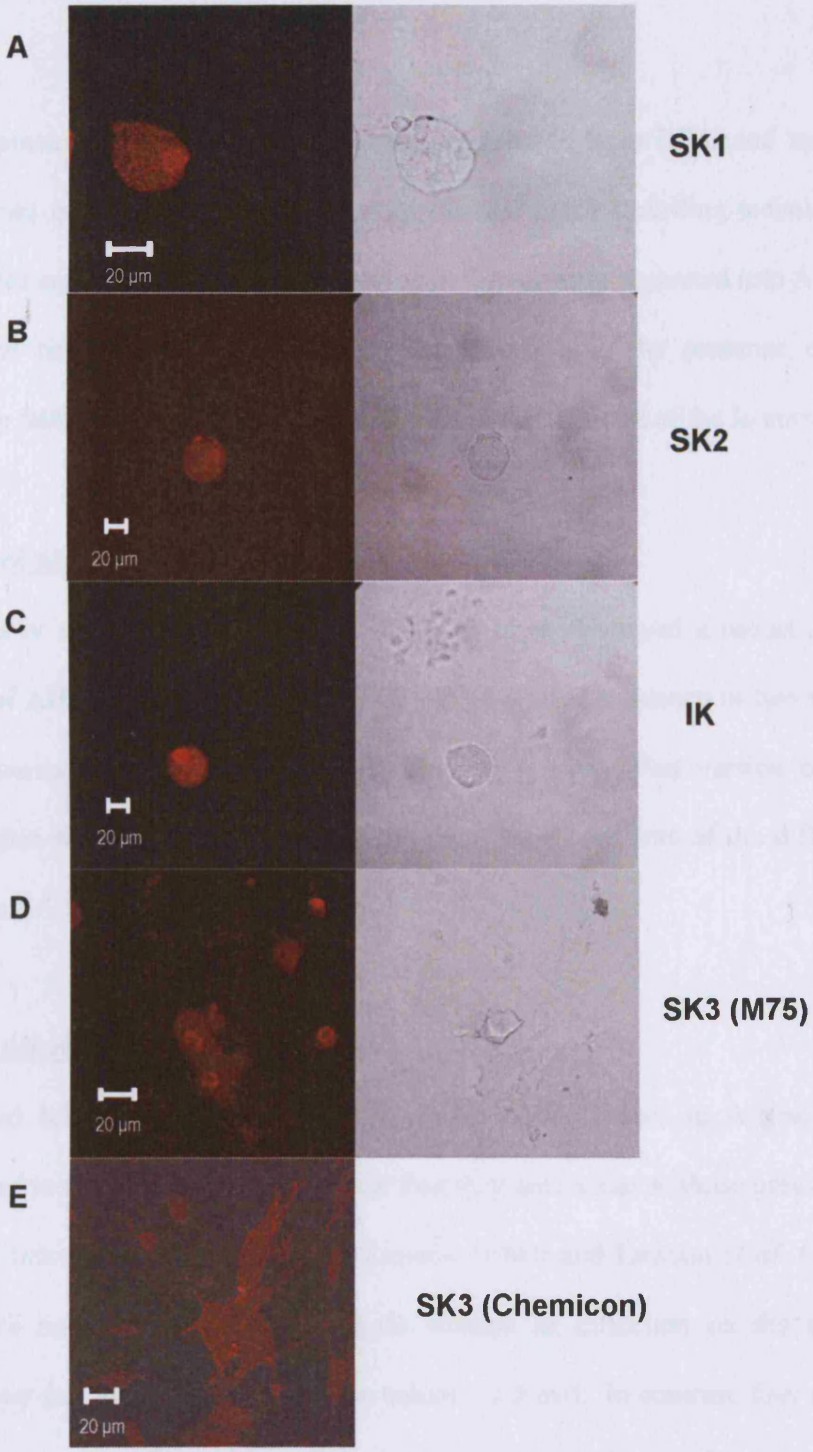

Figure 4.26 Staining of guinea pig nodose ganglion cells with anti-SK/IK channel antibodies. In each case the left panel shows the antibody staining and the right, the brightfield image (there is no brightfield image for panel **E**). **A**, SK1 staining with the L155 antibody. **B**, SK2 staining with the M1 antibody. **C**, IK staining with the M4 antibody. **D** and **E**, SK3 staining with the M75 and Chemicon antibodies respectively. There was no positive signal seen except for the punctate staining see with the Chemicon anti-SK3 antibody.

4.4 Discussion

This chapter presents results from voltage recordings made from DRG and nodose ganglion neurones using either intracellular or perforated patch recording techniques. The initial studies examined AHPs in DRG neurones. These were separated into A- and C-type neurones on the basis of several properties; cell size, the presence of an inflection on the falling phase of the action potential and the presence of the I_H current.

4.4.1 Analysis of AHP kinetics

Following one or more action potentials, DRG cells often displayed a robust AHP. The durations of AHPs following a single action potential were examined in two ways, firstly by measuring the AHP_{80} and secondly by fitting a modified version of the Goldman-Hodgkin-Katz equation to estimate the decay time constants of the different AHP components.

4.4.1.1 AHP_{80} values

In the cultured cells used for these recordings, the AHP_{80} values in A-type cells AHP_{80}s appeared to cluster into two groups and thus they are similar to those previously reported in the literature where Waddell & Lawson (1990) and Lawson *et al.* (1996) showed that the majority of A-fibre neurones without an inflection on the action potential had very fast duration AHPs (AHP_{80} values < 7.5 ms). In contrast, they found that a large number of A-fibre cells with an inflection showed longer duration AHPs (AHP_{80} values > 9 ms). The two groups of AHP_{80} values described here, reflect these results to some extent. Of the A-type cells with AHP_{80} values < 30 ms only 5% of cells (6/44) had an inflection, but of the cells with an AHP_{80} > 35 ms 21% (6/28) had an inflection.

C-type cells tended not to have very short duration AHP_{80}s, with the lowest value being ~11 ms. As with the A-type neurones, the longest duration AHP had an AHP_{80} value of ~500 ms. Again, these results compare well with those of Waddell & Lawson (1990) who did not see AHP_{80} values shorter than 12 ms in C-fibre cells. However, the work presented here does differ from previous reports in that some AHP_{80}s were considerably longer in both A- and C-type neurones. Waddell & Lawson (1990) found that the longest duration AHP_{80} value was 70 ms in a A-type neurone with an action potential inflection compared with ~500 ms in the work described here. There are some differences in the methods used that may account for this. My work has been carried out on adolescent Sprague-Dawley rats using isolated cells in culture and perforated patch recording, whereas Waddell & Lawson (1990) worked on adult Wistar rats using whole ganglia and intracellular recording techniques.

4.4.1.2 AHPs fitted to a modified GHK equation

AHPs were also analysed by fitting them to a modified GHK equation to determine whether there were different temporal components to the AHPs (seen after a single action potential) that could be used to associate them with particular cell types. As with other types of neurone, the DRG cell AHPs appeared to have several components with decay time constants ranging from a few milliseconds to several seconds. In most cells the AHP was fitted to an equation with two variable K^+ components. As with AHP_{80} values, AHPs with very fast decay time constants (< 5 ms) were generally only seen in A-type neurones. Conversely, the slowest decay time constants (> 700 ms) were only seen in C-type neurones, although it would be necessary to repeat these experiments to determine whether such slow components are restricted to C-type cells. However, there were only a few cells from either group which exhibited τ values at either of these

extremes. Overall, there was a large spread of τ values which could be seen in both A- and C-type neurones. Thus it was not possible to identify a distinct type of AHP component, or combination of components, that corresponded to a particular cell type. Some cells also appeared to have AHPs with a Cl^- component, although again, this could not be attributed to a specific cell type.

A similarly large range of AHP durations has also been seen in work by Villière & McLachlan (1996) who examined both AHPs and the underlying currents. They showed that currents were generally best fitted by a series of exponentials and that decay time constants of similar duration were seen in $A_{\alpha/\beta}$, A_δ and C-fibre neurones. Apparently there was no particular type of AHP that occurred in a given cell type with the exception of very long duration AHPs, several seconds long, which were only seen in C-fibre neurones (Villière & McLachlan, 1996). My results are similar, suggesting that there may be a number of different channels involved in the generation of AHPs, possibly reflecting the functional diversity of DRG neurones. One point worthy of note is that many of the cells with two component AHPs could be separated into different groups on the basis of the time difference between their two components. These groups were not specific to A- or C-type cells and were therefore not as useful as had been hoped for the current work. However, they may provide a basis for future *in vivo* work; it may be possible to associate these groupings with a particular cellular function, for example they could be nociceptors or low threshold mechanoceptors.

4.4.2 Pharmacology of AHPs

Attempts were next made to characterise AHPs using a pharmacological approach. As described previously, AHPs in many cell types have been shown to be mediated by SK channels and these tend to be mAHPs (Kawai & Watanabe, 1986; Sah & McLachlan,

1991; Stocker *et al.*, 1999a; Faber & Sah, 2002). However, there are conflicting reports as to whether or not SK channels play a similar role in DRG neurones. In pigeon DRGs, the use of the non-selective Ca^{2+} channel blocker Co^{2+} reduces the amplitude of the AHP, which is consistent with an SK/IK-like component (Görke & Pierau, 1980). In addition, Co^{2+} also blocks a prominent outward current in guinea-pig DRG cells (Kameyama, 1983). Several groups have also described AHPs sensitive to apamin. Tokimasa *et al.*, (1990) made voltage-clamp recordings using bullfrog DRGs and showed that an outward current lasting several hundred milliseconds was reduced to ~25% of the control value in the presence of 3 nM apamin. In rat DRGs, some authors report AHPs that were abolished by apamin (Amir & Devor, 1997; Gold *et al.*, 1996a, Lüscher *et al.*, 1994). There are, however, a number of studies which contradict much of this data. Villière & McLachlan (1996) found that very few medium duration AHPs in different sized cells were sensitive to block by Co^{2+} and those cells that were sensitive only showed partial block. This would suggest that the conductance underlying AHPs in DRG cells is probably due to something other than K_{Ca} channels. Furthermore, Abdulla & Smith (2001) report that apamin application has little or no effect on the number of action potentials evoked in dissociated DRG neurones, again supporting the idea that SK channels are not involved in the generation of the medium duration AHP seen in these cells.

4.4.2.1 Pharmacology of mAHPs in DRG cells from p17 rats

In order to determine whether there was any involvement of SK channels in the mAHP in DRG neurones, UCL 1848 was used a concentrations of 10 nM and 50 nM, which are known to block both cloned and native channels (Benton *et al.*, 1999; Shah & Haylett, 2000a; Hosseini *et al.*, 2001; Shah *et al.*, 2001). Only one of twelve cells showed an

AHP which was sensitive to block by 10 nM UCL 1848, and this AHP was only partially blocked. There was no inhibition in the remaining cells. Similarly, most cells were insensitive to Cd^{2+} block, indicating that the channels underlying these AHPs were not Ca^{2+}-dependent. Finally cells tested with TEA and ChTx showed AHPs insensitive to block by either of these drugs confirming that K_{Ca} channels are unlikely to generate the majority of mAHPs in isolated p17 DRG cells. Cells tested with 4-AP also had AHPs insensitive to block by this compound, ruling out the involvement of a number of voltage-gated K^+ channels (Coetzee *et al.*, 1999).

4.4.2.2 Pharmacology of mAHPs in DRG cells from adult rats

The results presented in **Chapter 5** show that SK channel mRNA and the SK3 protein are up-regulated in rat DRGs with age. For this reason, the mAHP in adult (p40-45) rat DRG cells was also examined. However, as with the p17 cells, these AHPs were insensitive to 50 nM UCL 1848, 10 μM clotrimazole and 5 mM TEA suggesting that they are unlikely to be generated by SK, IK or BK channels respectively. This was supported by the fact that only 1 in 3 cells showed any sensitivity to 200 μM Cd^{2+}.

In addition to the blockers used, the mAHP in p40-45 DRG cells was also tested with the SK/IK channel enhancer 1-EBIO (300 μM). Assuming that SK channels are present and potentially functional in DRG neurones, it could be that they are not normally actived during AHP generation, so 1-EBIO was used in an attempt to enhance SK channel opening. Only one cell out of eight tested had an mAHP that was enhanced. Since a number of cells had AHPs that approached the expected value for E_K, this may have masked any small increases in potassium conductance in these cells. However, given that 1-EBIO should also have prolonged SK channel opening, this would have

been reflected as a prolonged AHP which was not seen. So it would thus appear that only a small proportion of cultured DRG cells have an AHP affected by 1-EBIO.

4.4.2.3 Possible candidates for the channel underlying the mAHP in DRG cells

What then might be the identity of the channel(s) underlying the mAHP in DRG cells? One possible candidate is the M-channel which is known to regulate cell excitability in a number of different types of neurone (Marrion, 1997; Robbins; 2001). The presence of the M-current and proposed M-channel subunits (KCNQ2 and KCNQ3) have recently been demonstrated in rat DRG neurones (Passmore *et al.*, 2003). It is already known that M-channels make a significant contribution to the mAHP seen in hippocampal neurones (Storm, 1989; Dutar & Nicoll, 1989), thus it is feasible that they have a similar role in DRG neurones. However the IC_{50} for TEA of KCNQ2/3 heteromers is in the low millimolar range (3.8-4.7 mM; Wang *et al.*, 1998; Hadley *et al.*, 2000; Passmore *et al.*, 2003), thus it should have been possible to observe some blocking effect of TEA at a concentration of 5 mM. It would thus appear that the M-channel does not play a major role in AHP generation.

Another potassium channel which may be involved in mAHP generation is the K_{Na} channel which is activated by a rise in intracellular Na^+ and Cl^- (Bhattacharjee *et al.*, 2003; Yuan *et al.*, 2003). Franceschetti and colleagues (2003) examined the properties of medium duration AHPs (~200 ms long) in intrinsically bursting neurones of the neocortex. They found that substituting extracellular NaCl with LiCl reduced the amplitude of AHPs in these cells which had the effect of increasing neuronal firing frequency. This has led to the suggestion that K_{Na} channels may underlie AHPs which regulate the rate of firing in some neurones. Cloned K_{Na} channels are insensitive to high concentrations of blockers such as ChTx (100 nM) and apamin (100 nM), and are

also relatively insensitive to external TEA with currents showing little or no inhibition at 1 mM (Bhattacharjee *et al.*, 2003). In this respect K_{Na} channels have a profile which is consistent with the channel underlying mAHPs in DRG cells, and are thus another potential candidate.

Finally, Wittekindt *et al.* (2004) have recently described an apamin and scyllatoxin-insensitive SK3 splice variant which remains sensitive to Ca^{2+}. This isoform may account for the mAHPs that were sensitive to Cd^{2+} or 1-EBIO but insensitive to UCL 1848.

4.4.2.4 Pharmacology of the sAHP in DRG cells

In addition to the mAHP, some DRG neurones also exhibited a sAHP which was usually best seen in response to a train of action potentials. As with the sAHP in other types of sensory neurone, the amplitude and duration of this sAHP frequently increased with increasing numbers of action potentials (Cordoba-Rodriguez *et al.*, 1999). Based on the pharmacological properties, three types of sAHP were observed in DRG cells. The first type was only seen in A-type neurones (with cell diameters > 35 μm) and was insensitive to UCL 1848, TEA and Cd^{2+} but could be blocked by UCL 2027. One common feature of the sAHPs reported to date is that they are modulated by neurotransmitters (Vogalis *et al.*, 2003). The sAHP seen in large DRG neurones was unusual as it was insensitive to histamine. One possibility for the origin of this AHP is the Na^{+}-K^{+} ATPase, which is reported to underlie hyperpolarisations following multiple action potentials in spinocerebellar and motorneurones of the cat (Kuno *et al.*, 1970; Kernell & Monster, 1982).

A second type of sAHP, observed in C-type neurones, was blocked by 200 μM Cd^{2+} implying that it is Ca^{2+}-dependent. This result agrees with previous data which showed

that very long duration slowly decaying AHPs in C-fibre neurones could be blocked by Co^{2+} (Villière & McLachlan, 1996). The Ca^{2+}-dependent sAHP reported here was also insensitive to 5 mM TEA and 10 nM UCL 1848. Thus the characteristics of this sAHP are more typical of the sAHPs known to produce spike-frequency adaptation in other neurones (Sah, 1996; Sah & Davies, 2000) and the underlying conductance is unlikely to be due to SK channel opening (Vogalis *et al.*, 2003; Bond *et al.*, 2004; Villalobos *et al.*, 2004). Interestingly, Gold and colleagues (1996a) found that sAHPs in DRG cells were sensitive to block by apamin. However, the relatively high concentrations of apamin used (1 μM) may have had a non-specific blocking effect on the channels underlying the sAHP.

There was also a third type of sAHP detected in isolated rat DRG cells. It too was seen in C-type neurones and was insensitive to UCL 1848 and ChTx though blocked by UCL 2027. What was particularly striking about this sAHP, however, was the blocking effect of 5 mM TEA which almost completely abolished the sAHP leaving just a small insensitive component. A similar effect was seen when histamine was applied. A TEA-sensitive sAHP has, to my knowledge, not previously been described. The sensitivity to such a low concentration of TEA would suggest that the channels underlying this AHP were voltage-gated. However, most channels of this type would not be expected to be active at such negative membrane potentials.

Certain KCNQ subunit proteins are known to form channels that are sensitive to TEA and the most sensitive of these is KCNQ2 (IC_{50} 0.1-0.3 mM; Hadley *et al.*, 2000; Shapiro *et al.*, 2000). This sensitivity has been attributed to a tyrosine residue in the pore loop (Wang *et al.*, 1998). KCNQ3 subunits, which have a threonine in the corresponding position, are highly insensitive to TEA giving an IC_{50} value of > 30 mM (Wang *et al.*, 1998; Hadley *et al.*, 2000; Shapiro *et al.*, 2000). Thus the intermediate

sensitivity of the channels formed when KCNQ2 and KCNQ3 genes are co-expressed is likely due to arise from co-assembly of the two different subunit proteins (Wang *et al.*, 1998; Hadley *et al.*, 2000)

Several factors point to a role for KCNQ2/3 channels underlying the TEA-sensitive sAHP. Firstly several studies report that heteromeric KCNQ2/3 channels are blocked by relatively low concentrations of TEA (IC_{50} of 3.8-4.7 mM; Wang *et al.*, 1998; Hadley *et al.*, 2000; Passmore *et al.*, 2003). This may account for the small component of the sAHP which remained after applying 5 mM TEA; a higher concentration of the drug may have blocked the AHP more fully. Secondly, M-currents are known to be attenuated by a number of agonists which bind to G-protein coupled receptors including: substance P (Simmons *et al.*, 1994), glutamate (Choi *et al.*, 1996), bradykinin (Cruzblanca *et al.*, 1998) and angiotensin (Shapiro *et al.*, 1994). The TEA-sensitive sAHP was significantly reduced by histamine which has also been suggested to inhibit M-channel activity via H1 receptors (Guo *et al.*, 2002).

In addition to the pharmacology, it is necessary to consider the kinetics of the channels underlying the TEA-sensitive sAHP. Recent work on KCNQ2 has shown that there are a number of possible splice variants and that transcripts for different isoforms could be detected in rat SCG tissue (Pan *et al.*, 2001). One of the intriguing aspects of this work was that expressed channels containing exon 15a were found to have much slower kinetics than the other isoforms (decay time constants of slow components of activation and deactivation were ~1600 and ~500 ms respectively; Pan *et al.*, 2001). This held true when such channel proteins were co-expressed with the KCNQ3 subunit proteins; heteromeric channels activated and deactivated 2.5 times more slowly than those formed with the other isoforms (Pan *et al.*, 2001). Taken together, these reports and the results presented in this chapter provide evidence for a novel sAHP in DRG neurones

which might well be generated by heteromultimers of KCNQ2 (containing exon 15a) and KCNQ3 subunits. The possibility that this is the case could be further explored by testing DRG sAHPs with selective blockers of the M-current, such as linopirdine (Aiken *et al.*, 1995; Lamas *et al.*, 1997) and XE991 (Wang *et al.*, 1998).

4.4.3 Pharmacology of AHPs in nodose ganglion cells

In addition to the work done on rat DRG cells, a series of experiments was also carried out using guinea-pig nodose ganglion neurones in culture. Following a train of seven action potentials, ~25% of nodose neurones exhibited a robust sAHP. As with the sAHPs in DRG neurones, the amplitude and duration of these AHPs increased when the cell was stimulated to fire increasing numbers of action potentials. This is in accord with the idea that more action potentials increase intracellular Ca^{2+} concentrations further, thus increasing the number of active channels and/or open probability of the channels underlying the sAHP (Cordoba-Rodriguez *et al.*, 1999).

As also reported by others, the sAHP in nodose neurones was sensitive to block by histamine (Undem & Weinreich, 1993; Jafri *et al.*, 1997) and bradykinin (Weinreich, 1986; Weinreich *et al.*, 1995), both of which are believed to regulate the sAHP via G-protein coupled receptors. The sAHP was insensitive to UCL 1848, which is consistent with the report that this sAHP was also insensitive to 100 nM apamin (Cordoba-Rodriguez *et al.*, 1999).

The sAHP in nodose neurones was also tested with the clotrimazole analogue UCL 2027 which blocked the AHP in a concentration-dependent manner. There are, as yet, no high affinity sAHP specific blockers, however, this compound has previously been shown to block the sAHP in hippocampal pyramidal neurones with an IC_{50} of ~1 μM (Shah *et al.*, 2001). In nodose ganglion neurones this value was considerably higher at

6.0 ± 1.4 μM. One interpretation of this is that it reflects differences in the properties of the channels underlying the sAHP in these two cell types. In hippocampal neurones, UCL 2027 appeared to show specificity for the current underlying the sAHP in that it did not have any effect on Ca^{2+} entry, the mAHP or currents generated by recombinant hSK1 or rSK2 channels expressed in HEK 293 cells (Shah *et al.*, 2001). This led to the tentative suggestion that UCL 2027 may be a specific blocker for the channel underlying the sAHP and may thus provide a useful tool in attempting to ascertain the identity of this channel. However, the effects of UCL 2027, described in the work presented here, appear to be less specific. For example, this compound almost completely abolished three types of sAHP seen in DRG neurones, which otherwise had clearly different pharmacologies. In addition, high concentrations (≥ 10 μM) of UCL 2027 tended to produce a significant depolarisation of the resting membrane potential. Shah *et al.* (2001) also reported a small reduction in the outward holding current seen in hippocampal cells clamped at -50 mV. Given that UCL 2027 was developed from a highly non-selective base compound, namely clotrimazole, which has a number of wide-ranging effects on K^+ channels (Brugnara *et al.*, 1993; Rittenhouse *et al.*, 1997; Wu *et al.*; 1999; Hatton & Peers, 1996) Ca^{2+} channels (Thomas *et al.*, 1999) and cytochrome P450 (Kahl *et al.*, 1980) it is possible that it exerts its effects via a variety of targets possibly including both ion channels and second messenger systems.

4.4.4 Staining for SK/IK channel proteins in nodose neurones

Staining of guinea-pig nodose ganglion neurones showed a small but detectable signal for the SK3 channel protein, though this was only seen with the Chemicon antibody. While both the M75 and Chemicon antibodies recognise a similar region of the SK3 protein sequence, the Chemicon antibody has an epitope with an additional 5 amino

acids. This may account for the difference in staining seen with the two antibodies. There was no positive signal seen with the anti-SK1, SK2 or IK channel antibodies.

There were no full guinea-pig SK channel protein sequences available to determine whether the antibodies would be expected to recognise them, although there was a partial SK2 sequence. To assess the likelihood of antibody recognition, a number of SK channel protein alignments were made using peptide sequences from different species. A comparison of the regions, in which the epitopes for the different antibodies lie, can be seen in **Figure 4.27**. There was also a predicted peptide sequence available for the guinea-pig IK channel protein (clone obtained from guinea-pig taenia by Dr Ramine Hosseini, Department of Pharmacology, UCL). The C-terminal region of this protein does differ from the epitope for the M4 antibody:

guinea-pig C-terminal	AALGPQQLPAPSQEAT
M4 epitope	CALGPRQLPEPSQQSK

From the alignments, it can be seen that the epitope regions for the anti-SK2 and –SK3 antibodies are highly conserved amongst mammalian species, so these antibodies should also be suitable for identifying the guinea-pig channel proteins. Indeed, the Chemicon anti-SK3 antibody does seem to produce a punctate staining pattern in the region of the cell membrane. However, in the case of the SK1 and IK channel proteins, a negative result would be likely to arise from a lack of antibody specificity for the guinea-pig peptide sequence, even if they are expressed in the nodose neurones.

In any event, in view of the lack of effect of 10 nM UCL 1848 on the sAHP in nodose neurones, it is unlikely that SK channels play a role in sAHP generation. There has been very little reported in the literature about the nature of the mAHP seen in nodose ganglion neurones. Cordoba-Rodriguez *et al.* (1999) found that these 50% of these AHPs were Ca^{2+}-sensitive and blocked by 10 mM TEA and have thus suggested that the

channel responsible is the BK channel. However, the duration of the AHP (50-300 ms) lies in the range of a typical apamin-sensitive AHP. This may present a role for the SK3 channel protein which is apparently expressed in some nodose ganglion neurones (**Figure 4.26**). It would be interesting then, in future experiments, to test the effects of UCL 1848 and apamin on the nodose ganglion mAHP.

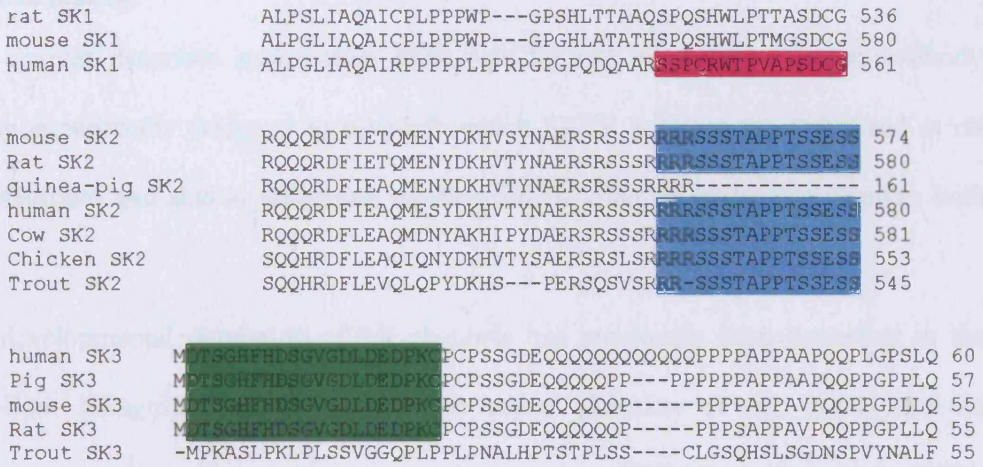

Figure 4.27 Sequence alignments of SK peptide sequences from different species in the epitope regions. The C-terminal epitope region for the anti-SK1 (L155; region seen in pink) antibody appears to be quite different between three species. The SK2 (blue) and SK3 (green) epitope regions, however, appear to be highly conserved between the different species. By extension, the guinea-pig SK2 and SK3 sequences in these regions are likely to be very similar and the antibodies should be able to detect the channel proteins. Genbank accession numbers for rat, mouse and human SK1 sequences were NP_062186, AAG43216 and AAB09562 respectively. For SK2 accession numbers for mouse, rat, human, cow, chicken and trout were AAM88568, AAB09563, AAK84039, BAD08234, NP_990129 and AAK39560 respectively. Genbank accession numbers for human, pig, mouse, rat and trout SK3 were NP_740752, NP_999150, NP_536714, AF292389 and AAK39561 respectively.

Chapter 5

Developmental regulation of SK/IK channel gene expression in DRGs

5.1 Introduction

This chapter describes quantitative PCR (qPCR) and immunofluorescent antibody staining experiments designed to establish which SK/IK proteins are expressed in rat DRG neurones and also to determine whether SK/IK channel expression changes with age.

The developmental regulation of SK channels has previously been described in the cerebellum (Cingolani *et al.*, 2002), the retina (Klöcker *et al.*, 2001) and in motorneurone terminals at the neuromuscular junction (NMJ; Roncarati *et al.*, 2001). However, to date, there have been no comparable studies of SK channels in neurones in sensory pathways.

In cerebellar Purkinje neurones, SK2 expression has been shown to be down-regulated with age, and it has consequently been suggested that SK2 plays an important role in regulating Ca^{2+} transients during the early stages of development thus contributing to the process of maturation (Cingolani *et al.*, 2002).

In retinal ganglion cells SK2 shows steady up-regulation within the first eight days following birth (Klöcker *et al.*, 2001). A third situation exists in motorneurone terminals at the neuromuscular junction. SK3 is absent from the NMJ until p35, when a clear immunofluorescent signal can be detected (Roncarati *et al.*, 2001). As NMJ maturation is believed to be functionally complete at this time it has been suggested that

SK3 probably does not play a role in developmental changes in motorneurones following birth (Navarrete & Vrbova, 1993; Roncarati *et al.*, 2001).

In Chapters 3 and 4 I have already demonstrated that SK3 immunoreactivity is present in DRG cells from a p17 animal using fluorescent antibody staining (see **Chapter 3**) so to look at possible developmental changes, SK channel expression was also examined at two time points either side of this age group i.e. p7 and p40-45. This also covers the range of ages used in other SK developmental studies reasonably well. The aim was to determine whether SK/IK channels were up- or down-regulated and therefore to establish whether, functionally, they might be more important at a certain ages.

5.2 Results

5.2.1 SK/IK channel mRNA expression in DRG cells

5.2.1.1 Positive controls using plasmid DNA

The levels of mRNA present in DRG cells were determined by reverse transcribing the RNA to produce complementary DNA (cDNA) and by using quantitative PCR (qPCR) as previously described (see Methods, **Chapter 2**). Positive controls were first carried out using plasmids containing each of the SK channels or in the case of the IK channel, a small fragment of DNA containing the amplicon for the IK primer/probe set. The results are shown in **Figure 5.1** where it can be seen that each set of primers and probes correctly amplified the target without producing any significant amplification of the other control DNAs. Thus, all primer-probe sets appeared to be specific for their targets.

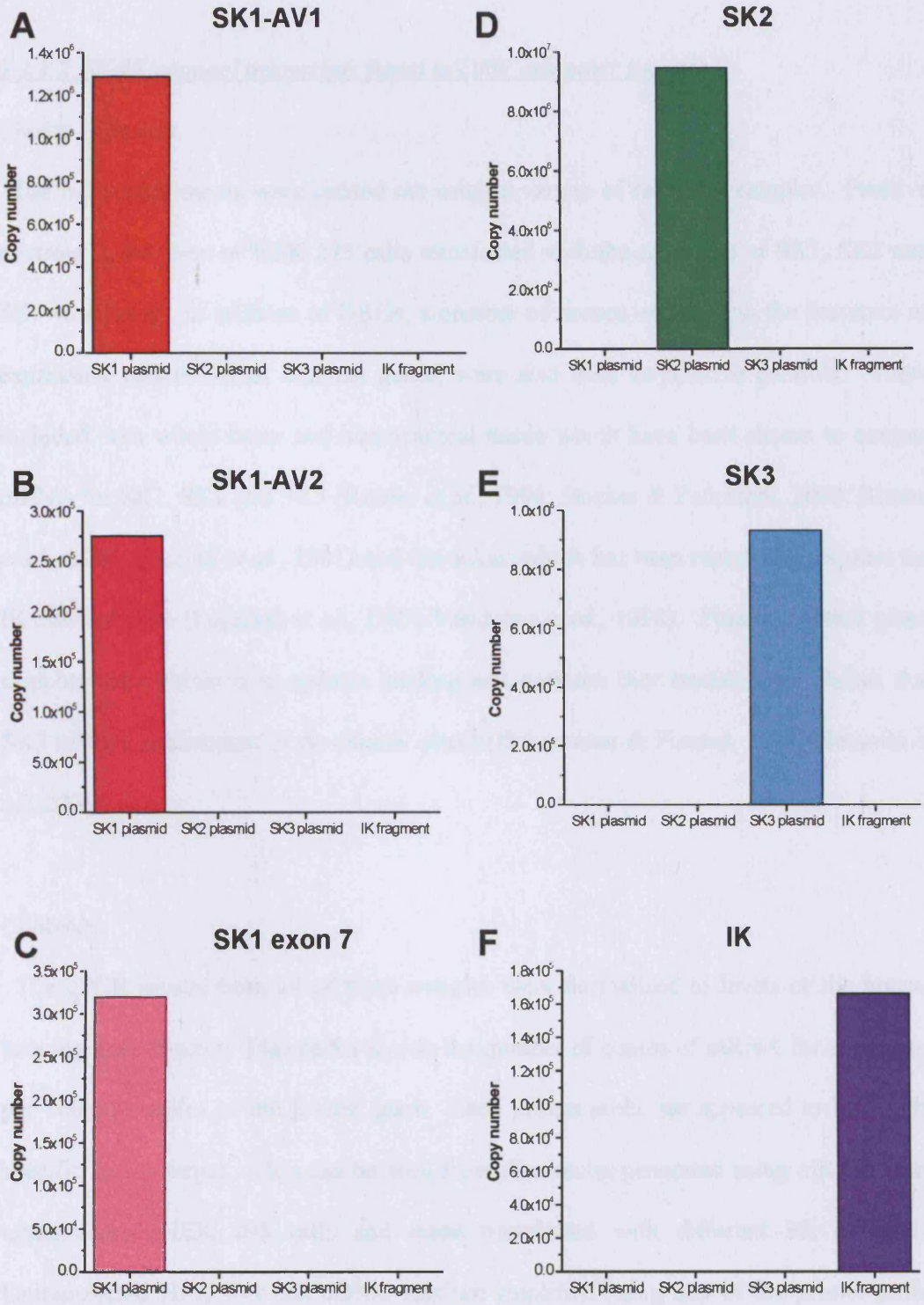

Figure 5.1 Positive controls for qPCR results show that the probes selectively amplify the appropriate gene. SK plasmids (2 ng) and the IK fragment were run with primers and probes that should amplify all variants (AV) of SK1 (**A** and **B**), SK1 variants containing exon 7 (**C**), SK2 (**D**), SK3 (**E**) and IK (**F**). In each case the appropriate DNA was amplified, while levels of the other control DNAs were all <1500 copies indicating the specificity of each primer and probe set for its target.

5.2.1.2 SK/IK channel transcripts found in DRG and other tissues

Choice of tissues

The next experiments were carried out using a variety of rat tissue samples. Positive controls in the form of HEK 293 cells transfected with the rat forms of SK1, SK2 and SK3 were used. In addition to DRGs, a number of tissues, reported in the literature as expressing certain SK/IK channel genes, were also used as positive controls. These included both whole brain and hippocampal tissue which have been shown to contain mRNA for SK1, SK2 and SK3 (Köhler *et al.*, 1996; Stocker & Pederzani, 2000; Rimini *et al.*, 2000; Tacconi *et al.*, 2001) and the colon, which has been reported to express the IK channel gene (Logsdon *et al.*, 1997; Vandorpe *et al.*, 1998). Finally, adrenal gland samples were obtained as apamin binding and northern blot studies have shown that SK3 mRNA is abundant in rat adrenal gland (Habermann & Fischer, 1979; Hosseini *et al.*, 2001).

Controls

The qPCR results from all of these samples were normalised to levels of the house-keeping gene β-actin. **Figure 5.2** shows the number of copies of mRNA for each gene per 100,000 copies of the β-actin gene. Each primer/probe set appeared to be highly specific for its target. This can be seen from the results generated using mRNA from untransfected HEK 293 cells and those transfected with different SK plasmids. Untransfected HEK 293 cell cDNA was not amplified using any of the primer-probe sets. However, cDNA from cells expressing one of the plasmids, for example SK2, was selectively amplified by the SK2 primer/probe set whilst cDNA from HEK 293 cells transfected any of the other plasmids were not. Thus all primer/probe sets specifically amplified their targets. However, absolute copy numbers from these HEK cell control

samples must be interpreted with caution as they depend on the transfection efficiency of the HEK 293 cells with each of the plasmids, which is variable. For example, SK3 mRNA levels in hippocampus appeared to be roughly equal to those in SK3 transfected HEK 293 cells (**Figure 5.2**). Although SK3 mRNA levels are high in the hippocampus, it may well be that the transfection efficiency was low, so that the comparison with HEK cells is not very informative.

Tissue results

In contrast to the other tissues used in this study, DRGs seemed to show fairly high levels of expression for SK1 (all variants and those containing exon 7), and for the SK2, SK3 and IK channel genes (**Figure 5.2**). These qPCR reactions demonstrate that the primer/probe sets amplify cDNA obtained from physiological levels of mRNA in those tissues. As expected SK1 (all variants and those including exon 7), SK2 and SK3 were all expressed in the whole brain and hippocampal samples (Köhler *et al.*, 1996; Stocker & Pederzani, 2000; Rimini *et al.*, 2000; Tacconi *et al.*, 2001). More specifically, there appeared to be a very high level of SK3 expression in the hippocampus ($>10^4$ copies). There were also very low levels of IK channel cDNA seen in these samples. As expected, from other work, it was possible to detect comparatively high levels of IK channel cDNA from the colonic tissue sample (Logsdon *et al.*, 1997; Vandorpe *et al.*, 1998). There was, in addition, a small amount of SK3 expression, but there was no sign that SK1 or SK2 cDNAs were present.

Adrenal gland tissue from a p17 animal showed only low levels of SK1, SK3 and IK gene expression; the estimated number of mRNA copies being a few hundred in each

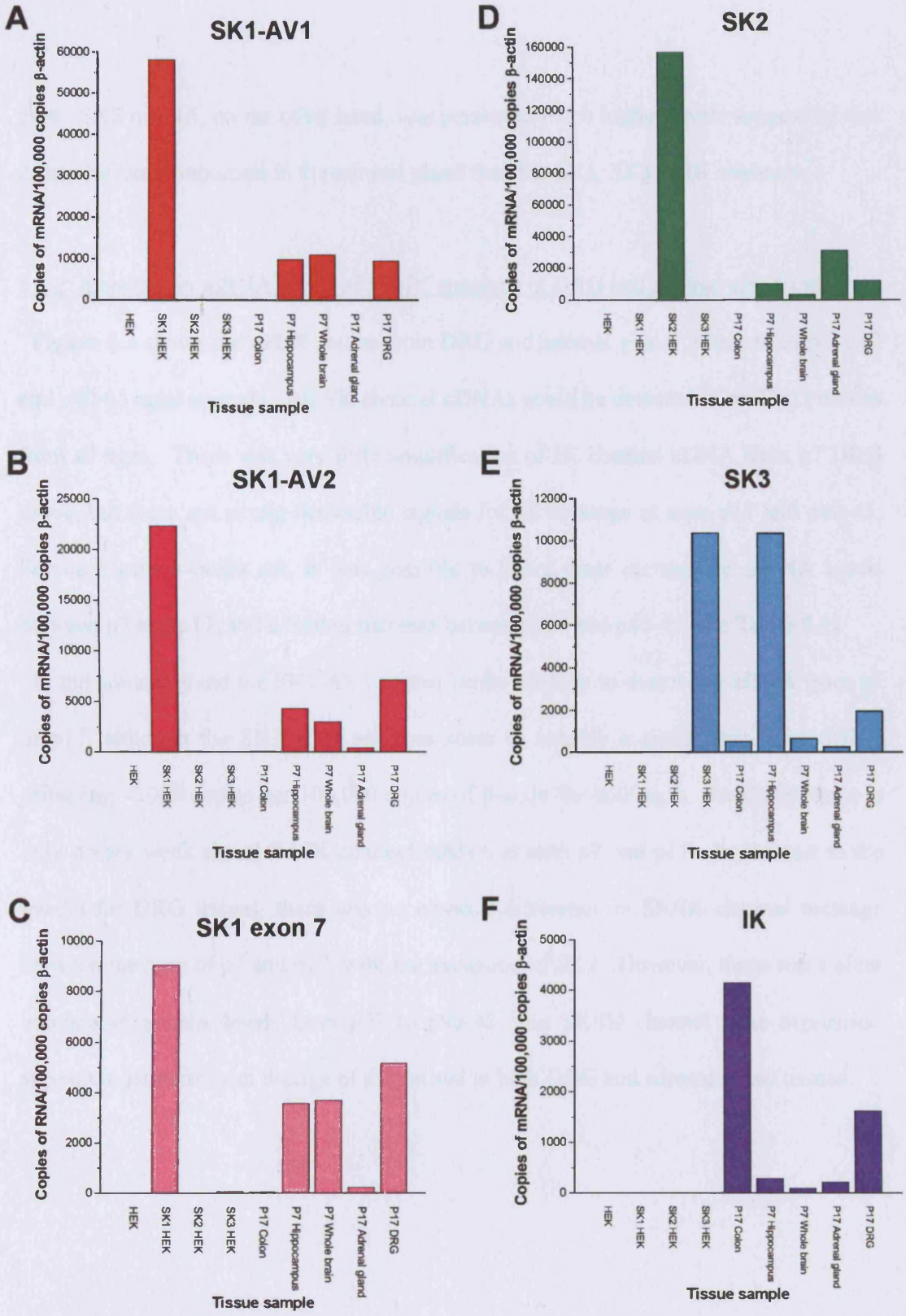

Figure 5.2 Levels of SK/IK channel mRNA expressed in different tissues detected by qPCR. Tissue samples were run with the six different primer/probe sets alongside cDNA from HEK 293 cells transfected with SK/IK channel constructs. In addition to the DRG samples, whole brain and hippocampal cDNA was included as a positive control for SK1, SK2 and SK3, adrenal gland cDNA for SK3 and cDNA from colon tissue was included as a positive control for IK channel gene expression.

case. SK2 mRNA, on the other hand, was present at much higher levels suggesting that it may be more important in the adrenal gland than the SK1, SK3 or IK channels.

5.2.2 Increases in mRNA levels of SK/IK channels in DRG and adrenal gland tissue

Figure 5.3 shows the qPCR results from DRG and adrenal gland tissues from p7, p17 and p40-45 aged animals. All SK channel cDNAs could be detected in rat DRG tissues from all ages. There was very little amplification of IK channel cDNA from p7 DRG tissue, but there are strong detectable signals for IK message at ages p17 and p40-45. For each primer-probe set, it was possible to see a clear increase in mRNA levels between p7 and p17, and a further increase between p17 and p40-45 (see **Table 5.1**).

In the adrenal gland the SK1 AV1 primer/probe set fails to detect any cDNA from p7 or p17, although the SK1 AV2 set does seem to amplify a small amount of cDNA reflecting <1000 copies per 100,000 copies of β-actin for both ages. Similarly, there is only a very weak signal for IK channel mRNA at ages p7 and p17. In contrast to the results for DRG tissues, there was no obvious difference in SK/IK channel message between the ages of p7 and p17, with the exception of SK2. However, there was a clear increase in mRNA levels from p17 to p40-45. So SK/IK channel gene expression appears to increase with the age of the animal in both DRG and adrenal gland tissues.

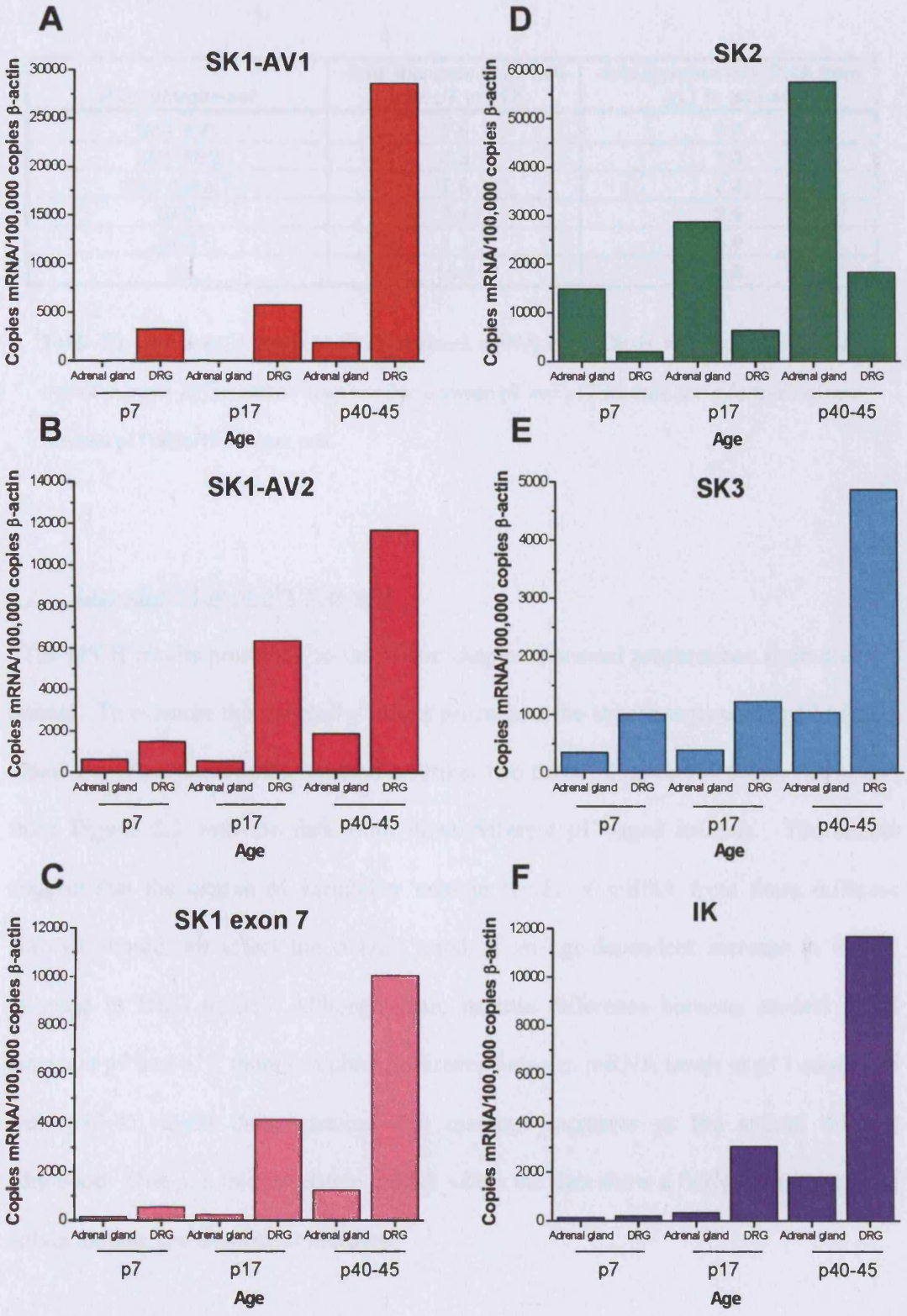

Figure 5.3 SK/IK channel mRNA expressed in adrenal gland and DRG tissues for three different age groups. Adrenal gland and DRG samples were obtained from p7, p17 and p40-45 rats. These were run with the six different SK/IK primer-probe sets (described in **Chapter 2**).

Primer/probe set	-fold increase of mRNA from p7 to p17	-fold increase of mRNA from p17 to p40-45
SK1 AV1	1.8	5.0
SK1 AV2	4.3	1.8
SK1 exon 7	7.6	2.4
SK2	3.4	2.9
SK3	1.2	4.0
IK	16.9	3.8

Table 5.1 Increases in levels of SK/IK channel mRNA in rat DRGs with age. There is an overall increase in the mRNA copy number between p7 and p17 animals and a further increase between p17 and p40-45 aged rats.

5.2.3 Reproducibility of qPCR results

The qPCR results presented so far in this chapter represent preparations from a single animal. To examine the variability of this procedure, the experiments using p17 adrenal gland and DRG tissue were repeated a further two times. **Figure 5.4** shows the results from **Figure 5.3** with the data from three different p17 aged animals. The results suggest that the degree of variability seen in levels of mRNA from three different animals should not affect the overall trend of an age-dependent increase in SK/IK message in DRG tissue. Although there is little difference between adrenal gland results at p7 and p17, there is a clear difference between mRNA levels at p17 compared with p40-45, again demonstrating that message increases as the animal reaches adulthood. One possible exception is SK2 where the data show a fairly high scatter and only a modest age-dependent increase.

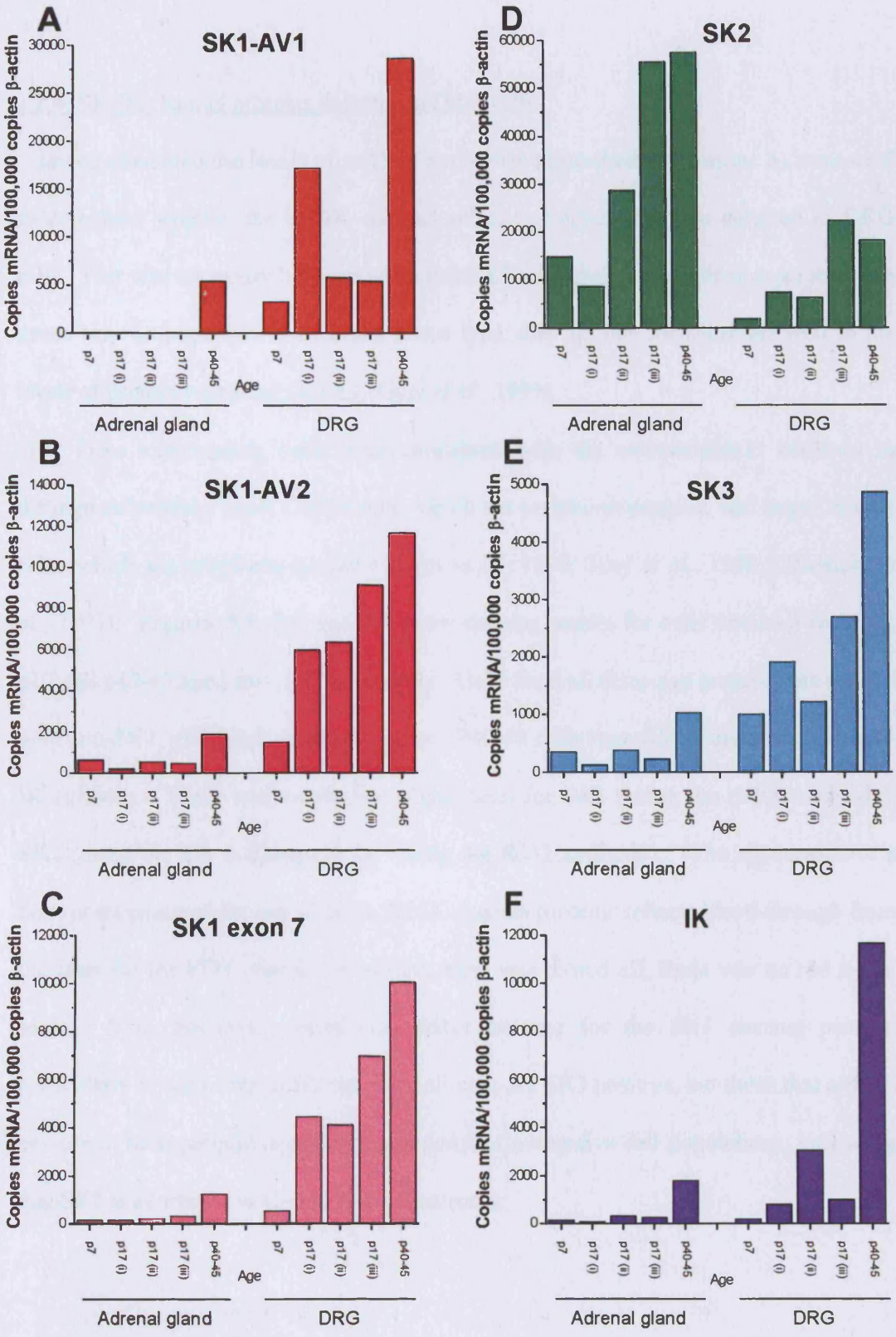

Figure 5.4 The variability of the results for different animals should not affect the overall trend of an age-dependent increase in DRG mRNA levels. The results from adrenal gland and DRG samples obtained from p17 rats [p17 (i), (ii) and (iii)] show data from three different animals. With the degree of variability seen, there is still trend for an increase in mRNA levels with an increase in age with rat DRG tissue.

5.2.4 SK/IK channel proteins detected in DRG cells

Having examined the levels of mRNA, antibodies (described in **Chapter 3**) were used to determine whether the SK/IK channel subunit proteins could be detected in DRG cells. This was necessary because while mRNA levels give some indication as to which genes may be important in a certain tissue type, they do not always relate well to the levels of protein expressed (see e.g. Gygi *et al.*, 1999).

For these experiments, cells were co-stained with the anti-peripherin antibody to distinguish between small C-type cells, which are peripherin positive, and larger A-type cells, which are peripherin negative (Ferri *et al.*, 1990; Troy *et al.*, 1990; Goldstein *et al.*, 1991). **Figures 5.5**, **5.6**, and **5.7** show staining results for cells obtained from p7, p17 and p40-45 aged animals respectively. Cells from all three age groups were stained with anti-SK1, -SK2 and –SK3 antibodies. P40-45 cells were also stained with the anti-IK antibody. There was no positive signal seen for SK1 (using the rb200 antibody), SK2 (using the M1 antibody) or IK (using the R212 antibody). (The appearance of a faint positive signal for any of these SK/IK channel proteins reflects bleed-through from the laser for the FITC signal. When this laser was turned off, there was no red signal seen.) It is, however, possible to detect staining for the SK3 channel protein, particularly in cells from adult rats. Not all cells are SK3 positive, but those that are can be seen in both peripherin-positive and peripherin-negative cell populations, indicating that SK3 is expressed in C- and A-type neurones.

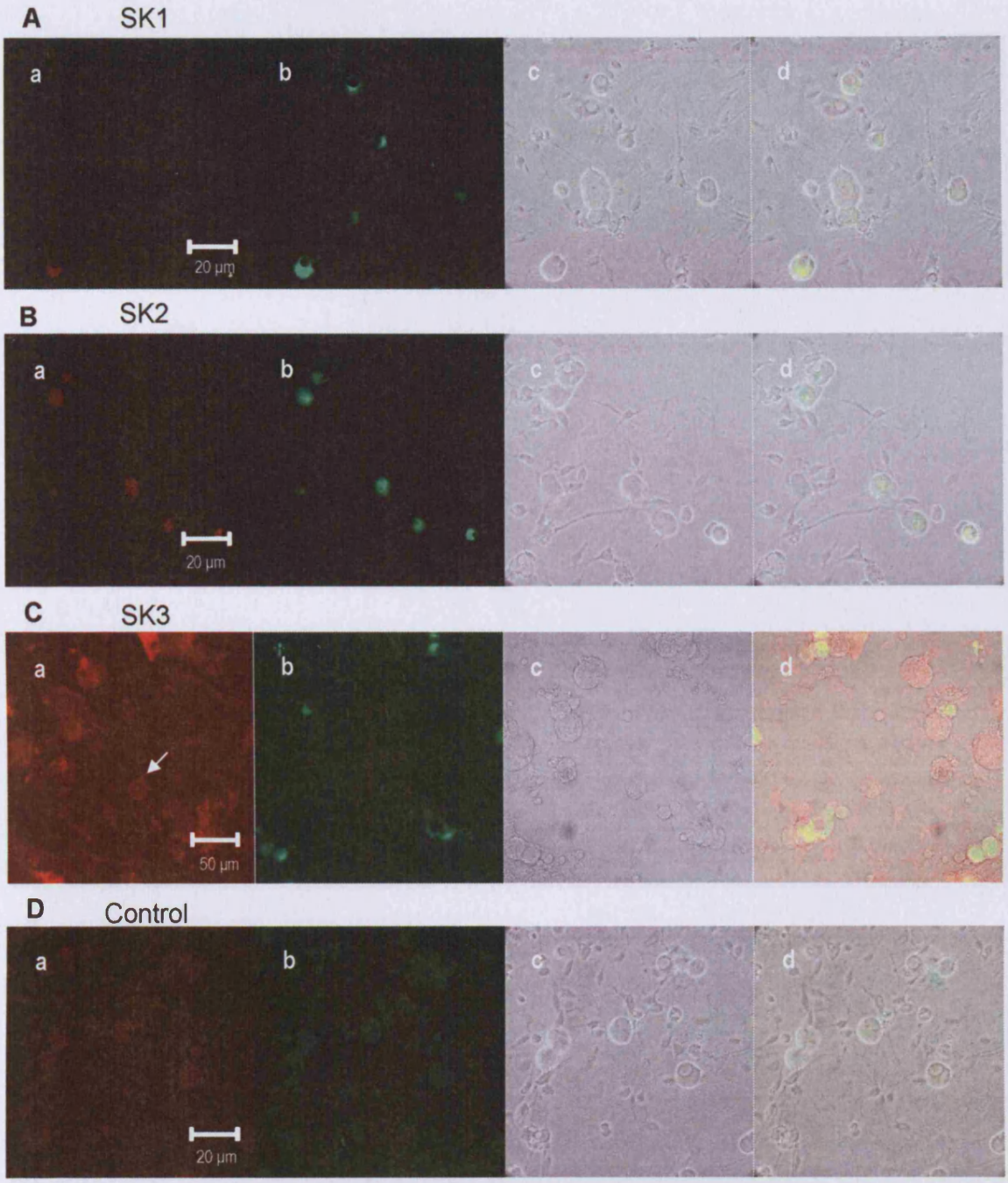

Figure 5.5 SK channel antibody staining in p7 DRG cells. **A**, staining seen with the anti-SK1 antibody rb200; there is no clear positive signal. **B**, cells stained with the M1 (anti-SK2) antibody. As with SK1, there is no positive staining seen for the SK2 protein. **C**, SK3 immunofluorescence can be detected in a small number of cells stained with the M75 antibody. One example of this is highlighted by the arrow and shows a weak but detectable signal at or near the cell membrane. **D**, negative controls, cells stained with the secondary antibodies alone (Cy3 and FITC labelled **a** and **b** respectively). In **A**, **B** and **C**, **a** shows staining with the anti-SK channel antibodies, **b** shows staining for peripherin. **c** shows the brightfield and **d** the overlay.

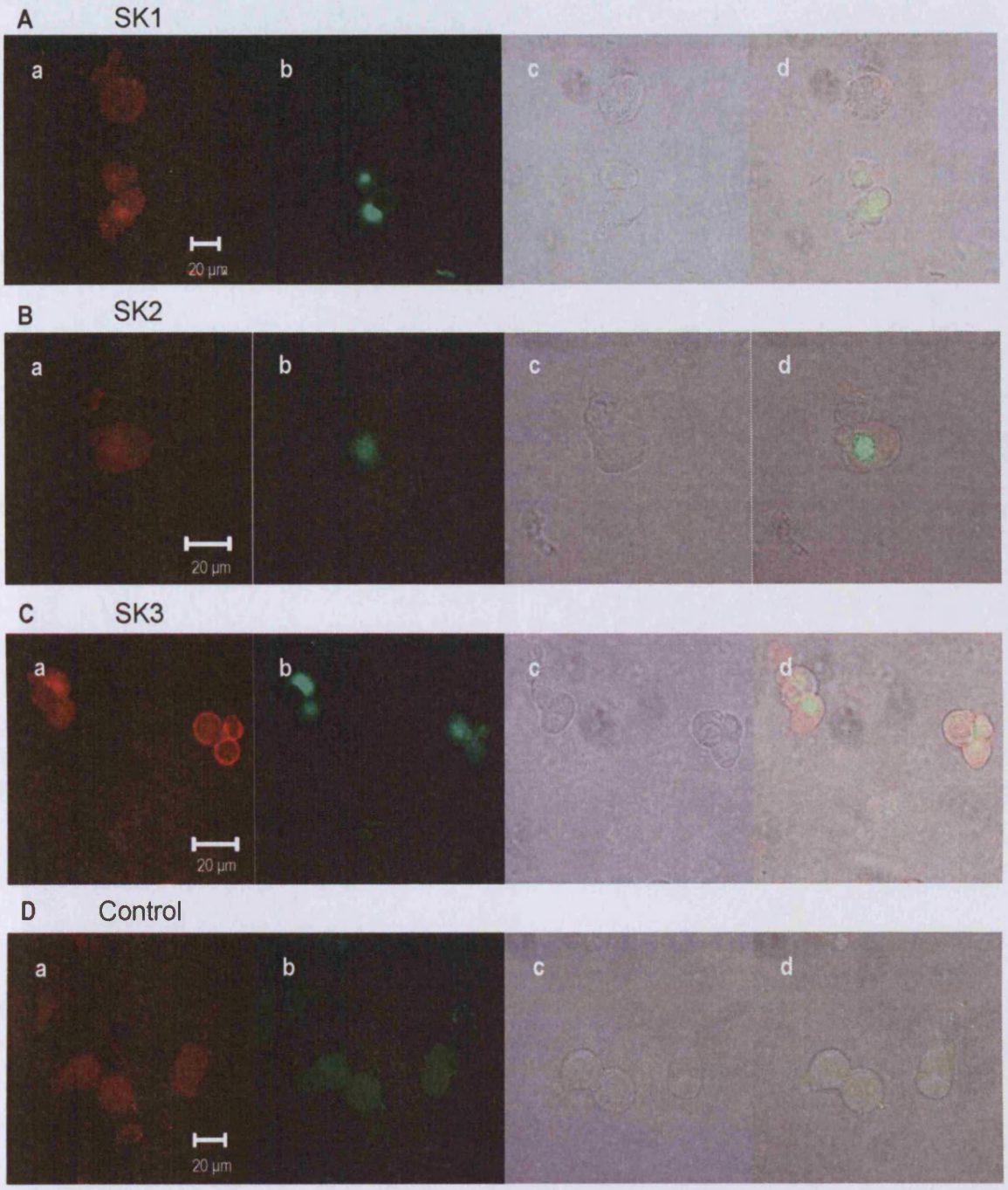

Figure 5.6 SK channel antibody staining in p17 DRG cells. **A**, staining seen with the anti-SK1 antibody rb200. **B**, cells stained with the M1 (anti-SK2) antibody. **C**, staining seen with the anti-SK3 antibody (M75). The pattern of staining seen in cells from a p17 animal is the same as for a p7 animal. There is no staining seen for SK1, or SK2. However there is a bright positive signal with the SK3 antibody, highlighting protein close to the cell membrane in some, but not all, cells. In panels **A**, **B** and **C**, **a** shows staining with anti-SK channel antibodies and **b** with the anti-peripherin antibody. **D**, shows negative controls; cells stained with the secondary antibodies alone (Cy3 and FITC labelled, **a** and **b** respectively). Brightfields (**c**) and overlays (**d**) are also shown.

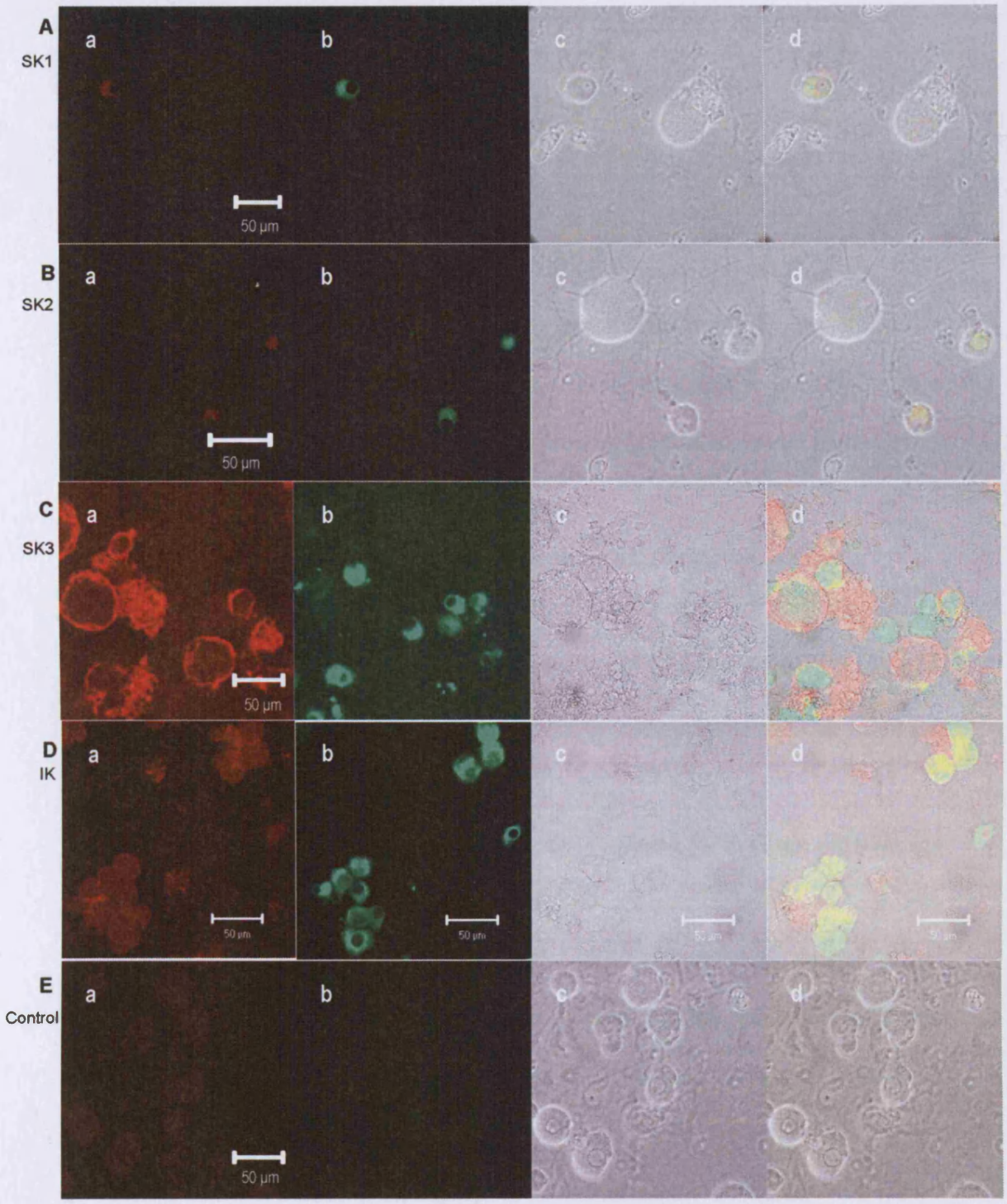

Figure 5.7 SK/IK antibody staining in p40-45 DRG cells. **A**, staining seen with the anti-SK1 antibody rb200. **B**, cells stained with the M1 (anti-SK2) antibody. **C**, pattern of staining seen with the anti-SK3 (M75) antibody. **D**, cells stained with the R212 anti-IK antibody. Cells were co-stained with anti-SK or IK channel antibodies (**a**) and an antibody to peripherin (**b**). There is no detectable signal for SK1, SK2 or IK. However there is a bright positive stain from the anti-SK3 antibody in a large number of cells from adult animals. The SK3 channel protein appears to be expressed in peripherin-positive and peripherin-negative cells indicating that it is present in A-type and C-type cells. **E**, negative controls, cells stained with the secondary antibodies alone (Cy3 and FITC labelled). Brightfields (**c**) and overlays (**d**) are also shown.

5.2.5 Quantification of the SK3 changes in DRG cells with age

To see whether the increases in SK/IK channel mRNA reflected changes in the amount of translated protein in DRGs, cells isolated from p7, p17 and p40-45 animals and stained with the anti-SK3 and peripherin antibodies were examined more closely. This is because the increase in SK3 signal could occur in one of several ways:

1. There might be no change in the number of cells staining positively for SK3, just a change in the intensity indicating that the same proportion of cells express higher levels of SK3.
2. There could be a greater number of cells expressing SK3 as the animal ages.
3. It could be due to a combination of both 1 and 2.

The co-staining with peripherin allows identification of A- and C-type neurones thus making it possible to see whether there is any change in the type of cell that expresses SK3

Figure 5.8 shows typical examples of SK3 antibody staining for the three different age groups. As before it is possible to see that SK3 appears to be detected in both peripherin-positive and peripherin-negative cells. What is particularly striking is that not only does the intensity of staining appear brighter, but the number of cells that appear to be SK3 positive increase with the age of the animal. The plot in **Figure 5.8 (D)** shows the relative proportions of SK3-positive cells for the three different age groups. At p7, only 9% of DRG cells showed a detectable SK3 signal. At p17, the number of SK3 antibody-positive cells increased so that 26% gave a positive signal and at p40-45 this value rose to 53%. The proportion of SK3 antibody-positive cells that were also peripherin-positive was the same for all three age groups, so of all the cells that stained positively for SK3, ~40% were also positive for peripherin. The different populations of cells are shown in **Table 5.2**.

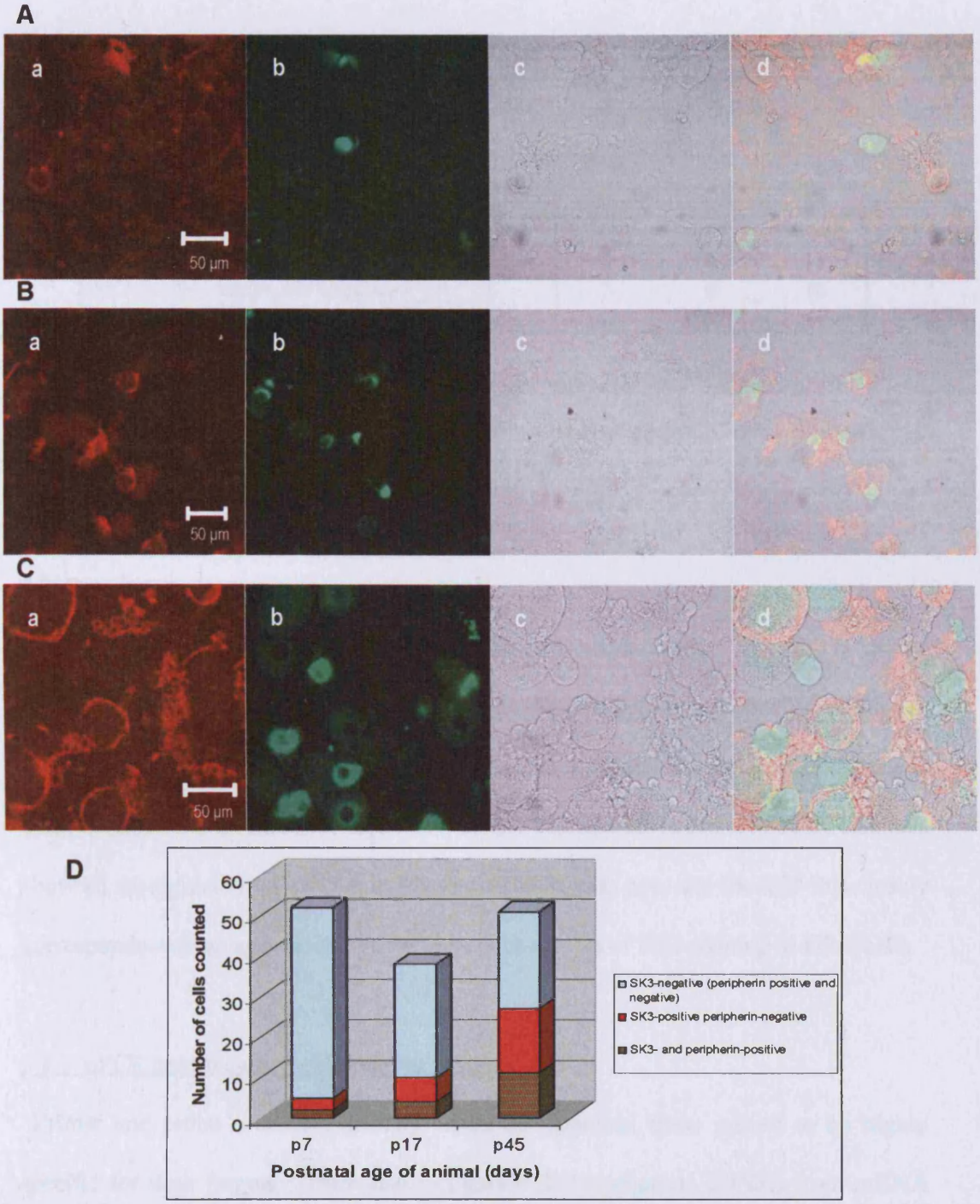

Figure 5.8 Age-dependent increase in SK3 staining in DRG cells. Cells were stained with the anti-SK3 antibody M75 (**a**) and the anti-peripherin antibody (**b**). Brightfields (**c**) and overlays (**d**) are also shown. **A**, SK3 staining in cells from a p7 animal, a weak positive signal can be detected in a small number of cells. **B**, cells from a p17 animal stained with SK3 show a more intense signal than p7 cells. There is also a higher proportion of SK3-positive cells. **C**, cells from p40-45 animals show a bright and easily detectable signal for SK3 in approximately half of the cells examined. **D**, the relative numbers of SK3 antibody-positive cells at different ages. At p7 only 9% of cells stained positively for SK3. At p17 this value increased to 26% and at p40-45 it reached 53%. In each case ~40% of the SK3 positive cells also expressed the peripherin protein indicating that SK3 was present in roughly equal proportions in A- and C-type cells.

Immunofluorescence	Number of cells counted		
	p7	p17	p40-45
SK3 and peripherin positive	2	4	11
SK3 positive peripherin negative	3	6	16
SK3 negative (peripherin positive and negative)	47	28	24

Table 5.2 The number of SK3 positive cells increase with age. However the proportions of SK3 antibody-positive cells that are also peripherin positive/negative (C-type or A-type) remain the same.

5.3 Discussion

There are two major findings of the work presented in this chapter. The first is that by qPCR SK and IK channel mRNA expression can be detected in a number of rat tissues, including that from DRG, but only antibodies that recognise the SK3 protein showed detectable protein levels in isolated DRG cells. The second is that all SK/IK channels show an up-regulation of mRNA levels in rat DRGs with age, and for SK3 this closely corresponds with an age-dependent increase in the levels of SK3 staining in DRG cells.

5.3.1 qPCR controls using different rat tissues

Primer and probe sets were initially tested on plasmids; these proved to be highly specific for their targets. They also recognised the appropriate cDNAs from mRNA obtained from HEK 293 cells transiently transfected with the SK/IK plasmids. In addition, they amplified cDNA from tissues expressing mRNA for native channels (see **Figure 5.2**).

5.3.1.1 SK/IK mRNA levels in brain tissues

In accordance with the literature, hippocampal and whole brain tissue showed detectable levels of SK1, SK2 and SK3 mRNA (Stocker & Pederzani, 2000; Rimini *et*

al., 2000). There were also low levels of IK signal. However, functional IK channels in the brain have, to date, only been described in neurones of the rat supraoptic nucleus (Greffrath *et al.*, 1998).

5.3.1.2 SK/IK mRNA levels in colon

As expected, there were high levels of IK mRNA seen in rat colon tissue and there was also a detectable amount of SK3 mRNA present. However, there was virtually no SK1 or SK2 mRNA expression. Several other groups have also reported IK mRNA in colonic tissue (Logsdon *et al.*, 1997; Vandorpe *et al.*, 1998) and more specifically in the epithelium (Furness *et al.*, 2003; Joiner *et al.*, 2003). Transcripts encoding SK channels have also been detected in colonic tissue samples (Joiner *et al.*, 2003). Ro and colleagues (2001) found that all subtypes of SK channels can be detected in murine colon (relative abundances: SK2 > SK3 > SK1) although apparently very little SK channel mRNA is present in canine tissue. Northern blots using rat colon also show high levels of SK2 expression (Joiner *et al.*, 2003). There may be several reasons for the difference in SK channel levels described here with those reported previously. Ro *et al.* (2001) carried out much of their studies on mouse tissue, and as the work described in this chapter involved using rat tissue, the levels of SK channels detected may reflect species differences. The work by Joiner *et al.* (2003), however, was also carried out on rat colon, but from adults, and they showed that high levels of SK2 mRNA were present, which is in contrast with the work presented here which shows that SK2 cDNA is not amplified. This may be explained by differences in the ages of the animals; I used adolescent animals (p17) and, as discussed in this chapter, at least in some tissues SK and IK channel mRNA is up-regulated as animals get older. This may be why SK2 is not detected in p17 rat colon. Joiner *et al.* (2003) also report that there is no SK3

detected, however they use northern blots to look at mRNA expression, which needs high levels of starting material to be effective. The qPCR technique is able to amplify up small amounts of cDNA thus making it more sensitive, which might explain why, in this study, it was possible to detect a low level of SK3 in colon tissue.

5.3.1.3 SK/IK mRNA levels in adrenal gland

Adrenal gland tissue shows very low levels of SK1 mRNA compared to the brain and hippocampal samples. There was virtually no amplification with the SK1-AV1 primer/probe set, however there was some amplification with the SK1-AV2 and SK1 exon 7 primer/probe sets suggesting that low levels of these mRNAs were present. There were similarly low levels of SK3 and IK mRNA. In contrast to these results, there were high levels of SK2 mRNA suggesting that it may be functionally more important than the other SK/IK channels. In fact, a recent study has highlighted a role for SK2 channels in the hypoxia-evoked catecholamine release from the adrenal medulla (Keating *et al.*, 2001).

5.3.1.4 SK/IK mRNA levels in DRG tissue

The qPCR results for the DRG tissues apparently show high levels of mRNA for all of the SK channels and also IK channels. There is very little work showing functional expression of IK channels in neurones, however, there is some suggestion of a role in AHP generation in neurones of the supraoptic nucleus (Greffrath *et al.*, 1998) so it is interesting to find evidence for IK channel mRNA expression in DRG cells.

5.3.1.5 Levels of SK channel splice variants

One of the primer/probe sets was designed to detect particular SK1 splice variants. Alternate splicing of SK1 transcripts is predicted to generate 16 different polypeptides which could generate considerable functional heterogeneity. Several of the putative polypeptides would lead to a loss of the calmodulin-binding domain (CaMBD) and these are unlikely to form functional channels. One way this could happen is via the loss of exon 7. In the currently described experiments, high levels of rSK1 mRNA can be detected in whole brain, hippocampal and DRG tissue using primer/probe sets designed to recognise all variants of SK1 and those containing exon 7. Similar levels of these transcripts can be seen in brain and DRG tissue with all three primer/probe sets suggesting that there are few or no transcripts lacking exon 7 in these tissues.

Since this work was done, there have also been reports of different splice variants of SK3 (Tomita *et al*, 2003; Kolski-Adreaco *et al*, 2004; Wittekindt *et al*, 2004). SK3-1B and SK3-1C constitute truncated isoforms of the SK3 channel that lack a region of the N-terminus and have been shown to have a dominant negative effect on SK/IK channel currents (Tomita *et al*, 2003; Kolski-Adreaco *et al*, 2004). However, while message for SK3-1B has been detected in the brain, SK3-1C mRNA has so far only been described in non-neuronal tissues (Tomita *et al*, 2003; Kolski-Adreaco *et al*, 2004). A third SK3 isoform, which has reported by Wittekindt *et al* (2004), contains an additional 15 amino acids inserted between the S5 and P regions (hSK3-ex4). Transcripts for this protein are present in both neuronal and non neuronal tissues. What is particularly interesting about this splice variant is that whilst these channels and hSK3 channels are activated by similar Ca^{2+} concentrations, hSK3-ex4 is insensitive to block by high concentrations of apamin (up to 100 nM) and scyllatoxin (up to 500 nM; Wittekindt *et al*, 2004).

However, from the current experiments it is not possible to determine the extent to which any of these splice variants might be important in DRG neurones.

5.3.2 Age-dependent changes in mRNA levels

The second aim of the work in this chapter was to examine age-related changes in SK/IK expression in rats. The results from qPCR experiments indicate that there are increases in mRNA levels in rat DRG and adrenal gland suggesting that the importance of a role for SK/IK channels may increase with age.

5.3.3 SK/IK channel proteins expressed in cultured DRG neurones

While studies into mRNA levels provide some indication as to which channels might be important in certain tissues, when considered alone they are not sufficient to predict levels of channel protein translated. Work in yeast comparing protein and mRNA abundances suggests that there is not always a good correlation between the two (Gygi *et al.*, 1999), so in addition to the qPCR, DRG cells were stained with SK/IK channel specific antibodies. Only the anti-SK3 antibody produced clear detectable staining, implicating a role for SK3 in DRG cells. However, the optimal antibody concentrations were established using transiently transfected HEK 293 cells over-expressing the SK/IK channel genes (see **Chapter 3**). So it is also possible that the other SK/IK channel proteins are present but are expressed at low levels and are below the threshold for detection in my experiments.

Interestingly, the SK3 protein can be detected in both peripherin-positive C-fibre cells and in peripherin-negative A-fibre cells. This suggests that SK3 may have a functional role regulating excitability in a range of different types of sensory neurone. As with mRNA levels the number of cells staining positively with the anti-SK3 antibodies

increases with the age of the animal suggesting that the channel becomes more important as the animal reaches adulthood.

5.3.5 Possible mechanisms by which SK/IK channels are up-regulated

K^+ channel gene expression is extensively controlled. Regulation occurs by a number of means including physiological stimuli e.g. hormones, neurotransmitters etc, drugs e.g. opioids, and pathophysiological conditions such as hypertension and epilepsy (Levitan & Takimoto, 1998). Gene expression can also be altered during development to produce other long term effects (Levitan & Takimoto, 1998). Oestrogen has been shown to increase SK3 transcription in guinea pig brain (Bosch *et al.*, 2002) and in a rat skeletal muscle cell line (Jacobson *et al.*, 2003). As mammalian development and the onset of puberty is associated with an increase in sex hormones such as oestrogen, this may explain partially why SK3 protein levels in rat DRG cells appear to increase with age. However, given that both male and female rats show age-dependent increases in SK/IK expression levels, it is unlikely to be the only mechanism. In addition to oestrogen, growth hormone (whose levels also increase with age) has been shown to up-regulate K_V channel expression (Chen, 2002) providing another possible means by which levels of SK channel transcripts could be regulated.

5.3.6 Possible functional significance of SK3 up-regulation

What might be the functional significance of this age-dependent increase in SK channel expression? One of the major differences in the transmission of sensory information between neonates and adults lies in the response to nociceptive stimuli. In newborns, reflex responses to even innocuous stimuli are greatly exaggerated compared with those of adults (Wolf, 1999; Fitzgerald & Jennings, 1999). Sensory neurones,

which are functional in neonates, have been shown to form connections with dorsal horn cells in the spinal cord in the foetus (Wolf, 1999), so one might expect that sensory transduction in neonates would be similar to that in adults. However, this is not the case. There are several suggestions for the differences in transmission of sensory information. These include changes in the glutamate receptor subunits expressed in dorsal horn neurones, which alter cell excitability, and functional changes in $GABA_A$ and glycine receptors of the dorsal horn (Alvares & Fitzgerald, 1999; Pattinson & Fitzgerald, 2004). These changes reflect maturation of cells in the spinal cord. However, DRGs are also likely to undergo extensive changes during development as highlighted by work on $GABA_A$ receptors which show different kinetic properties in embryonic and adult DRG cells (Valeyev *et al.*, 2000).

Cutaneous withdrawal reflexes have long been used to provide information on nervous sensitivity to nociceptive stimuli and are particularly pronounced in the newborn rat (Fitzgerald & Jennings, 1999). Interestingly, this effect begins to change after the first postnatal week (Fitzgerald & Gibson, 1984) and thresholds to mechanical skin stimulation decrease with the age of the animal (Fitzgerald & Jennings, 1999) until in the adult, only noxious stimuli produce a reflex response (Wolf, 1999). It is possible, therefore, that SK3 might have some functional involvement in this process because these timings correspond reasonably well with the presence of low levels of SK3 channel protein in p7 cells, which increase as animals get older. Also, the correlation with SK3 expression in the "right direction" i.e. increased levels of the potassium channel are expected to reduce excitability.

Although the work described here allows one to speculate that SK channels might be important to changes in DRG cell function, their physiological role for them is examined further in adult animals in the next chapter.

Chapter 6

SK/IK channel gene expression in rat spinal cord and putative role in sensory nerve terminals

6.1 Introduction

This chapter describes results from immunofluorescent antibody staining experiments designed to examine the presence and localisation of different SK/IK channel subunit proteins in the lumbar region of rat spinal cord. Some of these localisations within the spinal cord are compared with those of the vanilloid receptor (VR1 or more recently called TRPV1). Also in this chapter results are presented from *in vivo* recordings made to explore a possible physiological role for SK channels in sensory transmission. These later experiments were performed as part of a collaboration with Prof Anthony Dickenson and Dr. Rie Suzuki (Department of Pharmacology, UCL).

SK channels in DRG cell bodies may be transported to the peripheral and/or the central terminals of these neurones. Many of these central terminals appear in the outer laminae of the spinal cord where, for example, the vanilloid receptor VR1 appears in C-fibre terminals. Even though the results from isolated cells (presented in **Chapter 4)** suggest that SK channels do not play a prominent role, at least in terms of AHP generation, in the cell bodies of DRG neurones, these SK channels may still have a significant role in sensory transmission at nerve terminals. Other proteins for example, the neuropeptide Y receptors Y1 and Y2, are present in both central terminals and DRG cell bodies but they appear to have different degrees of influence at these locations (Zhang *et al.*, 1994; Brumovsky *et al.*, 2002; Abdulla & Smith 1999). Thus, it is still

possible that SK channels have a prominent role in regulating sensory transmission even if they have very limited activity in cell bodies.

The VR1 receptor, used as a marker for comparison with SK channel antibody staining, is a Ca^{2+} permeable cation channel that opens in response to heat and ligands, such as capsaicin, to increase cell excitability (Catrina et al., 1997). It has recently been shown to also respond to endogenous ligands, for example, anandamide and eicosanoids (Benham *et al.*, 2003). The protein is expressed in small diameter nociceptive nerve fibres (Szallasi & Blumberg, 1999) and is not detected in fast conducting A-fibre cells or high threshold mechanoreceptive cells (Szolcsanyi *et al.*, 1988). Immunocytochemical experiments suggest that the VR1 protein is present not only in DRG peripheral terminals but in cell somata, spinal terminals and also post-synaptically in dorsal horn neurones of the spinal cord (Tominaga *et al.*, 1998; Guo *et al.*, 1999; Valtschanoff, 2001). The pattern of staining for VR1 protein in the spinal cord is largely restricted to the superficial laminae I and II where nociceptive afferents are expected to terminate (Tominaga *et al.*, 1998; Guo *et al.*, 1999). Because of the extensive characterisation of its distribution and its important functional role in sensory transmission, the VR1 receptor makes an interesting comparison with SK channels when examining protein distributions.

To investigate further SK channel activity in sensory pathways from the periphery to the spinal cord, SK channel activators and blockers were applied while *in vivo* extracellular recordings were made from lamina V wide dynamic range neurones. An outline of the methods used in these recordings is described later in this chapter. These experiments were carried out by Dr Rie Suzuki as part of a collaborative investigation. My role in these experiments included design, in the form of drugs selected and the concentrations chosen. I also did some of the subsequent data analysis.

6.2 Results

6.2.1 Controls

Slices were initially stained with secondary antibodies alone to establish background levels of staining (see **Figure 6.1**). The secondary antibodies did not produce any specific pattern of staining and low levels of background were observed in all experiments.

6.2.2 SK/IK channel staining in the spinal cord

The anti-SK/IK antibodies used subsequent experiments were: rb196 (N- terminal anti-rSK1), rb200 (C-terminal anti-rSK1), M1 (anti-rSK2), M75 (anti-rSK3) and R212 (anti-rIK). Neither the anti-rSK1 antibodies nor the anti-rSK2 antibody produced any positive selective staining in spinal cord slices at concentrations used to stain transfected HEK 293 cells (see **Figure 6.2**).

6.2.3 SK3 staining in the spinal cord

Figure 6.3 shows SK3 immunoreactivity in the spinal cord. In sharp contrast to the SK1 and SK2 channel antibody results, the anti-SK3 antibody produces a bright positive signal in the superficial dorsal horn. This fine fibrous pattern of staining is particularly pronounced in lamina I and lamina II and probably also extends into lamina III. Dark spots in this pattern of staining correspond to the cell bodies of spinal neurones and thus the staining is consistent with SK3 protein being present in the incoming DRG terminals.

The ventral horn has a quite different pattern of SK3 antibody staining. Certain cells, most likely to be alpha motorneurones, show SK3 immunofluorescence in the region of

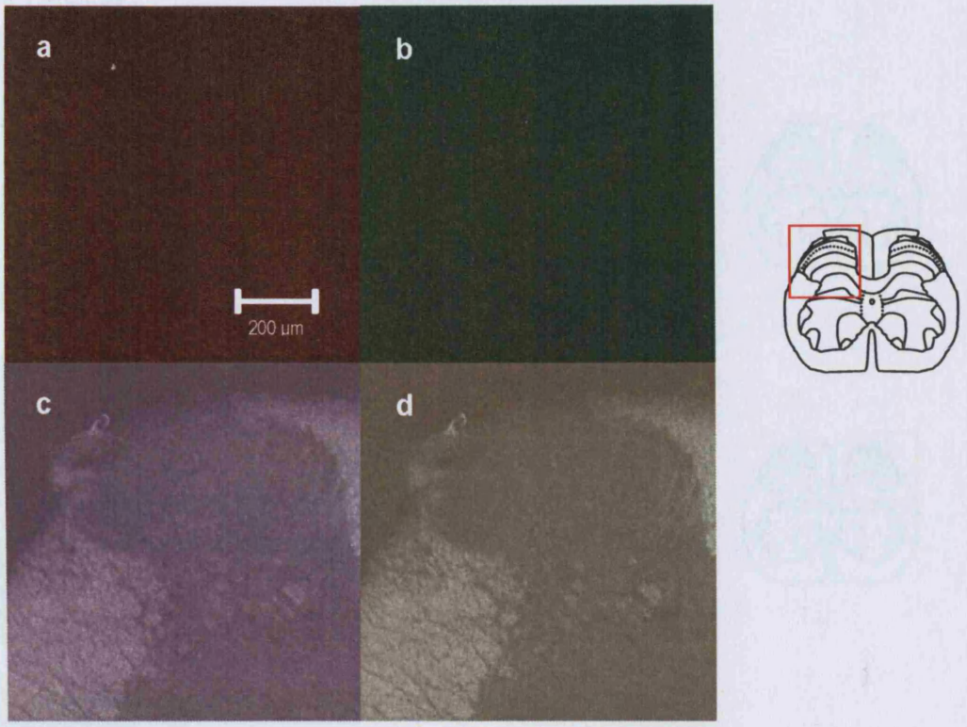

Figure 6.1 Secondary antibodies produce very low levels of background staining in rat spinal cord slices. A negative control where slices were stained with the CY3-labelled goat anti-rabbit secondary antibody (**a**) and the fluorescein-labelled goat anti-guinea pig secondary antibody (**b**) to determine levels of background staining. A brightfield image (**c**) and overlay (**d**) are also shown. The illustration to the right indicates the region of the spinal cord depicted in the confocal images.

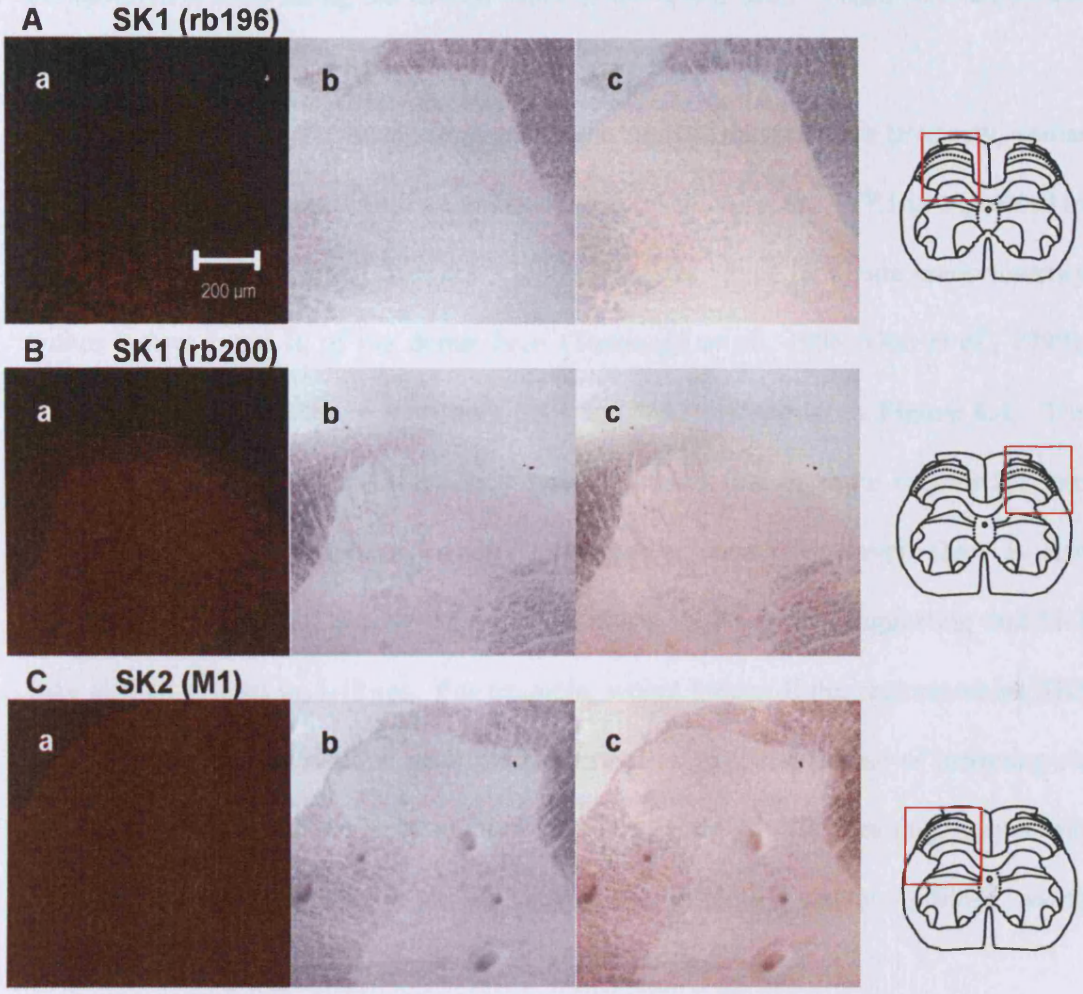

Figure 6.2 Anti-SK1 and SK2 antibodies do not produce selective positive staining in rat spinal cord slices. **A**, SK1 staining seen with the rb196 antibody. **B**, SK1 staining seen with the rb200 antibody. **C**, SK2 staining seen with the M1 antibody. In each case **a** shows SK1/SK2 antibody staining using the CY3 labelled secondary antibody, **b** shows the brightfield, and **c** shows the overlay. To the right of each image is a schematic of the spinal cord showing the region depicted. The scale bar in **A** also applies to **B** and **C**. Illustrations to the right show the region of spinal cord depicted.

the cell membrane. This signal extends beyond the soma into the processes for these cells. Finally, there is a strong SK3 antibody signal at or near the plasma membrane of the ependymal cells lining the central canal of the spinal cord. These cells are of the epithelial type (Bruni, 1998).

In order to examine the localisation of SK3 immunoreactivity more precisely, spinal slices were also co-stained with an antibody to the VR1 receptor. VR1 is expressed in the nerve terminals of small diameter C-fibre neurones which terminate predominantly within lamina I and II_i of the dorsal horn (Tominaga *et al.*, 1998; Guo *et al.*, 1999). Spinal cord sections stained with both SK3 and VR1 are shown in **Figure 6.4**. The overlay of the VR1 and SK3 antibody staining shows that in some regions the two proteins might be co-expressed in the same nerve fibres. However, there is also extensive SK3 immunoreactivity in regions that are VR1-negative suggesting that SK3 may also be present in A-fibres. For example, within lamina II the regions where SK3 appears to be expressed alone most likely correspond to the terminals of incoming A_δ fibres. Where the SK3 antibody staining extends beyond the VR1 staining, deeper into the dorsal horn, it may well reflect SK3 expression in large diameter A_β fibres, which are known to terminate in lamina III (Woolf & Fitzgerald, 1986).

The apparent localisation of SK3 in different types of afferent fibre terminals is consistent with staining in isolated DRG cells as shown in **Chapter 5** and **Figure 6.4 B**. By using peripherin as a marker for C-type neurones it can be seen that SK3 is present in the small diameter peripherin-positive cells. There is also strong staining in the small and very large diameter A-fibre cells which are peripherin-negative indicating that SK3 is likely to be expressed in A_δ and A_β type cells. In addition, there are some peripherin-positive and peripherin-negative DRG cells that do not show a positive signal for SK3.

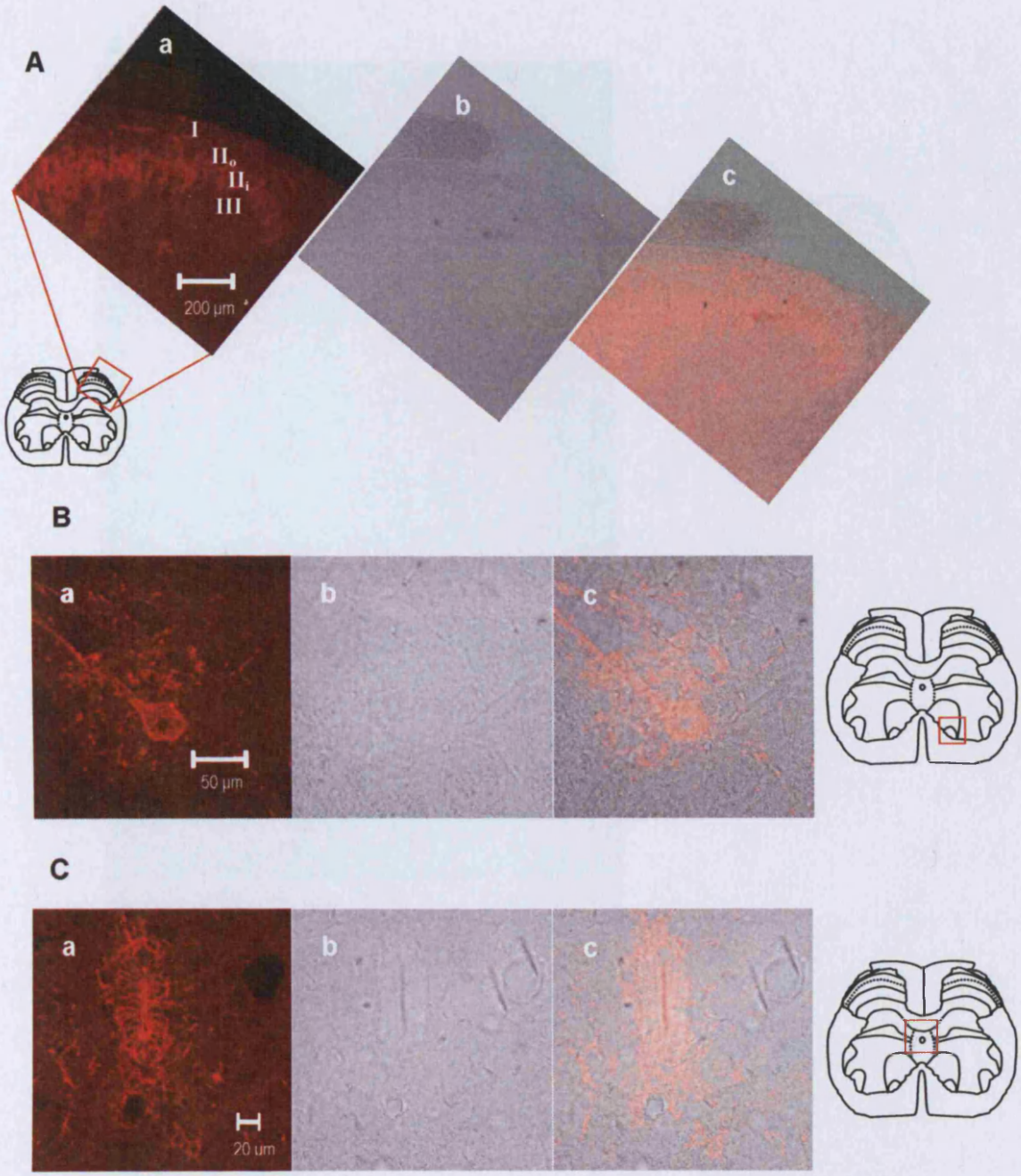

Figure 6.3 SK3 antibody staining is seen in several regions of the spinal cord. In each set of images **a** shows the SK3 antibody staining, **b** shows the brightfield and **c** shows the overlay of the first two images. **A**, SK3 staining in the superficial dorsal horn. There is a bright positive signal in lamina I and a fainter but detectable signal in the outer region of lamina II (II_o). There is also a strong SK3 antibody signal in the inner region of lamina II (II_i) which probably continues into lamina III. **B**, an example of staining in a large diameter neurone in the ventral horn of the spinal cord. Staining can be seen in the region of the cell membrane of the soma and this extends into the cell's processes. **C**, a bright SK3 antibody signal is detected at or near the plasma membrane of the ependymal cells lining the central canal. In each case the "boxed" region of the spinal cord diagram indicates the region shown in the staining images.

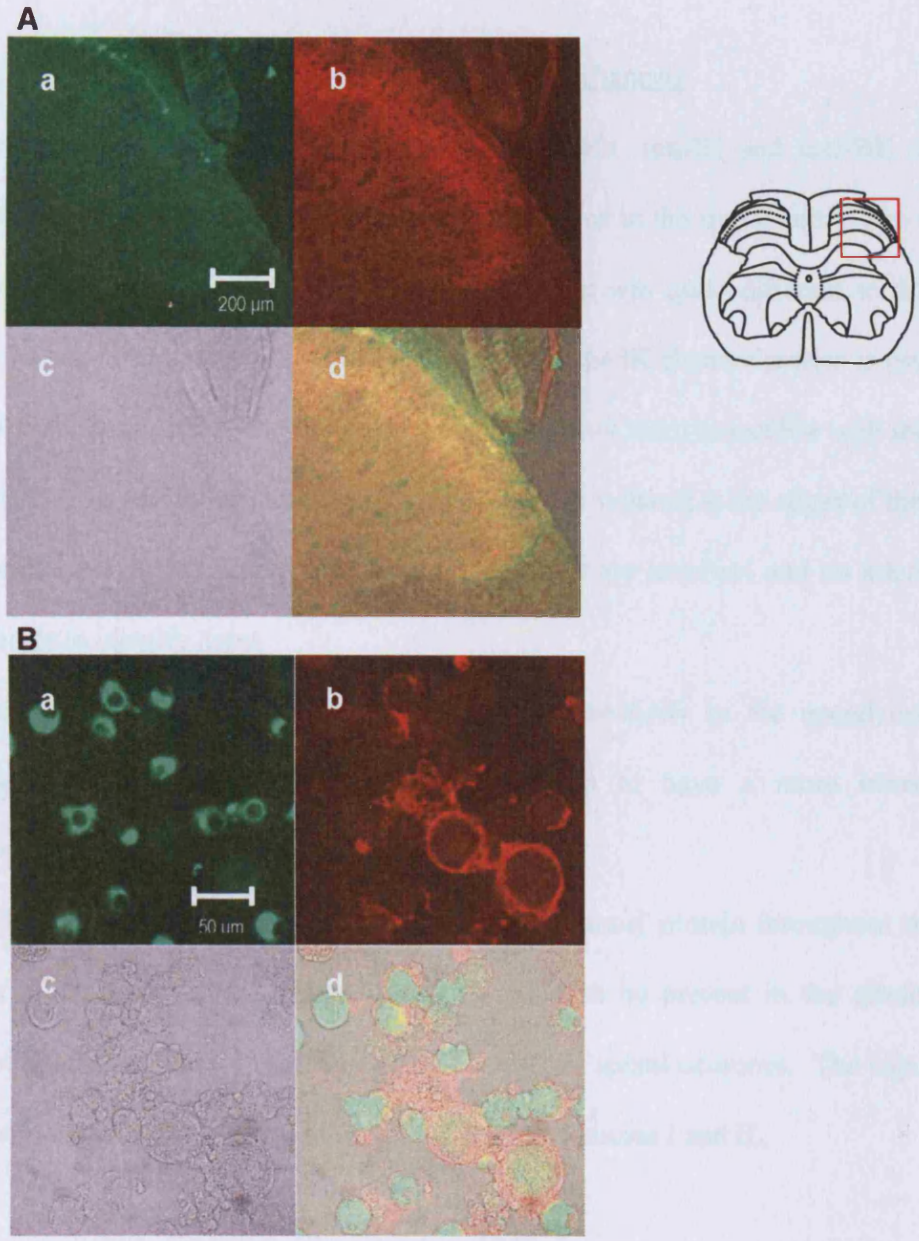

Figure 6.4 SK3 antibody staining in spinal cord and cultured DRG neurones is consistent with expression in both A- and C-type cells. **A**, spinal cord slices stained with VR1 (**a**), and SK3 (**b**). (**c**) shows the brightfield and (**d**) the overlay. VR1 antibody staining is seen in lamina I and more faintly in lamina II_i. SK3 antibody staining, can be seen in lamina I, II and most likely III as the SK3 immunoreactivity extends beyond the VR1 staining (**d**). The schematic to the right shows the region of the spinal cord depicted. **B**, isolated DRG cells stained with an antibody to the C-fibre marker peripherin (**a**) and with the SK3 antibody (**b**). The brightfield is shown in (**c**) and the overlay in (**d**). SK3 immunoreactivity can be clearly seen in both A- and C-type cells, which is consistent with the termination pattern in the spinal cord. Note that this pattern of staining forms an unbroken ring around the DRG cells suggesting that it is unlikely to be due to positive staining of satellite cell sheath.

6.2.4 Staining for other calcium-activated potassium channels

As well as testing for the presence of SK channels, anti-IK and anti-BK channel antibodies were used to look for these channel proteins in the spinal cord. The anti-IK antibody produced a striking pattern of staining that was quite different to that seen using the anti-SK3 antibody. **Figure 6.5** shows that the IK channel protein is present in a large number of cells in the spinal cord, but it does not seem to localise with incoming terminals. The density of these cells becomes slightly reduced at the edges of the dorsal and ventral horns, but it is not clear what cell types are involved and no attempt has been made to identify them.

As with the SK3 antibody, there is IK immunoreactivity in the ependymal cells although the IK antibody staining signal appears to have a more intracellular distribution.

The BK channel antibody appears to detect the channel protein throughout the grey matter of the spinal cord (**Figure 6.6**). It may thus be present in the terminals of incoming afferent fibres and also in the cell bodies of spinal neurones. The signal only appears weaker in two regions of the spinal cord, in laminae I and II_o.

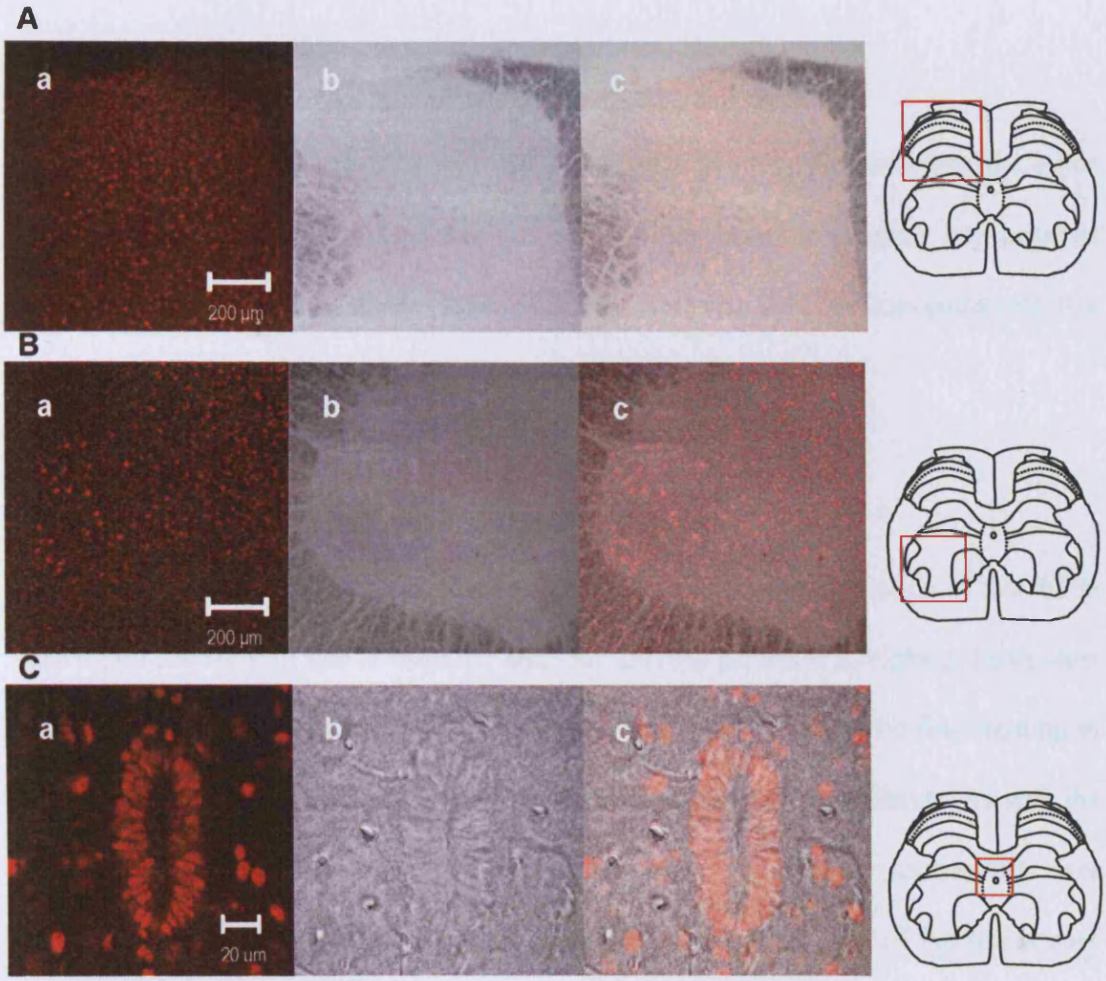

Figure 6.5 The IK channel antibody produces selective staining in the spinal cord. **A**, IK positive staining of cells in the dorsal horn and **B** in the ventral horn. **C**, positive signal seen in the ependymal cells surrounding the central canal of the spinal cord. In each case **a** shows the IK channel antibody staining, **b** shows the brightfield image and **c** shows an overlay. The schematic to the right indicates the region of the spinal cord depicted.

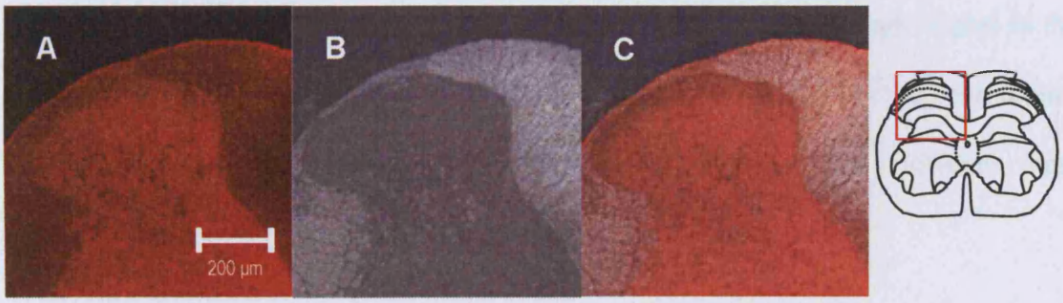

Figure 6.6 The BK channel antibody produces positive staining throughout the grey matter of the spinal cord. **A**, positive staining with the anti-BK channel antibody. There is a strong positive signal for the BK channel protein throughout the grey matter of the spinal cord. Thus, it may be present in incoming afferent terminals and/or in the somata of spinal neurones. The signal is, however, weaker in the region of lamina I and lamina II_o. **B**, a brightfield image and **C** an overlay. The schematic to the right shows the spinal cord region depicted.

6.2.5 Staining for SK1 and SK2 with higher antibody concentrations

It is possible that the anti-SK1 and –SK2 antibodies are less sensitive than the other anti-K_{Ca} channel antibodies and that this is why they failed to produce any positive staining in the spinal cord slices. As a result they were also tested at concentrations 10x and 50x higher than the original concentrations.

6.2.5.1 rSK1 staining at high antibody concentrations

Figure 6.7 shows the results of staining with a 10x higher concentration of the rb196 and rb200 antibodies. The N-terminal antibody (rb196) produces a bright positive stain of spinal neurones in both the dorsal and ventral horns but there was no fine staining in the dorsal horn indicating an absence of SK1 in terminating afferent fibres. As with the transfected HEK 293 cells the rSK1 signal appears to be largely intracellular (see **Chapter 3**). In contrast, there was no selective staining seen in any of the spinal cord regions with the C-terminal antibody (rb200).

6.2.5.2 rSK2 staining at high antibody concentrations

SK2 staining was only seen when the M1 antibody concentration was increased to 50x the original (**Figure 6.8**). In the dorsal horn, there was a relatively bright signal in the region of lamina I, where the incoming C-fibre afferents are found. In the ventral horn there appeared to be some selective staining of large diameter cells. However, there was no SK2 signal seen in the ependymal cells.

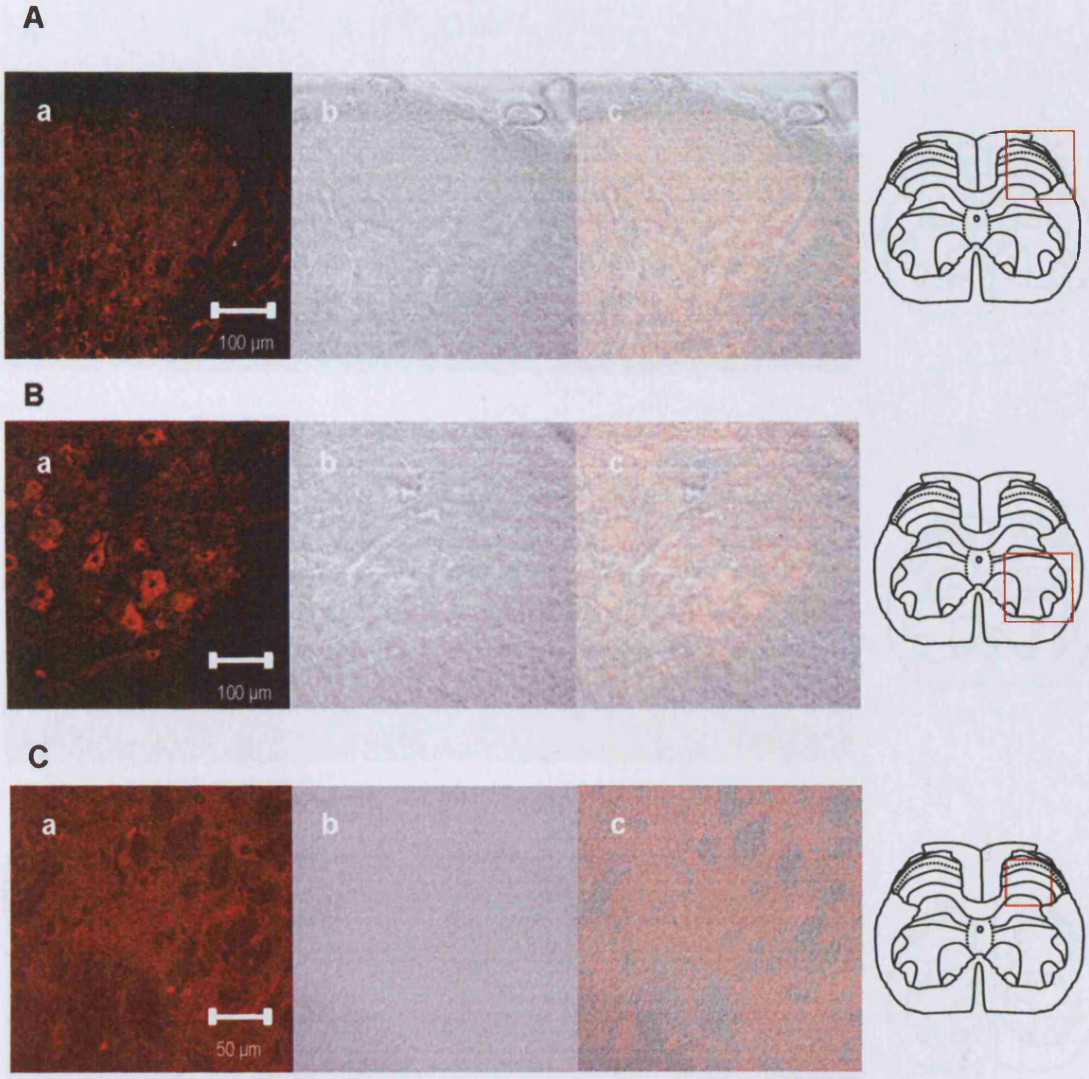

Figure 6.7 Staining of spinal sections with higher concentrations of the anti-SK1 antibodies. **A** (dorsal horn) and **B** (ventral horn) show positive staining with the N-terminal anti-rSK1 antibody rb196 and **C** shows a lack of selective staining with the C-terminal antibody rb200. In each case **a** shows the antibody fluorescence, **b** the brightfield image and **c** the overlay. Both antibodies were used at a concentration ten times higher than that used to stain HEK 293 cells transfected with rSK1. The rb196 antibody produces bright positive staining of the cell bodies of neurones in the dorsal and ventral horns. As expected, the pattern of staining appears to be intracellular. In contrast there is no selective positive staining seen with the rb200 antibody (**C**).

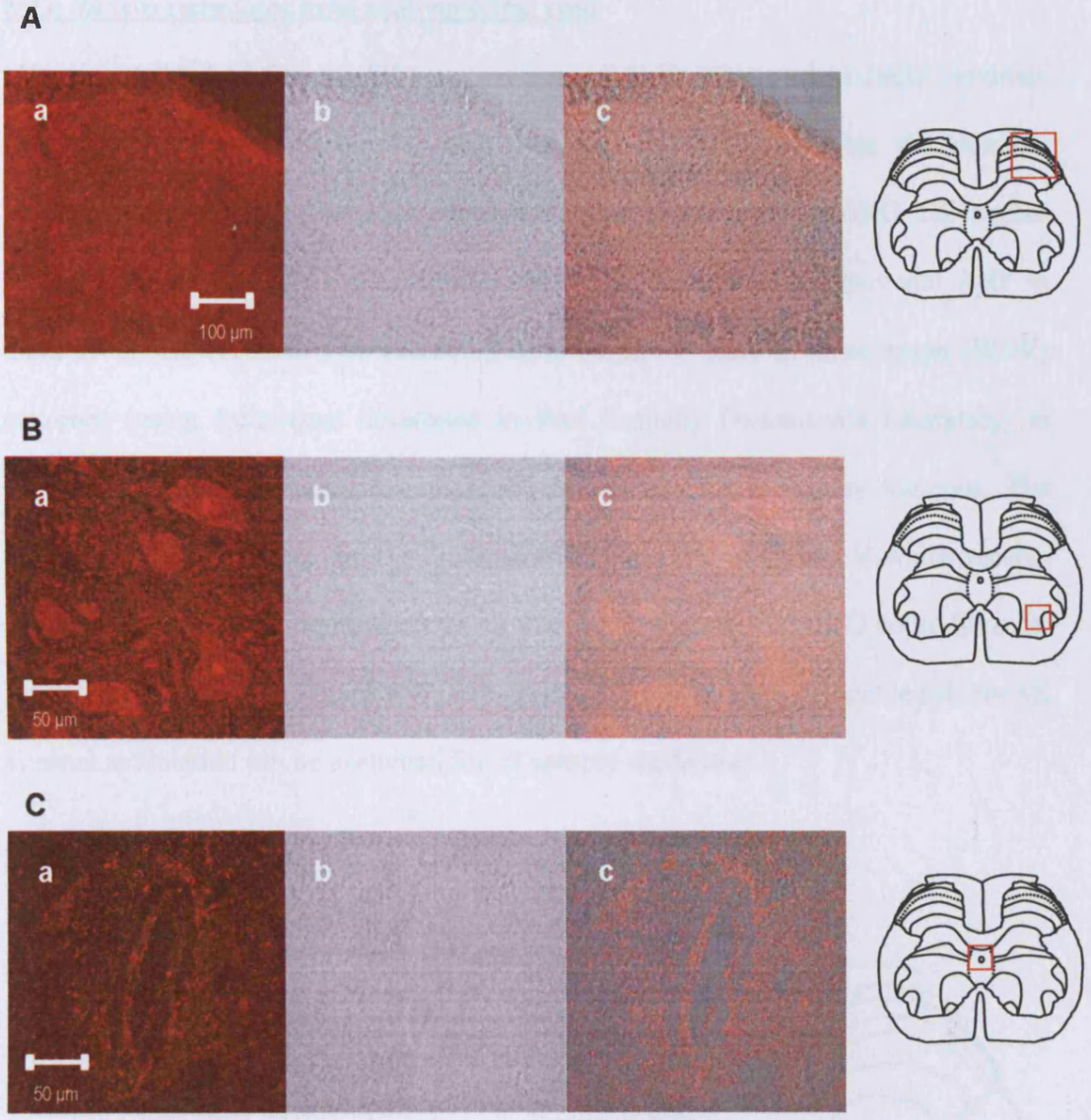

Figure 6.8 Positive staining of spinal neurones with higher concentrations of the anti-rSK2 antibody (M1). The M1 antibody was used at a concentration fifty times higher than that used to stain HEK 293 cells transfected with SK2. **A**, shows staining in lamina I of the dorsal horn. **B**, shows staining of large diameter neurones in the ventral horn and **C** shows staining in the region of the ependymal cells. In each case **a** shows the antibody staining, **b** shows the brightfield and **c** the overlay of **a** and **b**. There appears to be a positive SK2 antibody signal in the region of lamina I. In the ventral horn, the motorneurones also show signs of SK2 immunoreactivity. However, the ependymal cells are not stained by the antibody.

6.2.6 *In vivo* recordings from adult rat spinal cord

Having established that the SK3 protein appears to be expressed in DRG terminals from both A- and C-fibres, the next step was to determine what the possible physiological role might be. Electrophysiological experiments in DRG cell bodies provided little evidence for the contribution of SK channels to the neuronal AHP in these cells. However, *in vivo* recording from lamina V wide dynamic range (WDR) neurones (using techniques developed in Prof Anthony Dickenson's laboratory, in UCL) provides another means to explore SK channel function in sensory neurones. The method utilises recordings from individual WDR neurones in lamina V which receive inputs via second order neurones from all three different types of DRG nerve fibre i.e. A_β, A_δ, and C-fibre (see **Figure 6.9**; Dickenson, 1995). Therefore a possible role for SK channel modulation can be examined for all sensory modalities.

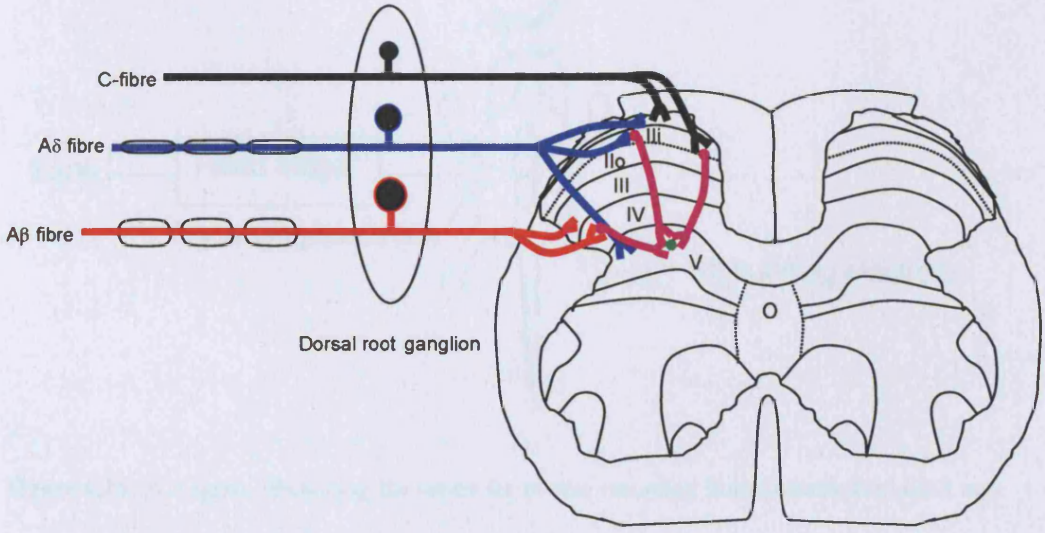

Figure 6.9 A schematic representation of the principal connections between primary afferents and spinal neurones. *In vivo* recordings are made from wide dynamic range neurones in lamina V (•). Stimulation of DRG afferents in the periphery affects spinal neurone firing generally via second order neurones (•) which synapse upon lamina V cells.

6.2.6.1 Method for in vivo recordings

The *in vivo* work described in this thesis was designed in collaboration with and carried out by Dr Rie Suzuki and Prof Anthony Dickenson (Department of Pharmacology, UCL), therefore only an outline of the methods will be provided here. For a fuller description of the technique see Urch & Dickenson (2003).

Anaesthetised adult rats (200-250g) were used in all experiments, in accordance with Home Office guidelines. The spinal cord was exposed via a laminectomy at vertebrae L1-L3. Single-unit extracellular recordings were made from lamina V wide-dynamic range neurones using a parylene-coated tungsten electrode (see **Figure 6.10**). Recordings were made from one neurone in each animal and each animal received a single pharmacological treatment.

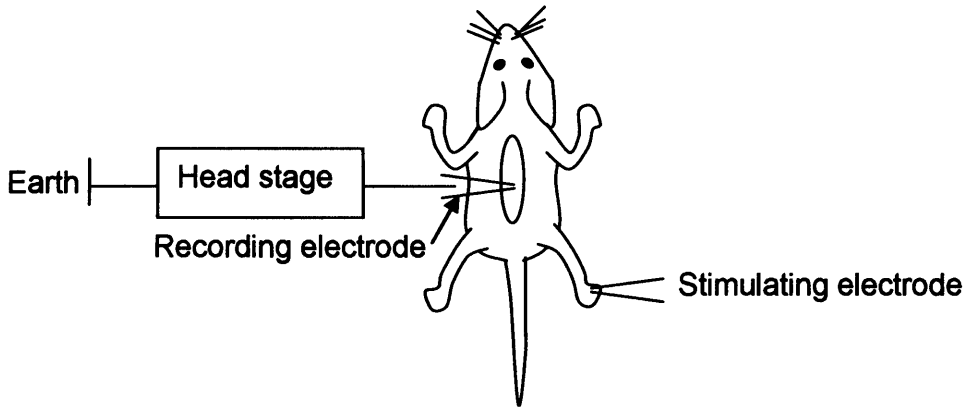

Figure 6.10 A diagram illustrating the set-up for *in vivo* recording from anaesthetised adult rats. Lumbar regions L1-L3 of the spinal cord are exposed and extracellular recordings are made from a single lamina V neurone using an electrode inserted into the spinal cord. Various stimuli are applied via the hind-paw. Electrical stimulation is produced via two needles inserted into the paw. A number of naturally evoked responses were also produced; heat (via a 45 °C water jet), innocuous touch (via soft brushing of the paw) and noxious pressure (via 9 g and 75 g von Frey filaments). Figure adapted from Urch & Dickenson (2003).

Neurones were stimulated electrically and naturally using a range of noxious and innocuous stimuli applied to the rat hind-paw. For electrical stimulation, neurones were given a train of pulses, at a magnitude of three times the threshold current for C-fibres via two stimulating needles inserted into the receptive field of the hind paw. A post-stimulus histogram was then constructed and Aβ-(0-20 ms), Aδ- (20-90 ms) and C-fibre (90-300 ms) evoked neuronal responses (number of action potentials fired) were separated and quantified on the basis of latency (see **Figure 6.11**). Neuronal responses occurring after the C-fibre latency band were taken to be the postdischarge of the cell (300-800 ms). The postdischarge (PD) is a result of the phenomenon of "wind-up" whereby prolonged C-fibre firing results in sensitisation and increased electrical activity of the dorsal horn neurones.

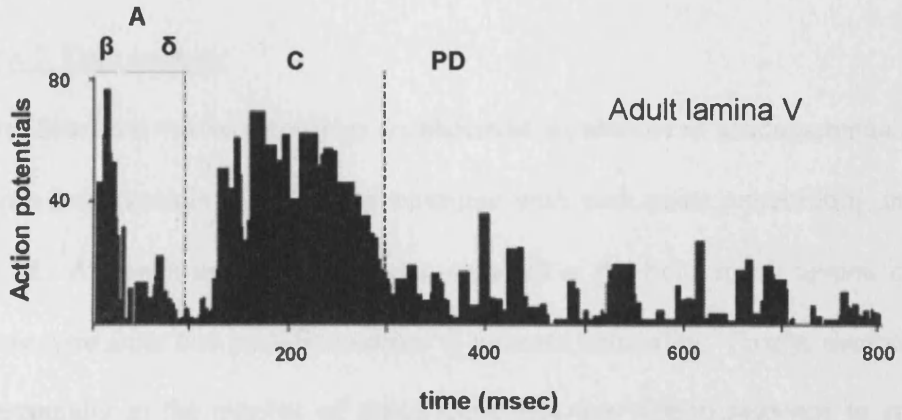

Figure 6.11 Data separation from a single lamina V neurone. The number of action potentials elicited in response to a given stimulus can be recorded and separated on the basis of their latency to determine the effects on A_β (β), A_δ (δ) and C-fibres (C) and also the post discharge (PD). Figure adapted from Urch & Dickenson (2003).

A number of innocuous and noxious stimuli were used to characterise neuronal responses to natural (mechanical and thermal) stimuli. For thermal responses, water at a temperature of 45 °C was applied to the centre of the receptive field of the hind paw using a water jet. For mechanical stimulation, a brush was used to gently stroke the hind paw and von Frey filaments (Scientific Marketing Associates) were applied in ascending order (9 g then 75g) to provide a mechanical stimulus of increasing intensity.

A 10 µl volume of the appropriate drug was applied directly into a small well created in the spinal cord. Prior to drug administration, three stable control responses were obtained at 10 min intervals. All drug effects were followed for 40 minutes per dose and tests were carried out at 10 minute intervals to avoid desensitisation.

Responses to natural stimuli cannot be separated into fibre types and so were simply recorded as the total number of action potentials.

6.2.6.2 Data analysis

The data from *in vivo* recordings are shown as the number of action potentials recorded in pre-drug controls vs post-drug treatment with each point representing the mean ± S.E.M. Although this method is quite standard in the field, it has several drawbacks. These stem from two problems related to neurone variability. Firstly, neurones vary in substantially in the number of action potentials they fire in response to stimulation. Secondly, they vary considerably in the individual responses to drug application. This means that repeated measurements from individual neurones are not repeated attempts to measure the same parameter. For this reason, the S.E.M.s cannot be considered a measure of error in the normal way.

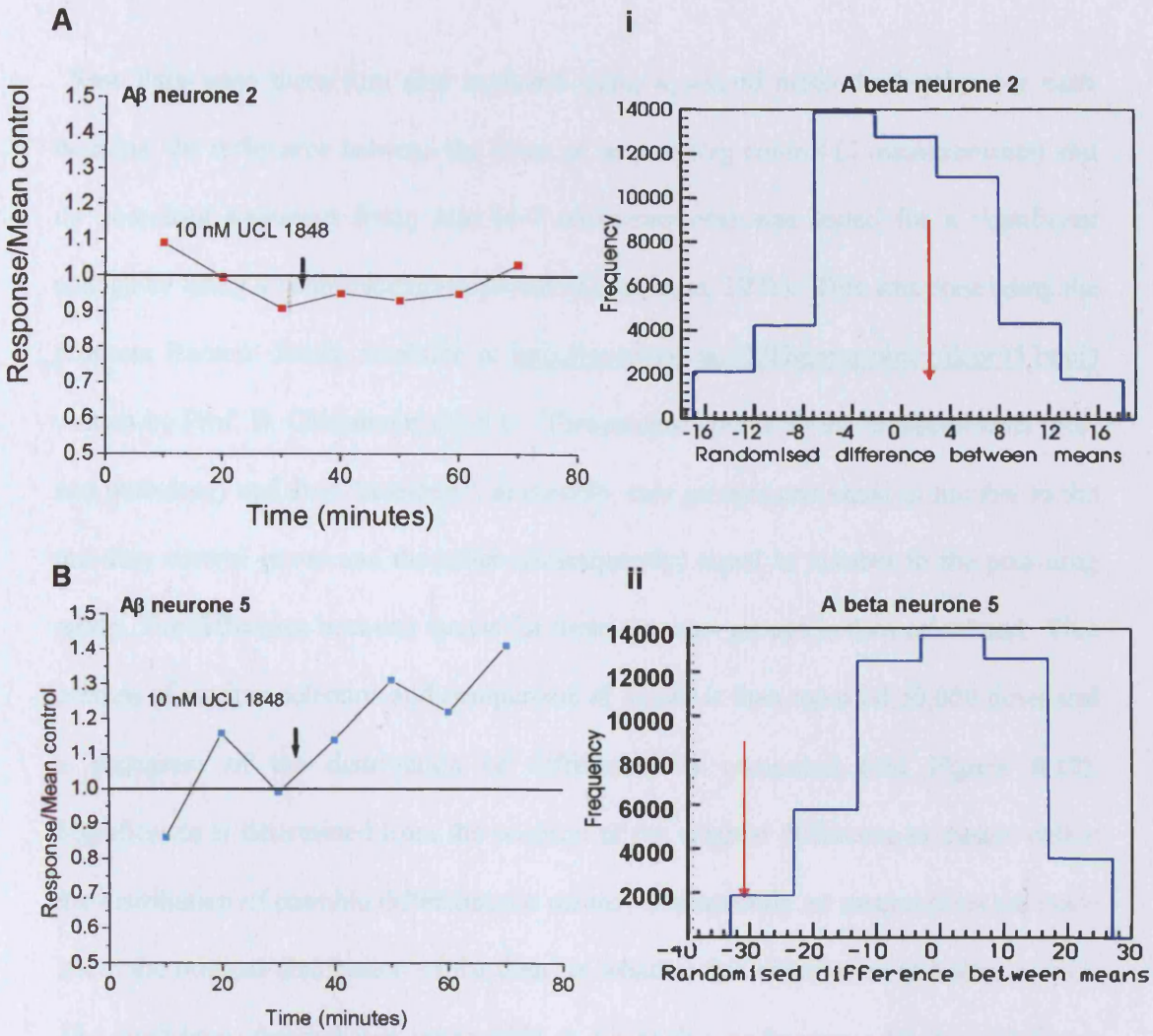

Figure 6.12 Raw data from two different A_β neurones along with histograms generated using the Rantest program to calculate the significance of the differences in means of data generated pre- and post- the drug application (in this case following the application of 10 nM UCL 1848). **A** and **B** show the number of action potentials fired relative to the mean control for that cell. UCL 1848 does not appear to have any effect the number of action potentials fired in cell shown in **A**. However, the cell in **B** appears to show an increase in firing. **i** and **ii** show the corresponding histograms (for **A** and **B** respectively) with the distribution of the possible differences in means (following 50,000 randomisations). The red arrow shows the difference in means of the original data. Where the randomised difference between means is zero there is no effect of the drug. The Rantest histograms confirm that "**A beta neurone 2**" firing was not significantly affected while "**A beta neurone 5**" showed a highly significant change in response to UCL 1848.

Raw data were there fore also analysed using a second method whereby, for each neurone, the difference between the mean of its pre-drug control (3 measurements) and its post-drug treatment firing rate (4-7 measurements) was tested for a significant change by using a randomisation approach (Colquhoun, 1971). This was done using the program Rantest (freely available at http://www.ucl.ac.uk/Pharmacology/dcpr95.html) written by Prof. D. Colquhoun at UCL. This program pools all the measurements (pre- and post-drug) and then "reselects", at random, two groups; one equal in number to the pre-drug control group and the other (consequently) equal in number to the post-drug group. The difference between means for these two new groups is then calculated. This process of random selection and comparison of means is then repeated 50,000 times and a histogram of the distribution of differences is computed (see **Figure 6.12**). Significance is determined from the position of the original difference in means within the distribution of possible differences in means; consequently no assumptions are made about the original distribution of the data i.e. whether this distribution is normal or not. The confidence interval was set to 95% to establish significance. All the significant changes referred to in the proceeding sections were calculated using Rantest results.

6.2.6.3 Effects of drugs that alter SK channel activity

UCL 1848

To examine possible SK channel involvement in sensory nerve transmission, the first set of experiments was done by applying UCL 1848 at two concentrations, first 10 nM and then 50 nM. Such low concentrations of UCL 1848 have been shown to block neuronal SK3 channels *in vitro* (Hosseini *et al.*, 2001). The effects of UCL 1848 on the responses of a single lamina V neurone were determined by stimulating the rat hind-paw both electrically and using a set of natural stimuli. The effects of UCL 1848 on responses to electrical stimulation in the periphery, can be seen in **Figure 6.13**. In the simplest model, the application of SK channel blockers should increase the excitability of the afferent neurone and thus increase the input to the lamina V neurone and the results in **Figure 6.13** suggest that this is indeed the case. The averaged results from five to six neurones show that the overall trend is for increased excitability of the lamina V neurone in response to UCL 1848 application (**Figure 6.13 A** and **B**). This can be seen more clearly in recordings from individual dorsal horn neurones (**Figure 6.13 a**, **b**, **c** and **d**). The effects of UCL 1848 proved to be rapid, occurring within ~10 mins of application, and the increases seen in neurone firing were dose-dependent. There was a significant increase in the input for 3 out of 5 lamina V neurones from A_β fibres, 2 out of 6 neurones show a significantly increased input from A_δ fibres, and 4 out of 6 from C-fibres. There is also an increase in the postdischarge of 3 out of 6 neurones. In contrast to the cells that showed increased excitability, only one cell showed reduced input from C-fibres and another from A_δ fibres. The remaining cells showed no significant change in response to UCL 1848 application.

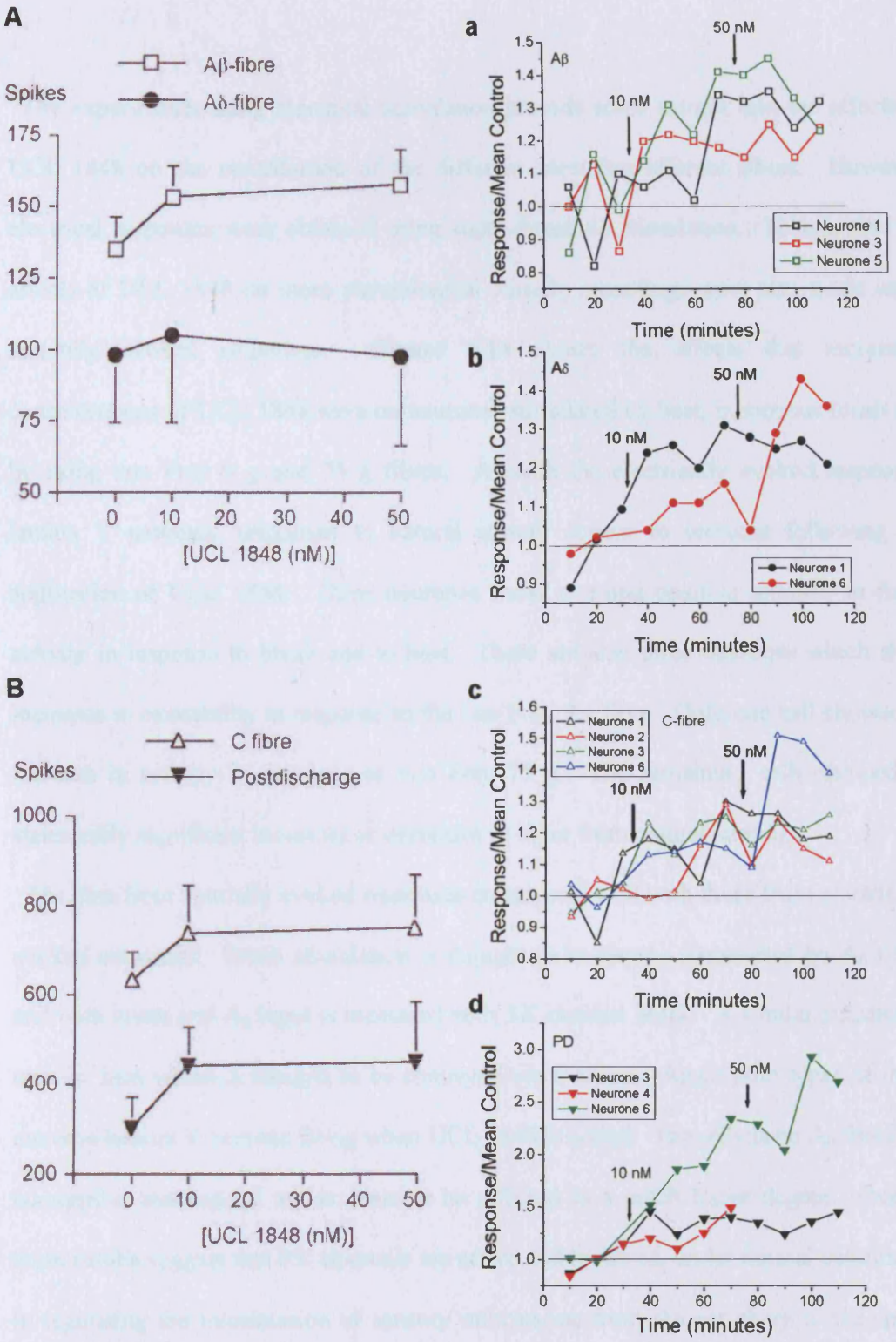

Figure 6.13 UCL 1848 increases spinal cord input from electrically evoked stimuli recorded as the firing of a lamina V neurone. **A** and **B** show the averaged responses from 6 different neurones, except for A_β which shows the results from 5 neurones. **a-d** show statistically significant effects on individual neurones (data has been normalised to the control responses). Overall there is an increase in electrical excitability of the lamina V neurones in response to increasing concentrations of UCL 1848. This is true for A_β, A_δ and C-fibre input.

The experiments using electrical stimulation provide some insight into the effects of UCL 1848 on the contribution of the different incoming afferent fibres. However, electrical responses were obtained using supra-threshold stimulation. To examine the effects of UCL 1848 on more physiological stimuli, recordings were also made using naturally evoked responses. **Figure 6.14** shows the effects that increasing concentrations of UCL 1848 have on neurones stimulated by heat, innocuous brush and by using von Frey 9 g and 75 g fibres. As with the electrically evoked responses, lamina V neuronal responses to natural stimuli appear to increase following the application of UCL 1848. Three neurones show a strong positive increase in firing activity in response to brush and to heat. There are also three neurones which show increases in excitability in response to the von Frey 9 g fibre. Only one cell showed an increase in activity in response to von Frey 75 g. The remaining cells showed no statistically significant increases or decreases in input from natural stimuli.

The data from naturally evoked responses correspond well with those from electrically evoked responses. Brush stimulation is thought to be largely transmitted by A_β fibres and both brush and A_β input is increased with SK channel block. A similar situation is true for heat which is thought to be conveyed via C-fibres. Again both types of input increase lamina V neurone firing when UCL 1848 is added. The effects on A_δ fibre and nociceptive mechanical inputs seem to be affected to a much lesser degree. Overall these results suggest that SK channels are active and involved, under normal conditions, in regulating the transmission of sensory information from the periphery to the spinal cord.

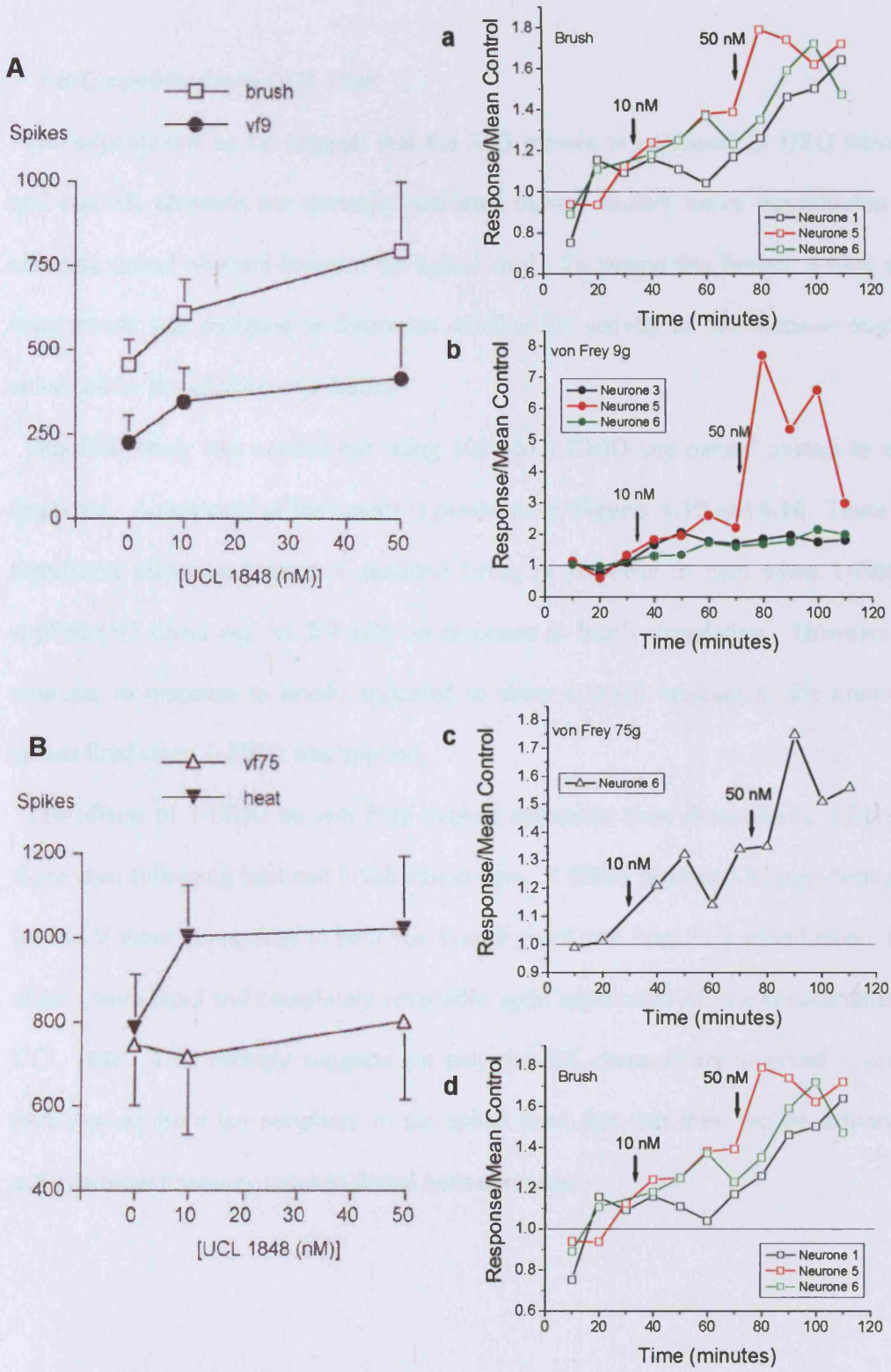

Figure 6.14 UCL 1848 increases spinal input from most naturally evoked responses. **A** and **B** show the averaged responses from 6 different neurones. **a-d** show statistically significant effects on individual neurones (data has been normalised to the control responses). Overall there is an increase in the number of action potentials fired by lamina V neurones in response to increasing concentrations of UCL 1848. This is true for several sensory modalities including heat, brush and von Frey 9 g, although with von Frey 75 g only one neurone showed a significant increase.

1- EBIO combined with UCL 1848

The experiments so far suggest that the SK3 protein is expressed in DRG terminals and that SK channels are normally activated during sensory nerve transmission thus affecting dorsal neurone firing in the spinal cord. To pursue this further, a final set of experiments was designed to determine whether the activity of SK channels might be enhanced by the addition of 1-EBIO.

This final study was carried out using 300 μM 1-EBIO and natural stimuli to evoke responses. A summary of the results is presented in **Figures 6.15** and **6.16**. There is no significant effect on lamina V neurone firing in response to heat when 1-EBIO is applied (3/3 cells) nor for 2/3 cells in response to brush stimulation. However, one neurone, in response to brush, appeared to show a small increase in the number of spikes fired when 1-EBIO was applied.

The effects of 1-EBIO on von Frey evoked responses were dramatically different to those seen following heat and brush stimulation. 1-EBIO produced a large decrease in lamina V input in response to both von Frey 9 g and von Frey 75 g stimulation. These effects were rapid and completely reversible upon application of low concentrations of UCL 1848. This strongly suggests not only that SK channels are involved in sensory transmission from the periphery to the spinal cord, but that they can be activated in order to reduce sensory input to dorsal horn neurones.

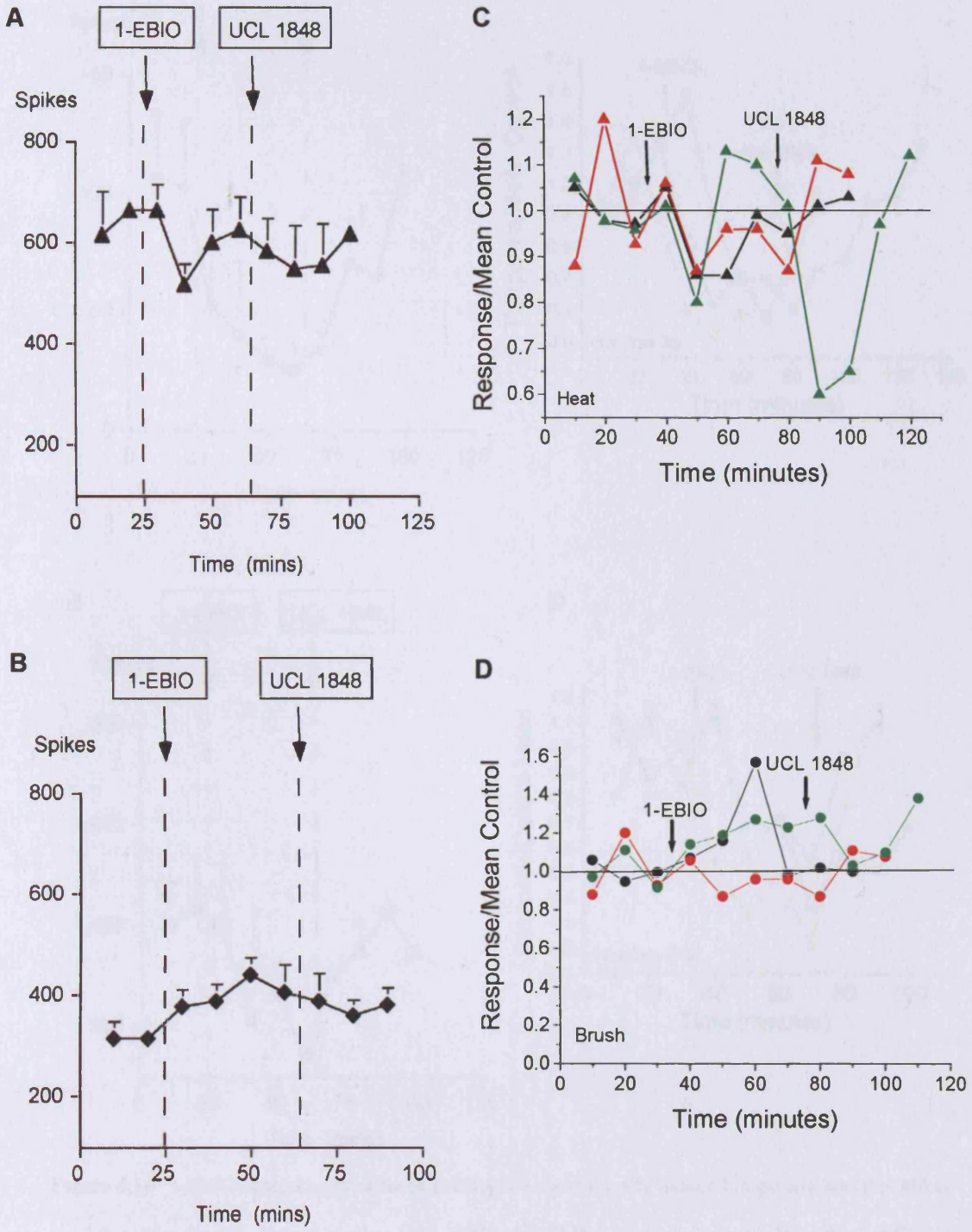

Figure 6.15 1-EBIO and UCL 1848 have very little effect on responses evoked using heat and innocuous brush. **A** and **B**, averaged responses from three different neurones stimulated using heat or brush respectively. **C** and **D** show the effects on individual lamina V neurones responses seen as a result of heat or brush stimulation respectively. There was no significant effect of 1-EBIO on heat evoked responses and only one out of three lamina V cells (●) responding to brush showed a possible change, an increase.

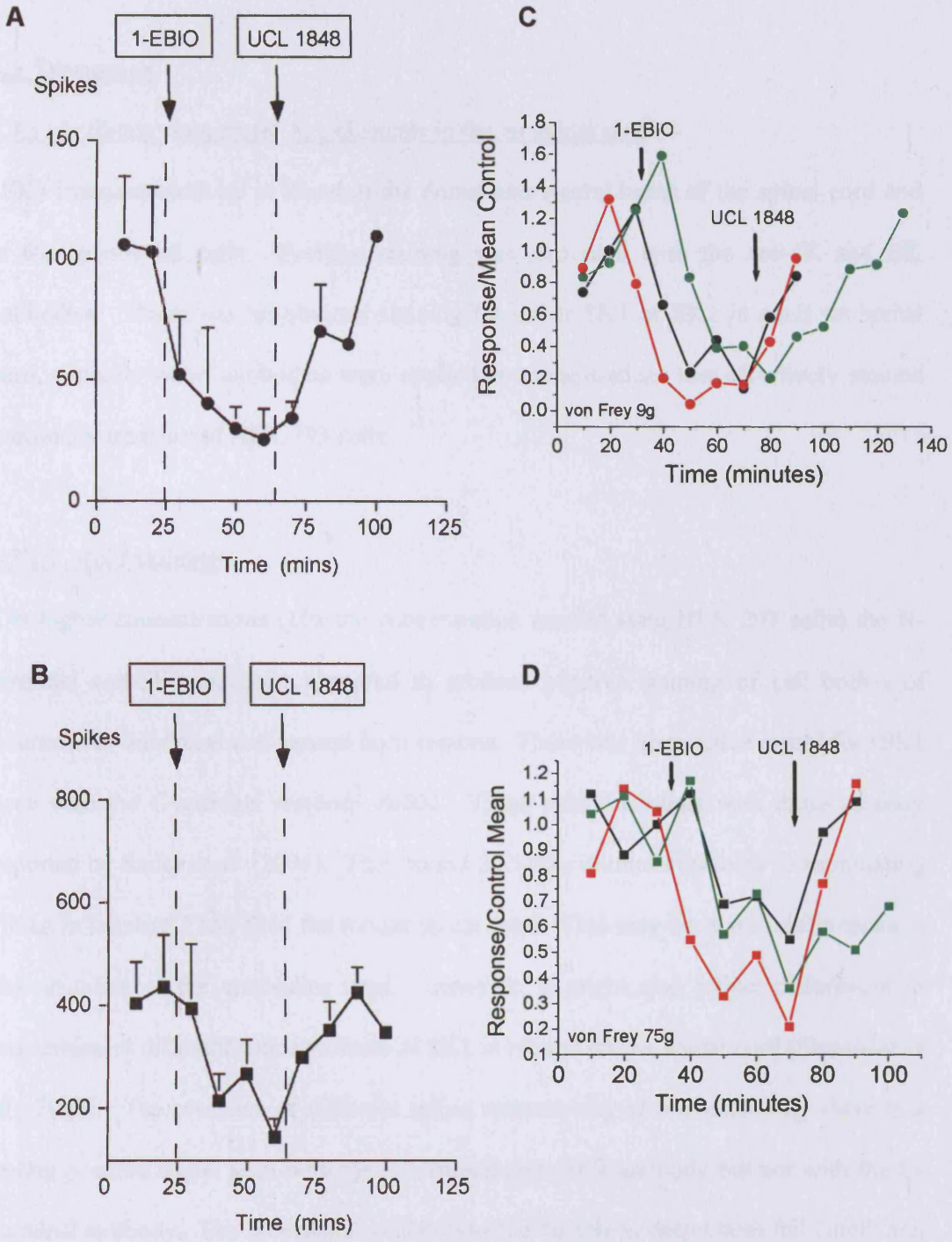

Figure 6.16 1-EBIO dramatically reduces nociceptive mechanically induced responses and this effect is inhibited by the SK channel blocker UCL 1848. **A** and **B**, averaged responses from three different neurones stimulated using von Frey 9 g and von Frey 75 g respectively. **C** and **D**, effects on individual lamina V neurones responses seen as a result of von Frey 9 g and von Frey 75 g stimulation respectively. The application of 300 μM 1-EBIO causes a massive inhibition of lamina V neurone firing in response to noxious mechanical stimulation. This effect is clearly reversed by 10 nM UCL 1848. These data indicate that SK channels involved in sensory transmission can be activated further to inhibit spinal cord input and that these effects can then be selectively blocked by UCL 1848.

6.3 Discussion

6.3.1 Antibody staining for K_{Ca} channels in the rat spinal cord

SK3 immunoreactivity is found in the dorsal and ventral horns of the spinal cord and in the ependymal cells. Positive staining was also seen with the anti-IK and BK antibodies. There was no obvious staining for either SK1 or SK2 in adult rat spinal cord, certainly when antibodies were applied at concentrations that effectively stained transiently transfected HEK 293 cells.

6.3.1.1 rSK1 staining

At higher concentrations (10x the concentration used to stain HEK 293 cells) the N-terminal anti-SK1 antibody appeared to produce positive staining of cell bodies of neurones in the dorsal and ventral horn regions. There was no positive signal for rSK1 seen with the C-terminal antibody rb200. These results contrast with those recently reported by Sailer *et al.* (2004). They found SK1-like immunoreactivity in terminating fibres in laminae I and II of the mouse spinal cord. This may be due to differences in the affinities of the antibodies used. However, it might also reflect differences in expression of different splice variants of SK1 in rat and mouse spinal cord (Shmukler *et al.*, 2001). The presence of different splice variants may also explain why there is a strong positive signal seen with the N-terminal anti-rSK1 antibody but not with the C-terminal antibody. The N-terminal antibody would be able to detect both full length and truncated forms of rSK1. The C-terminal antibody, however, would not be able to detect the shorter isoforms. Thus, if high levels of the truncated rSK1 were expressed they would be detected by the N-terminal but not the C-terminal antibodies.

6.3.1.2 rSK2 staining

Higher concentrations of the anti-SK2 antibody (50x) also made it possible to detect SK2 immunoreactivity in the rat spinal cord, although given the high concentrations used, these results must be interpreted cautiously. The few regions staining positively are largely in agreement with the results of Sailer *et al.* (2004). Thus there appears to be a signal for SK2 in the region of lamina I and large diameter neurones (possibly motorneurones) in the ventral horn. Sailer and colleagues saw staining in both those regions but, in addition, found SK2 immunoreactivity in neuronal fibres branching out into the white matter. This was not evident in my results.

6.3.1.3 IK and BK staining

There was a strong positive signal with the anti-IK channel antibody. This staining was localised within the cell bodies of spinal neurones throughout the grey matter. There was also positive staining seen within the ependymal cells. The role of IK channels has been well documented in various epithelia in controlling secretion (Jensen *et al.*, 2001). The ependyma likely regulates the transport of ions, small molecules and water between the cerebrospinal fluid and neuronal tissue (Bruni, 1998) so it is probable that IK channels have a similar role in controlling secretion here.

BK channels are widely expressed in DRG cells, motorneurones and other types of nerve cell (Simonneau *et al*, 1987; McLarnon, 1995; Safronov & Vogel, 1998). So it is not surprising to see bright positive staining for this channel protein in spinal cord slices.

6.3.1.4 SK3 staining

The pattern of staining seen with the SK3 antibody M75 was reproduced by the Chemicon anti-SK3 antibody (not shown). Sailer *et al.* (2004) used a third antibody which produced positive staining in the same spinal cord regions. Taken together, the results suggest that it is highly likely that SK3 immunoreactivity seen in the current report and in previous work corresponds to the presence of the SK3 channel protein.

The SK3 antibody staining in the ventral horn of the spinal cord probably represents staining of alpha motorneurones. This staining is similar to that of SK3 in SCG neurones in that both the cell body and processes stain positively (Hosseini *et al.*, 2001). Like SCGs, motorneurones in the cat and turtle are known to exhibit an apamin-sensitive AHP (Zhang & Krnjevic, 1987; Hounsgaard *et al.*, 1988). So, SK3 provides a candidate for the channel underlying this apamin-sensitive hyperpolarisation. However, Safronov & Vogel (1996) have reported K_{Na} currents which could also play a role in AHP generation in rat motorneurones. The relative contributions of these currents requires further study.

SK3 antibody staining was also pronounced in the ependymal cells of the central canal, which is interesting as recent work on the human lens has shown that SK channels may well be important in other epithelial cell types (Rhodes *et al.*, 2003).

With respect to sensory nerve transmission, the most pertinent pattern of staining was that seen for SK3 in the dorsal horn of the spinal cord. There was a clear and bright positive signal for the SK3 antibody in the superficial laminae. When co-stained with VR1, which is known to be expressed in sensory fibres that terminate in lamina I and lamina II_i (Tominaga *et al.*, 1998; Guo *et al.*, 1999), it is possible to see that SK3 immunoreactivity has a similar pattern of termination with some of the SK3 signal co-localising with VR1. However, the SK3 antibody signal is also seen in regions which

are largely VR1-negative. Overall, SK3 antibody staining is seen in lamina I, II (outer and inner regions) and it extends beyond the VR1 staining into regions which probably form part of lamina III. This pattern of localisation strongly suggests that SK3 is expressed in both C-fibre cells (which also express the VR1 receptor) and A-fibre cells. This localisation is thus consistent with the pattern of staining seen in cultured DRG neurones. In these co-staining with the C-fibre cell marker peripherin made it possible to see that both peripherin-positive and peripherin-negative cells expressing the SK3 protein. There is also a proportion of cells that do not express SK3 and again these are of both the peripherin-positive and peripherin-negative type. So it appears that SK3 is expressed in different DRG cell types and is presumably transported from the cell bodies to the central terminals in the spinal cord.

6.3.2 *In vivo* recording from the rat spinal cord

Functional evidence for SK channel activity in sensory transmission was obtained using *in vivo* recordings from dorsal horn neurones of adult rats. There was considerable variability seen in the responses to pharmacological treatment. This is probably not surprising when one considers the potential number of inputs a single lamina V neurone receives from the periphery and the extent to which different types of incoming fibres may affect the firing of such a spinal neurone. It is also important to note that the concentrations of the drugs applied in these studies were remarkably low for an *in vivo* preparation (chosen in order to maintain specificity for SK channels). The finding that some neurones were largely unaffected by drug application could thus reflect poor diffusion through the tissue. Higher concentrations of drug may have provided greater effects.

6.3.2.1 Increasing concentrations of UCL 1848 increase firing in spinal neurones

Effects at both 10 nM and 50 nM UCL 1848 were observed on electrically and naturally evoked responses of a single lamina V neurone. At such low concentrations, UCL 1848 is expected to be highly selective for SK channels. At both doses, UCL 1848 application increased input to the lamina V neurone, an effect which usually more pronounced with the higher concentration of 50 nM. Such an increase in excitability is most likely to be due to the block of SK3 channels and possibly also SK2 channels in the terminals of primary afferents the result of which is an increased input to spinal neurones. There are several aspects of my work that support such a role for SK channels in the presynaptic terminals. The first is the SK3 staining in the dorsal horn which corresponds well with the termination pattern of incoming afferent fibres. The second comes from the *in vivo* recordings. If the effects of UCL 1848 had been on postsynaptic SK channels expressed in the lamina V neurone, one would expect all types of peripheral nerve stimulation to increase neuronal firing. However, the effects on some sensory modalities are greater than on others. For example, only one neurone showed significant input in response to von Frey 75 g stimulation. Again, the staining experiments, which showed that only a subset of DRG neurones appear to be SK3-positive, support the idea that certain types of peripheral stimulation may show increased sensory input into the spinal cord in response to UCL 1848, whilst others may not.

There are now several well-documented examples of SK3 expression in nerve terminals in other types of neurone (Obermair *et al.*, 2001; Roncarati *et al.*, 2001). For example, recent work on central neurones has demonstrated the presence of the SK3 channel protein in the presynaptic glutaminergic terminals of hippocampal neurones (Obermair *et al.*, 2001). Given that BK channels, with a similar localisation, have been

shown under certain conditions to contribute to the modulation of glutamate release from such terminals (Hu *et al.*, 2001), this has led to the suggestion that presynaptic SK3 channels may serve a similar role (Obermair *et al.*, 2001).

6.3.2.2 Activation of SK channels by 1-EBIO is reversed by UCL 1848

When 1-EBIO was applied in an attempt to activate SK channels, there was substantially reduced sensory input in response to von Frey 9 g and 75 g evoked stimuli, though little or no effect on brush or heat. This attenuation of excitability appears to be attributable to SK channel activation, as it is effectively reversed by 10 nM UCL 1848. An interesting point to note is that the firing rate of one lamina V neurone may have increased in response to brush stimulation when 1-EBIO was applied. More work is needed to see how frequently this effect occurs but it may perhaps be explained by the presence of IK channels in certain spinal neurones. 1-EBIO is a non-selective compound which acts on a number of channels, including SK and IK channels to enhance their activity (Devor *et al.*, 1996; Pedersen *et al.*, 1999; Syme *et al.*, 2000; Pederzani *et al.*, 2001). Spinal neurones can form a complex network of inhibitory and excitatory synapses converging onto single cells. It is known, for example, that A_β fibres synapse onto inhibitory interneurones which in turn affect the firing properties of wide dynamic range neurones in the dorsal horn (Millan, 1999). It is quite possible that as well as input from the periphery, certain lamina V neurones receive information from IK-expressing spinal neurones. If so, 1-EBIO activation might have the effect of increasing cell excitability in the spinal cord. However, the present experiments do not allow this to be settled.

One exciting aspect of the work with 1-EBIO is the possiblity for identification of novel analgesic drugs. Enhancing SK channel activity has the effect of reducing

sensory input and this may be utilised to design new drugs that may reduce the transmission of painful stimuli. Two possible conditions for treatment with SK channel openers would include mechanical allodynia (the perception of pain in response to an innocuous stimulus) which can arise by nerve damage resulting in cross-excitation of C-fibres by A_β fibres, and hyperalgesia (increased sensitivity to nociceptive input). Both of these conditions are most commonly linked with chronic pain states such as those arising from nerve injury (neuropathy).

Musso and colleagues (2003a; 2003b) have already provided evidence showing that compounds which are structurally very similar to 1-EBIO have muscle relaxant, antiinflammatory, and analgesic properties. One particular compound, (E)-2-(4,6-difluoro-1-indanylidene) acetamide (GW275919X), developed at GlaxoWellcome, has recently been described as a potent enhancer of SK and IK channel activity (Cryan *et al.*, 2003). Similarly, the muscle relaxant and analgesic chlorzoxazone, which is thought to be a centrally acting agent, has also been shown to enhance SK channel activation (Syme *et al.*, 2000; Cao *et al.*, 2001). Although much work needs to be done on determining the exact mechanism of action of these 1-EBIO-like drugs, the work described here, and elsewhere by others, points to a role for drugs targeting SK channels in the development of novel analgesic agents.

In summary, the work in this chapter demonstrates that SK3 immunoreactivity can be detected in the lumbar region of the spinal cord, apparently in the terminals of dorsal root afferents. Here SK channels appear to be involved in the transmission of sensory information and activation of these SK channels can reduce sensory input to the spinal cord.

Chapter 7

Discussion

In this chapter I discuss some of the main findings of my thesis in a wider context and examine possible future directions for the work.

At the outset of this PhD little was known about the functional properties of the rat rSK1 protein and data about the co-assembly of SK channel subunits was also limited. Further, there was little firm evidence to suggest that any of these SK channels played a role in sensory neurones with the existing reports being both limited and largely conflicting. The experimental findings presented in this thesis make advances in each of these areas.

7.1 SK channel subunits and their interactions

Several points of interest arise from the experiments with SK channels expressed in cell lines. Firstly, given the different subcellular distributions of the subunit proteins, it would appear that there are differences in subunit trafficking. Even SK2 and SK3, which both reach the cell surface and form functional channels, appear to be transported differently within the cell because these two proteins appear (predominantly) in distinct compartments. Furthermore, though rSK1 has a pattern of staining similar to rSK2, it does not form functional channels at the cell surface suggesting that the rSK1 protein remains trapped intracellularly. Experiments to address this issue specifically, possibly by using surface biotinylation stategies, would be an interesting future direction.

Some progress towards understanding these differences in trafficking has been made by D'hoedt *et al.*, (2004) who describe experiments using rSK1, hSK1 and rSK2 chimeras. Based on their findings they suggest that one reason for the lack of functional rSK1 channels is that the subunit protein is unable to form assemblies with itself. Since assembly is intimately associated with trafficking, this would be likely to contribute substantially to the differences seen in SK protein distributions. Further, D'hoedt and colleagues highlight the carboxyl terminal region as one that may be responsible for this "failure" of rSK1 to form functional channels. Although this is clearly an interesting suggestion, there is still a great deal of work needed to understand, at the molecular level, how SK channel proteins assemble and/or are transported in the cell. One noteworthy observation from the work presented in **Chapter 3** is that rSK1 interacts with rSK2 resulting in a complex that appears to be transported to the cell surface, possibly more efficiently than rSK2 alone. However, when rSK1 (or indeed hSK1) is co-expressed with rSK3, the proteins appear to remain trapped inside the cell. These results demonstrate that no single subunit dominates the trafficking.

Given the lack of functional expression and the apparently "silent" nature of rSK1, this protein seems very unlikely to underlie the neuronal sAHP, as has been suggested in the past (Vergara *et al.*, 1998; Bond *et al.*, 1999; Bowden *et al.*, 2001). Work recently reported by Bond *et al.* (2004) provide more conclusive evidence for this (see section **7.3**).

Finally, although much of the focus surrounding rSK1 has been to suggest that it co-assembles with SK2 (e.g Ishii *et al.*, 1997b), it is possible that it also acts to regulate rSK3 expression levels. So it may be that rSK1 acts in a way that is similar to certain K_V channel β subunits which regulate the levels of functional protein reaching the cell surface membrane (Martens *et al.*, 1999).

The co-expression experiments presented in this thesis demonstrate that heteromeric assembly could be a means for increased functional diversity of SK channels may arise. However, it is not yet known whether such assemblies of SK channel subunits occurs *in vivo*. Sailer and colleagues (2002) report that SK channel subunits do not appear to co-assemble in rat brain on the basis of co-immunoprecipitation experiments using synaptosomes. However, this does not exclude the possibility of rSK1 and rSK3 co-assembly as one would not necessarily expect these complexes to be found in plasma membranes. Furthermore, it remains possible that SK channel heteromers may form in peripheral tissues.

7.2 SK/IK channel expression in DRGs

7.2.1 Expression of SK/IK mRNA splice variants in DRGs

mRNA for SK1, SK2, SK3 and IK channels is present in DRG tissue. The abundance of exon 7 splice variants of rSK1 was examined (**Chapter 5**) and in general, the levels of transcripts containing exon 7 matched the "all variants" levels of SK1. This suggests that most SK1 transcripts will code for channels containing a calmodulin binding region that is intact and should therefore be functional.

Since this work was completed, there have also been reports of splice variants for SK3; SK3-1B and SK3-1C that are thought to act as dominant negatives, while hSK3-ex4 forms a channel that is insensitive to the potent SK blockers apamin and scyllatoxin (Tomita *et al.*, 2003; Kolski-Adreaco *et al.*, 2004; Wittekindt *et al.*, 2004). From the current work it is not possible to determine the extent to which any of these splice variants might be important in DRG neurones. This could be another interesting line to pursue.

7.2.2 Developmental regulation of SK/IK channels

There are many examples of regulated K^+ channel expression which reflect important developmental changes (Yool *et al.*, 1988; Ribera & Spitzer, 1992; Wang *et al.*, 1996). Such developmental changes have also been described for SK channels in the retina, where levels of SK channel mRNA increase, and in Purkinje neurones where mRNA and protein levels decrease (Klöcker *et al.*, 2001; Cingolani *et al.*, 2002). However, recent work suggests that the functional significance of these changes in the Purkinje neurons may be less than was first thought (Womack & Khodakhah, 2003).

Age-dependent changes in SK channel expression in DRGs were examined using qPCR and antibody staining techniques (**Chapter 5**). Both the message for SK/IK channels and the levels of SK3 antibody staining increase with age (in whole rat DRG tissues and DRG neurones respectively). This suggests that SK channel-mediated effects may increase with age in rats. One of the major differences in the transmission of sensory information between neonates and adults lies in the response to nociceptive stimuli (Wolf, 1999; Fitzgerald & Jennings, 1999). The cutaneous withdrawal reflex is particularly pronounced in the newborn rat but decreases with age until adults only show withdrawal in response to a noxious stimulus (Fitzgerald & Jennings, 1999). A large number of changes occur in sensory pathways during this period. The net result is that the activity of sensory neurones involved in the withdrawal reflex decreases. The age-dependent increase in levels of SK3 may play a part in this. Interestingly, the *in vivo* experiments described in **Chapter 6** show that UCL 1848, used to block SK channels, increases spinal neurone firing in response to innocuous brush and von Frey 9 stimulation. This indicates that SK channels are normally active in sensory neurones to reduce activity in response to innocuous stimuli. Thus, when SK channels are blocked we may have a situation similar to that in the neonate.

7.3 The diversity of AHPs in DRG and nodose ganglion neurones

AHPs in sensory neurones vary greatly in their kinetics. The DRG AHPs described in this thesis closely match previous reports with respect to AHP_{80} values and decay time constants (Waddell & Lawson, 1990; Lawson *et al.*, 1996; Villière & McLachlan, 1996). Neither AHP_{80} values nor decay time constants of different durations appear to associate with neurones of a particular fibre type *i.e.* both fast and slow AHPs are seen in A- and C-type neurones. Interestingly however, those cells with AHPs that had two K^+ components could be grouped on the basis of the separation between the two different components. While these groups do not correspond to A- or C-type neurones, it is still possible that they may reflect certain phenotypes. A similar situation has been suggested for action potential inflections, which are believed to correspond quite closely to nociceptors (Traub & Mendell, 1988; Ritter & Mendell, 1992).

7.3.1 Which channel(s) underlie the mAHPs in DRG neurons?

One of the most surprising outcomes of the current work was that, despite strong positive SK3 staining in DRG cell bodies, there was little indication that SK channels play a role in mAHP generation in these cells. Most of the medium duration AHPs in DRG cells were not only insensitive to UCL 1848 but also to Cd^{2+} indicating that the underlying channels were not Ca^{2+}-dependent. In addition, there was no block seen with TEA or 4-AP which rules out a number of voltage-gated K^+ channels. One possibility is that K_{Na} channels, which have been shown to underlie AHPs in neocortical neurones, may be involved (Franceschetti *et al.*, 2003). However, whilst K_{Na} currents have been detected in DRG cells (Bischoff *et al.*, 1998), their role in AHPs has not yet been investigated. In the absence of selective blockers, the involvement of K_{Na} channels could be explored further using bath solutions with Li^+ substituted for Na^+

(Franceschetti *et al.*, 2003). However, the observation of multiple components in the AHP decay phase and partial cadmium sensitivity, suggests that there may be multiple channel contributions to these DRG hyperpolarisations.

7.3.2 Which channel(s) underlie the sAHPs in DRG and nodose neurones?

There were at least three types of sAHP detected in DRG neurones:

1. Those that were insensitive to Cd^{2+}, histamine and the K^+ channel blockers used in this study; these were only seen in A-type cells.
2. Those that were insensitive to UCL 1848 and TEA but blocked by Cd^{2+} and histamine.
3. Finally, those that were insensitive to UCL 1848 but blocked by low concentrations of TEA (5 mM) and histamine.

The sAHPs described in the current study (in DRG and nodose neurones) along with the results of the rSK1 experiments support previous work which suggests that SK channels do not make any contribution to this AHP type (Vogalis *et al.*, 2003). Recently, two different groups have provided more conclusive evidence for this. Bond *et al.* (2004) have shown that in hippocampal neurones from SK channel "knock-out" mice the sAHP is unaffected, although SK2 knock-outs no longer generate mAHPs. Similarly, Villalobos and colleagues (2004) used a dominant negative strategy to assess whether SK channels were involved in the sAHP in cortical neurones. They too found that there was a pronounced inhibition of the mAHP without any obvious effect on the sAHP. So in central neurones, at least, there appears to be no involvement of SK channels in sAHP generation.

One possibility for the first type of DRG sAHP (found in A-type cells) is that it is due to an electrogenic pump. To see whether the A-type sAHP is due to the Na^+/K^+ ATPase

activity, the cardioactive steroid ouabain could be used to inhibit the pump and observe whether there is any corresponding inhibition of the AHP.

The second type of sAHP recorded from C-type cells, which was blocked by Cd^{2+} and histamine but not by the SK blocker UCL 1848, resembled the sAHPs described in hippocampal and nodose neurones (Vogalis *et al.*, 2003). There are few characteristics to indicate its likely molecular correlate, but perhaps the apparently weak voltage dependence is a useful starting point. This observation could implicate either "two-pore" domain potassium channels or K_{ir} channels. However, other possibilities remain open because voltage-dependent channels interacting with beta subunits can become voltage independent over the physiological range (Schroeder *et al.*, 2000).

The third type of sAHP, also present in C-type neurones, was sensitive to block by relatively low concentrations of TEA. Sensitivity to TEA appears to be dictated (primarily) by a single amino acid in the pore of the channel (MacKinnon & Yellen, 1990). On this basis possible alpha subunit proteins include KCNA1,6, KCNB1,2, KCNC1,2,3,4, KCNG3, KCNJ1,3,10,13 and KCNQ2. Of these candidates, two observations support the possibility that it might be an M-channel (KCNQ2 containing). Firstly, these channels, are composed of KCNQ2 and KCNQ3 subunits and can be blocked by low (mM) concentrations of TEA and also by neurotransmitters such as histamine. Secondly, certain KCNQ2 splice variants show very slow activation and deactivation kinetics which could result in the generation of a sAHP though this has not been described before. There are a number of selective blockers (e.g. linopirdine and XE991) and openers (e.g. retigabine) which could, in future experiments, be used to determine the involvement of these channels (Aiken *et al.*, 1995; Wang *et al.*, 1998; Main *et al.*, 2000; Tatulian *et al.*, 2001).

7.3.3 SK channels in DRG neuronal cell bodies

As mentioned already, it is intriguing, given the pattern of staining seen with the anti-SK3 antibodies, that there is no major role of SK channels in AHP generation. It is possible that SK channels in DRG cell bodies might be present in the cell membrane but are not functional and/or they may have important roles other than regulation of excitability in the cell body. SK channel opening regulates Ca^{2+} entry and is thus thought to affect processes such as gene transcription (Faber & Sah, 2003). One specific example where SK channels are thought to be involved in this way is in learning and memory. For example, studies using mouse hippocampi have shown that apamin induces the expression of c-fos and c-jun genes, which are thought to be initial markers for memory formation (Heurteaux *et al.*, 1993).

However, tempting as it is to suggest from the pattern of staining that the localisation of SK3 is at the plasma membrane of cell bodies and that the channels are somehow activated in specific circumstances, it must be remembered that the resolution of confocal microscopy is not sufficient to determine whether this is so. Thus it may be that the channel proteins are trapped in organelles that lie just below the cell surface membrane before being transported to peripheral terminals. Such a situation appears to occur in PC12 cells (an adrenal pheochromocytoma cell line). Staining with the anti-SK3 antibodies produces a bright punctate staining pattern which extends around the circumference of the cells (data not included), however, there is little or no current detected in these cells (unpublished observations with D.C.H. Benton, see also Kolski-Andreaco *et al.*, 2004).

7.4 SK/IK expression in rat spinal cord and putative role in sensory nerve terminals

The anti-SK3 antibody produced the most prominent staining in adult rat spinal cord. Of particular interest was the staining seen in the region of incoming DRG afferent terminals, which, in conjunction with *in vivo* recordings, suggests that SK channels could be important in controlling sensory transmission from the periphery by regulating neurotransmitter release. A similar functional role has been proposed for BK and SK channels in terminals of hippocampal neurones (Hu *et al.*, 2001; Obermair *et al.*, 2003). While the patterns of staining in **Chapter 6** strongly suggest that SK3 is predominantly expressed in DRG afferents rather than in spinal neurones, it is important to rule out more definitively the possibility that the SK channels involved in sensory transmission are present in spinal neurones. One way this could be done is by performing dorsal rhizotomy and staining spinal cord slices to observe whether there is any change in the pattern of SK3 immunoreactivity. Additionally, the presence of functional SK channels in spinal neurones could be explored by making electrophysiological recordings from spinal cord slices and examining the effects of SK-specific blockers such as UCL 1848 and apamin, and openers such as 1-EBIO.

If SK channels were found, unambiguously, to work by inhibiting neurotransmitter release it suggests that other important proteins in the control of sensory transmission may, like SK3, have a large influence at central terminals but show little activity in the cell body. This raises a further interesting question about SK channels; do they have a role to play at peripheral terminals that is also not evident from the work carried out to date? Again, this is an area where further experiments might be useful.

7.5 Do SK channels make suitable targets for analgesic drug development?

Initially the idea of using SK channel activation for analgesia does not look promising. This is because SK channels are expressed in a wide variety of tissues. In addition, drugs which activate these channels including 1-EBIO, chlorzoxazone and the GlaxoWellcome compound GW275919X, do not discriminate well between the various SK/IK subtypes (Devor *et al.*, 1996; Syme *et al.*, 2000; Cao *et al.*, 2001; Musso *et al.*, 2003a; 2003b). It would thus be desirable to develop more selective compounds. However, even if more selective drugs were available, so that one could target SK3 exclusively, the wide expression pattern of this channel suggests at first sight that it is an unpromising target. Several observations indicate that things are not as bleak as they might appear. First, many drugs, for example, local anaesthetics, can be systemically administered (e.g. to treat dysrhythmia), even when their target is found in many tissues: clearly multiple tissue expression does not exclude the possibility of drugs targeting proteins in a particular tissue for a specific condition. Indeed, Passmore and colleagues (2003) were able to demonstrate a therapeutic potential for other K^+ (KNCQ) channel openers as novel analgesics, even though KCNQ channels occur in a number of neuronal tissues. So, SK channel openers might, similarly, be useful analgesics. In particular, since 1-EBIO reduces sensory input in response to noxious mechanical stimulation, similar compounds may be effective in treating specific conditions such as mechanical allodynia and hyperalgesia.

In conclusion, the work presented in my thesis suggests a possible functional link between the "centrally acting" analgesic action of drugs such as chlorzoxazone and their ability to activate SK channels. It would therefore seem well worthwhile to examine further SK channel openers as potentially novel analgesics in certain pain states.

Appendix 1. A summary of some of the basic properties of all p17 DRG cells recorded from using the perforated patch technique.

Cell	cell size (μm)	Em (mV)	AP inflection	Voltage sag	AHP type present			Slow ADP
					fast only	medium	slow	
1	25	-51	no	?			Yes	
2	25	-58	yes	?		Yes	Yes	
3	37.5	-61	yes	?		Yes	Yes	
4	22.5	-52	no	?	Yes			
5	42.5	-55	no	?	Yes			
6	25	-60	no	?				
7	25	-60	yes	?		Yes	Yes	
8	37.5	-60	?	?		Yes	Yes	
9	37.5	-55	no	?			Yes	
10	30	-50	yes	?	Yes			
11	37.5	-60	no	?	Yes			
12	25	-65	?	?	Yes			
13	32.5	-60	no	?	Yes			
14	30	-58	yes	?			Yes	
15	35	-50	no	yes			Yes	
16	37.5	-56	no	yes	Yes			
17	32.5	-60	no	?		Yes	Yes	
18	35	-67	no	yes	Yes			
19	25	-60	?	no		Yes	Yes	
20	35	-60	?	?	Yes			
21	35	-50	?	?	Yes			
22	40	-50	no	yes		Yes	Yes	
23	32.5	-50	no	yes	Yes			
24	42.5	-59	no	yes		Yes	Yes	
25	42.5	-60	no	yes		Yes		
26	25	-52	no	yes	Yes			
27	27.5	-52	no	yes	Yes			
28	30	-51	yes	yes		Yes	Yes	
29	29	-52	yes	no		Yes		
30	32.5	-58	no	?		Yes	Yes	
31	25	-57	yes	?		Yes		
32	25	-50	yes	?	Yes			
33	27.5	-59	yes	yes			Yes	
34	27.5	-55		?		Yes		
35	42.5	-50	no	yes		Yes		
36	47.5	-55	no	yes			Yes	
37	45	-53	no	yes			Yes	
38	42.5	-52	no	yes		Yes	Yes	
39	47.5	-59	no	yes		Yes	Yes	
40	47.5	-64	no	yes	Yes			
41	50	-54	no	yes			Yes	
42	42	-60	no	yes		Yes	Yes	
43	42.5	-63	no	yes	Yes			
44	42.5	-67	no	yes	Yes			
45	40	-66	no	yes		Yes		
46	37.5	-68	no	?		Yes		
47	42.5	-60	no	?		Yes		
48	40	-60	no	yes	Yes			
49	42.5	-58	no	yes		Yes		

Cell	cell size (μm)	Em (mV)	AP inflection	Voltage sag	AHP type present			Slow ADP
					fast only	medium	slow	
50	40	-58	no	yes	Yes			
51	42.5	-52	no	yes		Yes		
52	45	-61	no	yes	Yes			
53	42.5	-50	no	yes	Yes			
54	42.5	-56	no	yes	Yes			
55	45	-57	no	yes	Yes			
56	43.8	-56	no	yes	Yes			
57	37.5	-59	no	yes	Yes			
58	27.5	-79	no	?			Yes	
59	35	-55	no	yes	Yes		Yes	
60	35	-58	no	yes	Yes			
61	42.5	-68	?	yes		Yes		
62	37.5	-52	no	?	Yes			
63	42.5	-50	no	yes			Yes	
64	40	-65	no	yes			Yes	
65	25	-56	no	yes		Yes	Yes	
66	27.5	-50	?	no			Yes	
67	40	-53	no	no		Yes		
68	42.5	-50	?	yes		Yes	Yes	
69	37.5	-50	?	?		Yes		
70	40	-53	no	?	Yes			
71	42.5	-52	no	?	Yes			
72	35	-59	no	?		Yes	Yes	
73	42.5	-50	no	?	Yes			
74	40	-53	no	?	Yes			
75	42.5	-50	no	?			Yes	
76	40	-50	no	?	Yes			
77	37.5	-62	no	?	Yes			
78	50	-50	no	?	Yes			
79	50	-50	no	?	Yes			
80	37.5	-55	no	?	Yes			
81	40	-50	no	?	Yes			
82	50	-58	?	?	Yes			
83	42.5	-56	no	?		Yes	Yes	
84	37.5	-66	no	?				
85	50	-51	no	?		Yes		
86	40	-56	no	?		Yes		
87	42.5	-51	?	?		Yes		
88	37.5	-55	?	?		Yes		
89	42.5	-62	no	?	Yes			
90	37.5	-50	no	?	Yes			
91	30	-50	?	?	Yes			
92	25	-65	?	yes		Yes	Yes	
93	35	-52	no	yes		Yes		
94	27.5	-57	?	yes	Yes			
95	27.5	-65	no	yes		Yes		
96	30	-64	?	?				Yes
97	20	-55	yes	?			Yes	
98	25	-57	yes	?			Yes	
99	25	-73	yes	yes		Yes		Yes
100	25	-50	no	no		Yes	Yes	
101	25	-50	yes	yes			Yes	

Cell	cell size (µm)	Em (mV)	AP inflection	Voltage sag	AHP type present			Slow ADP
					fast only	medium	slow	
102	25	-54	yes	no		Yes		Yes
103	25	-60	no	yes		Yes		
104	27.5	-50	no	no		Yes		Yes
105	25	-60	no	?		Yes		
106	25	-51	no	yes		Yes		Yes
107	29	-51	?	yes	Yes			
108	27.5	-53	no	yes	Yes			
109	27.5	-50	?	yes	Yes			
110	25	-57	yes	yes		Yes	Yes	
111	25	-64	no	yes				Yes
112	30	-56	?	yes	Yes			
113	27.5	-55	no	yes		Yes		
114	27.5	-70	no	?		Yes	Yes	
115	25	-50	yes	no	Yes			
116	27.5	-72	yes	?		Yes		Yes
117	25	-59	yes	?		Yes		
118	25	-56	yes	?		Yes		Yes
119	25	-52	yes	?		Yes		Yes
120	27.5	-66	?	?		Yes	Yes	
121	25	-60	?	?		Yes		
122	25	-51	yes	?			Yes	
123	25	-65	yes	?		Yes	Yes	
124	25	-57	yes	?		Yes	Yes	
125	25	-56	yes	yes		Yes		
126	30	-55	no	yes		Yes		
127	27.5	-56	no	?		Yes	Yes	
128	25	-58	?	?		Yes		
129	25	-76	?	?		Yes	Yes	
130	20	-55	no	no		Yes		
131	20	-54	no	no		Yes		
132	22.5	-56	yes	?		Yes	Yes	
133	22.5	-60	yes	no		Yes		
134	22.5	-50	yes	no			Yes	
135	20	-56	yes	yes		Yes		Yes
136	20	-65	yes	no		Yes	Yes	
137	20	-52	yes	?		Yes	Yes	
138	25	-53	?	no	Yes			
139	22.5	-50	yes	no	Yes			
140	25	-56	no	?		Yes		
141	25	-66	yes	?		Yes		
142	22.5	-59	yes	yes		Yes		
143	20	-55	yes	no		Yes		Yes
144	22.5	-50	yes	no		Yes		
145	20	-60	yes	?		Yes		
146	22.5	-66	yes	?		Yes	Yes	
147	25	-56	yes	yes		Yes		
148	25	-57	yes	yes		Yes	Yes	
149	25	-55	yes	yes		Yes		
150	25	-52	yes	?	Yes			
151	25	-60	yes		Yes			
152	27.5	-63		yes	Yes			

Appendix 2. A summary of the effects of different drugs used to try and identify the K^+ channels underlying the AHPs in DRG cells.

Effects of drugs on mAHPs from p17 cells		
	Cell Type	
Drug applied	A-Type	C-type
UCL 1848	1/9	0/2
Cd2+	1/6	1/3
ChTx	0/2	
TEA	0/3	0/2
4-AP	0/1	0/1

Effects of drugs on mAHPs from p45	
Drug applied	p45 C-type cells
UCL 1848	0/8
Cd2+	1/3
1-EBIO	1/8
TEA	0/1
Clotrimazole	0/2

Effects of drugs on sAHPs from p17 cells		
	Cell Type	
Drug applied	A-Type	C-type
UCL 1848	0/4	0/3
Cd2+	0/6	1/1
ChTx		0/1
TEA	0/7	2/3
UCL 2027	2/2	2/2
Histamine	0/2	2/2

Appendix 3. A summary of the different components underlying the AHPs in DRG cells.

	Cell type	
AHP components	A	C
1 hyperpolarising	4	1
2 hyperpolarising	20	6
3 hyperpolarising	1	
2 hyperpolarising and 1 depolarising	1	1

References

1. Abdulla FA, Smith PA (1999) Nerve injury increases an excitatory action of neuropeptide Y and Y2-agonists on dorsal root ganglion neurons. Neuroscience 89: 43-60.

2. Abdulla FA, Smith PA (2001) Axotomy- and autotomy-induced changes in Ca2+ and K+ channel currents of rat dorsal root ganglion neurons. J Neurophysiol 85: 644-658.

3. Adelman JP, Shen KZ, Kavanaugh MP, Warren RA, Wu YN, Lagrutta A, Bond CT, North RA (1992) Calcium-activated potassium channels expressed from cloned complementary DNAs. Neuron 9: 209-216.

4. Aiken SP, Lampe BJ, Murphy PA, Brown BS (1995) Reduction of spike frequency adaptation and blockade of M-current in rat CA1 pyramidal neurones by linopirdine (DuP 996), a neurotransmitter release enhancer. Br J Pharmacol 115: 1163-1168.

5. Alvares D, Fitzgerald M (1999) Building blocks of pain: the regulation of key molecules in spinal sensory neurones during development and following peripheral axotomy. Pain Suppl 6: S71-S85.

6. Alvarez J, Montero M, Garcia-Sancho J (1992) High affinity inhibition of Ca(2+)-dependent K+ channels by cytochrome P-450 inhibitors. J Biol Chem 267: 11789-11793.

7. Amir R, Devor M (1997) Spike-evoked suppression and burst patterning in dorsal root ganglion neurons of the rat. J Physiol 501 (Pt 1): 183-196.

8. Andreasen M, Lambert JD (1995) The excitability of CA1 pyramidal cell dendrites is modulated by a local Ca(2+)-dependent K(+)-conductance. Brain Res 698: 193-203.

9. Atkinson NS, Robertson GA, Ganetzky B (1991) A component of calcium-activated potassium channels encoded by the Drosophila slo locus. Science 253: 551-555.

10. Baccaglini PI, Hogan PG (1983) Some rat sensory neurons in culture express characteristics of differentiated pain sensory cells. Proc Natl Acad Sci U S A 80: 594-598.

11. Banks BE, Brown C, Burgess GM, Burnstock G, Claret M, Cocks TM, Jenkinson DH (1979) Apamin blocks certain neurotransmitter-induced increases in potassium permeability. Nature 282: 415-417.

12. Barfod ET, Moore AL, Lidofsky SD (2001) Cloning and functional expression of a liver isoform of the small conductance Ca2+-activated K+ channel SK3. Am J Physiol Cell Physiol 280: C836-C842.

13. Barrett JN, Magleby KL, Pallotta BS (1982) Properties of single calcium-activated potassium channels in cultured rat muscle. J Physiol 331: 211-230.

14. Bekkers JM (2000) Distribution of slow AHP channels on hippocampal CA1 pyramidal neurons. J Neurophysiol 83: 1756-1759.

15. Benham CD, Gunthorpe MJ, Davis JB (2003) TRPV channels as temperature sensors. Cell Calcium 33: 479-487.

16. Benton DCH, Dunn PM, Chen JQ, Galanakis D, Ganellin CR, Malik-Hall M, Shah M, Haylett DG, Jenkinson DH (1999) UCL 1848; A novel bis-quinolinium cyclophane which blocks apamin-sensitive K+ channels with nanomolar affinity. Br J Pharmacol 128: 39P.

17. Benton DCH, Monaghan AS, Hosseini R, Bahia PK, Haylett DG, Moss GWJ (2003) Small conductance Ca2+-activated K+ channels formed by the expression of rat SK1 and SK2 genes in HEK 293 cells. J Physiol 553: 13-19.

18. Bhattacharjee A, Joiner WJ, Wu M, Yang Y, Sigworth FJ, Kaczmarek LK (2003) Slick (Slo2.1), a rapidly-gating sodium-activated potassium channel inhibited by ATP. J Neurosci 23: 11681-11691.

19. Bischoff U, Vogel W, Safronov BV (1998) Na+-activated K+ channels in small dorsal root ganglion neurones of rat. J Physiol 510 (Pt 3): 743-754.

20. Blair NT, Bean BP (2002) Roles of tetrodotoxin (TTX)-sensitive Na+ current, TTX-resistant Na+ current, and Ca2+ current in the action potentials of nociceptive sensory neurons. J Neurosci 22: 10277-10290.

21. Blank T, Nijholt I, Kye MJ, Radulovic J, Spiess J (2003) Small-conductance, Ca2+-activated K+ channel SK3 generates age-related memory and LTP deficits. Nat Neurosci 6: 911-912.

22. Blatz AL, Magleby KL (1986) Single apamin-blocked Ca-activated K+ channels of small conductance in cultured rat skeletal muscle. Nature 323: 718-720.

23. Blatz AL, Magleby KL (1987) Calcium-activated potassium channels. Trends Neurosci 10: 463-467.

24. Boettger MK, Till S, Chen MX, Anand U, Otto WR, Plumpton C, Trezise DJ, Tate SN, Bountra C, Coward K, Birch R, Anand P (2002) Calcium-activated potassium channel SK1- and IK1-like immunoreactivity in injured human sensory neurones and its regulation by neurotrophic factors. Brain 125: 252-263.

25. Bond CT, Maylie J, Adelman JP (1999) Small-conductance calcium-activated potassium channels. Ann N Y Acad Sci 868: 370-378.

26. Bond CT, Herson PS, Strassmaier T, Hammond R, Stackman R, Maylie J, Adelman JP (2004) Small conductance Ca2+-activated K+ channel knock-out mice reveal the identity of calcium-dependent afterhyperpolarization currents. J Neurosci 24: 5301-5306.

27. Bosch MA, Kelly MJ, Ronnekleiv OK (2002) Distribution, neuronal colocalization, and 17beta-E2 modulation of small conductance calcium-activated K(+) channel (SK3) mRNA in the guinea pig brain. Endocrinology 143: 1097-1107.

28. Bowden SE, Fletcher S, Loane DJ, Marrion NV (2001) Somatic colocalization of rat SK1 and D class (Ca(v)1.2) L-type calcium channels in rat CA1 hippocampal pyramidal neurons. J Neurosci 21: RC175.

29. Brenner R, Jegla TJ, Wickenden A, Liu Y, Aldrich RW (2000) Cloning and functional characterization of novel large conductance calcium-activated potassium channel beta subunits, hKCNMB3 and hKCNMB4. J Biol Chem 275: 6453-6461.

30. Brugnara C, de Franceschi L, Alper SL (1993) Inhibition of Ca(2+)-dependent K+ transport and cell dehydration in sickle erythrocytes by clotrimazole and other imidazole derivatives. J Clin Invest 92: 520-526.

31. Brumovsky PR, Shi TJ, Matsuda H, Kopp J, Villar MJ, Hokfelt T (2002) NPY Y1 receptors are present in axonal processes of DRG neurons. Exp Neurol 174: 1-10.

32. Bruni JE (1998) Ependymal development, proliferation, and functions: a review. Microsc Res Tech 41: 2-13.

33. Caffrey JM, Eng DL, Black JA, Waxman SG, Kocsis JD (1992) Three types of sodium channels in adult rat dorsal root ganglion neurons. Brain Res 592: 283-297.

34. Campos Rosa J., Galanakis D, Piergentili A, Bhandari K, Ganellin CR, Dunn PM, Jenkinson DH (2000) Synthesis, molecular modeling, and pharmacological testing of bis- quinolinium cyclophanes: potent, non-peptidic blockers of the apamin- sensitive Ca(2+)-activated K(+) channel. J Med Chem 43: 420-431.

35. Cao Y, Dreixler JC, Roizen JD, Roberts MT, Houamed KM (2001) Modulation of recombinant small-conductance Ca(2+)-activated K(+) channels by the muscle relaxant chlorzoxazone and structurally related compounds. J Pharmacol Exp Ther 296: 683-689.

36. Caterina MJ, Schumacher MA, Tominaga M, Rosen TA, Levine JD, Julius D (1997) The capsaicin receptor: a heat-activated ion channel in the pain pathway. Nature 389: 816-824.

37. Catterall WA, Striessnig J (1992) Receptor sites for Ca2+ channel antagonists. Trends Pharmacol Sci 13: 256-262.

38. Cesare P, McNaughton P (1996) A novel heat-activated current in nociceptive neurons and its sensitization by bradykinin. Proc Natl Acad Sci U S A 93: 15435-15439.

39. Chen C (2002) The effect of two-day treatment of primary cultured ovine somatotropes with GHRP-2 on membrane voltage-gated K+ currents. Endocrinology 143: 2659-2663.

40. Chen JQ, Galanakis D, Ganellin CR, Dunn PM, Jenkinson DH (2000) bis-Quinolinium cyclophanes: 8,14-diaza-1,7(1, 4)- diquinolinacyclotetradecaphane (UCL 1848), a highly potent and selective, nonpeptidic blocker of the apamin-sensitive Ca(2+)-activated K(+) channel. J Med Chem 43: 3478-3481.

41. Chen MX, Gorman SA, Benson B, Singh K, Hieble JP, Michel MC, Tate SN, Trezise DJ (2004) Small and intermediate conductance Ca(2+)-activated K+ channels confer distinctive patterns of distribution in human tissues and differential cellular localisation in the colon and corpus cavernosum. Naunyn Schmiedebergs Arch Pharmacol 369: 602-615.

42. Choi S, Lovinger DM (1996) Metabotropic glutamate receptor modulation of voltage-gated Ca2+ channels involves multiple receptor subtypes in cortical neurons. J Neurosci 16: 36-45.

43. Christie MJ, North RA, Osborne PB, Douglass J, Adelman JP (1990) Heteropolymeric potassium channels expressed in Xenopus oocytes from cloned subunits. Neuron 4: 405-411.

44. Cingolani LA, Gymnopoulos M, Boccaccio A, Stocker M, Pedarzani P (2002) Developmental regulation of small-conductance Ca2+-activated K+ channel expression and function in rat Purkinje neurons. J Neurosci 22: 4456-4467.

45. Coetzee WA, Amarillo Y, Chiu J, Chow A, Lau D, McCormack T, Moreno H, Nadal MS, Ozaita A, Pountney D, Saganich M, Vega-Saenz dM, Rudy B (1999) Molecular diversity of K+ channels. Ann N Y Acad Sci 868: 233-285.

46. Coggan JS, Gruener R, Kruelen DL (1991) Electrophysiological properties and cholinergic responses in guinea-pig celiac ganglion neurons in primary culture. J Auton Nerv Syst 34: 147-155.

47. Colquhoun D (1971) Lectures on Biostatistics: An Introduction to Statistics with Applications in Biology and Medicine. Oxford University.

48. Cordoba-Rodriguez R, Moore KA, Kao JP, Weinreich D (1999) Calcium regulation of a slow post-spike hyperpolarization in vagal afferent neurons. Proc Natl Acad Sci U S A 96: 7650-7657.

49. Cruzblanca H, Koh DS, Hille B (1998) Bradykinin inhibits M current via phospholipase C and Ca2+ release from IP3-sensitive Ca2+ stores in rat sympathetic neurons. Proc Natl Acad Sci U S A 95: 7151-7156.

50. Cryan JE, Dale TJ, Chen MX, Robertson G, Trezise DJ (2003) Identification of (E)-2-(4,6-difluoro-1-indanylidene)acetamide (GW275919X) as a novel opener of human recombinant IK and SK Ca2+-activated K+ channels. Proceedings of the British Pharmacological Society at http://www pa2online org/Vol1Issueabst062P html.

51. D'hoedt D, Hirzel K, Pedarzani P, Stocker M (2004) Domain Analysis of the Calcium-activated Potassium Channel SK1 from Rat Brain: Functional Expression and Toxin Sensitivity. J Biol Chem 279: 12088-12092.

52. Dale TJ, Cryan JE, Chen MX, Trezise DJ (2001) Partial apamin sensitivity of hSK-1 Ca2+ - activated K+ channels stably expressed in CHO cells. J Physiol 535: 5P.

53. Devor DC, Singh AK, Frizzell RA, Bridges RJ (1996) Modulation of Cl- secretion by benzimidazolones. I. Direct activation of a Ca(2+)-dependent K+ channel. Am J Physiol 271: L775-L784.

54. Dickenson AH (1995) Spinal cord pharmacology of pain. Br J Anaesth 75: 193-200.

55. Djouhri L, Bleazard L, Lawson SN (1998) Association of somatic action potential shape with sensory receptive properties in guinea-pig dorsal root ganglion neurones. J Physiol 513 (Pt 3): 857-872.

56. Doyle DA, Morais CJ, Pfuetzner RA, Kuo A, Gulbis JM, Cohen SL, Chait BT, MacKinnon R (1998) The structure of the potassium channel: molecular basis of K+ conduction and selectivity. Science 280: 69-77.

57. Dryer SE (1994) Na(+)-activated K+ channels: a new family of large-conductance ion channels. Trends Neurosci 17: 155-160.

58. Dryer SE (2003) Molecular identification of the Na+-activated K+ channel. Neuron 37: 727-728.

59. Dunn PM (1994) Dequalinium, a selective blocker of the slow afterhyperpolarization in rat sympathetic neurones in culture. Eur J Pharmacol 252: 189-194.

60. Dutar P, Nicoll RA (1989) Pharmacological characterization of muscarinic responses in rat hippocampal pyramidal cells. EXS 57: 68-76.

61. Dworetzky SI, Boissard CG, Lum-Ragan JT, McKay MC, Post-Munson DJ, Trojnacki JT, Chang CP, Gribkoff VK (1996) Phenotypic alteration of a human BK (hSlo) channel by hSlobeta subunit coexpression: changes in blocker sensitivity, activation/relaxation and inactivation kinetics, and protein kinase A modulation. J Neurosci 16: 4543-4550.

62. Faber ES, Sah P (2002) Physiological role of calcium-activated potassium currents in the rat lateral amygdala. J Neurosci 22: 1618-1628.

63. Faber ES, Sah P (2003) Calcium-activated potassium channels: multiple contributions to neuronal function. Neuroscientist 9: 181-194.

64. Fanger CM, Ghanshani S, Logsdon NJ, Rauer H, Kalman K, Zhou J, Beckingham K, Chandy KG, Cahalan MD, Aiyar J (1999) Calmodulin mediates calcium-dependent activation of the intermediate conductance KCa channel, IKCa1. J Biol Chem 274: 5746-5754.

65. Ferri GL, Sabani A, Abelli L, Polak JM, Dahl D, Portier MM (1990) Neuronal intermediate filaments in rat dorsal root ganglia: differential distribution of peripherin and neurofilament protein immunoreactivity and effect of capsaicin. Brain Res 515: 331-335.

66. Fitzgerald M, Gibson S (1984) The postnatal physiological and neurochemical development of peripheral sensory C fibres. Neuroscience 13: 933-944.

67. Fitzgerald M, Jennings E (1999) The postnatal development of spinal sensory processing. Proc Natl Acad Sci U S A 96: 7719-7722.

68. Fowler JC, Greene R, Weinreich D (1985) Two calcium-sensitive spike after-hyperpolarizations in visceral sensory neurones of the rabbit. J Physiol 365: 59-75.

69. Franceschetti S, Lavazza T, Curia G, Aracri P, Panzica F, Sancini G, Avanzini G, Magistretti J (2003) Na+-activated K+ current contributes to postexcitatory hyperpolarization in neocortical intrinsically bursting neurons. J Neurophysiol 89: 2101-2111.

70. Fukuda J, Kameyama M (1980) A tissue-culture of nerve cells from adult mammalian ganglia and some electrophysiological properties of the nerve cells in vitro. Brain Res 202: 249-255.

71. Furness JB, Robbins HL, Selmer IS, Hunne B, Chen MX, Hicks GA, Moore S, Neylon CB (2003) Expression of intermediate conductance potassium channel immunoreactivity in neurons and epithelial cells of the rat gastrointestinal tract. Cell Tissue Res 314: 179-189.

72. Galvez A, Gimenez-Gallego G, Reuben JP, Roy-Contancin L, Feigenbaum P, Kaczorowski GJ, Garcia ML (1990) Purification and characterization of a unique, potent, peptidyl probe for the high conductance calcium-activated potassium channel from venom of the scorpion Buthus tamulus. J Biol Chem 265: 11083-11090.

73. Garcia-Calvo M, Knaus HG, McManus OB, Giangiacomo KM, Kaczorowski GJ, Garcia ML (1994) Purification and reconstitution of the high-conductance, calcium-activated potassium channel from tracheal smooth muscle. J Biol Chem 269: 676-682.

74. Gardos G (1958) The function of calcium in the potassium permeability of human erythrocytes. Biochimica Biophysica Acta 30: 653-654.

75. Gold MS, Shuster MJ, Levine JD (1996a) Role of a Ca(2+)-dependent slow afterhyperpolarization in prostaglandin E2-induced sensitization of cultured rat sensory neurons. Neurosci Lett 205: 161-164.

76. Gold MS, Dastmalchi S, Levine JD (1996b) Co-expression of nociceptor properties in dorsal root ganglion neurons from the adult rat in vitro. Neuroscience 71: 265-275.

77. Goldstein ME, House SB, Gainer H (1991) NF-L and peripherin immunoreactivities define distinct classes of rat sensory ganglion cells. J Neurosci Res 30: 92-104.

78. Gordon-Weeks PR (2004) Microtubules and growth cone function. J Neurobiol 58: 70-83.

79. Görke K, Pierau FK (1980) Spike potentials and membrane properties of dorsal root ganglion cells in pigeons. Pflugers Arch 386: 21-28.

80. Greffrath W, Martin E, Reuss S, Boehmer G (1998) Components of after-hyperpolarization in magnocellular neurones of the rat supraoptic nucleus in vitro. J Physiol 513 (Pt 2): 493-506.

81. Griffith WH (1988) Membrane properties of cell types within guinea pig basal forebrain nuclei in vitro. J Neurophysiol 59: 1590-1612.

82. Grissmer S, Lewis RS, Cahalan MD (1992) Ca(2+)-activated K+ channels in human leukemic T cells. J Gen Physiol 99: 63-84.

83. Grunnet M, Jensen BS, Olesen SP, Klaerke DA (2001) Apamin interacts with all subtypes of cloned small-conductance Ca2+- activated K+ channels. Pflugers Arch 441: 544-550.

84. Guo A, Vulchanova L, Wang J, Li X, Elde R (1999) Immunocytochemical localization of the vanilloid receptor 1 (VR1): relationship to neuropeptides, the P2X3 purinoceptor and IB4 binding sites. Eur J Neurosci 11: 946-958.

85. Guo J, Schofield GG (2002) Histamine inhibits KCNQ2/KCNQ3 channel current via recombinant histamine H(1) receptors. Neurosci Lett 328: 285-288.

86. Guy HR, Conti F (1990) Pursuing the structure and function of voltage-gated channels. Trends Neurosci 13: 201-206.

87. Gygi SP, Rochon Y, Franza BR, Aebersold R (1999) Correlation between protein and mRNA abundance in yeast. Mol Cell Biol 19: 1720-1730.

88. Habermann E, Fischer K (1979) Bee venom neurotoxin (apamin): iodine labeling and characterization of binding sites. Eur J Biochem 94: 355-364.

89. Hadley JK, Noda M, Selyanko AA, Wood IC, Abogadie FC, Brown DA (2000) Differential tetraethylammonium sensitivity of KCNQ1-4 potassium channels. Br J Pharmacol 129: 413-415.

90. Hagiwara S, Byerly L (1981) Calcium channel. Annu Rev Neurosci 4: 69-125.

91. Halliwell JV, Adams PR (1982) Voltage-clamp analysis of muscarinic excitation in hippocampal neurons. Brain Res 250: 71-92.

92. Hanani M, Lasser-Ross N (1997) Activity-dependent changes in intracellular calcium in myenteric neurons. Am J Physiol 273: G1359-G1363.

93. Harper AA, Lawson SN (1985a) Conduction velocity is related to morphological cell type in rat dorsal root ganglion neurones. J Physiol 359: 31-46.

94. Harper AA, Lawson SN (1985b) Electrical properties of rat dorsal root ganglion neurones with different peripheral nerve conduction velocities. J Physiol 359: 47-63.

95. Hatton CJ, Peers C (1996) Effects of cytochrome P-450 inhibitors on ionic currents in isolated rat type I carotid body cells. Am J Physiol 271: C85-C92.

96. Heginbotham L, Lu Z, Abramson T, MacKinnon R (1994) Mutations in the K+ channel signature sequence. Biophys J 66: 1061-1067.

97. Heurteaux C, Messier C, Destrade C, Lazdunski M (1993) Memory processing and apamin induce immediate early gene expression in mouse brain. Brain Res Mol Brain Res 18: 17-22.

98. Hillsley K, Kenyon JL, Smith TK (2000) Ryanodine-sensitive stores regulate the excitability of AH neurons in the myenteric plexus of guinea-pig ileum. J Neurophysiol 84: 2777-2785.

99. Hodgkin AL, Huxley AF (1952) A quantitative description of membrane current and its application to conduction and excitation in nerve. J Physiol 117: 500-544.

100. Holden JE, Pizzi JA (2003) The challenge of chronic pain. Adv Drug Deliv Rev 55: 935-948.

101. Hosseini R, Benton DCH, Dunn PM, Jenkinson DH, Moss GWJ (2001) SK3 is an important component of K(+) channels mediating the afterhyperpolarization in cultured rat SCG neurones. J Physiol 535: 323-334.

102. Hounsgaard J, Kiehn O, Mintz I (1988) Response properties of motoneurones in a slice preparation of the turtle spinal cord. J Physiol 398: 575-589.

103. Hu G (1993) DNA polymerase-catalyzed addition of nontemplated extra nucleotides to the 3' end of a DNA fragment. DNA Cell Biol 12: 763-770.

104. Hu H, Shao LR, Chavoshy S, Gu N, Trieb M, Behrens R, Laake P, Pongs O, Knaus HG, Ottersen OP, Storm JF (2001) Presynaptic Ca2+-activated K+ channels in glutamatergic hippocampal terminals and their role in spike repolarization and regulation of transmitter release. J Neurosci 21: 9585-9597.

105. Isacoff EY, Jan YN, Jan LY (1990) Evidence for the formation of heteromultimeric potassium channels in Xenopus oocytes. Nature 345: 530-534.

106. Ishii TM, Silvia C, Hirschberg B, Bond CT, Adelman JP, Maylie J (1997a) A human intermediate conductance calcium-activated potassium channel. Proc Natl Acad Sci U S A 94: 11651-11656.

107. Ishii TM, Maylie J, Adelman JP (1997b) Determinants of apamin and d-tubocurarine block in SK potassium channels. J Biol Chem 272: 23195-23200.

108. Jacobson D, Pribnow D, Herson PS, Maylie J, Adelman JP (2003) Determinants contributing to estrogen-regulated expression of SK3. Biochem Biophys Res Commun 303: 660-668.

109. Jafri MS, Moore KA, Taylor GE, Weinreich D (1997) Histamine H1 receptor activation blocks two classes of potassium current, IK(rest) and IAHP, to excite ferret vagal afferents. J Physiol 503 (Pt 3): 533-546.

110. Jenkinson DH, Haylett DG, Cook NS (1983) Calcium-activated potassium channels in liver cells. Cell Calcium 4: 429-437.

111. Jensen BS, Strobaek D, Christophersen P, Jorgensen TD, Hansen C, Silahtaroglu A, Olesen SP, Ahring PK (1998) Characterization of the cloned human intermediate-conductance Ca2+- activated K+ channel. Am J Physiol 275: C848-C856.

112. Jensen BS, Strobaek D, Olesen SP, Christophersen P (2001) The Ca2+-activated K+ channel of intermediate conductance: a molecular target for novel treatments? Curr Drug Targets 2: 401-422.

113. Jiang Y, Pico A, Cadene M, Chait BT, MacKinnon R (2001) Structure of the RCK domain from the E. coli K+ channel and demonstration of its presence in the human BK channel. Neuron 29: 593-601.

114. Jiang Y, Lee A, Chen J, Cadene M, Chait BT, MacKinnon R (2002) Crystal structure and mechanism of a calcium-gated potassium channel. Nature 417: 515-522.

115. Jiang Y, Lee A, Chen J, Ruta V, Cadene M, Chait BT, MacKinnon R (2003) X-ray structure of a voltage-dependent K+ channel. Nature 423: 33-41.

116. Johnson SW, Seutin V (1997) Bicuculline methiodide potentiates NMDA-dependent burst firing in rat dopamine neurons by blocking apamin-sensitive Ca2+-activated K+ currents. Neurosci Lett 231: 13-16.

117. Joiner WJ, Wang LY, Tang MD, Kaczmarek LK (1997) hSK4, a member of a novel subfamily of calcium-activated potassium channels. Proc Natl Acad Sci U S A 94: 11013-11018.

118. Joiner WJ, Tang MD, Wang LY, Dworetzky SI, Boissard CG, Gan L, Gribkoff VK, Kaczmarek LK (1998) Formation of intermediate-conductance calcium-activated potassium channels by interaction of Slack and Slo subunits. Nat Neurosci 1: 462-469.

119. Joiner WJ, Basavappa S, Vidyasagar S, Nehrke K, Krishnan S, Binder HJ, Boulpaep EL, Rajendran VM (2003) Active K+ secretion through multiple KCa-type channels and regulation by IKCa channels in rat proximal colon. Am J Physiol Gastrointest Liver Physiol 285: G185-G196.

120. Kahl R, Friederici DE, Kahl GF, Ritter W, Krebs R (1980) Clotrimazole as an inhibitor of benzo[a]pyrene metabolite-DNA adduct formation in vitro and of microsomal mono-oxygenase activity. Drug Metab Dispos 8: 191-196.

121. Kameyama M (1983) Ionic currents in cultured dorsal root ganglion cells from adult guinea pigs. J Membr Biol 72: 195-203.

122. Kawai T, Watanabe M (1986) Blockade of Ca-activated K conductance by apamin in rat sympathetic neurones. Br J Pharmacol 87: 225-232.

123. Keating DJ, Rychkov GY, Roberts ML (2001) Oxygen sensitivity in the sheep adrenal medulla: role of SK channels. Am J Physiol Cell Physiol 281: C1434-C1441.

124. Keen JE, Khawaled R, Farrens DL, Neelands T, Rivard A, Bond CT, Janowsky A, Fakler B, Adelman JP, Maylie J (1999) Domains responsible for constitutive and Ca(2+)-dependent interactions between calmodulin and small conductance Ca(2+)-activated potassium channels. J Neurosci 19: 8830-8838.

125. Kenyon JL (2000) The reversal potential of Ca(2+)-activated Cl(-) currents indicates that chick sensory neurons accumulate intracellular Cl(-). Neurosci Lett 296: 9-12.

126. Kernell D, Monster AW (1982) Time course and properties of late adaptation in spinal motoneurones of the cat. Exp Brain Res 46: 191-196.

127. Khanna R, Chang MC, Joiner WJ, Kaczmarek LK, Schlichter LC (1999) hSK4/hIK1, a calmodulin-binding KCa channel in human T lymphocytes. Roles in proliferation and volume regulation. J Biol Chem 274: 14838-14849.

128. Klöcker N, Oliver D, Ruppersberg JP, Knaus HG, Fakler B (2001) Developmental expression of the small-conductance Ca(2+)-activated potassium channel SK2 in the rat retina. Mol Cell Neurosci 17: 514-520.

129. Knaus HG, Folander K, Garcia-Calvo M, Garcia ML, Kaczorowski GJ, Smith M, Swanson R (1994) Primary sequence and immunological characterization of beta-subunit of high conductance Ca(2+)-activated K+ channel from smooth muscle. J Biol Chem 269: 17274-17278.

130. Koh DS, Jonas P, Vogel W (1994) Na(+)-activated K+ channels localized in the nodal region of myelinated axons of Xenopus. J Physiol 479 (Pt 2): 183-197.

131. Köhler M, Hirschberg B, Bond CT, Kinzie JM, Marrion NV, Maylie J, Adelman JP (1996) Small-conductance, calcium-activated potassium channels from mammalian brain. Science 273: 1709-1714.

132. Kolski-Andreaco A, Tomita H, Shakkottai VG, Gutman GA, Cahalan MD, Gargus JJ, Chandy KG (2004) SK3-1C, a dominant-negative suppressor of SKCa and IKCa channels. J Biol Chem 279: 6893-6904.

133. Kostyuk PG, Veselovsky NS, Fedulova SA, Tsyndrenko AY (1981a) Ionic currents in the somatic membrane of rat dorsal root ganglion neurons-III. Potassium currents. Neuroscience 6: 2439-2444.

134. Kostyuk PG, Veselovsky NS, Tsyndrenko AY (1981b) Ionic currents in the somatic membrane of rat dorsal root ganglion neurons-I. Sodium currents. Neuroscience 6: 2423-2430.

135. Kostyuk PG, Veselovsky NS, Fedulova SA (1981c) Ionic currents in the somatic membrane of rat dorsal root ganglion neurons-II. Calcium currents. Neuroscience 6: 2431-2437.

136. Krapivinsky G, Gordon EA, Wickman K, Velimirovic B, Krapivinsky L, Clapham DE (1995) The G-protein-gated atrial K+ channel IKACh is a heteromultimer of two inwardly rectifying K(+)-channel proteins. Nature 374: 135-141.

137. Kress M, Reeh PW (1996) More sensory competence for nociceptive neurons in culture. Proc Natl Acad Sci U S A 93: 14995-14997.

138. Kubota M, Nakamura M, Tsukahara N (1984) Calcium-dependent potentials in mammalian red nucleus neurons in vitro. Neurosci Res 1: 185-189.

139. Kuno M, Miyahara JT, Weakly JN (1970) Post-tetanic hyperpolarization produced by an electrogenic pump in dorsal spinocerebellar tract neurones of the cat. J Physiol 210: 839-855.

140. Kuryshev YA, Gudz TI, Brown AM, Wible BA (2000) KChAP as a chaperone for specific K(+) channels. Am J Physiol Cell Physiol 278: C931-C941.

141. Lamas JA, Selyanko AA, Brown DA (1997) Effects of a cognition-enhancer, linopirdine (DuP 996), on M-type potassium currents (IK(M)) and some other voltage- and ligand-gated membrane currents in rat sympathetic neurons. Eur J Neurosci 9: 605-616.

142. Lancaster B, Nicoll RA (1987) Properties of two calcium-activated hyperpolarizations in rat hippocampal neurones. J Physiol 389: 187-203.

143. Lancaster B, Zucker RS (1994) Photolytic manipulation of Ca2+ and the time course of slow, Ca(2+)-activated K+ current in rat hippocampal neurones. J Physiol 475: 229-239.

144. Larsson HP, Baker OS, Dhillon DS, Isacoff EY (1996) Transmembrane movement of the shaker K+ channel S4. Neuron 16: 387-397.

145. Lasser-Ross N, Ross WN, Yarom Y (1997) Activity-dependent [Ca2+]i changes in guinea pig vagal motoneurons: relationship to the slow afterhyperpolarization. J Neurophysiol 78: 825-834.

146. Lawson SN, Harper AA, Harper EI, Garson JA, Anderton BH (1984) A monoclonal antibody against neurofilament protein specifically labels a subpopulation of rat sensory neurones. J Comp Neurol 228: 263-272.

147. Lawson SN, McCarthy PW, Prabhakar E (1996) Electrophysiological properties of neurones with CGRP-like immunoreactivity in rat dorsal root ganglia. J Comp Neurol 365: 355-366.

148. Lawson SN (2002) Phenotype and function of somatic primary afferent nociceptive neurones with C-, Adelta- or Aalpha/beta-fibres. Exp Physiol 87: 239-244.

149. Leal-Cardoso H, Koschorke GM, Taylor G, Weinreich D (1993) Electrophysiological properties and chemosensitivity of acutely isolated nodose ganglion neurons of the rabbit. J Auton Nerv Syst 45: 29-39.

150. Lesage F, Lazdunski M (2000) Molecular and functional properties of two-pore-domain potassium channels. Am J Physiol Renal Physiol 279: F793-F801.

151. Levitan ES, Takimoto K (1998) Dynamic regulation of K+ channel gene expression in differentiated cells. J Neurobiol 37: 60-68.

152. Light AR, Perl ER (2003) Unmyelinated afferent fibers are not only for pain anymore. J Comp Neurol 461: 137-139.

153. Logsdon NJ, Kang J, Togo JA, Christian EP, Aiyar J (1997) A novel gene, hKCa4, encodes the calcium-activated potassium channel in human T lymphocytes. J Biol Chem 272: 32723-32726.

154. Lüscher C, Streit J, Lipp P, Luscher HR (1994) Action potential propagation through embryonic dorsal root ganglion cells in culture. II. Decrease of conduction reliability during repetitive stimulation. J Neurophysiol 72: 634-643.

155. MacKinnon R, Reinhart PH, White MM (1988) Charybdotoxin block of Shaker K+ channels suggests that different types of K+ channels share common structural features. Neuron 1: 997-1001.

156. MacKinnon R, Yellen G (1990) Mutations affecting TEA blockade and ion permeation in voltage-activated K+ channels. Science 250: 276-279.

157. Main MJ, Cryan JE, Dupere JR, Cox B, Clare JJ, Burbidge SA (2000) Modulation of KCNQ2/3 potassium channels by the novel anticonvulsant retigabine. Mol Pharmacol 58: 253-262.

158. Marrion NV (1997) Control of M-current. Annu Rev Physiol 59: 483-504.

159. Martens JR, Kwak YG, Tamkun MM (1999) Modulation of Kv channel alpha/beta subunit interactions. Trends Cardiovasc Med 9: 253-258.

160. Martinez-Pinna J, Davies PJ, McLachlan EM (2000) Diversity of channels involved in Ca(2+) activation of K(+) channels during the prolonged AHP in guinea-pig sympathetic neurons. J Neurophysiol 84: 1346-1354.

161. Marty A (1981) Ca-dependent K channels with large unitary conductance in chromaffin cell membranes. Nature 291: 497-500.

162. McCarthy PW, Lawson SN (1989) Cell type and conduction velocity of rat primary sensory neurons with substance P-like immunoreactivity. Neuroscience 28: 745-753.

163. McCarthy PW, Lawson SN (1990) Cell type and conduction velocity of rat primary sensory neurons with calcitonin gene-related peptide-like immunoreactivity. Neuroscience 34: 623-632.

164. McFarlane S, Cooper E (1991) Kinetics and voltage dependence of A-type currents on neonatal rat sensory neurons. J Neurophysiol 66: 1380-1391.

165. McLarnon JG (1995) Potassium currents in motoneurones. Prog Neurobiol 47: 513-531.

166. McManus OB, Helms LM, Pallanck L, Ganetzky B, Swanson R, Leonard RJ (1995) Functional role of the beta subunit of high conductance calcium-activated potassium channels. Neuron 14: 645-650.

167. Meech RW, Strumwasser F (1970) Intracellular Calcium Injection Activates Potassium Conductance In Aplysia Nerve Cells. Fed Proc 834.

168. Meera P, Wallner M, Song M, Toro L (1997) Large conductance voltage- and calcium-dependent K+ channel, a distinct member of voltage-dependent ion channels with seven N-terminal transmembrane segments (S0-S6), an extracellular N terminus, and an intracellular (S9-S10) C terminus. Proc Natl Acad Sci U S A 94: 14066-14071.

169. Meera P, Wallner M, Toro L (2000) A neuronal beta subunit (KCNMB4) makes the large conductance, voltage- and Ca2+-activated K+ channel resistant to charybdotoxin and iberiotoxin. Proc Natl Acad Sci U S A 97: 5562-5567.

170. Millan MJ (1999) The induction of pain: an integrative review. Prog Neurobiol 57: 1-164.

171. Miller MJ, Rauer H, Tomita H, Rauer H, Gargus JJ, Gutman GA, Cahalan MD, Chandy KG (2001) Nuclear localization and dominant-negative suppression by a mutant SKCa3 N-terminal channel fragment identified in a patient with schizophrenia. J Biol Chem 276: 27753-27756.

172. Monaghan AS, Benton DCH, Bahia PK, Hosseini R, Shah YA, Haylett DG, Moss GWJ (2004) The SK3 subunit of small conductance Ca2+-activated K+ channels interacts with both SK1 and SK2 subunits in a heterologous expression system. J Biol Chem 279: 1003-1009.

173. Moore KA, Cohen AS, Kao JP, Weinreich D (1998) Ca2+-induced Ca2+ release mediates a slow post-spike hyperpolarization in rabbit vagal afferent neurons. J Neurophysiol 79: 688-694.

174. Morita K, Katayama Y (1989) Calcium-dependent slow outward current in visceral primary afferent neurones of the rabbit. Pflugers Arch 414: 171-177.

175. Musso DL, Orr GF, Cochran FR, Kelley JL, Selph JL, Rigdon GC, Cooper BR, Jones ML (2003a) Indanylidenes. 2. Design and synthesis of (E)-2-(4-chloro-6-fluoro-1-indanylidene)-N-methylacetamide, a potent antiinflammatory and analgesic agent without centrally acting muscle relaxant activity. J Med Chem 46: 409-416.

176. Musso DL, Cochran FR, Kelley JL, McLean EW, Selph JL, Rigdon GC, Orr GF, Davis RG, Cooper BR, Styles VL, Thompson JB, Hall WR (2003b) Indanylidenes. 1. Design and synthesis of (E)-2-(4,6-difluoro-1-indanylidene)acetamide, a potent, centrally acting muscle relaxant with antiinflammatory and analgesic activity. J Med Chem 46: 399-408.

177. Nagy JI, Hunt SP (1983) The termination of primary afferents within the rat dorsal horn: evidence for rearrangement following capsaicin treatment. J Comp Neurol 218: 145-158.

178. Navarrete R, Vrbová G (1993) Activity-dependent interactions between motoneurones and muscles: Their role in the development of the motor unit. Progress in Neurobiology 41: 93-124.

179. Neely A, Lingle CJ (1992) Two components of calcium-activated potassium current in rat adrenal chromaffin cells. J Physiol 453: 97-131.

180. Neylon CB, Lang RJ, Fu Y, Bobik A, Reinhart PH (1999) Molecular cloning and characterization of the intermediate-conductance Ca(2+)-activated K(+) channel in vascular smooth muscle: relationship between K(Ca) channel diversity and smooth muscle cell function. Circ Res 85: e33-e43.

181. Obermair GJ, Kaufmann WA, Knaus HG, Flucher BE (2003) The small conductance Ca2+-activated K+ channel SK3 is localized in nerve terminals of

excitatory synapses of cultured mouse hippocampal neurons. Eur J Neurosci 17: 721-731.

182. Ogden DC, Capiod T, Walker JW, Trentham DR (1990) Kinetics of the conductance evoked by noradrenaline, inositol trisphosphate or Ca2+ in guinea-pig isolated hepatocytes. J Physiol 422: 585-602.

183. Olesen SP, Munch E, Moldt P, Drejer J (1994) Selective activation of Ca(2+)-dependent K+ channels by novel benzimidazolone. Eur J Pharmacol 251: 53-59.

184. Ottschytsch N, Raes A, Van Hoorick D, Snyders DJ (2002) Obligatory heterotetramerization of three previously uncharacterized Kv channel alpha-subunits identified in the human genome. Proc Natl Acad Sci U S A 99: 7986-7991.

185. Pácha J, Vorlicek J, Teisinger J (1992) Identification of apamin binding sites in rat intestinal mucosa. Life Sci 51: 423-429.

186. Pallotta BS, Magleby KL, Barrett JN (1981) Single channel recordings of Ca2+-activated K+ currents in rat muscle cell culture. Nature 293: 471-474.

187. Pan Z, Selyanko AA, Hadley JK, Brown DA, Dixon JE, McKinnon D (2001) Alternative splicing of KCNQ2 potassium channel transcripts contributes to the functional diversity of M-currents. J Physiol 531: 347-358.

188. Park YB (1994) Ion selectivity and gating of small conductance Ca(2+)-activated K+ channels in cultured rat adrenal chromaffin cells. J Physiol 481 (Pt 3): 555-570.

189. Passmore GM, Selyanko AA, Mistry M, Al Qatari M, Marsh SJ, Matthews EA, Dickenson AH, Brown TA, Burbidge SA, Main M, Brown DA (2003) KCNQ/M currents in sensory neurons: significance for pain therapy. J Neurosci 23: 7227-7236.

190. Pattinson D, Fitzgerald M (2004) The neurobiology of infant pain: development of excitatory and inhibitory neurotransmission in the spinal dorsal horn. Reg Anesth Pain Med 29: 36-44.

191. Pedarzani P, Kulik A, Muller M, Ballanyi K, Stocker M (2000) Molecular determinants of Ca2+-dependent K+ channel function in rat dorsal vagal neurones. J Physiol 527 Pt 2: 283-290.

192. Pedarzani P, Mosbacher J, Rivard A, Cingolani LA, Oliver D, Stocker M, Adelman JP, Fakler B (2001) Control of electrical activity in central neurons by modulating the gating of small conductance Ca2+-activated K+ channels. J Biol Chem 276: 9762-9769.

193. Pedarzani P, D'hoedt D, Doorty KB, Wadsworth JD, Joseph JS, Jeyaseelan K, Kini RM, Gadre SV, Sapatnekar SM, Stocker M, Strong PN (2002) Tamapin, a venom peptide from the Indian red scorpion (Mesobuthus tamulus) that targets small conductance Ca2+-activated K+ channels and afterhyperpolarization currents in central neurons. J Biol Chem 277: 46101-46109.

194. Pedersen KA, Schroder RL, Skaaning-Jensen B, Strobaek D, Olesen SP, Christophersen P (1999) Activation of the human intermediate-conductance Ca(2+)-activated K(+) channel by 1-ethyl-2-benzimidazolinone is strongly Ca(2+)-dependent. Biochim Biophys Acta 1420: 231-240.

195. Pennefather P, Lancaster B, Adams PR, Nicoll RA (1985) Two distinct Ca-dependent K currents in bullfrog sympathetic ganglion cells. Proc Natl Acad Sci U S A 82: 3040-3044.

196. Post MA, Kirsch GE, Brown AM (1996) Kv2.1 and electrically silent Kv6.1 potassium channel subunits combine and express a novel current. FEBS Lett 399: 177-182.

197. Reichling DB, Levine JD (1997) Heat transduction in rat sensory neurons by calcium-dependent activation of a cation channel. Proc Natl Acad Sci U S A 94: 7006-7011.

198. Reimann F, Ashcroft FM (1999) Inwardly rectifying potassium channels. Curr Opin Cell Biol 11: 503-508.

199. Rexed B (1952) The cytoarchitectonic organization of the spinal cord in the cat. J Comp Neurol 96: 414-495.

200. Rhodes JD, Collison DJ, Duncan G (2003) Calcium activates SK channels in the intact human lens. Invest Ophthalmol Vis Sci 44: 3927-3932.

201. Ribera AB, Spitzer NC (1992) Developmental regulation of potassium channels and the impact on neuronal differentiation. Ion Channels 3: 1-38.

202. Rimini R, Rimland JM, Terstappen GC (2000) Quantitative expression analysis of the small conductance calcium- activated potassium channels, SK1, SK2 and SK3, in human brain. Brain Res Mol Brain Res 85: 218-220.

203. Rittenhouse AR, Parker C, Brugnara C, Morgan KG, Alper SL (1997) Inhibition of maxi-K currents in ferret portal vein smooth muscle cells by the antifungal clotrimazole. Am J Physiol 273: C45-C56.

204. Ritter AM, Mendell LM (1992) Somal membrane properties of physiologically identified sensory neurons in the rat: effects of nerve growth factor. J Neurophysiol 68: 2033-2041.

205. Ro S, Hatton WJ, Koh SD, Horowitz B (2001) Molecular properties of small-conductance Ca2+-activated K+ channels expressed in murine colonic smooth muscle. Am J Physiol Gastrointest Liver Physiol 281: G964-G973.

206. Robbins J (2001) KCNQ potassium channels: physiology, pathophysiology, and pharmacology. Pharmacol Ther 90: 1-19.

207. Romey G, Lazdunski M (1984) The coexistence in rat muscle cells of two distinct classes of Ca2+-dependent K+ channels with different pharmacological properties and different physiological functions. Biochem Biophys Res Commun 118: 669-674.

208. Roncarati R, Di Chio M, Sava A, Terstappen GC, Fumagalli G (2001) Presynaptic localization of the small conductance calcium-activated potassium channel SK3 at the neuromuscular junction. Neuroscience 104: 253-262.

209. Roy ML, Narahashi T (1992) Differential properties of tetrodotoxin-sensitive and tetrodotoxin-resistant sodium channels in rat dorsal root ganglion neurons. J Neurosci 12: 2104-2111.

210. Rozen S, Skaletsky HJ (2000) Primer3 on the WWW for general users and for biologist programmers. In: Bioinformatics Methods and Protocols: Methods in Molecular Biology (Krawetz S MS, ed), pp 365-386. Towata, NJ: Humana Press.

211. Ruppersberg JP, Schroter KH, Sakmann B, Stocker M, Sewing S, Pongs O (1990) Heteromultimeric channels formed by rat brain potassium-channel proteins. Nature 345: 535-537.

212. Safronov BV, Vogel W (1996) Properties and functions of Na(+)-activated K+ channels in the soma of rat motoneurones. J Physiol 497 (Pt 3): 727-734.

213. Safronov BV, Vogel W (1998) Large conductance Ca(2+)-activated K+ channels in the soma of rat motoneurones. J Membr Biol 162: 9-15.

214. Sah P, McLachlan EM (1991) Ca(2+)-activated K+ currents underlying the afterhyperpolarization in guinea pig vagal neurons: a role for Ca(2+)-activated Ca2+ release. Neuron 7: 257-264.

215. Sah P (1995) Properties of channels mediating the apamin-insensitive afterhyperpolarization in vagal motoneurons. J Neurophysiol 74: 1772-1776.

216. Sah P (1996) Ca(2+)-activated K+ currents in neurones: types, physiological roles and modulation. Trends Neurosci 19: 150-154.

217. Sah P, Davies P (2000) Calcium-activated potassium currents in mammalian neurons. Clin Exp Pharmacol Physiol 27: 657-663.

218. Sah P, Faber ES (2002) Channels underlying neuronal calcium-activated potassium currents. Prog Neurobiol 66: 345-353.

219. Sailer CA, Hu H, Kaufmann WA, Trieb M, Schwarzer C, Storm JF, Knaus HG (2002) Regional differences in distribution and functional expression of small-conductance Ca2+-activated k+ channels in rat brain. J Neurosci 22: 9698-9707.

220. Sailer CA, Kaufmann WA, Marksteiner J, Knaus HG (2004) Comparative immunohistochemical distribution of three small-conductance Ca(2+)-activated potassium channel subunits, SK1, SK2, and SK3 in mouse brain. Mol Cell Neurosci 26: 458-469.

221. Savic N, Pedarzani P, Sciancalepore M (2001) Medium afterhyperpolarization and firing pattern modulation in interneurons of stratum radiatum in the CA3 hippocampal region. J Neurophysiol 85: 1986-1997.

222. Scholz J, Woolf CJ (2002) Can we conquer pain? Nat Neurosci 5 Suppl: 1062-1067.

223. Schreiber M, Salkoff L (1997) A novel calcium-sensing domain in the BK channel. Biophys J 73: 1355-1363.

224. Schroeder BC, Waldegger S, Fehr S, Bleich M, Warth R, Greger R, Jentsch TJ (2000) A constitutively open potassium channel formed by KCNQ1 and KCNE3. Nature 403: 196-199.

225. Schwindt PC, Spain WJ, Crill WE (1989) Long-lasting reduction of excitability by a sodium-dependent potassium current in cat neocortical neurons. J Neurophysiol 61: 233-244.

226. Scroggs RS, Fox AP (1992) Calcium current variation between acutely isolated adult rat dorsal root ganglion neurons of different size. J Physiol 445: 639-658.

227. Seutin V, Johnson SW (1999) Recent advances in the pharmacology of quaternary salts of bicuculline. Trends Pharmacol Sci 20: 268-270.

228. Shah M, Haylett DG (2000a) The pharmacology of hSK1 Ca2+-activated K+ channels expressed in mammalian cell lines. Br J Pharmacol 129: 627-630.

229. Shah M, Haylett DG (2000b) Ca(2+) channels involved in the generation of the slow afterhyperpolarization in cultured rat hippocampal pyramidal neurons. J Neurophysiol 83: 2554-2561.

230. Shah MM, Miscony Z, Javadzadeh-Tabatabaie M, Ganellin CR, Haylett DG (2001) Clotrimazole analogues: effective blockers of the slow afterhyperpolarization in cultured rat hippocampal pyramidal neurones. Br J Pharmacol 132: 889-898.

231. Shapiro MS, Wollmuth LP, Hille B (1994) Angiotensin II inhibits calcium and M current channels in rat sympathetic neurons via G proteins. Neuron 12: 1319-1329.

232. Shapiro MS, Roche JP, Kaftan EJ, Cruzblanca H, Mackie K, Hille B (2000) Reconstitution of muscarinic modulation of the KCNQ2/KCNQ3 K(+) channels that underlie the neuronal M current. J Neurosci 20: 1710-1721.

233. Shen KZ, Lagrutta A, Davies NW, Standen NB, Adelman JP, North RA (1994) Tetraethylammonium block of Slowpoke calcium-activated potassium channels expressed in Xenopus oocytes: evidence for tetrameric channel formation. Pflugers Arch 426: 440-445.

234. Shmukler BE, Bond CT, Wilhelm S, Bruening-Wright A, Maylie J, Adelman JP, Alper SL (2001) Structure and complex transcription pattern of the mouse SK1 K(Ca) channel gene, KCNN1. Biochim Biophys Acta 1518: 36-46.

235. Simmons MA, Schneider CR, Krause JE (1994) Regulation of the responses to gonadotropin-releasing hormone, muscarine and substance P in sympathetic neurons by changes in cellular constituents and intracellular application of peptide fragments of the substance P receptor. J Pharmacol Exp Ther 271: 581-589.

236. Simonneau M, Distasi C, Tauc L, Barbin G (1987) Potassium channels in mouse neonate dorsal root ganglion cells: a patch-clamp study. Brain Res 412: 224-232.

237. Stocker M, Krause M, Pedarzani P (1999a) An apamin-sensitive Ca2+-activated K+ current in hippocampal pyramidal neurons. Proc Natl Acad Sci U S A 96: 4662-4667.

238. Stocker M, Hellwig M, Kerschensteiner D (1999b) Subunit assembly and domain analysis of electrically silent K+ channel alpha-subunits of the rat Kv9 subfamily. J Neurochem 72: 1725-1734.

239. Stocker M, Pedarzani P (2000) Differential distribution of three Ca(2+)-activated K(+) channel subunits, SK1, SK2, and SK3, in the adult rat central nervous system. Mol Cell Neurosci 15: 476-493.

240. Storm JF (1989) An after-hyperpolarization of medium duration in rat hippocampal pyramidal cells. J Physiol 409: 171-190.

241. Strobaek D, Jorgensen TD, Christophersen P, Ahring PK, Olesen SP (2000) Pharmacological characterization of small-conductance Ca(2+)-activated K(+) channels stably expressed in HEK 293 cells. Br J Pharmacol 129: 991-999.

242. Sugiura Y, Lee CL, Perl ER (1986) Central projections of identified, unmyelinated (C) afferent fibers innervating mammalian skin. Science 234: 358-361.

243. Sugiura Y, Terui N, Hosoya Y (1989) Difference in distribution of central terminals between visceral and somatic unmyelinated (C) primary afferent fibers. J Neurophysiol 62: 834-840.

244. Suzuki R, Dickenson AH (2000) Neuropathic pain: nerves bursting with excitement .. Neuroreport 11: R17-R21.

245. Syme CA, Gerlach AC, Singh AK, Devor DC (2000) Pharmacological activation of cloned intermediate- and small- conductance Ca(2+)-activated K(+) channels. Am J Physiol Cell Physiol 278: C570-C581.

246. Szallasi A, Blumberg PM (1999) Vanilloid (Capsaicin) receptors and mechanisms. Pharmacol Rev 51: 159-212.

247. Szolcsanyi J, Anton F, Reeh PW, Handwerker HO (1988) Selective excitation by capsaicin of mechano-heat sensitive nociceptors in rat skin. Brain Res 446: 262-268.

248. Tacconi S, Carletti R, Bunnemann B, Plumpton C, Merlo PE, Terstappen GC (2001) Distribution of the messenger RNA for the small conductance calcium-activated potassium channel SK3 in the adult rat brain and correlation with immunoreactivity. Neuroscience 102: 209-215.

249. Tatulian L, Delmas P, Abogadie FC, Brown DA (2001) Activation of expressed KCNQ potassium currents and native neuronal M-type potassium currents by the anti-convulsant drug retigabine. J Neurosci 21: 5535-5545.

250. Thomas GP, Karmazyn M, Zygmunt AC, Antzelevitch C, Narayanan N (1999) The antifungal antibiotic clotrimazole potently inhibits L-type calcium current in guinea-pig ventricular myocytes. Br J Pharmacol 126: 1531-1533.

251. Tokimasa T, Shiraishi M, Akasu T (1990) Morphological and electrophysiological properties of C-cells in bullfrog dorsal root ganglia. Neurosci Lett 116: 304-308.

252. Tominaga M, Caterina MJ, Malmberg AB, Rosen TA, Gilbert H, Skinner K, Raumann BE, Basbaum AI, Julius D (1998) The cloned capsaicin receptor integrates multiple pain-producing stimuli. Neuron 21: 531-543.

253. Tomita H, Shakkottai VG, Gutman GA, Sun G, Bunney WE, Cahalan MD, Chandy KG, Gargus JJ (2003) Novel truncated isoform of SK3 potassium channel is a potent dominant-negative regulator of SK currents: implications in schizophrenia. Mol Psychiatry 8: 524-35, 460.

254. Traub RJ, Mendell LM (1988) The spinal projection of individual identified A-delta- and C-fibers. J Neurophysiol 59: 41-55.

255. Troy CM, Brown K, Greene LA, Shelanski ML (1990) Ontogeny of the neuronal intermediate filament protein, peripherin, in the mouse embryo. Neuroscience 36: 217-237.

256. Tseng-Crank J, Foster CD, Krause JD, Mertz R, Godinot N, DiChiara TJ, Reinhart PH (1994) Cloning, expression, and distribution of functionally distinct Ca(2+)- activated K+ channel isoforms from human brain. Neuron 13: 1315-1330.

257. Tseng-Crank J, Godinot N, Johansen TE, Ahring PK, Strobaek D, Mertz R, Foster CD, Olesen SP, Reinhart PH (1996) Cloning, expression, and distribution of a Ca(2+)-activated K+ channel beta-subunit from human brain. Proc Natl Acad Sci U S A 93: 9200-9205.

258. Undem BJ, Weinreich D (1993) Electrophysiological properties and chemosensitivity of guinea pig nodose ganglion neurons in vitro. J Auton Nerv Syst 44: 17-33.

259. Urch CE, Dickenson AH (2003) In vivo single unit extracellular recordings from spinal cord neurones of rats. Brain Res Brain Res Protoc 12: 26-34.

260. Valeyev AY, Hackman JC, Holohean AM, Wood PM, Davidoff RA (2000) Pentobarbital-activated Cl(-) channels in cultured adult and embryonic human DRG neurons. Brain Res Dev Brain Res 124: 137-140.

261. Valtschanoff JG, Rustioni A, Guo A, Hwang SJ (2001) Vanilloid receptor VR1 is both presynaptic and postsynaptic in the superficial laminae of the rat dorsal horn. J Comp Neurol 436: 225-235.

262. Vandorpe DH, Shmukler BE, Jiang L, Lim B, Maylie J, Adelman JP, de Franceschi L, Cappellini MD, Brugnara C, Alper SL (1998) cDNA cloning and functional characterization of the mouse Ca2+-gated K+ channel, mIK1. Roles in regulatory volume decrease and erythroid differentiation. J Biol Chem 273: 21542-21553.

263. Varadi G, Mori Y, Mikala G, Schwartz A (1995) Molecular determinants of Ca2+ channel function and drug action. Trends Pharmacol Sci 16: 43-49.

264. Vergara C, Latorre R, Marrion NV, Adelman JP (1998) Calcium-activated potassium channels. Curr Opin Neurobiol 8: 321-329.

265. Villalobos C, Shakkottai VG, Chandy KG, Michelhaugh SK, Andrade R (2004) SKCa channels mediate the medium but not the slow calcium-activated afterhyperpolarization in cortical neurons. J Neurosci 24: 3537-3542.

266. Villière V, McLachlan EM (1996) Electrophysiological properties of neurons in intact rat dorsal root ganglia classified by conduction velocity and action potential duration. J Neurophysiol 76: 1924-1941.

267. Vogalis F, Furness JB, Kunze WA (2001) Afterhyperpolarization current in myenteric neurons of the guinea pig duodenum. J Neurophysiol 85: 1941-1951.

268. Vogalis F, Storm JF, Lancaster B (2003) SK channels and the varieties of slow after-hyperpolarizations in neurons. Eur J Neurosci 18: 3155-3166.

269. Waddell PJ, Lawson SN (1990) Electrophysiological properties of subpopulations of rat dorsal root ganglion neurons in vitro. Neuroscience 36: 811-822.

270. Wadsworth JD, Doorty KB, Strong PN (1994) Comparable 30-kDa apamin binding polypeptides may fulfill equivalent roles within putative subtypes of small conductance Ca(2+)-activated K+ channels. J Biol Chem 269: 18053-18061.

271. Wadsworth JD, Doorty KB, Ganellin CR, Strong PN (1996) Photolabile derivatives of 125I-apamin: defining the structural criteria required for labeling high and low molecular mass polypeptides associated with small conductance Ca(2+)-activated K+ channels. Biochemistry 35: 7917-7927.

272. Wadsworth JD, Torelli S, Doorty KB, Strong PN (1997) Structural diversity among subtypes of small-conductance Ca2+-activated potassium channels. Arch Biochem Biophys 346: 151-160.

273. Waibl H (1973) Zur topographie der medulla spinalis der albinoratte (Rattus norvegicus). Springer-Verlag, Berlin, New York.

274. Wang HS, Pan Z, Shi W, Brown BS, Wymore RS, Cohen IS, Dixon JE, McKinnon D (1998) KCNQ2 and KCNQ3 potassium channel subunits: molecular correlates of the M-channel. Science 282: 1890-1893.

275. Wang L, Feng ZP, Kondo CS, Sheldon RS, Duff HJ (1996) Developmental changes in the delayed rectifier K+ channels in mouse heart. Circ Res 79: 79-85.

276. Weinreich D (1986) Bradykinin inhibits a slow spike afterhyperpolarization in visceral sensory neurons. Eur J Pharmacol 132: 61-63.

277. Weinreich D, Wonderlin WF (1987) Inhibition of calcium-dependent spike after-hyperpolarization increases excitability of rabbit visceral sensory neurones. J Physiol 394: 415-427.

278. Weinreich D, Koschorke GM, Undem BJ, Taylor GE (1995) Prevention of the excitatory actions of bradykinin by inhibition of PGI2 formation in nodose neurones of the guinea-pig. J Physiol 483 (Pt 3): 735-746.

279. Wiener H, Klaerke DA, Jorgensen PL (1990) Rabbit distal colon epithelium: III. Ca2(+)-activated K+ channels in basolateral plasma membrane vesicles of surface and crypt cells. J Membr Biol 117: 275-283.

280. Wittekindt OH, Visan V, Tomita H, Imtiaz F, Gargus JJ, Lehmann-Horn F, Grissmer S, Morris-Rosendahl DJ (2004) An Apamin- and Scyllatoxin-Insensitive Isoform of the Human SK3 Channel. Mol Pharmacol 65: 788-801.

281. Wolf AR (1999) Pain, nociception and the developing infant. Paediatr Anaesth 9: 7-17.

282. Wolfart J, Neuhoff H, Franz O, Roeper J (2001) Differential expression of the small-conductance, calcium-activated potassium channel SK3 is critical for pacemaker control in dopaminergic midbrain neurons. J Neurosci 21: 3443-3456.

283. Womack MD, Khodakhah K (2003) Somatic and dendritic small-conductance calcium-activated potassium channels regulate the output of cerebellar purkinje neurons. J Neurosci 23: 2600-2607.

284. Womble MD, Moises HC (1993) Muscarinic modulation of conductances underlying the afterhyperpolarization in neurons of the rat basolateral amygdala. Brain Res 621: 87-96.

285. Woolf CJ, Fitzgerald M (1986) Somatotopic organization of cutaneous afferent terminals and dorsal horn neuronal receptive fields in the superficial and deep laminae of the rat lumbar spinal cord. J Comp Neurol 251: 517-531.

286. Wu SN, Li HF, Jan CR, Shen AY (1999) Inhibition of Ca2+-activated K+ current by clotrimazole in rat anterior pituitary GH3 cells. Neuropharmacology 38: 979-989.

287. Xia XM, Fakler B, Rivard A, Wayman G, Johnson-Pais T, Keen JE, Ishii T, Hirschberg B, Bond CT, Lutsenko S, Maylie J, Adelman JP (1998) Mechanism of calcium gating in small-conductance calcium-activated potassium channels. Nature 395: 503-507.

288. Yool AJ, Dionne VE, Gruol DL (1988) Developmental changes in K+-selective channel activity during differentiation of the Purkinje neuron in culture. J Neurosci 8: 1971-1980.

289. Yuan A, Santi CM, Wei A, Wang ZW, Pollak K, Nonet M, Kaczmarek L, Crowder CM, Salkoff L (2003) The sodium-activated potassium channel is encoded by a member of the Slo gene family. Neuron 37: 765-773.

290. Zhang L, Krnjevic K (1987) Apamin depresses selectively the after-hyperpolarization of cat spinal motoneurons. Neurosci Lett 74: 58-62.

291. Zhang X, Bao L, Xu ZQ, Kopp J, Arvidsson U, Elde R, Hokfelt T (1994) Localization of neuropeptide Y Y1 receptors in the rat nervous system with

special reference to somatic receptors on small dorsal root ganglion neurons. Proc Natl Acad Sci U S A 91: 11738-11742.

292. Zhu J, Watanabe I, Gomez B, Thornhill WB (2003) Heteromeric Kv1 potassium channel expression: amino acid determinants involved in processing and trafficking to the cell surface. J Biol Chem 278: 25558-25567.